Author:
Franchini, Daniela

Title:
Changes in Dendritic and Synaptic Function During Early Postnatal Development of the Mouse Barrel Cortex

Changes in Dendritic and Synaptic Function During Early Postnatal Development of the Mouse Barrel Cortex

Daniela Franchini

A dissertation submitted to the University of Bristol in accordance to the requirement for award of the degree of PhD in the Faculty of Life Science

School of Physiology, Pharmacology and Neuroscience

September 2019

Word count: 51,000

Abstract

Neuronal dendrites are the main recipients of glutamatergic synaptic input and participate in active integration of information via the generation of local, regenerative events called dendritic spikes. Whilst these regenerative events have been mostly characterised in adult cortical and hippocampal neurons, it is unclear whether dendritic spikes require mature, fully established synapses or whether they can occur early during development. To explore this possibility, focal synaptic stimulation was used to induce dendritic spiking in postnatal day 7-20 spiny stellate neurons of the layer 4 barrel cortex. However, no nonlinearity characteristic of dendritic spiking was observed in these young neurons, suggesting dendritic spikes are a feature of mature synapses.

During the first 3 postnatal weeks, functional and structural synaptic formation and maturation is accompanied by several changes in the morphology and protein content of postsynaptic spines. Correct function of synaptic transmission relies on the precise apposition between pre- and post-synaptic compartments. Synaptic components, such as ion channels, adhesion proteins and neurotransmitter receptors, are recruited to the post-synaptic sites to establish synaptic function. In excitatory synapses, these proteins are spatially organized and held in place in the spines by members of the membrane-associated guanylate kinase family of proteins. Two members of this family, PSD95 and SAP102, have been identified as major players of synaptic maturation and receptor trafficking, respectively. Developmental profiling of these two proteins revealed a layer-specific, developmentally regulated pattern of expression. Both proteins are highly enriched from P4 in L1 and L4, while the protein levels in L2/3 increase sharply over time. L5A is enriched with PSD95, but not SAP102, from the earliest age and this layer receives inputs from Cplx3-positive subplate neurons.

Acknowledgements

I would like to extend my gratitude to all members, past and present, of the Ashby lab. Firstly, thank you to Mike for his constant, invaluable support during the toughest and the most exciting parts of my PhD. It has been an absolute pleasure.

Thank you to all the members of the Ashby lab. Sarah Hulme, who was there when it all began and inspired me to pursue this research; Fliss Inkpen, for all the poetry and the art, as well as the cracking science; Rob Lees, Christine Cross, Lasani Wijetunge, Jonathan Witton, Soraya Meftah and Laura Mediavilla Santos, for making this experience amazing and always being there to talk about science and life.

Thank you to all the people I have met in this lovely city that have make it feel like home. A massive thank you to Jennie and Richard (Dickie) who have shared this journey with me and have been through thick and thin. To Luis and Luke who have always brought a smile to my face. To Despoina who has always been there for me.

A special thank you goes to my amazing friend Victoria for her immensurable source of support, throughout my time in Bristol and especially during the final stages of my PhD, both morally and practically (all the food and cups of tea!).

Last but not least, I want to take this opportunity to thank my close and extended family, I could not have done this without their support even if from far away.

I would also like to thank the Wolfson Imaging facility, with special mention of Stephen Cross for the writing of the ImageJ macro and Alan Leard for the help with the facility's confocal and 2-photon imaging. Thanks also to the staff from the Histology Unit for their help and competence during training on the freezing microtome. Finally, many thanks to the Wellcome Trust which funded the whole PhD, allowing me to conduct this exciting research.

Author’s declaration

I declare that the work in this dissertation was carried out in accordance with the requirements of the University's Regulations and Code of Practice for Research Degree Programmes and that it has not been submitted for any other academic award.

Except where indicated by specific reference in the text, the work is the candidate's own work. Work done in collaboration with, or with the assistance of, others, is indicated as such. Any views expressed in the dissertation are those of the author.

SIGNED…….. DATE……

Table of contents

List of figures

List of tables

List of abbreviations

AMPA..... α-amino-3-hydroxy-5-methyl-4-isoxazolepropionic acid

AU.....Arbitrary units

bAP..... Backpropagating action potential

BDNF.....Brain-derived neurotrophic factor

Cplx3..... Complexin 3

CTFG.....Connective tissue growth factor

DIV..... Days *in vitro*

DLG..... Disc-large

E..... Embryonic day

EM..... Electron microscopy

EPSP..... Excitatory postsynaptic potential

GABA..... γ-aminobutyric acid

GFP.....Green fluorescent protein

GUK.....Guanylate kinase

L.....Layer

LGE.....Lateral ganglionic eminence

LTP..... Long-term potentiation

LTD.....Long-term depression

M1.....Primary motor cortex

MAGUK..... Membrane-associated guanylate kinases

mKO2..... Kusabira Orange 2

MGE..... Medial ganglionic eminence

MZ.....Marginal zone

NA.....Numerical aperture

NMDA ..... N-Methyl-d-aspartic acid

P .....Postnatal day

PBS.....Phosphate buffer solution

POM.....Posteromedial nucleus

PSD ..... Postsynaptic density

PSD95 ..... Postsynaptic density protein 95

PSD93 ..... Postsynaptic density protein 93

Ptx.....Picrotoxin

RGC..... Radial glial cells

RMTW..... rostromedial telencephalic wall

S1 .....Primary sensory cortex

S2 .....Secondary sensory cortex

SAP102……Synapse-associated protein 102

SAP97……..……Synapse-associated protein 97

Sh3 ..... SRC Homology 3 Domain

SP ..... Subplate

SPN ..... Subplate neurons

SVZ..... Subventricular zone

TAP..... Tandem affinity purification

TCA..... Thalamocortical afferents

Vm ..... Membrane potential

VPM..... Ventral posteromedial nucleus

VZ .....Ventricular zone

Summary statement of contributions:

All the following work, including the knock-in mouse breeding, electrophysiological and imaging experiments, diagrams, except where stated in the figure legend, was conducted by the author of this thesis.

The mouse lines used in this paper were acquired from Professor Seth Grant (University of Edinburgh).

The ImageJ macro to analyze the fluorescent puncta was made by Stephen Cross (Wolfson Imaging Facility, University of Bristol).

Introduction

1.1 Neocortical organization of sensory systems

The 3D spatial organization of the mammalian neocortex is striking and it is thought to underlie the efficiency of this system in dealing with the intricate neuronal circuits it comprises.

Horizontally, this structure is divided into 6 layers which host neurons with distinct morphologies, transcriptomic profiles, electrophysiological properties and connectivity patterns. Vertically, the neocortex is organized in cortical columns that further increase the organization and optimize neuronal circuit function, by the formation of topographically mapped connections that increase the parallel processing and global integration of inputs and outputs (Fujita et al., 1992; Hubel and Wiesel, 1963; Kanold et al., 2014; Mountcastle, 1957). Cortical columns, first described in the monkey somatosensory cortex, are a common organizing principle of several systems, including the motor, visual and auditory systems (Fujita et al., 1992; Hubel and Wiesel, 1963; Kanold et al., 2014; Mountcastle, 1957). Therefore, the neocortex is organized in cortical physically- and functionally-related modules to give rise to this extremely precise network in which anatomical topology is tightly linked to the precise functionality of this system. The laminar location of distinct types of cortical neurons is determined during development, via a strict spatiotemporal regulation of neuronal generation, migration and synapse formation (Rakic, 1988).

1.2 Neuronal transmission and computation

Neuronal communication underlies and directs the execution of brain functions, such as movement, sensory processing and higher cognitive processing. Efficient neuronal function is therefore essential for the interaction with the surrounding environment. The adult human brain has been estimated to contain around 100 billion neurons (Azevedo et al., 2009); these neurons form many connections between each other via specialised junctions, the synapses. Synapses are usually composed of a presynaptic terminal, a synaptic cleft and an electron dense postsynaptic compartment containing the postsynaptic density (PSD, Colonnier, 1968; Harris et al., 1992). Each neuron receives several inputs from functionally connected partners and propagates the signal to downstream neurons. These synaptic connections give rise to neuronal pathways, a collection of neurons that connect different areas of the brain that are specific to a specific function. The nervous system, therefore, is an extremely complex and organised structure that requires the proper establishment of each component to support widespread computation of signals.

Neurons collect information, in the form of chemical signals driven by synaptic transmission. When these signals reach the dendrite, they summate and if they cause the neuronal membrane potential to depolarise beyond a threshold voltage, an output, called action potential, is generated. Action potentials are initiated at the axonal initial segment, a Na^+ channel rich area located at the axon hillock, and propagate down the axon to presynaptic sites (Fig. 1.1). Action potentials trigger the fusion of neurotransmitter-filled synaptic vesicles in the presynaptic terminal, in specifically located active zones (Burns and Augustine, 1995; Phillips et al., 2001). Neurotransmitters (mainly glutamate in excitatory neocortical neurons) are thus released in the synaptic cleft, the 20-25 µm area between the pre- and post-synaptic neurons (Schikorski and Stevens, 1997). The released glutamate binds to glutamate receptors found on the membrane of the postsynaptic partner; a variety of receptors and cell adhesion proteins are present in the electron dense PSD (Kennedy, 2000). Most excitatory synapses in the brain are located in dendritic protrusions, named dendritic spines (Nimchinsky et al., 2002). Within spines, N-methyl-D-aspartate (NMDA) and α-amino-3-hydroxy-5-methyl-4-isoxazolepropionic acid (AMPA) receptors (NMDARs and AMPARs), which are the two main classes of ionotropic glutamate receptors (Hollmann and Heinemann, 1994), are clustered at the postsynaptic density. The activation of excitatory synapses via binding of neurotransmitters at dendritic spines leads to an influx of Na^+ ions that drives a depolarisation of the membrane potential. The summation of these depolarising synaptic potentials drives the cell towards action potential threshold, repeating the cycle of information transmission. Importantly, neuronal dendrites are not simply passive recipients of electric signals, but instead exhibit electrogenic properties that can dynamically process received information locally. This active role in information processing is a product of the presence of many voltage-gated ion channels in the dendritic membrane that allow nonlinear amplification and active propagation of electric signals. In the neocortex, neuronal dendritic arbours can exhibit a variety of shapes and sizes, depending on the cell type and the location within the cortical layers. These morphological differences in this postsynaptic structure have an impact on the way neurons process information. The location and density of dendrites within a neuronal dendritic arbour determine the type and number of inputs that neurons can sample. Furthermore, the size and shape of single dendrites, can determine its passive electrotonic properties. Whilst these morphological features can affect the passive properties of the dendrite, the type, number and distribution of ion channels along dendritic length affect its active membrane conductances.

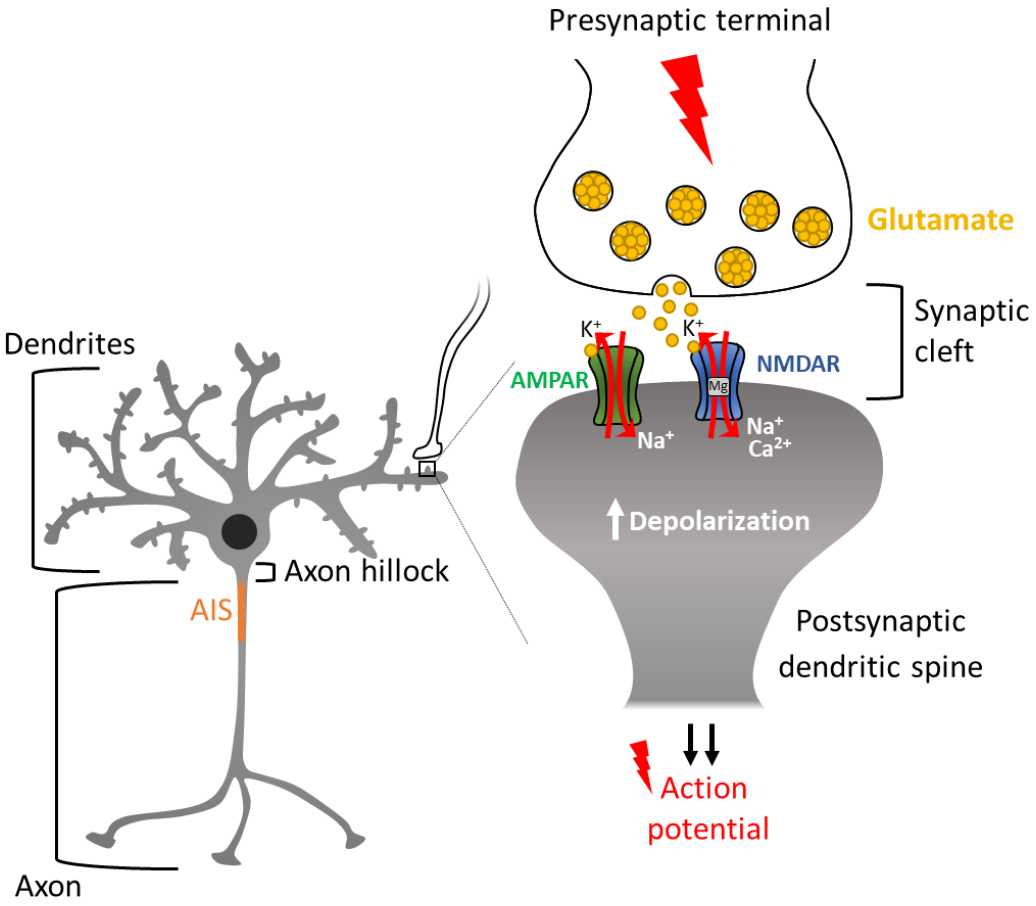

Figure 1. 1 Basic components of a cortical excitatory synapse

Action potentials, here symbolised as a red lightning, reach the presynaptic axonal terminal and cause the release of neurotransmitters. Neurotransmitters, glutamate in this case, diffuse across the synaptic cleft and bind to receptors present on the postsynaptic membrane of the synapsing neuron. This event causes the opening of AMPA receptors, which lead to depolarisation of the dendritic spine which in turn releases the magnesium block from NMDA receptors which open and allow more positive ions to enter the cell. When a threshold is reached, an action potential is propagated down the axon to excite downstream dendrites.

1.3 Active dendrite processing

Dendritic arbours can be extremely large, meaning that currents resulting from distal synapses are considerably attenuated when they reach the soma (Berger et al., 2001; Harnett et al., 2015; Larkum et al., 2009; Magee, 1998; Nevian et al., 2007; Stuart and Spruston, 1998; Williams and Stuart, 2002). Dendrites have been shown to exhibit active properties, which can compensate for this geometrically imposed dissipation of distal synaptic inputs. For example, action potentials generated at the axonal initial segment have been shown to propagate back into the dendritic arbor (backpropagating action potentials, bAPs) and this phenomenon is actively supported in dendrites via activation of voltage-dependent Na^+ and K^+ channels (Colbert et al., 1997; Hoffman et al., 1997; Jung et al., 1997; Vetter et al., 2001). Additionally, by virtue of their active properties, dendrites have also been shown to sustain local generation of regenerative potentials, called dendritic spikes, that can boost spatiotemporally synchronised inputs (Antic et al., 2010; Branco and Häusser, 2011; Brandalise et al., 2016; Golding et al., 2002; Lavzin et al., 2012; Schiller and Schiller, 2001). Backpropagating action potentials and dendritic spikes have distinct spatiotemporal features; bAPs occur after somatic action potential generation and spread on a proximal to distal manner (from the soma); on the other hand, dendritic spike generation is usually restricted to individual dendritic branches and while it contributes to the depolarised state of the neurons, it does not always trigger somatic action potentials.

1.3.1 Dendritic spikes

Dendritic spikes and active dendritic processing have received extensive interest in the past 30 years. These electrophysiological features of neurons are thought to dramatically expand neuronal computational repertoire and provide an additional mechanism to integrate inputs from different parts of the brain (Antic et al., 2010; Branco and Häusser, 2011; Brandalise et al., 2016; Golding et al., 2002; Lavzin et al., 2012; Schiller and Schiller, 2001).

These nonlinear regenerative events are restricted to a portion of a single dendritic branch. They emerge as consequence of the dendritic electrogenic properties, i.e. the distribution of voltage-gated channels along their lengths. When a sufficient number of synapses is active on a single dendrite, the ionic influx in the spines causes a depolarisation that can trigger the opening of voltage-gated channels present in the vicinity, even in synapses which are not directly engaged. The resulting membrane potential response triggered by these regenerative events is therefore larger than the linear sum of the synapses activated (Antic et al., 2010; Branco and Häusser, 2011;

Brandalise et al., 2016; Golding et al., 2002; Lavzin et al., 2012; Schiller and Schiller, 2001).

1.3.2 Dendritic spiking in pyramidal cells

Dendritic spiking has been most extensively characterised in neocortical layer (L) 5 and L2/3 pyramidal and hippocampal pyramidal neurons (Magee, 1998; Spruston, 2008). The dendritic arbour of pyramidal neurons comprises of a thick apical dendrite and thin basal, oblique and tuft dendrites. At the time when these regenerative membrane potentials were first being described, the more easily identified thick apical dendrites were the main subjects of study, because technical limitations made the visualisation of smaller dendrites very difficult. These dendrites contain voltage-gated channels that allow active processing of currents and exhibit Na^+ and Ca^{2+} spikes (Magee, 1998; Spruston, 2008; Stuart and Spruston, 1998). With the improvement of imaging techniques, the thin dendrites of pyramidal cells started being investigated and it was uncovered that these dendrites can also support local dendritic spikes mediated by voltage-gated Na^+ or Ca^{2+} channels and NMDARs (Larkum et al., 2009; Major et al., 2008; Rhodes, 2006; Schiller and Schiller, 2001).

Why do dendritic spikes appear to be such a prominent feature of pyramidal neurons? These cells have a larger dendritic arbour, with long apical dendrites that reach the outermost cortical layer and receive top-down inputs. This means that the inputs that need to get integrated in the axonal initial segment have a long distance to travel down and the signal dissipates quickly. A dendritic spike, therefore, would help to boost the signal in these distal apical synapses, compensating for the dissipation and helping to counterbalance the higher synaptic impact of synapses in the more proximal dendrites. *In silico* models of backpropagating action potential has shown that dendritic spikes can provide a mechanism by which spatiotemporally clustered inputs affect synaptic plasticity; especially in the case of distal synapses, dendritic filtering greatly dissipates the bAP, dendritic spikes provide a mechanism by which long-term potentiation (LTP) or long-term depression (LTD) can be achieved without feedback from the bAP (Golding et al., 2002). This is especially important in pyramidal neurons because due to their large dendritic arbour, they span many cortical layers and therefore can receive layer-specific inputs (Spruston, 2008). Dendritic spikes have been recorded in proximal dendrites of L5 pyramidal cells as well, so they probably provide additional processing power and mechanisms that affect neuronal computation.

1.3.3 Dendritic spiking in L4 spiny stellate cells

In contrast to the large dendritic arbors of pyramidal neurons, L4 spiny stellate neurons of the barrel cortex exhibit a much smaller dendritic arbour. These cells receive direct input from thalamocortical afferents (TCAs) and interconnect to each other extensively within each barrel, before sending their axons to L2/3 (Harris and Woolsey, 1983). Cells within the barrels have been shown to respond maximally to whisker deflections at a specific angle (Bruno et al., 2003; Lavzin et al., 2012). Active dendritic integration has been speculated to play a role in the sharpening of neuronal tuning curves during sensory processing (Archie and Mel, 2000; Branco and Häusser, 2010; Poirazi and Mel, 2001; Polsky et al., 2004). Therefore, dendritic spiking in L4 barrel cortex neuron may provide a way to establish and regulate this specificity by potentiating spatiotemporally clustered synaptic inputs triggered by whisker deflections at a specific angle. Indeed, Lavzin and colleagues showed that blocking NMDAR-mediated dendritic spikes also significantly decreases the orientation tuning of these cells to specific angular whisker deflections (Lavzin et al., 2012).

1.3.4 Types and kinetics of dendritic spikes

Regenerative membrane potentials are named after the main type of channels that mediates them, each exhibiting specific kinetics and preferential location of origin along the dendritic branch (Fig 1.2, Antic et al., 2010; Branco and Häusser, 2011; Brandalise et al., 2016; Golding et al., 2002; Lavzin et al., 2012; Schiller and Schiller, 2001). Dendritic spikes have been shown to be mediated by voltage-gated Na^+ channels (sodium spikes), Ca^{2+} channels (calcium spikes) and NMDA receptors (NMDA spikes). Sodium spikes are usually very narrow in width (less than 5 ms); as it is the case for most types of dendritic spikes, they can occur in the absence of somatic action potential generation, which distinguishes them from backpropagating action potentials (Golding and Spruston, 1998; Losonczy and Magee, 2006; Stuart et al., 1997; Sun et al., 2014). Calcium spikes are much broader (more than 10 ms in duration) and they are usually elicited by more prolonged depolarisations (Amitai et al., 1993; Golding and Spruston, 1998; Llinás and Sugimori, 2012; Pockberger, 1991; Stuart et al., 1997; Wong et al., 1979). NMDA spikes have been reported to be between 40-50 mV in amplitude (Nevian et al., 2007) and are the longest in duration, lasting for 50-100 ms (Major et al., 2008; Polsky et al., 2004; Rhodes, 2006; Schiller et al., 2000). Due to the high Ca^{2+} permeability of NMDARs, Ca^{2+} imaging of the dendritic arbour can be used to extract spatiotemporal information about dendritic spikes. Using this technique and modelling, NMDA spikes were found to occur within short dendritic segments between 10-40 µm (Larkum et al., 2009; Major et al., 2008; Rhodes, 2006; Schiller et al., 2000). While Ca^{2+} spikes occurring in the pyramidal

apical thick dendrites usually propagate into the soma and trigger action potentials (Amitai et al., 1993; Connors and Gutnick, 1990; Helmchen et al., 1999; Kim and Connors, 1993; Larkum et al., 1999; Larkum and Zhu, 2002; Schiller et al., 1997), NMDA spikes in the thin dendrites usually involve only one sister branch and rarely lead to action potential generation (Holthoff et al., 2004; Larkum et al., 2009; Major et al., 2008; Milojkovic et al., 2005; Oakley et al., 2001; Schiller et al., 2000); however, multiple NMDA spikes can induce Ca^{2+} spiking that in turn can trigger somatic action potential (Larkum et al., 2009; Lavzin et al., 2012; Milojkovic et al., 2005; Palmer, 2014; Polsky et al., 2004).

1.3.5 Location-specific generation of dendritic spikes

Studies on cortical pyramidal neurons show that different portions of the dendritic arbor usually preferentially support a specific type of dendritic spike. Sodium spikes occur throughout the length of the arbour, while calcium spikes are generally generated in the thick apical dendrites and NMDA spikes occur preferentially in the thin apical tuft and basal dendrites (Harnett et al., 2015; Larkum et al., 2009; Nevian et al., 2007; Schiller et al., 1997; Stuart et al., 1997; Yuste et al., 1994). Additionally, to date, only NMDAR-mediated regenerative events have been observed in the spiny stellate neurons of the mouse barrel cortex (Lavzin et al., 2012).

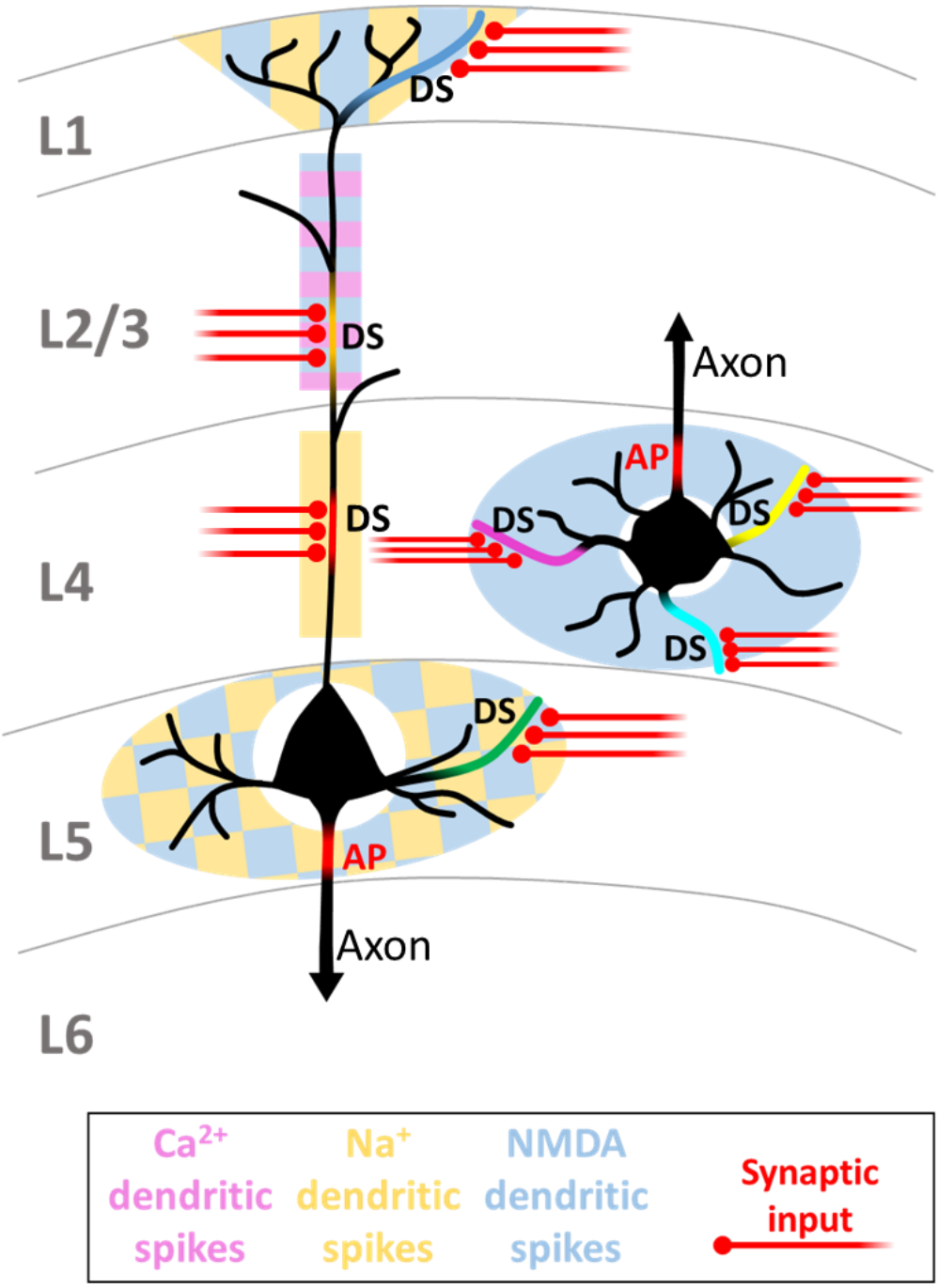

Figure 1. 2 Dendritic spikes in two types of cortical neurons

Dendritic spikes are generated by spatiotemporally synchronous synaptic input. They can be mediated by Ca^{2+}, Na^{+} and NMDAR are generated in specific areas of the dendritic tree. (Left) diagram of a L5 pyramidal cell. While Na+ spikes can be elicited almost ubiquitously in the dendritic tree, Ca^{2+} are specific to the apical trunk and NMDA spikes to tufts and basal dendrites. (Right) diagram of a L4 spiny stellate neuron. These cells support NMDA spikes. DS: dendritic spike; AP: action potential. Adapted from Stuart and Spruston (2015).

1.3.6 Effects and implications of dendritic spike generation

Dendritic spike generation causes an increase in intracellular concentration of Ca^{2+} (Major et al., 2008; Milojkovic et al., 2005; Takahashi and Magee, 2009) which, by acting as a second messenger, can affect short- and long-term plasticity (Golding et al., 2002; Holthoff et al., 2004; Johnston and Narayanan, 2008; Kampa et al., 2007; Kim et al., 2018; Lau et al., 2009; Losonczy and Magee, 2006; Nimchinsky et al., 2002; Sjöström et al., 2001; Spruston, 2008; Takahashi and Magee, 2009; Zucker and Regehr, 2002). This modulation of synaptic plasticity has been shown to occur even in the absence of action potential generation at the soma (Gambino et al., 2014; Golding et al., 2002).

Computer modelling studies have supported the idea that dendritic spiking may contribute to the compartmentalisation of inputs on the dendritic arbour, so that each dendritic branch can act as an independent computational unit (Archie and Mel, 2000; Gollo et al., 2009; Poirazi and Mel, 2001). This has important implications for neuronal computations as it allows parallel processing of information, as well as integration of inputs from different pathways converging onto the same neuron.

Due to their nonlinear nature, dendritic spikes can amplify spatially clustered and temporally synchronised synaptic inputs. From a biological point of view, this also means that functionally related inputs that are also spatially clustered can influence local plasticity to a level which can be disproportionate to their objective synaptic weight (i.e. spatiotemporal patterns are important, as well as input strength). Therefore, this would favour a model where synaptic inputs are clustered, over a “salt and pepper” model where synaptic inputs relating to the same function are sparsely distributed across the dendritic arbour. Indeed, physical clustering of functionally related synapses enhances the probability of reaching the threshold for a local dendritic spike, leading to more efficient cooperation between inputs related to the same functional task.

1.3.7 Distribution of synaptic inputs: evidence for and against synaptic clustering

Modelling studies have, indeed, shown that the activation of clustered synapses (~ 40 µm apart) can produce a supralinear response, while inputs resulting from the co-activation of synapses located farther apart (~60 µm) summate linearly (Araya et al., 2006). Electrophysiology data further corroborated the computational data, showing how in L5 pyramidal neuron dendrites, a 2-fold larger response is obtained by

activation of neighbouring inputs (20-40 µm apart); this nonlinearity was found to be NMDAR-dependent (Polsky et al., 2004).

Therefore, dendritic spikes simultaneously actively reinforce and thrive in a network that favours synaptic clustering of spatiotemporally synchronised and putatively functionally related inputs. However, it is unclear whether this synaptic organization is present universally across all regions and various neuronal cell types of the nervous system.

In order to shed light on whether inputs are randomly distributed on postsynaptic sites or whether structured organisation underlies their location, computational models and empirical studies have been employed to address this question in several ways.

In support of a clustered organisation of functionally related inputs, Poirazi and Mel's computational model predicted that, over time, pairing activations of synapses tends to cluster and segregate activated inputs from asynchronous others (Poirazi and Mel, 2001). McBride and colleagues showed the formation of a new circuit in the inferior colliculus in owls that were raised with prism glasses that shifts the field of view by 19° (McBride et al., 2008). This new circuit forms alongside the original visual circuit, providing a way to compare the synaptic organisation of functionally relevant and functionally suppressed circuits. In the newly formed, functionally learned circuit, the intercontact distances of putative synapses was never observed to be <20 µm, while in the original functionally suppressed circuit a mixture of <10 µm but also a substantial fraction of >20 µm inter-contact distances was found. This suggests that functional circuitry favours the clustering of inputs. Furthermore, 2-photon imaging of developing hippocampal pyramidal cells in rat pups also revealed that synapses located within 16 µm of each other are more likely to be co-active; this arrangement is an activity-dependent feature, since the presence of tetrodotoxin significantly dispersed the distribution of synapses (Kleindienst et al., 2011). *In vivo* studies involving calcium imaging of spontaneous activity in the developing visual system uncovered a synaptic plasticity mechanism whereby transmission efficiency of desynchronised synapses becomes depressed; this suggests that synchronisation of neighbouring synapses is important not only for efficient transmission but also for plastic changes occurring within the developing neural circuit (Winnubst et al., 2015). Additionally, in the CA3 of pyramidal cells of postnatal day (P) 7 rats, 10 µm of inter-synaptic distance was determined to be the threshold for high probability of co-activation (Takahashi et al., 2012). Task learning was also found to cause the appearance of new clustered synapses on the L5 pyramidal neurons of the motor cortex, albeit in a much smaller scale (2µm average inter-synaptic distance, Fu et al.,

2012). Furthermore, the learning of a new task induced the generation of new clusters of synapses, spatially segregated from those formed in the learning of the previous task (Fu et al., 2012). The principle of clustering of functionally related synaptic inputs appears to extend to inhibitory synaptic inputs. Studies on inhibitory synaptic inputs onto cortical L2/3 pyramidal neurons show that dynamic changes of these inputs are spatially clustered and that this plastic organisation is influenced by sensory inputs (Chen et al., 2012). Finally, a recent EM study provided structural evidence that synaptic inputs onto CA1 pyramidal neurons are spatially clustered in the distal, but not proximal dendrites (Bloss et al., 2018). This collection of studies suggests that synapses that are functionally related tend to cluster together and this spatial organisation is activity dependent.

However, not all studies show evidence for the clustering of synaptic inputs. The Konnerth laboratory has produced a series of 2-photon imaging studies investigating spatial distribution of dendritic calcium transient elicited via sensory stimulation in the L2/3 cells of the mouse visual cortex (Jia et al., 2014), L2 cells of the mouse barrel cortex (Varga et al., 2011) and in the L2/3 cells of the mouse auditory cortex (Chen et al., 2011). In all these studies, examples were found where specific sensory features, to which all the examined cells were tuned, would elicit a calcium response in different non-neighbouring dendrites. On the other hand, different stimulus features could activate synapses that were close by on the same dendrite. This spatial arrangement of functionally related inputs appears to be geared more towards a “salt and pepper” distribution of inputs, which directly contrasts with previously discussed clustering of inputs. Additionally, correlated light and electron microscopy of retrogradely traced thalamic neurons onto L4 spiny stellate neurons of the visual cortex of the cat also presented no evidence of synaptic clustering onto these dendrites (Costa and Martin, 2011).

Therefore, the prevalence of clustered synapses or dispersed synapses remains an open question. It is unclear whether the presence of a more clustered organisation of synaptic inputs is a universally applied feature of neural networks, or whether it is restricted to certain regions, cell types or developmental timepoints. The establishment and maintenance of a clustered input regime would involve the elimination of spatially isolated synapses and the formation of co-active synapses localised near each other. Indeed, a mechanism for the bidirectional regulation of this process has been proposed by a recent paper, whereby brain-derived neurotrophic factor (BDNF) and pro-BDNF act to stabilise clustered synapses and suppresses unsynchronised synapses, respectively (Niculescu et al., 2018).

1.3.8 Behavioural relevance of dendritic spikes in vivo

Several studies have probed the behavioural relevance of these local nonlinear events *in vivo.* Takahashi and colleagues showed that in mice (Takahashi et al., 2016), Ca^{2+} spiking affects the perception of whisker stimulation. Indeed, the probability of the detection of the movement increased when dendritic activity was induced and decreased when activity was inhibited. Furthermore, Ca^{2+} spikes were found to be generated during whisking behaviour, when the vibrissal motor cortex and thalamic inputs combined, suggesting that this type of dendritic spikes play an active role during sensory-motor integration. Finally, NMDA spikes in L2/3 and L4 neurons were detected during whisker deflection (Gambino et al., 2014; Lavzin et al., 2012). These types of spikes were found to be important for neuronal tuning in the somatosensory and visual cortex (Lavzin et al., 2012; Smith et al., 2013).

In conclusion, dendritic spikes can participate in three processes:

1. Synaptic plasticity: even in the absence of action potential, synapses have been shown to modify their strength after dendritic spike generation (Gambino et al., 2014; Golding et al., 2002).
2. Increase of the neuronal computational power: by providing a mechanism for supralinear summation of inputs and allowing dendrite-specific independent integration of signals.
3. Sharpening of neuronal tuning of behavioural responses (Lavzin et al., 2012; Smith et al., 2013).

Because of these characteristics, dendritic spikes have the potential to play an important role during synapse formation and maturation, a developmental stage during which activity has a dramatic effect on shaping neuronal circuitry. However, it is unclear whether these events require functionally mature synapses in order to occur, or whether they can occur during synaptic development and contribute to this process.

1.3.9 Experimental electrophysiological features of dendritic spikes

Experimentally, dendritic spikes have been investigated by the detection a nonlinear response to an increasing stimulus intensity. Two main methods have been employed to stimulate an increasing number of neighbouring synapses on a single dendritic branch: focal synaptic stimulation at different intensities or glutamate uncaging on an increasing number of dendritic spines (Antic et al., 2010; Branco and Häusser, 2011; Brandalise et al., 2016; Golding et al., 2002; Lavzin et al., 2012; Schiller and Schiller, 2001). Dendritic spikes are characterised by a nonlinear response to increasing input

when it exceeds a certain threshold. This ”jump” in the response is thought to be due to the activation of voltage-gated receptors on nearby dendritic areas, caused by the overflow of depolarisation from the activated synapses.

Furthermore, as dendritic spikes have been shown to be mediated by either Na^+, Ca^{2+} or NMDA receptors, pharmacological or physiological blockage that significantly abolishes the characteristic nonlinearity can be used to investigate the contribution of the ion channel or receptor, thus determining the type of dendritic spike that is being generated. For example, in the case of NMDAR-mediated dendritic spike, washing the brain slice with extracellular (2R)-amino-5-phosphonovaleric acid; (2R)-amino-5-phosphonopentanoate (APV), using internal solution containing intracellular MK801 or hyperpolarising the cells thus preventing the activation of the receptors via Mg^+ block release, have been shown to prevent the generation of dendritic spikes. Blocking the ion channels or receptors that mediate the generation of a dendritic spike linearizes the input/output curve; i.e. it abolishes the supralinear summation of inputs (e.g. Lavzin et al., 2012). This method has been used to prove the mechanism by which dendritic spikes can be generated and to ascertain which voltage-gated components are involved in this phenomenon.

Recently Lavzin and colleagues showed that they were able to elicit nonlinear responses in the spiny stellate neurons of the mouse barrel cortex between P15-20. In their hands, these dendritic spikes were NMDAR-dependent and were visualised by performing calcium imaging, which highlighted the branch-specificity of these events (Lavzin et al., 2012). Furthermore, their study showed that preventing the occurrence of NMDAR-dependent events, acutely in an *in vivo* mouse brain, significantly decreased the angular tuning to whisker deflection of layer 4 spiny stellate neurons.

1.4 Stages of the development of sensory systems

The development of the neocortex relies on an intricate and precisely spatiotemporally regulated interplay between genetic factors and neuronal activity that can be grossly divided in two stages:

1. an embryonic stage where genetically specified programs govern neurogenesis and neuronal migration
2. an early postnatal, activity-dominated stage during which the immature template of the neural circuit is refined

1.4.1 Embryonic stage of neural development

The mammalian embryonic CNS originates from the neuroepithelial cells that constitute the neural tube (Götz and Huttner, 2005). The two main classes of cortical neurons, excitatory and inhibitory gamma-Aminobutyric acid (GABA) -ergic, emerge from distinct developmental lineages.

Excitatory neurons are generated via asymmetric division of progenitor cells located in the subventricular and ventricular zone (Fig. 1.3). The major progenitor cells are radial glial cells (RGCs, Williams and Price, 1995). RGCs are a transient population of non-neuronal cells that are fundamental for the generation of the vast majority of neurons and glial cells (Campbell and Götz, 2002; Kriegstein and Gotz, 2003; Noctor et al., 2001). They exhibit a characteristic cell morphology, bipolar cells with radial processes that span the whole depth of the cortex (Bentivoglio and Mazzarello, 1999; Cameron and Rakic, 1991) and they provide structural scaffolding for neurons migrating radially towards the cortical plate (Levitt and Rakic 1980; Rakic 1988; Hatten, 2002). After an intense period of neurogenesis, RGC cells switch to gliogenesis, giving rise to astrocytes and oligodendrocytes (Kriegstein and Alvarez-Buylla, 2009).

Newly-generated postmitotic neurons make their way to the cortical plate to establish distinct cortical layers. The stereotypic laminar structure is essential for the correct functioning of the neocortex. Cortical layers have been shown to be established in an “inside-out” fzashion, whereby early born neurons populate the deeper layers and neurons generated later migrate through the early-born neurons and locate in the more superficial layers (Angevine et al., 1961, Berry et al, 1965). There are two modes of radial migration that excitatory neurons can adopt. During early development the most prominent mode is somal translocation (Miyata et al., 2001; Morest, 1970; Nadarajah et al., 2001); neurons develop a long radial process and drag their somas towards the pial surface (Nadarajah et al., 2001). During later stages of development,

newly-born neurons predominantly migrate via radial glia guided locomotion (Nadarajah and Parnavelas, 2002; Noctor et al., 2004; Sidman and Rakic, 1973). Migrating neurons follow the cortical plate spanning RCG processes towards the marginal zone and when their leading process makes contact with this layer, they detach from the radial glia (terminal translocation phase, Nadarajah et al. 2001).

Appropriate radial migration leading to correct laminar organization in the cortex has been shown to rely on the secretion of an extracellular glycoprotein, reelin, from Cajal-Retzius cells located in the marginal zone (Marin-Padilla and Marin-Padilla, 1982; Río et al., 1997; Marín-Padilla, 1998). In fact, in the *reeler* mouse, where this protein is absent due to a mutation, the cortical layers are organized in a reversed "outside-in" fashion (Caviness and Rakic, 1978; D'Arcangelo, 2001; Drakew et al., 2002; Forster et al., 2002; Magdaleno et al., 2002; Ogawa et al., 1995). This mouse is characterized by motor dysfunctions, ataxic and reeling gait

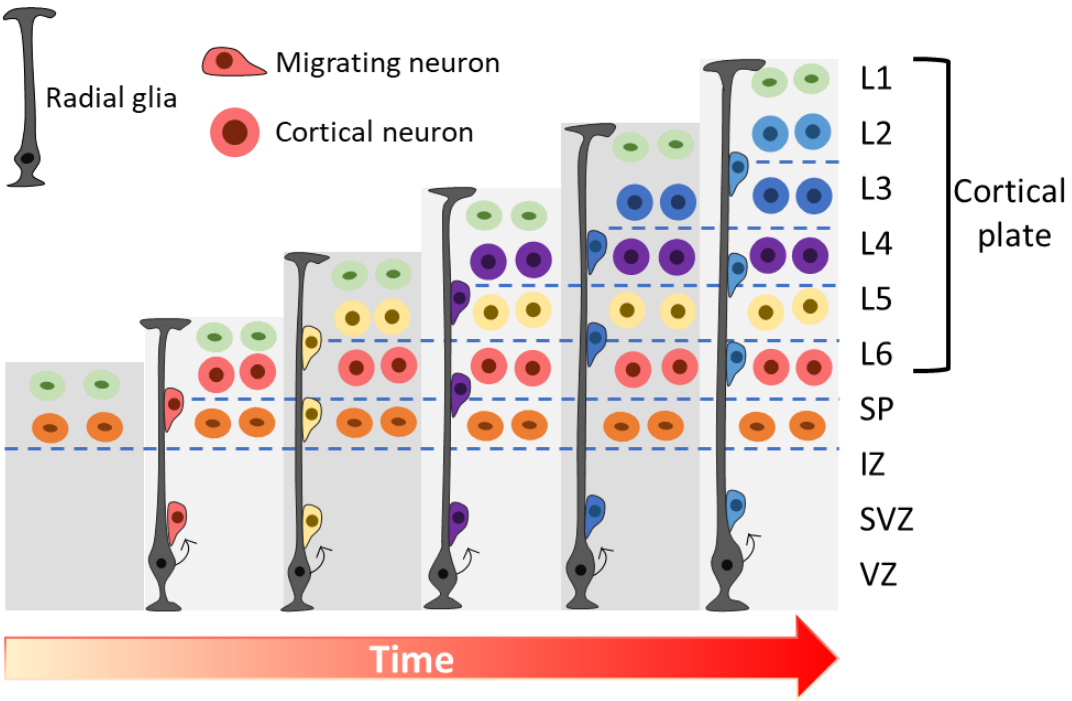

Figure 1. 3 Cortical development of excitatory neurons
The diagram shows the developmental growth of the cortical plate. The red arrow is showing the direction of increased time. Neurons are generated in the proliferative zone and migrate towards the superficial layers along radial glia processes. They stop their migration just below the marginal zone/L1, and establish cortical layers in an inside-out manner.
IZ, intermediate zone; SVZ, subventricular zone; VZ, ventricular zone.

GABAergic cortical interneurons are generated in the extracortical areas of the ventral telencephalon, mainly the medial ganglionic eminence (MGE, Lavdas et al., 1999; Wichterle et al., 1999), the caudal ganglionic eminence (CGE, Nery et al., 2002; Xu et al., 2004), and the preoptic area (POA, Gelman et al., 2011). RCGs in the MGE have been shown to undergo asymmetric cell division to generate neocortical interneurons (Brown et al., 2011). Due to the distal location of the ganglionic eminences compared to the origin of excitatory neurons, neocortical interneurons embark in a prolonged tangential migration to reach the appropriate layer in the developing cortical plate (Anderson et al., 1999, 2001; Jimenez et al., 2002; Lavdas et al., 1999; Miyoshi et al., 2010; Nery et al., 2002; Polleux et al., 2002; Tan et al., 1998; Ware et al., 1999; Wichterle et al., 1999; Yozu et al., 2005). Once the migrating neocortical interneurons finally reach the neocortex, they continue to diffuse tangentially in the MZ, SP and SVZ (Lavdas et al., 1999), until eventually they switch to radial migration to reach their final destination in the correct cortical layer (Polleux et al., 2002; Tanaka et al., 2010).

The excitatory and inhibitory neurogenesis and migration appears to be an extremely coordinated and co-dependent event; indeed, despite the different duration of migration from the place of origin, excitatory and inhibitory neurons with similar birthdates end up populating the same cortical layer (Fairen et al., 1986; Miller, 1985; Nery et al., 2002; Valcanis and Tan, 2003). Additionally, interneurons are added to the neocortex only after their excitatory partners, suggesting the former cells follow signals from the latter cells (López-Bendito et al., 2004).

1.4.2 Early postnatal stages of neural development

Two types of activity sculpt the developing sensory neural system: spontaneous activity, which comprises of electrical events not evoked by overt external stimuli, and sensory-triggered activity, which is activity generated in response to experiencing the surrounding environment via peripheral sensory receptors.

Spontaneous activity is the most prominent type of activity during the earliest postnatal stages of development of many mammalian sensory systems; this type of activity has been most extensively studied in the visual system of several mammals, including cats and rats, but has also been found in the developing auditory system and in the rodent somatosensory cortex (Allene and Cossart, 2010; Clause et al., 2014; Torborg and Feller, 2005). Most spontaneous activity reported in these systems is associated with spontaneous activity in the pertinent sensory organ, e.g. the retinal waves (Ackman et al., 2012; Feller et al., 1996; Meister et al., 1991; Wong et al., 1993), auditory hair cell activation (Tritsch and Bergles, 2010; Wang and Bergles,

2015), whisker twitch (Tiriac et al., 2012). In the mouse barrel cortex, *in vivo* Ca^{2+} imaging in the neonatal pups has revealed “patchwork” patterns of activity in correspondence to the barrel cortex map (Mizuno et al., 2018). This activity was evoked from the periphery and was relayed to the cortex via thalamocortical axons. Spontaneous activity, therefore, appears to be a common and robust feature of developing sensory systems.

Early postnatally, neurons are maturing and forming connections between each other, and spontaneous activity is thought to help shape the emerging neural circuits, before the organism has had a chance to experience the surrounding world via the senses, e.g. before eye opening. (Ackman et al., 2012; Cang and Feldheim, 2013; Kandler et al., 2009; Kirkby et al., 2013). Spontaneous activity is thought to be a mechanism for priming the system for the advent of sensory experience; this way when, for example, the eyes open, a neural system is already in place and the incoming information can immediately undergo processing to, at least, some extent.

During early postnatal ages, developing synaptic connections are extremely plastic and very amenable to perturbations. These phases are termed critical periods (Erzurumlu and Killackey, 1982). As distinct neuronal components within a circuit develop at different times, they also have specific critical periods related to their synaptogenesis and synapse maturation timeframe.

At the onset of sensory perception and processing, experience-dependent plasticity is thought to instruct the addition or removal of synapses that contribute to the refinement of immature overly interconnected neural circuits (Holtmaat and Svoboda, 2009; Lichtman and Colman, 2000). The uncovering of this phenomenon is mainly due to studies involving sensory manipulation, especially in the visual system and the barrel cortex. Changes in sensory perception achieved via perturbing light exposure, retinal lesions, whisker trimming, for example, has been shown to cause changes in spine morphology and dynamics (Fagiolini and Hensch, 2000; Hofer et al., 2009; Holtmaat et al., 2006; Keck et al., 2008; Lendvai et al., 2000; Trachtenberg et al., 2002; Tropea et al., 2010; Zuo et al., 2005).

Therefore, while a template of neuronal circuits is genetically specified and largely established during embryonic and perinatal stages of development, the refinement of this immature network of cells relies on activity-dependent mechanisms that occur during the first few weeks after birth.

1.5 Morphological and functional changes during synaptic formation and maturation

1.5.1 Synaptic maturation

The formation and maturation of glutamatergic synapses are accompanied by many morphological and functional changes.

During early development, thin dendritic protrusions called filopodia are predominant (Fig. 1.4). As the brain matures, however, the proportion of these dynamic structures gradually declines (Zuo et al., 2005). The daily turn over of filopodia is in contrast to the stable nature of dendritic spines (Grutzendler et al., 2002; Zuo et al., 2005). In mice, substantial synaptic pruning occurs between 1-4 months, as around 30% of spines are lost and not replaced (Grutzendler et al., 2002; Zuo et al., 2005). Generally, the dynamics of dendritic spines greatly declines with age; however, this is not to say that the adult brain is uncapable of changing and adapting. On the contrary, an ever-growing plethora of data shows that plastic mechanisms in the brain are retained throughout life (Bavelier et al., 2010; Chen et al., 2010; Holtmaat and Svoboda, 2009; Zito and Svoboda, 2002).

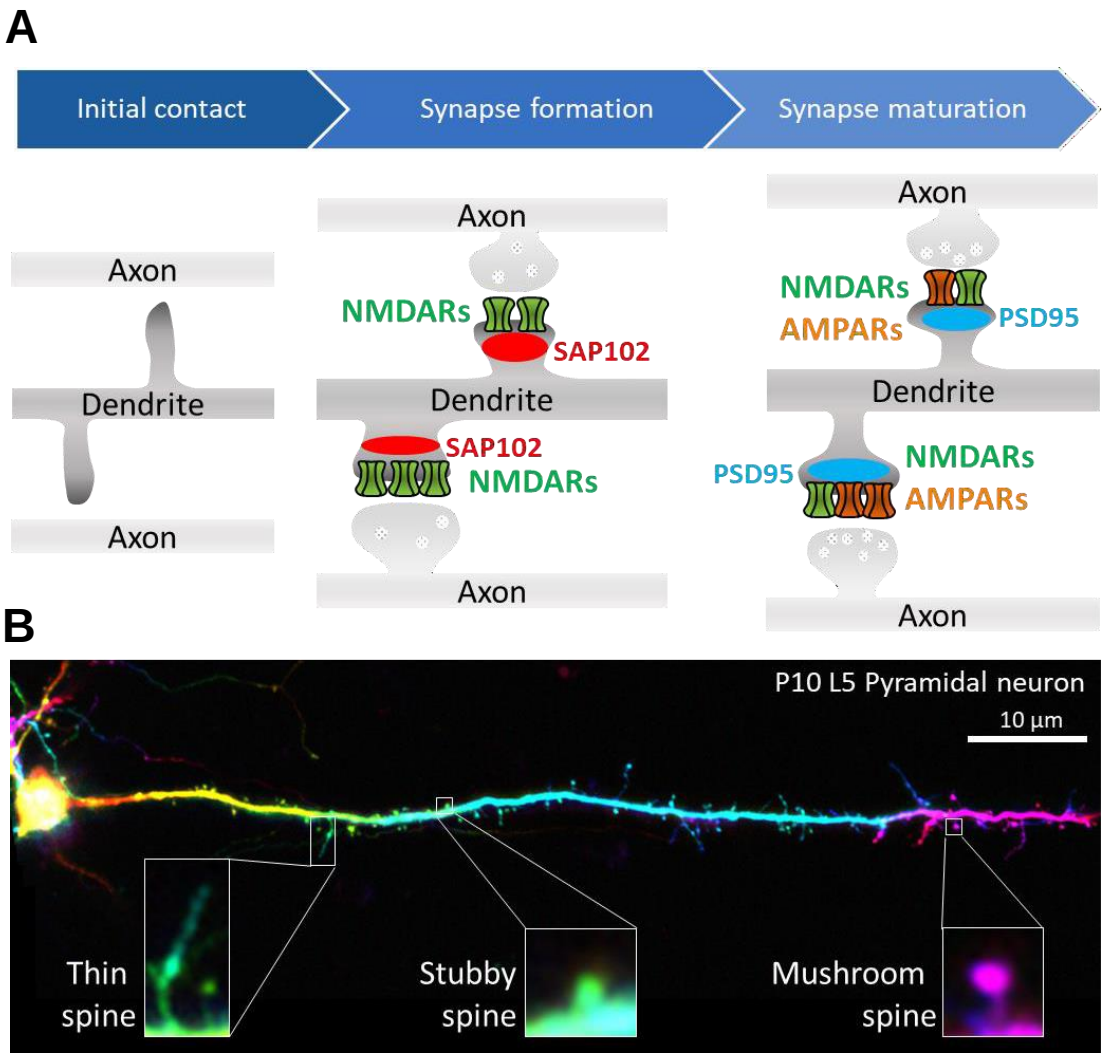

Figure 1. 4 Morphological changes during synapse formation and maturation

A. Diagram showing developing synapses at different maturational stages. During synapse maturation, the shape of the dendritic spine transitions from being filopodia-like to being mushroom-shaped. NMDAR-containing silent synapses become unsilenced via the insertion of AMPARs. The diagram also shows a switch in the major scaffolding protein at the synapse, changing from SAP102 to PSD95.

B. Maximum projected 2-photon image of the apical dendrite of a L5 pyramidal neuron from a P10 mouse. The neuron was patched and filled with Alexa 594. As this neurons is developing the three main spine morphologies can be observed, from a thin, filopodial like spine, to a stubby spine to a mushroom-shaped spine. Image is false-coloured reflecting the depth within the slice.

1.5.2 Protein repertoire of synaptic compartments

A remarkably large number of proteins are incorporated into the presynaptic terminal and PSD (Fig. 1.5, Collins et al., 2006). The presynaptic terminal contains many proteins involved with ensuring the correct localization and fusion of synaptic vesicles (Sudhof, 2004). Synaptic vesicles are tethered to the active zone and to the actin cytoskeleton by several scaffolding proteins (Phillips et al., 2001).

Proteins in the excitatory postsynaptic compartment, such as glutamate receptors and other ion channels, are linked to a large number of scaffolding proteins to form a dense molecular network. This interaction is crucial for ensuring correct trafficking of receptors, synaptic transmission and plasticity (Kennedy, 2000; Kim and Sheng, 2004; Montgomery et al., 2004). Organization in the PSD is orchestrated by an extremely conserved group of scaffolding proteins, the membrane-associated guanylate kinase proteins (MAGUKs).

Additionally, transsynaptic adhesion proteins bind to each other across the synaptic cleft, to regulate synapse formation and synaptic plasticity (Craig et al., 2006; Garner et al., 2006; Scheiffele, 2003; Waites et al., 2005).

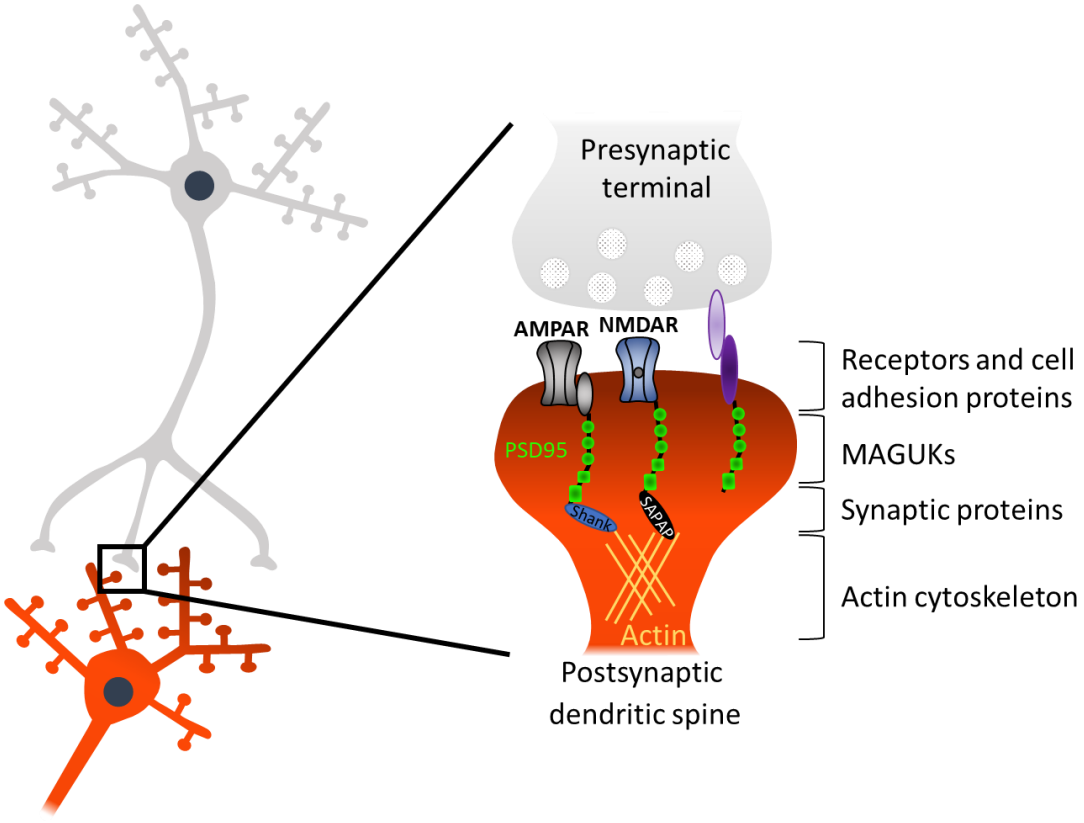

Figure 1. 5 Pre- and post-synaptic compartment
Diagram of a presynaptic neuron (grey) and a postsynaptic neuron (orange). Zoomed in area shows a synapse with its basic components: presynaptic vesicles, postsynaptic glutamate receptors and scaffolding proteins linking to the actin cytoskeleton.

1.5.3 Silent synapses

During perinatal development glutamatergic chemical synapses are mostly “silent” (Khazipov and Luhmann, 2006; Lohmann and Kessels, 2014). These synapses are called silent because they contain mainly NMDARs, which require depolarisation-induced release of a Mg^+ block additionally to glutamate binding for their activation, and are therefore inactive at normal neuronal resting potentials (Nowak et al., 1984). The presence of silent synapses decreases with increase in developmental age (Isaac et al., 1997; Rumpel et al., 2004, 1998). As experimental induction of LTP drives the insertion of AMPARs, thereby causing the unsilencing of synapses, this is thought to be an important step for the correct establishing of mature neural circuits (Kerchner and Nicoll, 2008).

Indeed, during the first 2 postnatal weeks in mice and rats, the number of gap junctions and silent synapses decrease (Valiullina et al., 2016; Vitali and Jabaudon, 2014), whereas an increase in chemical synapses occurs from the 2nd postnatal week (De Felipe et al., 1997).

In layer 4 neurons of barrel cortex, silent synapses are present in the early stages of postnatal development (P2-5) but disappear by P8-9 (Isaac et al., 1997). The disappearance of silent synapses has been reported to be activity dependent both in the barrel cortex and the visual system (Ashby and Isaac, 2011; Funahashi et al., 2013; Han et al., 2017).

As unsilencing of synapses can be triggered by activity, and experiments involving visual deprivation or whisker trimming during critical periods causes an extension of the existence of silent synapse in the visual and barrel cortex, respectively (Ashby and Isaac, 2011; Funahashi et al., 2013; Han et al., 2017), it is speculated that a combination of extrinsic and intrinsic factors contribute to the developmentally regulated insertion of AMPARs (Kanold et al., 2019).

Furthermore, during this first postnatal week, a switch from depolarising to hyperpolarising action of GABA occurs, mediated by changes in expression of Cl^- transporters NKCC1 and KCC2 (Kilb, 2012).

1.5.4 Subunit switches in glutamate receptors

NMDARs are heteromeric tetramers containing an essential NR1 subunit (which binds to glycine or D-serine), and one or more glutamate-binding NR2 (subunit A-D) and/or glycine-binding NR3 (Dingledine et al., 1999; Wenthold et al., 2003). These glutamate receptors and scaffolding proteins can be found in dendrites before synapses form (Barrow et al., 2009; Craig et al., 2006; Washbourne et al., 2004, 2002).

The expression of NMDAR subunits is developmentally-regulated and region-specific. *In situ* hybridization studies on the whole mouse brain have shown that the obligatory NR1 subunit is expressed embryonically and its levels gradually increase during postnatal development (Watanabe et al., 1992). On the other hand, NR2A is mainly detected postnatally and its expression levels undergo a striking increase between P7 and P21. NR2B is expressed embryonically in the cortical plate and its levels are observed to peak around birth and then decline slightly. NR2C is expressed postnatally in the cerebellum and the olfactory bulb and in L4 barrel cortex spiny stellate cells (Binshtok et al., 2006). Finally, NR4 is expressed in the diencephalon and brainstem during embryonic development. Its levels peak around P7 and then decline sharply.

In cultured neurons, NR2B is expressed from 2 days *in vitro* (DIV) until 15 DIV, then its expression abruptly declines (Bustos et al., 2014). On the other hand, NR2A cannot be detected at 2 DIV, then its expression increases, peaking in mature hippocampal neurons. Either reducing the expression of NR2B or increasing the expression of NR2A and PSD95 leads to an enhancement of dendritogenesis in immature neurons. This effect is dependent on the level of maturity of the neuronal cultures, as both manipulations are required to reach the same effect in mature neurons. Knock-down of PSD95 has a direct effect on synaptic clustering of NR2B, which suggests that the increasing levels of this MAGUK during development lead to the halting of NR2B clustering, thereby preventing further dendritic branching (Bustos et al., 2014).

Additionally, acute manipulations in *in vivo* and *in vitro* preparations have shown that NR2B regulates dendritogenesis (Espinosa et al., 2009; Sepulveda et al., 2010).

Destabilization of NR2A subunit at synapse leads to an increase in NR2B to compensate the lack of this subunit; this suggests that distinct, independent, mechanisms are employed to anchor at PSD (Bard et al., 2010).

However, a recent study examining the molar ratio of NR2A to NR2B expression found that there is a region-specific difference in expression of these two subunits. Consistently with previous literature, in the cerebellum of adult mice the NR2A subunit

was most prevalent in the adult mouse. Surprisingly, NR2B subunit was 6- and 3- fold more abundant than NR2A in the cortex and hippocampus, respectively (Frank et al., 2016). By the end of the 4th postnatal week, the extensive period of synaptogenesis and dendritic remodelling reached a more stable balance (De Felipe et al., 1997). The reported developmental NMDA subunit switch occur concomitantly with a switch in members of the MAGUK family of proteins – from early developmentally expressed SAP102 to the later-expressed marker for mature synapses PSD95. Additionally, several PSD95 direct and indirect interactors (such as GKAP and Shank) have also been reported to be developmentally regulated (Kawashima et al., 1997; Kelly and Vernon, 1985; Lim et al., 1999).

These changes in protein content and morphological features of the pre- and postsynapses, have a great effect on the functional properties of these developing synapses (Fig. 1.6). Changes in the morphology of the postsynaptic dendritic spine is likely to have important implication in calcium concentrations and the compartmentalization of biochemical gradients. Furthermore, the developmental NMDAR subunit change NR2B➐NR2A increases the kinetics of channel opening of this receptor (Monyer et al., 1994). These two NMDAR subunits have been linked to the induction of plasticity, such as LTP and LTD (Bartlett et al., 2007; Massey et al., 2004). Because of this closely interlinked relationship between structure and function, the study of changes in the prominent MAGUK proteins can help further uncovering mechanisms underlying synaptogenesis, such as receptor trafficking and synapse maturation.

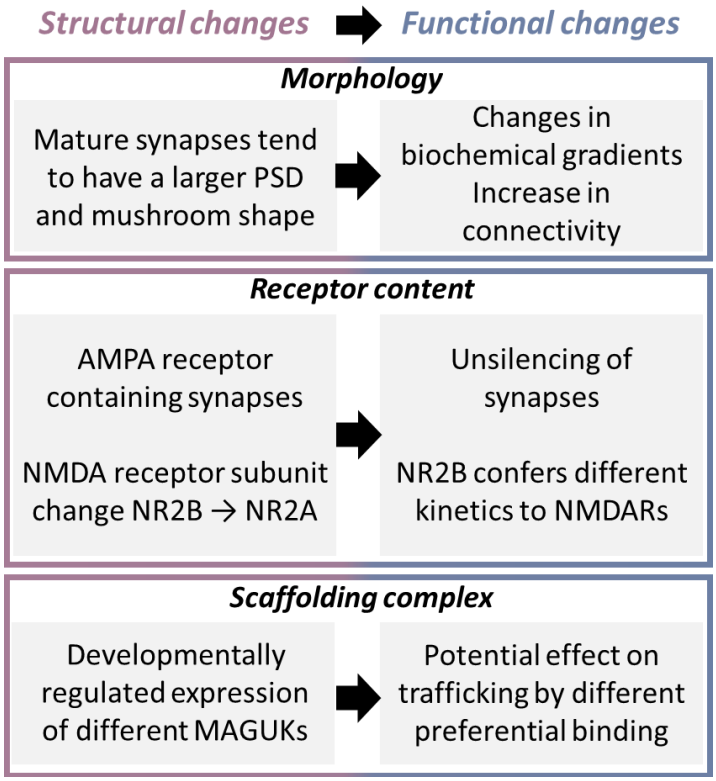

Figure 1. 6 Structural and functional changes during synapse formation and maturation
Structure and function are closely linked. This diagram shows a few developmental structural changes and how they affect the functional features of neurons and circuitry.

1.6 MAGUKs

The MAGUK proteins are a highly conserved superfamily of scaffolding proteins. They have been shown to be involved in a wide variety of cellular processes such as cell proliferation and differentiation and neuronal function.

1.6.1 DLG subfamily of scaffolding proteins

The DLG subfamily members of MAGUK proteins include synapse-associated protein 97 (SAP97), synapse-associated protein 102 (SAP102), postsynaptic density protein 93 (PSD93) and postsynaptic density protein 95 (PSD95). These proteins bind to glutamate receptors (either directly or indirectly) and adhesion proteins and participate in their trafficking, clustering and retention at the postsynapse (Fig. 1.7). All the DLG family members are characterized by the inclusion of 3 PDZ domains and a SH3-GK tandem domain. MAGUKs form protein networks at neuronal synapses and provide a functional link to the actin cytoskeleton, which can be modulated by them (Murata and Constantine-Paton, 2013). On top of providing a structural role and being essential for receptor synaptic targeting, they can also regulate changes in synaptic function. Aberrant expression of many components of the postsynaptic density have been linked to psychiatric disorders, including neurodevelopmental disorders, such as autism spectrum disorder and schizophrenia. For example, post-mortem studies of patients have uncovered decreased expression of PSD95 and SAP102 which underlie synaptic disfunctions observed in these conditions (de Bartolomeis et al., 2014; Tarpey et al., 2004; for reviews see Gardoni et al., 2009; Kaizuka and Takumi, 2018). This highlights the importance of these family of proteins for the correct development and functioning of neural circuits.

This study focuses on the expression of two MAGUKs: SAP102 and PSD95. Despite their similar molecular composition, SAP102 and PSD95 exhibit distinct expression pattern, preferential binding partners and functional roles. These differences are thought to at least partially be due to different protein regulation based on activity-dependent and developmentally-regulated splicing and posttranslational modifications that these proteins undergo.

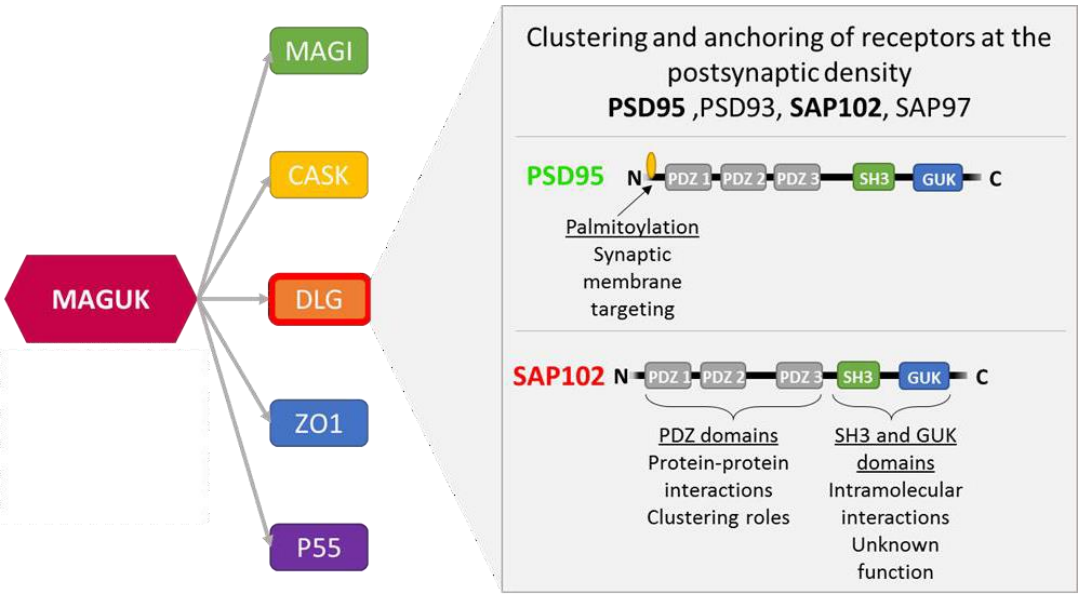

Figure 1. 7 The MAGUK family of scaffolding proteins
The MAGUK family of protein is comprised of 5 subfamilies. The DLG subfamily comprises of PSD95, PSD93, SAP102 and SAP97. All the members of this subfamily containg 3 PDZ domains, an SH3 and a GUK domain. Additionally, PSD95 has a palmitoylation site at its N-terminus.

1.6.2 Proteins and their regulatory sites

SAP102 is a cytoplasmic MAGUK that is enriched at the PSD, but has also been observed in dendritic shafts and axons, albeit more diffusely (El-Husseini et al., 2000; Müller et al., 1996; Sans et al., 2005; Zheng et al., 2010). Its expression levels are high both in young and mature neurons and it has been shown to have a major role during the synaptic trafficking and clustering of NMDARs during early brain development (Elias et al., 2008; Sans et al., 2003; Washbourne et al., 2002). This protein exists in 3 developmentally-regulated splice variants which regulate its synaptic targeting and receptor binding (Chen et al., 2011; Müller et al., 1996). SAP102 binds to the NR2B subunit of NMDARs, which is the dominant NMDAR subunit in immature synapses (Chen et al., 2011; Sans et al., 2000). This binding is specific to the SH3-GK hinge region of one of SAP102 splice variants, which has been shown to be upregulated during critical periods of filopodial development in the dendrite (Chen et al., 2011). This SH3/GK domain is also required for the synaptic localisation of SAP102 (Zheng et al., 2010).

On the other hand, PSD95 is one of the most abundant proteins at the post-synaptic density of mature glutamatergic synapses (Chen et al., 2011; Cheng et al., 2006; Kennedy, 1997; MacGillavry et al., 2013; Nair et al., 2013). In fact, it was estimated that an average synapse contains approximately 300 copies of this protein (Cheng et

al., 2006). While both SAP102 and PSD95 are enriched at the PSD, PSD95 appears more discretely densely packed within this structure (Zheng et al., 2010). This protein can directly bind NMDARs via its PDZ domain, and indirectly bind AMPARs via stargazing (Schnell et al., 2002). AMPARs are recruited to the PSD by interactions with the first two PDZ domains of PSD95 (Schnell et al., 2002).

Membrane targeting of both PSD95 and PSD93 has been shown to rely on the palmitoylation of cystine residues at the C-terminus of these proteins (Craven et al., 1999; Fukata et al., 2004; Jeyifous et al., 2016; Topinka and Bredt, 1998). This posttranslational modification is also essential for the retention of PSD95 and clustering of AMPARs at the PSD (El-Husseini et al., 2000). PSD95 requires palmitoylation to bind to receptors because this modification induces a conformational change from compact to elongated form, allowing the binding to occur (Jeyifous et al., 2016). While SAP102 preferentially binds to NR2B, PSD95 shows preferential binding to NR2A, specifically in mature brains (Sans et al., 2000). In baseline conditions, PSD95 undergoes continuous cycles of depalmitoylation and repalmitoylation, which ensure the maintenance of PSD95 clusters at the PSD (Fukata et al., 2013). This protein has a constitutive rate of turnover that can be bidirectionally modulated by synaptic activity (El-Husseini et al., 2000; Noritake et al., 2009).

The direct binding of the L27 domain of SAP97 to both NMDARs and AMPARs requires a similar conformational change (from compact to elongated version of the protein) and this is mediated by CASK binding. Interestingly, this conformational change dictates whether this protein binds to AMPAR (compact form) or NMDARs (extended, Jeyifous et al., 2016).

1.6.3 Assemblies at synaptic sites

A recent paper highlighted how synaptic proteins follow a rigid structurally hierarchical organisation, forming complexes, supercomplexes and nanoclusters (Frank and Grant, 2017; Frank et al., 2016). During the maturation of synapses, NMDARs can assemble in either small complexes, or can be incorporated in larger supercomplexes containing PSD95 and PSD93 and other proteins (Frank et al., 2016). Interestingly, these *in vivo* studies showed that both PSD95 and PSD93 are necessary for the formation of these supercomplexes, giving rise to the ‘tripartite rule’ (Frank et al., 2016); according to this rule, PSD95, PSD93 and NR2B subunit are all required for the assembly of supercomplexes. Furthermore, these MAGUK-containing supercomplexes were found to be upregulated in the mature forebrain (Frank et al., 2016). Whilst all PSD95 assembles into supercomplexes, only 3% of these supercomplexes contain NMDARs (Frank and Grant, 2017). As PSD95 can bind to

AMPARs, via adaptor proteins (Schnell et al., 2002), the proportion of the PSD95 supercomplexes that lack NMDARs likely contain AMPARs. In fact, colocalization between AMPAR nanodomains and PSD95 synaptic clusters was found prominent, albeit not systematic (Nair et al., 2013).

1.6.4 Developmental regulation

The expression of each MAGUK follows a distinct expression pattern during brain development. Western blots of whole brain, hippocampal and cortical lysates show that the expression of PSD95 steadily increases with development, starting from very low to being most highly expressed in the adult brain (Sans et al., 2000; Song et al., 1999). PSD93 and SAP97 follow a similar trajectory of expression (Cai et al., 2006; Sans et al., 2000). Whilst, PSD95 and PSD93 show different patterns of expression across the whole brain, but are both shown to increase in expression over time (E13-P21, Fukaya et al., 1999).On the other hand, the expression levels of SAP102 are considerably higher than those of the other MAGUKs at birth, and they increase during early postnatal ages (Müller et al., 1996). There is some controversy as to whether the expression of this protein plateaus in the adult brain or whether it significantly, but slightly, declines (Müller et al., 1996; Sans et al., 2000). It was reported, however, that the adult rat cortex and cerebellum is considerably less abundant in SAP102 than PSD95 (Al-Hallaq et al., 2001).

1.6.5 Experimental manipulation

The MAGUK subfamily proteins exhibit considerable functional overlap. This makes it difficult to experimentally disentangle individual contribution of the different member proteins as they tend to compensate for each other following a perturbation.

For example, following a PSD93/95 knock-out, SAP102 was found to be upregulated. Nevertheless, chronic and acute manipulations of these proteins have uncovered their different roles during the recruitment and retention of receptors at developing synapses. Further evidence for compensatory mechanisms is provided by studies showing that while removal of SAP102 has little or no effect on AMPAR concentration at the PSD under normal conditions (Schnell et al., 2002), in PSD95/PSD93 knock-out mice, the knock-down of SAP102 causes a significant reduction in the remaining AMPAR-mediated current (Elias et al., 2006).

The parameters affected by the acute knock-down of endogenous PSD95 was successfully rescued by overexpressing SAP102. The significant decrease in

AMPAR-mediated currents and frequency of mini EPSCs were brought to control levels following expression of SAP102 (Liu et al., 2018).

Knock-down studies have shown that both SAP102 and PSD95 are necessary for excitatory synapse formation and localization of glutamate receptors at the synapse (Chen et al., 2015; Murata and Constantine-Paton, 2013). SAP102 has been shown to promote spine lengthening (Chen et al., 2011), while PSD95 promotes spine maturation (El-Husseini et al., 2000).

Overexpression of PSD95 causes a selective increase in AMPAR-, but not NMDAR, mediated EPSCs and an increase in number and size of dendritic spines (Ehrlich et al., 2007; Ehrlich and Malinow, 2004; El-Husseini et al., 2000; Schnell et al., 2002; Stein et al., 2003). A premature NR2B to NR2A subunit switch was also observed (Elias et al., 2008). Knocking down this protein, instead, causes the increase of silent synapses (Béïque et al., 2006) and a reduction in AMPA-mediated transmission, with little effect on NMDARs (Béïque et al., 2006; Chen et al., 2011). Furthermore, an increase in the NR2B subunit contribution to NMDAR-mediated current has been detected following a reduction in PSD95 expression (Béïque et al., 2006; Elias et al., 2008). This protein is involved in behavioral outcomes, as impaired spatial learning has been reported in mice lacking this protein (Gandhi et al., 2014).

SAP102 overexpression promotes synapse formation, but the effects of a manipulation of SAP102 expression mainly manifest themselves when perturbations are delivered during the critical period of development (Chen et al., 2011; Elias et al., 2008). Reduction in expression of this protein early during development leads to a significant reduction in both NMDAR- and AMPAR-mediated currents (Elias et al., 2008). While overexpressing SAP102 led to an only slight increase in AMPARs, knock-down had no effect on these glutamate receptors (Schnell et al., 2002).

Since each protein contributes to synaptic transmission by receptor binding, unsurprisingly, simultaneous acute knock-down of PSD95, PSD93 and SAP102 in rat hippocampal cultures caused a 80% decrease of total synaptic transmission, an increase in silent synapses and a decrease of PSD size (Chen et al., 2015).

Within the ultrastructure of the PSD, PSD95 is mostly uniformly distributed, whereas glutamate receptors appear clustered. NMDARs are preferentially located at center of the PSD, while AMPARs are mostly situated at the periphery (Chen et al., 2011). Electron microscopy (EM) tomography following PSD95 knock-down also revealed a patchy loss of filaments perpendicular to the PSD, preferentially occurring at the periphery of the PSD, rather than the center (Chen et al., 2011). AMPARs-type

structures were identified and estimated to decrease by approximately 30%, while putative NMDARs were largely unaffected (Chen et al., 2011). This is likely due to the fact that NMDARs are more strongly tethered to the PSD, while AMPARs are loosely attached thus favoring their movement into and out of the synapse (Malinow et al., 2000; Nicoll and Malenka, 1999). Indeed, at the PSD PSD95 is thought to provide dynamic slots that AMPARs can bind to as they diffuse into and out of the postsynaptic compartment (Bats et al., 2007; Opazo et al., 2012; Schnell et al., 2002). An additional factor that may be contributing to the AMPAR-dominated effect is that the stoichiometry is different; while there is a 1:1 ratio between PSD95 and AMPAR, there is a 2:1 ratio between PSD95 and NMDARs, which would render the PSD95-NMDAR interaction less susceptible to perturbations. Finally, PSD95 binds directly to NMDARs, but requires an adaptor protein to bind to AMPARs, so the strength of the binding might differ.

1.6.6 Synaptic trafficking of receptors and MAGUK dynamics

NMDARs and PSD95 are thought to be recruited to the synapse independently of each other (Barrow et al., 2009; Bresler et al., 2001; Friedman et al., 2000; Washbourne et al., 2004, 2002). Discrete transports packets containing NMDARs have been shown to move bidirectionally along the dendrite (Washbourne et al., 2004, 2002). SAP102, but not PSD95, has been shown to colocalise with NMDAR mobile packets that are being transported to the nascent synapse (Barrow et al., 2009; Sans et al., 2000; Washbourne et al., 2004). However, a proportion of these mobile packets also contained AMPARs (Washbourne et al., 2002). NMDAR transport packets have been shown to cycle with the plasma membrane during their journey, this may be a way to sense glutamate to direct their transport (Washbourne et al., 2004). However, contrasting evidence has provided evidence that NMDAR exist in a diffuse cytoplasmic pool and get recruited to the synapse, rather than being transported in packets (Bresler et al., 2001).

In contrast to the relatively fast transport of SAP102-NMDARs, PSD95 is recruited on a slower timescale, independently from other MAGUKs and in a palmitoylation-dependent manner (Barrow et al., 2009). Some studies have provided evidence of immobile clusters of PSD95 prior to synapse formation (Bresler et al., 2001; Friedman et al., 2000; Marrs et al., 2001; Okabe et al., 2001, 1999; Rao et al., 1998; Sans et al., 2000; Washbourne et al., 2002), whilst other reports described modular transport of PSD95 or even pre-assembled complexes comprising of PSD95, GKAP and Shank (Gerrow et al., 2006; Prange and Murphy, 2001) .

A study on the accumulation of MAGUKs at nascent hippocampal synapses revealed that these proteins are asynchronously enriched at the PSD (Lambert et al., 2017). SAP102 was the first MAGUK to reach mature levels at the synapse, followed by SAP97 and PSD93. PSD95 was the last MAGUK to reach mature levels (compared to neighboring spines). Longitudinal *in vivo* studies in the adult brain also showed while PSD95 does not immediately accumulate at new synapses, the presence of a PSD containing PSD95 increased the probability of that newly formed spine to survive (Cane et al., 2014; Gray et al., 2006). SAP102 exhibits a greater mobility than PSD95 in spines, and these kinetics are related to actin dynamics (Zheng et al., 2010).

In adult brains, PSD95 within spines has an estimated turnover of 10 hours; its mobility under basal conditions is relatively low, but the kinetics can be upregulated following increase in synaptic activity (Fortin et al., 2014; Noritake et al., 2009; Steiner et al., 2008; Yoshii and Constantine-Paton, 2007). However, studies conducted in L2/3 of the developing barrel cortex (P10-21) show that this protein is much more mobile in younger neurons, displaying an average turnover of 22-63 mins. The stability of PSD95 at the PSD increased with age and was found to be experience-dependent (Gray et al., 2006).

A picture emerges from this evidence where SAP102 assumes a particularly crucial trafficking role during early development, when it binds to NR2B-containing NMDARs, while PSD95 reaches the PSD at a later timepoints and it can induce synaptic maturation and regulates synaptic strength. This study aims to characterize changes in expression of SAP102 and PSD95 in cortical layers, in order to relate these changes to pre-existing literature on barrel cortex development and expand our knowledge on the sequence of events leading to the establishment of a functional barrel cortex. Furthermore, the results from this study can be extrapolated and generalized to other developing areas of the brain.

1.7 The barrel cortex

The rodent barrel cortex is a well-suited model to study the formation and refinement of neural circuits. This area of the somatosensory cortex is responsible for processing information from the animal's whiskers, via several cortical relays (Fig. 1.8, Woolsey and Van der Loos, 1970). Since mice and rats are nocturnal animals, active whisking is an extremely important sensory modality of perception. Whiskers are used by rodents to build an internal representation of the surrounding environment by locating objects and discriminating between textures around them. As active whisking movement commences around the second postnatal week (Landers et al., 2006; Welker et al., 1988), in younger animals, processing of passive information transmitted via sensory receptors in the whisker pad are thought guide their huddling and suckling behavior, crucial for their survival (Arakawa and Erzurumlu, 2015). Indeed, applying pressure or moving the whiskers has been shown to evoke activity in the somatosensory cortex from as early as P2 (Akhmetshina et al., 2016; Arakawa and Erzurumlu, 2015; Sullivan et al., 2003).

The name of the highly specialized area of the somatosensory cortex derives from the barrel-like shape formed by clusters of neurons in cortical L4, which are the prime recipient of subcortical inputs from the thalamus (Wimmer et al., 2010). This system is an extremely well characterized synaptic pathway in literature; its components follow a stereotypical topographic pattern from the whisker pad to the somatosensory cortex, relaying in several subcortical regions. From the trigeminal ganglion, bipolar neurons project to the whiskers and to the brainstem, which in turn send its projections to the thalamus. Thalamocortical afferents innervate the cortical layers of the barrel cortex, mainly L4. The neurons within this pathway are highly organized in a somatotopic arrangement, whereby each whisker can be mapped to a single barrel in the cortex. Finally, another advantage of this model is that it allows interference with experience-dependent plasticity, both in an invasive (follicle lesions or transection of whisker related nerves) or non-invasive manner (daily whisker trimming from birth). Because of all these reasons, the barrel cortex constitutes a great model to study postnatal neurodevelopment.

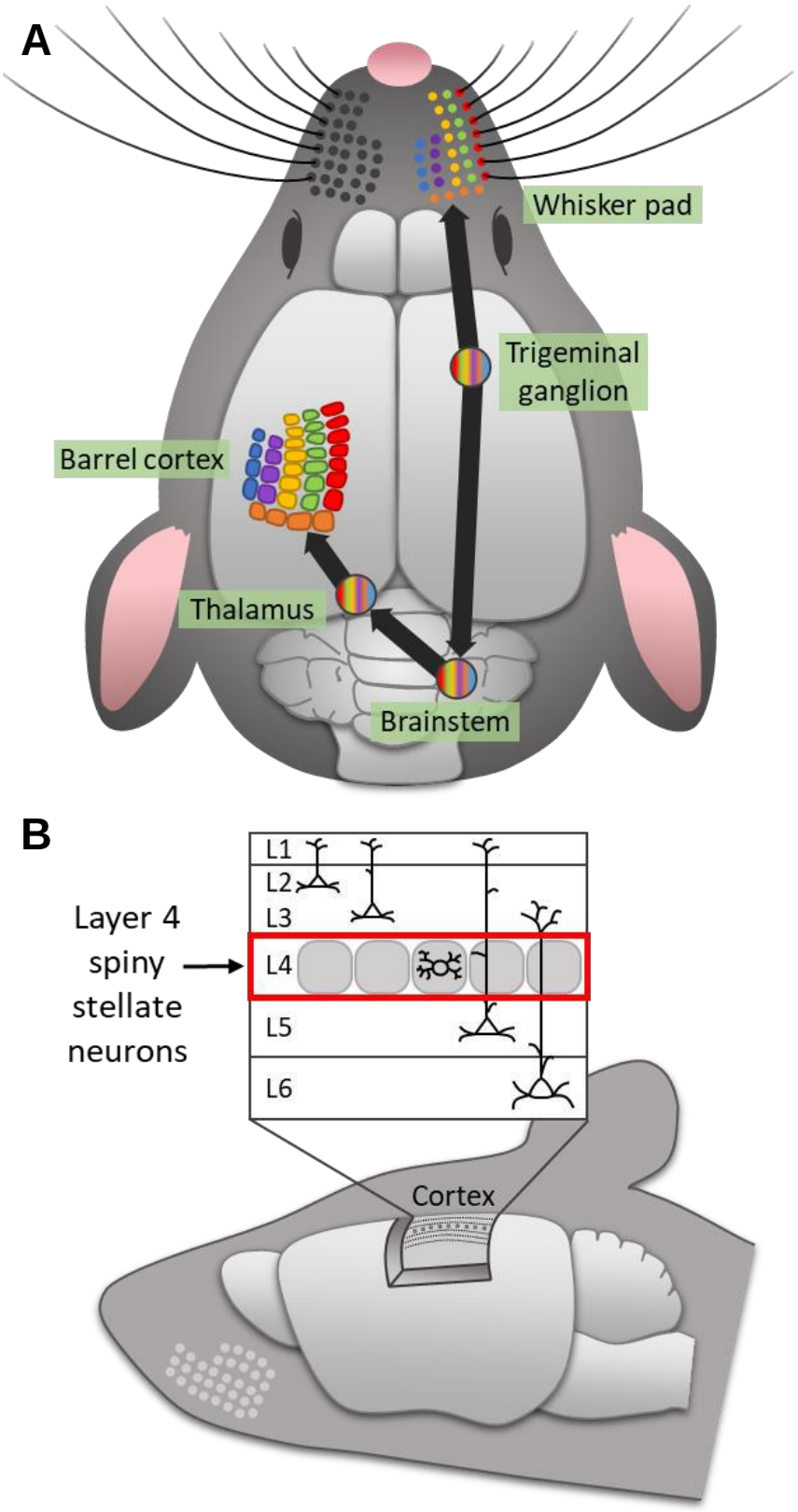

Figure 1. 8 The mouse barrel cortex

A. Whisker-related pathways. Whisker inputs get relayed in the trigeminal ganglion, then to the brainstem, then the thalamus and finally to the barrel cortex. The input from each whisker remains spatially segregated at every step.

B. In cortical L4, spiny stellate neurons form barrel-shaped clusters. These, barrels organise across the cortical plane in a map that resembles the map of whiskers in the whisker pad.

1.7.1 Neuronal types populating L4 barrel cortex

The most prominent cell type in L4 barrels is the spiny stellate neuron. These glutamatergic neurons constitute around 80% of all barrel cells (Lefort et al., 2009; Simons and Woolsey, 1984; White and DeAmicis, 1977). They have circular cell bodies of approximately 10 µm in diameter and large nuclei (Simons and Woolsey, 1984; White and DeAmicis, 1977). Spiny stellate neurons receive strong innervation from the ventro-posterior medial (VPM) thalamic nucleus and then project their axons to L2/3, after considerable ramification within their L4 barrel (Harris and Woolsey, 1983). A much more sparsely present glutamatergic cell type is the star pyramidal neuron (around 18%, Lefort et al., 2009). These neurons are characterised by the presence of an apical dendrite that extends into L3 (Simons and Woolsey, 1984; White and DeAmicis, 1977). The axonal morphology of these cells is similar to that of spiny stellate neurons (Lübke et al., 2000; Staiger et al., 2004). Even though spiny stellate neurons and star pyramidal neurons exhibit similar synaptic and intrinsic properties (Cowan and Stricker, 2004; Feldmeyer et al., 1999, Schubert et al., 2003), Schubert and colleagues showed that these two types of barrel neurons integrate in non-overlapping circuits, spiny stellate neurons participating in intra-barrel processing of inputs and star pyramidal neurons being integrated in a wider horizontal and top-down information flow (Schubert et al., 2003). Finally, about 20% of neurons in the L4 barrels are sparsely spiny or aspiny neurons, which are putatively inhibitory neurons (Simons and Woolsey, 1984; White and DeAmicis, 1977). Interneuron population of the L4 barrels is heterogeneous, with up to 3 types of neurons that have been described (Koelbl et al., 2015).

1.7.2 Parallel barrel cortex pathways

The barrel cortex pathway starts with neurons innervating hair follicles on the mouse snout (Fig. 1.8 and 1.9). The whisker pad is composed of 5 rows of mystacial vibrissa and an array of sinus hairs. Deflections of the whisker is thought to open mechanosensing ion channels on innervating trigeminal ganglion neurons, thus eliciting a response. The trigeminal ganglion projects to the brainstem, which then projects to the thalamus. The thalamus finally projects to the primary somatosensory cortex (S1). Throughout the whisker-related pathway, there is a remarkable somatotopic arrangement whereby individual whiskers map onto likewise discretely organized “barrellettes” in the brainstem, which, in turn, project to spatially separated “barrelloids” in the thalamus and finally “barrels” in the primary somatosensory area of the neocortex. There are three identified pathways that follow this sequence of

innervations but that specifically target distinct nuclei or layers within each part of the circuit: the lemniscal, paralemniscal and extralemniscal pathway.

These whisker-to-cortex parallel pathways have been suggested to mediate slightly different aspects of whisker-related sensory processing (Mo et al., 2017; Yu et al., 2006). The lemniscal pathway is the primary glutamatergic route in this system. After a relay in the principal trigeminal nucleus, neurons carrying whisker information via this route project to the dorsomedial portion of the VPM nucleus in the thalamus. Thalamocortical afferents then innervate the neocortical layers. The main target of these projection neurons are the center-projecting dendritic arbors of L4 neurons contained in L4 barrels. L2/3, 5 and 6A also receive VPM thalamic inputs, albeit to a considerable lesser extent. The lemniscal pathway is thought to drive information bearing and to convey a combination of sensorymotor signals (whisking and touch, (Mo et al., 2017; Yu et al., 2006). The paralemniscal pathway acts via the spinal trigeminal nucleus and the ventrolateral VPM in the thalamus. In the cortex the thalamic inputs from this pathway preferentially innervate L5A and L1 of S1 and also send projections to S2 and M1. Experimental stimulations of this pathway revealed that it exhibits predominantly modulatory functions and is involved in conveying whisking signals (Mo et al., 2017; Yu et al., 2006). The third, most recently discovered pathway, is the extralemniscal pathway (Pierret et al., 2000). Neurons in this pathway project to the caudal portion of the spinal trigeminal nucleus, which then form synapses with the ventrolateral posteromedial (POM) in the thalamus. Thalamocortical POM projections then reach the septal area between the L4 barrels and also send axons to S2. The axons within this pathway have been suggested to be involved in transmitting contact-related signals. Furthermore, all these circuits communicate between each other via S1-S2-M1 connections, giving rise to precisely integrated motor control and object identification and discrimination (Chakrabarti and Alloway, 2006; Welker et al., 1988; White and DeAmicis, 1977).

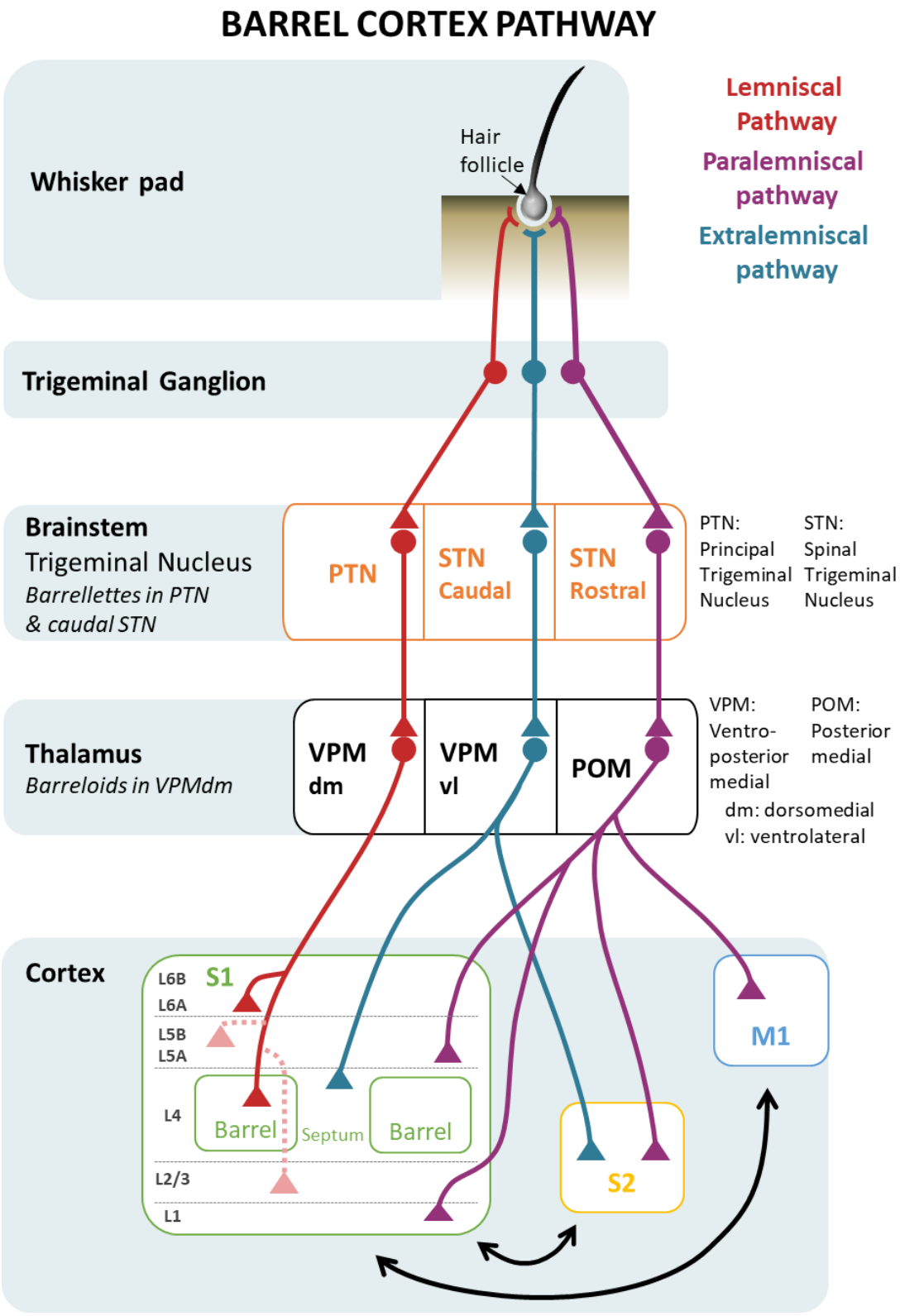

Figure 1. 9 Parallel pathways of the mouse barrel cortex
Whisker-related pathways segregate into three parallel routes, the lemniscal, paralemniscal and extralemniscal pathway. These pathways project to different nuclei within the brainstem and thalamus, and specifically target distinct cortical regions.

1.7.3 Cortical organization of microcircuits

The 6 cortical layers house several lamina-specific inhibitory and excitatory cell types, which render this structure extremely specialized. The whisker-related somatosensory cortex is characterized by the presence of barrel-shaped clusters of neurons in L4. Each cortical layer is specifically targeted by well described long-range projections from subcortical regions or other cortical regions, and in turn innervates well defined areas (Fig. 1.10).

In the adult brain, L1 is rich in apical dendritic arbors and axonal projections and, except for excitatory Cajal-Retzius cells, it mainly contains GABAergic interneurons. The rest of the layers (L2-6) contain both glutamatergic neurons and GABAergic interneurons.

L4 is the main recipient of thalamic inputs coming from the VPM (lemniscal pathway). The main cell type within this layer is the spiny stellate neuron (SSN). The dendritic arbors of these excitatory neurons are restricted to the barrel borders and they exhibit biased orientation towards the center of the barrel (Jeanmonod et al., 1981; Steffen and Van der Loos, 1980; Woolsey et al., 1975). Discrete bundles of VPM axons synapse onto these oriented dendrites; a single axon primarily innervates a single barrel (Arnold et al., 2001; Furuta et al., 2011; Jensen and Killackey, 1987) and this organization causes each barrel to respond predominantly to a single “primary” whisker (Armstrong-James and Fox, 1987; Chapin and Lin, 1984; Simons, 1985; Simons and Carvell, 1989; Simons and Woolsey, 1984).

VPM thalamic afferents make glutamatergic synapses mainly in L4, and to a much smaller extent to L3, 5 and 6 (Jensen and Killackey, 1987; Wimmer et al., 2010). The neurons contained within the L4 barrels make numerous connections to other SSNs within the same barrel and also send their axons to the layer just above, L2/3 (Feldmeyer et al., 2002). The L2/3 target neurons are mainly the cells located just above the barrel. This anatomical arrangement of ordered projections from thalamocortical afferents to L4 to L2/3 gives rise to cortical columns. These functional modules exhibit a structural basis, whereby the width of the column is determined by the width of each barrel and the signal travels towards the surface of the brain in a columnar fashion, for each barrel.

L2/3 cells project to the pyramidal cells in L5 (Reyes and Sakmann, 1999). L5 excitatory pyramidal neurons are considered the main output cells of the cortex. They can be split into two types, L5 intratelencephalic (IT) and L5 pyramidal tract (PT) neurons, based on distinct morphology and functional connectivity (Ahissar et al., 2001; Larsen and Callaway, 2006; Manns et al., 2004; Wise and Jones, 1976). L5 PT

are present only in L5B (the deeper portion of L5). These neurons exhibit very few local axons, while the main bulk of their output is projected to subcortical areas, such as the striatum, POM, pons, and brainstem (Bureau et al., 2006; Guo et al., 2017; Oberlaender et al., 2012). L5 IT, on the other hand, are present in both L5A and L5B and they strongly project to S1, as well as to other neocortical layers and the striatum (Kiritani et al., 2012; Oberlaender et al., 2012). The thalamic POM projects specifically to L5A IT neurons (Audette et al., 2018; Bureau et al., 2006; Wimmer et al., 2010). The neurons in this layer are also preferentially targeted by L2, 5A and 5B neurons (Lefort 2009; Bureau 2006; Schubert 2007). Therefore, L5A neurons receive direct innervation from POM neurons (Ahissar et al., 2001; Bureau et al., 2006; Chmielowska et al., 1989; Koralek et al., 1988) and indirectly from the VPM, via L4 (Feldmeyer et al., 2005; Schubert et al., 2003); so the lemniscal and paralemniscal pathway converge into L5A neurons which integrate the information and, in turn, projects to the caudate nucleus, secondary somatosensory cortex and motor cortex (Alloway et al., 2004; Chmielowska et al., 1989; Donoghue and Parham, 1983; Hoffer et al., 2003; Koralek et al., 1988). L5 neurons form glutamatergic connections with L6 neurons. L6 contains a heterogenous population of neurons, which includes corticothalamic neurons that project back to the VPM and POM nuclei in the thalamus. This long-range feedback pathway is thought to have a modulatory function (Varela, 2014).

This intracortical local connectivity of L4 ➔ L2/3 ➔ L5 ➔ L6 ➔ Thalamus constitutes the “canonical cortical circuit” (Fig. 1.11)

Functional studies involving imaging of voltage-sensitive dyes following stimulation of a single whisker show that at first the response can be observed in the corresponding L4 barrel (Laaris and Keller, 2002; Petersen and Sakmann, 2001), then the signal spreads across the width of the barrel column, engaging L2/3 cells (Ferezou et al., 2006; Harris et al., 1992; Peron et al., 2015) and finally extends to a large portion of the barrel field (Brecht et al., 2003; Estebanez et al., 2012; Zhu et al., 1999).The lateral spread is probably due to extensive horizontal connections between L2/3 that are performing large-scale computations and integration of whisker-related signals.

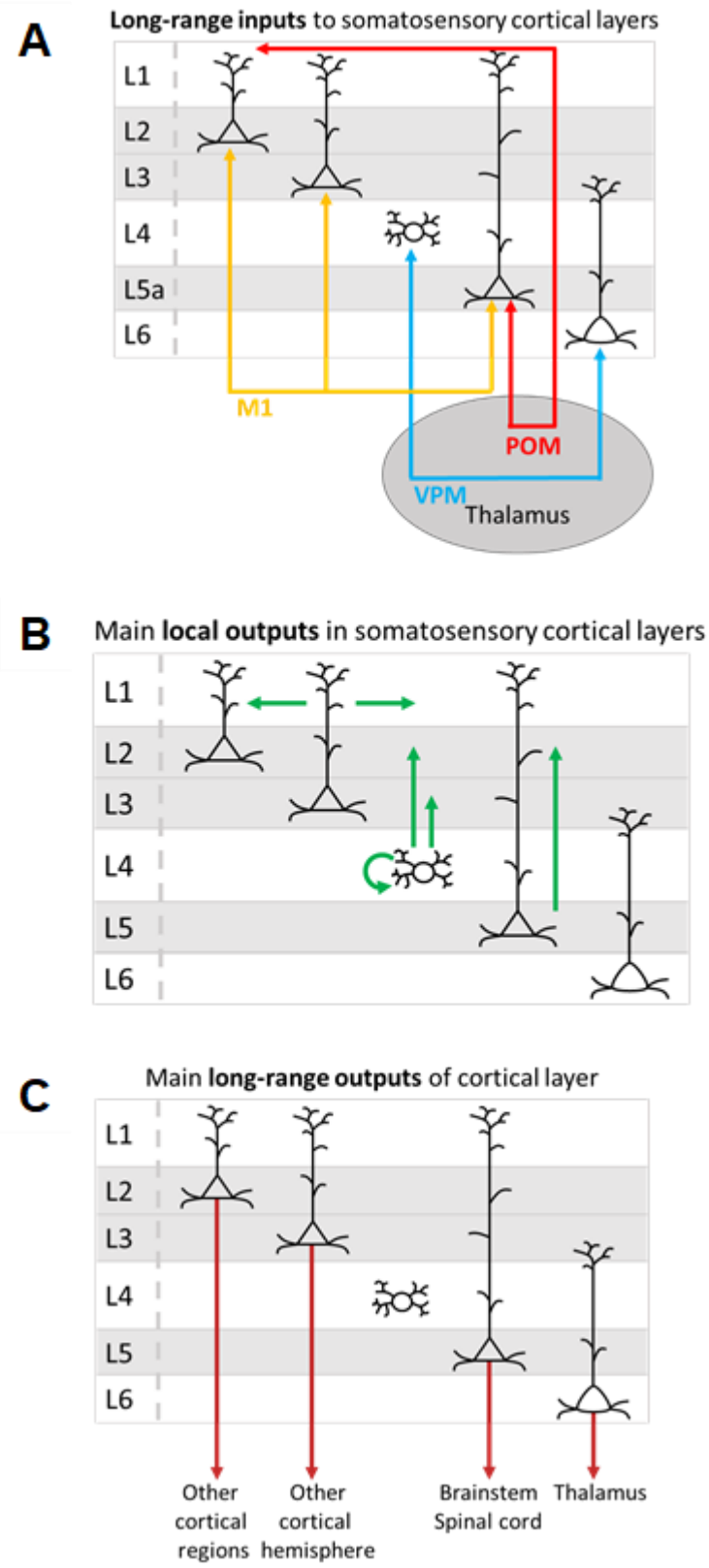

Figure 1. 10 Long-range inputs and outputs of distinct barrel cortical layers

Main long-range inputs into the cortical layers of the barrel cortex (A), main local outputs (B) and main long-range outputs (C). M1, motor cortex; VPM, ventroposterior medial nucleus; POM, posteromedial nucleus.

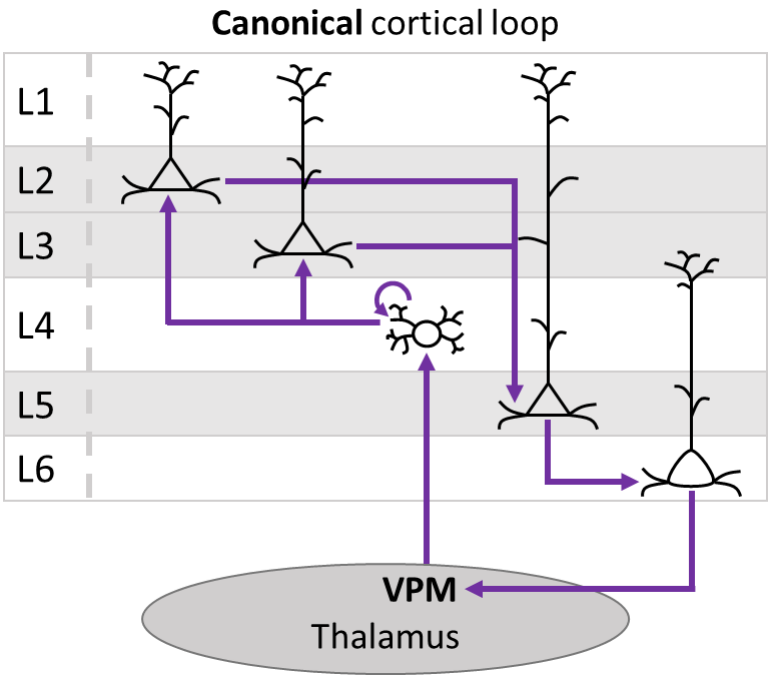

Figure 1. 11 The canonical cortical loop
In this canonical loop, thalamic VPM innervates L4 neurons, which in turn project to L2/3. L2/3 neurons then project to L5, which then projects to L6. L6 closes the loop by providing feedback to the VMP.

1.7.3 Development of barrel cortex circuits and critical periods for plasticity

The development of the barrel-related circuitry occurs in a sequential orderly manner, from the periphery to the subcortical regions of the brainstem and the thalamus and finally to the cortex (Sehara and Kawasaki, 2011, Fig. 1.12 and Fig. 1.13).

Perinatally, spontaneous whisker movement can be observed and tactile reflexes can be evoked from as early as P2-4 (Akhmetshina et al., 2016; Arakawa and Erzurumlu, 2015; Grant et al., 2012; Sullivan et al., 2003). Proper onset of active whisking emerges around P10 (Arakawa and Erzurumlu, 2015).

Specification of barrel field area is directed by the expression of intrinsic genetically instructed signals, e.g. fibroblast growth factor 8, whose gradient expression have been implicated with the correct positioning of this area (O'Leary et al., 2007; Shimogori et al., 2004; Sur and Rubenstein, 2005).

The patterning of the whisker circuits in brainstem occurs around birth, and it is shortly followed by patterning of the thalamic terminals around P3 (Agmon et al., 1993; Erzurumlu and Jhaveri, 1990; Rebsam et al., 2002; Senft and Woolsey, 1991).

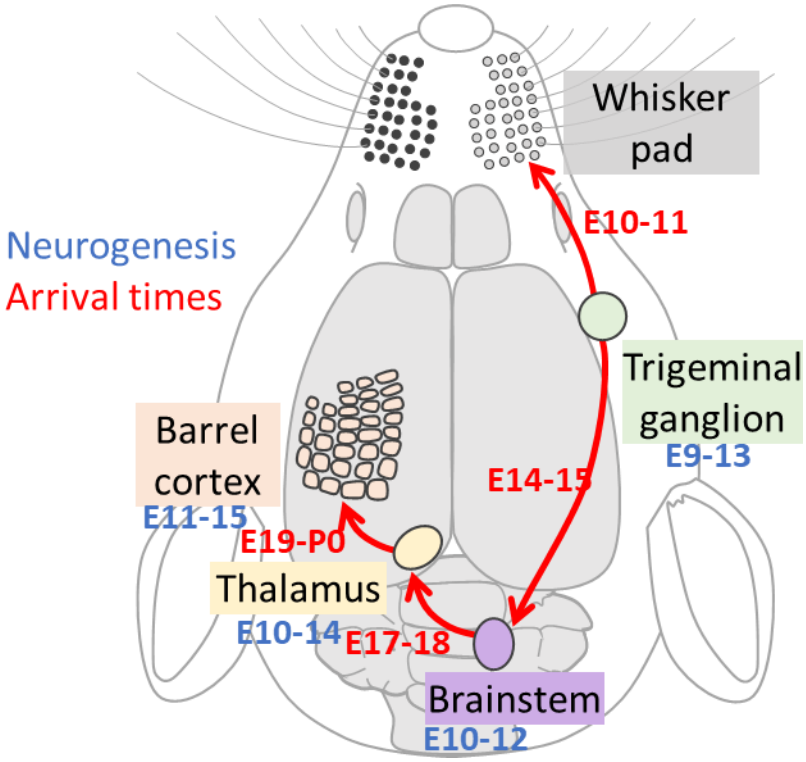

Figure 1. 12 Neurogenesis and innervation periods of whisker-related pathways
Diagram of the mouse head showing the whisker-related pathway and times relative to neurogenesis (blue) and arrival (red) of the components within the pathway.

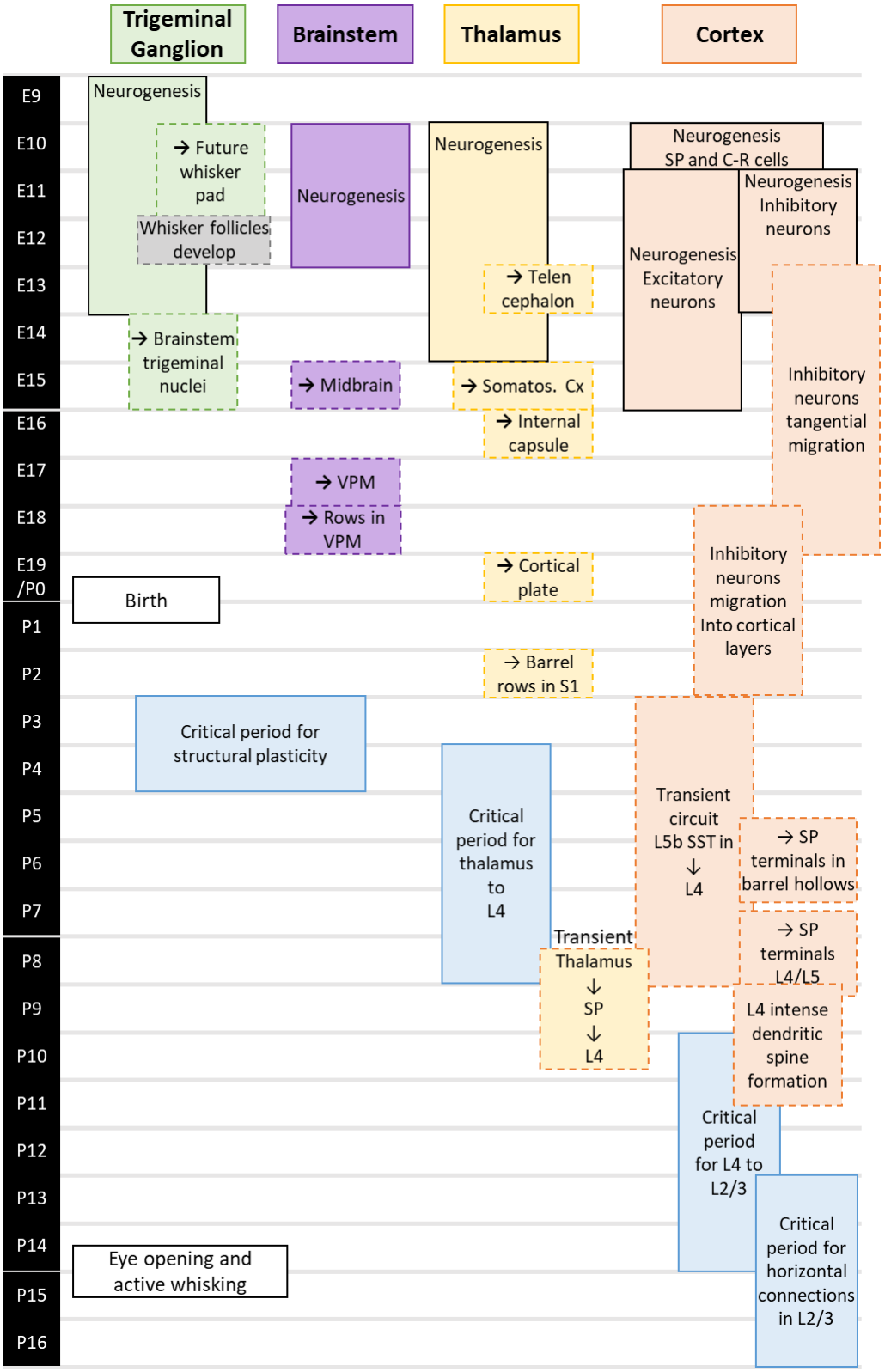

Figure 1. 13 Embryonic and postnatal development of the whisker-related network
Timeline of developmental time point for various aspects of development of the trigeminal ganglion (green), brainstem (purple), thalamus (yellow), cortex (orange). In white are behavioral events. In blue are the critical periods for synaptic connections. Dashed lines indicate dynamic events like migration or innervation, while solid contour designate neurogenesis events.

1.7.3.1 Neural activity and pattering of somatosensory maps

Similarly to the inside-out pattern of formation of cortical layers (Rakic, 1988; Takahashi et al., 1999), synapse formation and relative critical periods follow the same sequential developmental trajectory (Blue and Parnavelas, 1983; Zielinski and Hendrickson, 1992).

Around E18, thalamocortical afferents reach the subplate (SP), which is an early born cellular layer situated below the growing cortical plate. Subplate neurons are among the first cortical neurons to be generated during embryonic development (subplate will be discussed in depth in the next section). After a short waiting period in this layer, the thalamocortical axons invade the cortical plate shortly after birth (López-Bendito et al., 2006; López-Bendito and Molnár, 2003). Between P2-4, these afferents transition from being diffusely spread across the cortical plate to specifically target L4 in a periphery-related pattern (Higashi et al., 2005, 2002).

Around this perinatal stage, L4 neurons form sparsely distributed and immature synapses (Dufour et al., 2016). A steep increase in the synaptic maturation occurs from P4 onwards (Dufour et al., 2016), culminating in an extensive period of synaptogenesis between P9-11 (Ashby and Isaac, 2011).The maturation of these synapses are most likely driven by in increase and refinement in the thalamocortical inputs as well as intralaminar connectivity within this layer, which peaks around P14. This stage is followed by a substantial period of synaptic pruning (Ashby and Isaac, 2011; Tarusawa et al., 2016).

GABAergic interneurons present in L4 receive substantial thalamic innervation around P7 (Daw et al., 2007), followed by intense synaptogenesis between excitatory and inhibitory neurons between P7-11; this occurs coincidentally with the switch from depolarising to hyperpolarising effect of GABA (Chittajallu and Isaac, 2010; Daw et al., 2007).

The initial innervation of L4 spiny stellate neurons to pyramidal neurons in L2/3 is spatially spread wider than the barrel boundaries, but then acquires a columnar organisation by P11-14 (Bender et al., 2003). Functional studies have, however, revealed that this spatial organisation is present earlier on, around P8, suggesting synaptic connections between L4 and L2/3 are biased towards the area just above the barrel (Bureau et al., 2004). Additionally, *in vivo* studies reported the refinement of receptive fields of L2/3 by P10 (Bureau et al., 2004).

1.7.3.2 Critical periods of the barrel cortex

Critical periods are developmental stages during which the establishment of sensory maps takes place; this process requires peripheral sensory input. Perturbations, such as damage to sensory organs or sensory deprivations, during these periods have a significant effect on the normal development of the system being perturbed (Erzurumlu and Killackey, 1982). Several ways to induce sensory disruptions experimentally have been used to study this phenomenon. In the context of the barrel cortex, sensory deprivation studies have involved either the transection of the infraorbital nerve or lesion of hair follicles, or daily whisker trimming from birth has been used to greatly diminish sensory inputs in a non-invasive manner. These studies have been crucial to identify important critical periods during barrel cortex formation.

The critical period for barrel formation is up to P4, meaning lesions and other perturbations inflicted past this postnatal age do not disrupt the correct formation of this structure (Durham and Woolsey, 1984; Iwasato et al., 2000; Van der Loos and Woolsey, 1973; Wong-Riley and Welt, 1980).

Thalamocortical synapses have been shown to be insensitive to induction of LTP after the first postnatal week (Crair and Malenka, 1995), and LTD plasticity was found dramatically reduced shortly after (Feldman et al., 1998). This time period coincides with the developmentally regulated increase of AMPAR-mediated currents (Crair and Malenka, 1995).

The critical period for connections from L4 to L2/3 has been discovered to be between P10 and P14 (Lendvai et al., 2000; Maravall et al., 2004; Shoykhet et al., 2005), which then is followed by a longer critical period for L2/3 intralaminar synapses which terminates around P18 (Wen and Barth, 2011).

Therefore, after a period of intense synaptogenesis in the early postnatal days of mouse development, synaptic plasticity is seen to significantly decline following the $1^{st}/2^{nd}$ postnatal week, depending on the cell type (Barth and Malenka, 2001).

1.8 The subplate

The subplate is an enigmatic layer in the developing cortex that dynamically integrates in early intra- and extracortical functional circuits and plays a crucial role in the correct establishment of neocortical connectivity.

This area is anatomically defined as a 50 µm-thick layer situated below the cortical plate and above the white matter in the developing brain (Fig. 1.14, Hoerder-Suabedissen and Molnár, 2012). The SP contains glutamatergic and GABAergic neurons, as well as glial cells.

The subplate neurons (SPNs) are heterogeneous in terms of electrophysiological properties, connectivity, cell morphology and molecular markers (Antonini and Shatz, 1990; Hanganu et al., 2001; Hevner and Zecevic, 2006; Kostovic and Rakic, 1990; Watakabe et al., 2007).

The diverse morphology of SPNs includes pyramidal, multipolar and neurogliaform cells (De Carlos and O'Leary, 1992; Hanganu et al., 2002, 2001; Hoerder-Suabedissen and Molnár, 2012; Luhmann et al., 2000; Molnár et al., 1998a, 1998b; Rio et al., 1992; Robertson et al., 2000; Valverde et al., 1989).

Furthermore, during early postnatal stages, developing cortical neurons migrate through the SP to reach the cortical plate (Erzurumlu et al., 2006; Kanold and Luhmann, 2010).

In the rat, subplate cells have been shown to receive inputs mediated via AMPA, NMDA, $GABA_A$ and α/β heteromeric glycine receptors (Hanganu et al., 2001; Kilb et al., 2008). Glutamatergic inputs come from cortical as well as subcortical regions (Kanold and Luhmann, 2010) and the interneurons within this layer synapses with other SPNs thus forming extensive intrinsic GABAergic circuits, the function of which is uncertain (Hanganu et al., 2002).

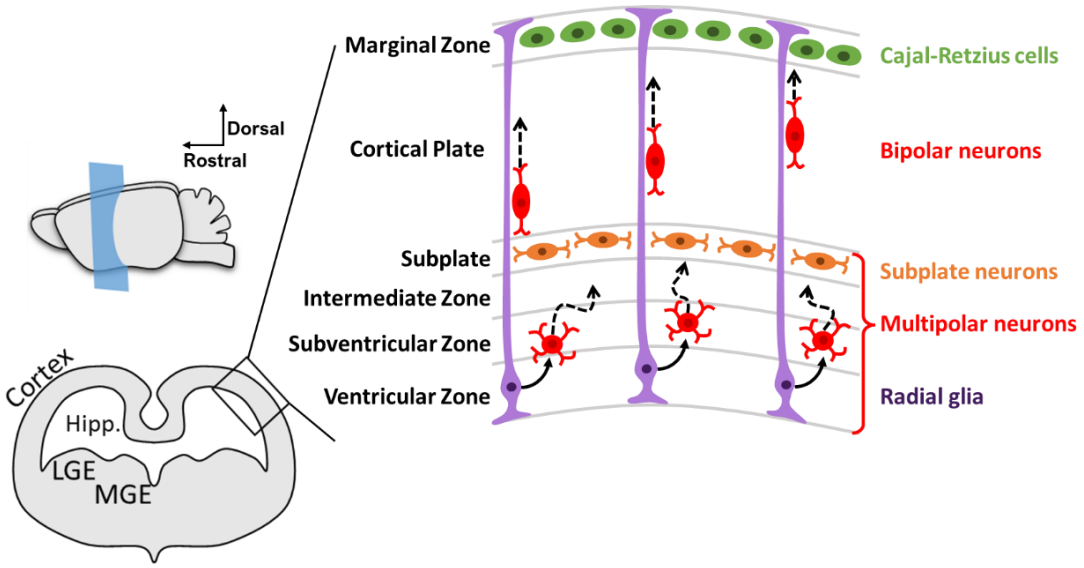

Figure 1. 14 The subplate layer during cortical development of glutamatergic neurons
Diagram of a developing brain and cortical layers during cortical neuronal migration. Neurons are generated in the ventricular zone by radial glial cells. These newly generated neurons are at first multipolar, then they switch to directed migration after interacting with the subplate. They then migrate along the process of the radial glia until they find the marginal zone. They stop their migration and join a cortical layer. LGE: lateral ganglionic eminence; MGE: medial ganglionic eminence.

1.8.1 Molecular markers

Molecular profiling uncovered the existence of several subpopulations of SPNs that express partially overlapping markers. For example the SPNs in the embryonic mouse express UNC5C and CDH10 (Oeschger et al., 2012) and Lpar1 (Hoerder-Suabedissen et al., 2013). In the postnatal brain, some identified SPN markers are CTGF, NURR1, CPLX3, Tmem193, MoxD1 (Hoerder-Suabedissen et al., 2009). The expression of CTGF, NURR1, CPLX3 partially overlaps (Hoerder-Suabedissen et al., 2013). Since CTGF, CPLX3, NURR1, and Lpar1 are not expressed in interneurons, it is thought that these markers are specific to glutamatergic SPNs (Boon et al., 2019; Hoerder-Suabedissen et al., 2013, 2009). Cplx3 and CTGF have been shown localised in the SP layer from early postnatal ages into adulthood (Hoerder-Suabedissen et al., 2013, 2009).

1.8.2 Age-specific connectivity and electrophysiological properties

SPNs are among the earliest neurons to be generated, around E11 (Angevine and Sidman, 1961; Bystron et al., 2008; Hoerder-Suabedissen et al., 2013; Price et al., 1997; Smart et al., 2002). Extending their neuronal projections around E13, they are

the first neurons to establish functional neuronal connections (De Carlos and O'Leary, 1992; Molnár et al., 1998a). Indeed, they have been shown to be the first cortical neuron to respond to auditory stimuli in neonatal ferrets, before L4 neurons become responsive (Wess et al., 2017). Conflicting experimental data exists regarding the fate of these early cell population in the adult brain. Some data suggests that SPNs are a largely transient population of neurons and that a great proportion of these cells die via apoptosis towards the end of the first postnatal week (Ferrer et al., 1990; Price et al., 1997; Rakic and Zecevic, 2000); on the other hand, different experiments show very minimal cell death (Valverde et al., 1995). Furthermore, numerous SP cells have been observed to persist until adulthood and SP molecular markers label a layer of cells in L6B in adult brains (Clancy et al., 2001; Friedlander and Torres-Reveron, 2009; Hoerder-Suabedissen et al., 2013, 2009; Jacobs et al., 2007; Reep, 2000; Valverde et al., 1989; Woo et al., 1991).

SPNs receive a variety of inputs, from the cortical plate as well as from the thalamus (Meng et al., 2014; Viswanathan et al., 2017). In turn, these early born neurons have been shown to project back to the cortical plate and the thalamus (Myakhar et al., 2011; Viswanathan et al., 2017). The thalamus–subplate–cortical plate circuit is thought to be essential for the correct establishment of thalamocortical connections (Allendoerfer and Shatz, 1994; Friauf and Shatz, 1991; Kanold and Shatz, 2006). The functional interactions between these layers change dynamically during development of the barrel cortex.

SPNs originate both from the cortical VZ and the extracortical rostromedial telencephalic wall (RMTW, Pedraza et al., 2014). The newly generated neurons migrate radially or tangentially, from the VZ or RMTW, respectively, to reach the SP cortical area (Pedraza et al, 2014). Cajal-Retzius neurons (CRN) are generated around the same time from the cortical hem (García-Moreno et al., 2007); Cortical GABAergic interneurons are generated in the ganglion eminence, preoptic area or the VZ (Gelman et al., 2011). Subsequently, they migrate tangentially towards the final destination in the cortex (Marín, 2013), appearing at the cortex around E12 (Rio et al., 1992).

TCAs start travelling towards the SP around E11; concomitantly, the SP axons migrate toward the thalamus. The projections from these two populations of neurons make contact around E13, when, according to the 'handshake hypothesis', molecular signals instruct the TCAs to follow the SPN path to the SP area (Molnár and Blakemore, 1995). Indeed, TCAs project to the SP by E15.5 (Antón-Bolaños et al., 2018; Auladell et al., 2000; Gezelius and López-Bendito, 2017; López-Bendito and

Molnár, 2003). In this location the thalamocortical projections sustain a waiting period during which activity-directed interactions with SPNs occur (Catalano and Shatz, 1998; Kanold and Luhmann, 2010).

Before thalamic innervation of the developing cortical plate, SPNs have been shown to project to the marginal zone and send axon collaterals into the cortical plate (Friauf and Shatz, 1991). Monosynaptic connections have been described between SPn interneurons and Cajal Retzius cells in marginal zone (Myakhar et al., 2011). This connection occurs via a primary dendrite that is retracted to L4 or below by P7 (Hoerder-Suabedissen and Molnár, 2012).

Around birth, thalamic afferents invade the developing cortical plate (Catalano et al., 1991, Fig. 1.15). The innervation pattern of TCAs in the cortical plate is refined during development as the projections are restricted to the L4 barrels, the main targets of these afferents in the adult somatosensory cortex.

Voltage-sensitive dyes have been used to investigate the functional connections between the thalamus and the cortex in the rat developing somatosensory cortex (Higashi et al., 2005, 2002). A functional connection was observed in embryos as young as E17. Soon after birth (P0-2), the activation pattern was diffuse, spanning the whole cortical depth. Between P2 and P4, the functional spread changed from being restricted to individual columns, still across the whole cortical depth, to being confined to L4 and L6.

This developmental pattern is consistent with a study that characterised SP and TCA innervation of L4 in the mouse somatosensory cortex (Piñon et al., 2009). In fact, TCA labelling in Golli-tau-eGFP transgenic mice, where SPNs are labelled with eGFP (Jacobs et al., 2007), has shown that between late embryonic and early postnatal development, the distribution of GFP-labelled SP fibres and thalamocortical afferents is reorganised in relation to the L4 barrels. From E17 until the perinatal stages, a diffuse distribution pattern of both SP neurites and thalamic afferents is observed in L4. By P4-6, both sets of projections organised in a periphery-related pattern, showing a preference to the barrel hollows. Gradually this pattern changes and by P10 the GFP-positive SPN fibres accumulate in the barrel septa, at the L4/L5 border, while the thalamic afferents persist in the barrel hollows.

This temporal sequence is consistent with the notion of SPNs pioneering the connections to the cortical plate, and the thalamic inputs using these projections as substrate to find the correct cortical location to innervate.

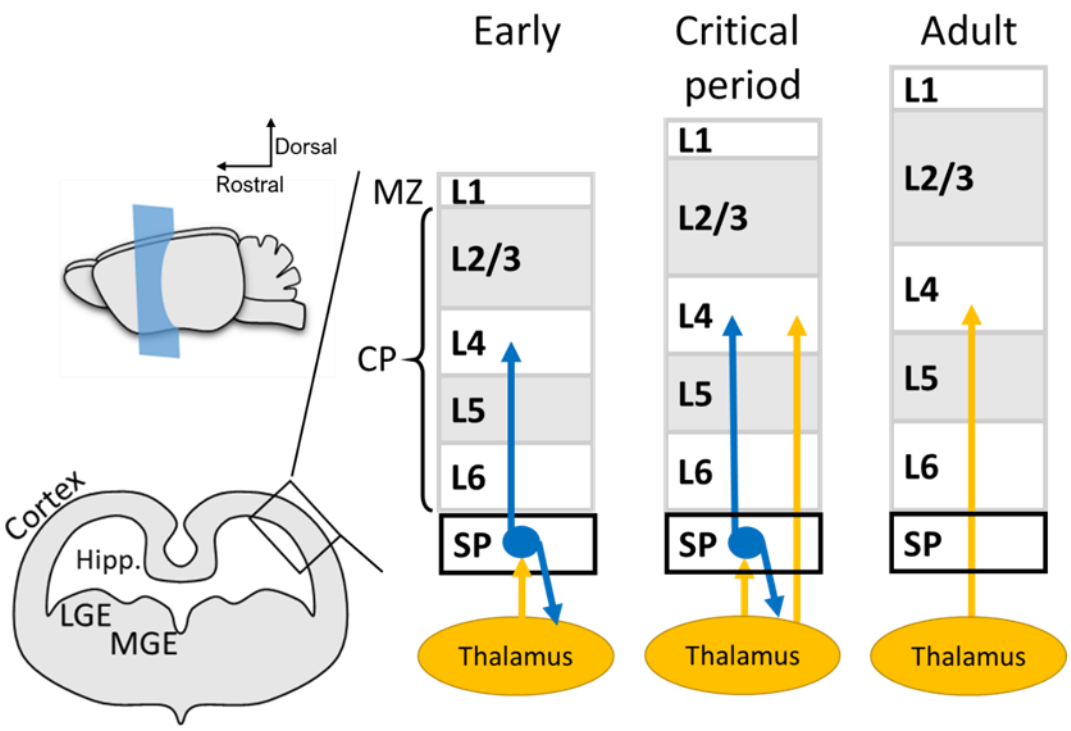

Figure 1. 15 The relationship between subplate, thalamus and cortex over development
Diagram of a developing brain and cortical layers during early development, critical period and adulthood. During early development the thalamus projects to the subplate, which in turn projects to L4 and back to the thalamus. During the critical period the thalamus also starts to project to L4 until during adulthood the thalamus directly synapses with L4 neurons. LGE: lateral ganglionic eminence; MGE: medial ganglionic eminence; SP: subplate; MZ: marginal zone; CP: cortical plate;

1.8.3 Proposed functions

SPNs are present in the brain from embryonic development and the expression of SP markers is seen in L6B in the adult brain. These neurons are thought to assume distinct roles at different developmental stages and thereby impact brain development and maturation.

In the embryonic brain, SPNs have been implicated in axon guidance of corticofugal and corticopetal projections from the thalamus (Ghosh et al., 1990; Grant et al., 2012; McConnell et al., 1994). Studies involving ablation of the SP layer in the cat's primary visual system show the importance of this area for appropriate thalamocortical targeting and the correct establishment of ocular dominance and orientation columns (Allendoerfer and Shatz, 1994; Kanold et al., 2003; Kanold and Shatz, 2006). Furthermore, the barrel cortex fails to develop properly following ablation of the SP (Tolner et al., 2012).

Perinatally, these neurons have been suggested to be involved in the generation of cortical oscillations in gap junction coupled neurons (Dupont et al., 2006). Moreover, SPNs are thought to be pivotal in the process of innervation of the L4 barrels in the visual system, as subplate ablation experiments have shown (Ghosh and Shatz, 1992).

Elimination of the subplate also causes the failure to upregulate genes involved in mature GABAergic function, thus preventing the switch of excitatory to inhibitory GABA action (Kanold et al., 2003; Kanold and Shatz, 2006). Additionally, it has also been proposed that SPNs transiently assume a secretory function, by secreting the serine protease inhibitor neuroserpin, which impacts the formation of cortical circuits during early postnatal development (Kondo et al., 2015)

Finally, as previously mentioned, at least a subset of this early-generated neuronal population is still present in the adult brain. The role of the SP during adulthood is less clear, but is speculated that these neurons can provide support to the cortico-cortical networks (Friedlander and Torres-Reveron, 2009; Kostović et al., 2011; Kostovic and Rakic, 1990; Suarez-Sola et al., 2009).

1.9 Aims and hypotheses

A wide variety of interlinked structural and functional changes occur during early postsynaptic development. All these modifications at the levels of synapses and neural circuits are essential to ensure the correct functioning of the adult brain.

During my PhD, I addressed 2 main questions regarding the development of the mouse barrel cortex within the first 3 postnatal weeks:

1. It is established that dendritic spikes occur in the adult brain and there is evidence for NMDA spikes in P15-20 L4 barrel neurons. When do these regenerative, branch specific events first emerge during development of the barrel cortex?
2. SAP102 and PSD95 are crucial in developing and mature neurons, respectively. Does their pattern of expression mirror the timeline of synaptic development in the different cortical layers of the barrel cortex accordingly?

The hypotheses regarding aim 1 were that during the first postnatal week neurons would be too immature (i.e. would not be expressing the correct number/density of voltage-gated receptors) to support dendritic spiking, but around P15 (so between 4-6 days after the critical period for these cells) the electrophysiological features of these neurons would suffice to be able to elicit dendritic spiking.

Regarding aim 2, we hypothesized that since there is a well-documented succession of maturation of the neurons in the different layers (which, following the innervation pattern, goes L4 ➔ L2/3 ➔ L5 ➔ L6), the expression of MAGUKs would follow a similar laminar enrichment pattern, with SAP102 levels increasing before PSD95 levels.

Ultimately this research will provide further information about the synaptic events that occur during synaptic formation and maturation in a healthy, developing brain.

Chapter 2: Emergence of dendritic spikes during development.

2.1 Dendritic spikes

The vast majority of evidence around dendritic spikes is based on studies conducted in L2/3 or L5 pyramidal neurons, in mature (6 weeks of age or older) murine models (Larkum et al., 2009; Magee and Johnston, 1995; Major et al., 2008; Rhodes, 2006; Schiller et al., 2000; Spruston et al., 1995; Stuart and Sakmann, 1994). The local and regenerative nature of these events, however, and the fact that they can greatly amplify incoming inputs, make them a great candidate to play a role during development. This is because during the establishment of new synapses and the plasticity occurring during this period of substantial change, neuronal activity has a major role on sculpting the developing neural circuits. On the other hand, it is unclear whether the electrophysiological state of the neurons is required to be mature in order to support dendritic spikes. A recent paper reported the presence of dendritic spikes in layer 4 spiny stellate neurons as early as P15-20 (Lavzin et al., 2012). The aim of the present study is to replicate these results and perform the same experiments at earlier ages to characterise the emergence of dendritic spikes. Understanding the timings of emergence of these events would allow the exploration of the possible interaction between regenerative membrane potentials and synapse formation and maturation using a combination of electrophysiological and imaging techniques.

2.1.4 Aim: Are dendritic spikes present in the developing brain?

The aim of the present study is to assess the emergence of dendritic spikes during the developmental ages of P7-20. This developmental timeframe encompasses the critical period for L4 spiny stellate neurons (P9-11, Ashby and Isaac, 2011) and the ages at which NMDA spikes were detected in previous literature (P15-21, Lavzin et al., 2012).

2.2 Methods

2.2.1 Thalamocortical slice preparation

For these experiments, PSD95-eGFP or C57BL/6J mouse pups between P7 and P20 were used (see Table 1 for exact number of animals and cells).

Postnatal day	***Number of animals***	***Number of cells***	***Genotype***	***Cell type***
7	1	2	PSD95	SS, Pyr
8	1	4	WT	SS
9	1	2	PSD95	SS
10	1	3	WT	SS, SS, IN
11	1	1	WT	SS
12	1	1	WT	SS
13	0	0	n/a	n/a
14	3	4	PSD95	SS
15	1	2	PSD95	SS
16	1	1	PSD95	SS
17	0	0	n/a	n/a
18	1	1	PSD95	SS
19	1	1	PSD95	SS
20	1	2	WT	SS
21	1	1	WT	SS

Table 1. Summary of animal numbers used for dendritic spike experiments

For each postnatal day examined, a list of n numbers of animals and cells, the genotype of the mice used and the type pf cell type patched are indicated.
WT, wild type;SS, spiny stellate neurons; Pyr, pyramidal cells; IN, interneurons.

The pups were euthanised by cervical dislocation in accordance with Home Office guidelines and as directed by the Home Office Licensing Team at the University of Bristol. The PSD95-eGFP mouse line is a knock-in mouse line where all endogenous PSD95 is fused to GFP and expressed under the endogenous promoter (Zhu et al., 2018). The brains were dissected and placed in ice-cold cutting solution containing (in mM): 119 NaCl, 2.5 KCl, 11 D-Glucose, 1 NaH_2PO_4, 26.5 $NaHCO_3$, 9 $MgSO_4$, 2.5 $CaCl_2$. To obtain thalamocortical slices, the brain was cut at a 45/55° angle (as described in Agmon and Connors 1991). Using a VT1200 vibratome (Leica), 4-5 thalamocortical brain slices (400 µm thick) were cut at the plane containing the barrel field of the somatosensory cortex, using the hippocampal anatomy as landmark to identify the approximate area. The freshly cut brain slices were submerged in artificial cerebrospinal fluid (ACSF) containing (in mM): 119 NaCl, 2.5 KCl, 11 D-Glucose, 1 NaH_2PO_4, 26.5 $NaHCO_3$, 1.3 $MgSO_4$, 2.5 $CaCl_2$. ACSF was bubbled with carbogen (95% O_2, 5% CO_2) throughout experiments. The tissue was left to rest at room temperature for at least 30-45 minutes in CO^2 bubbling ACSF before beginning electrophysiological experiments.

2.2.2 Whole-cell patch clamp

Whole-cell patch clamp technique was used to visualise the neuronal structure of layer 4 neurons within the barrels and record their membrane potential. Thalamocortical slices were placed in a recording chamber on the microscope rig which was continually superfused with carbonated ACSF. The recordings were performed at physiological temperature by heating the imaging bath to 37°C. The brain slices were first inspected using a 4X objective (Olympus, 0.06 NA) to check for the presence of visible barrels in the cortex (Fig. 2.1A). Care was taken to align the pial surface of the brain slice so it was parallel to the top edge of the field of view. The slice was then stabilised in the imaging bath using a tissue anchor to minimize motion during imaging and electrophysiological recordings. Spiny stellate neurons of L4 were identified using oblique brightfield imaging through a 60X water immersion objective (Olympus, 1 NA, Fig. 2.1B). Starting from the pia, L1 was recognizable because mostly devoid of cells, L2/3 presented densely packed small pyramidal cells. The spiny stellate neurons in L4 can be distinguished because their cell body is more circular then the pyramidal cell bodies of L2/3, and the neurons also appear more densely packed. Furthermore, the sparse and large pyramidal cells in L5, located below the barrels in L4, constitute another clearly distinguishable landmark for the position within the cortex.

Patch pipettes with tip resistance of 3-5 MΩ were made from borosilicate filamented glass capillaries (Harvard Apparatus) pulled using a p-87 micropipette puller (Sutter Instrument). These glass pipettes were filled with intracellular solution containing (in mM): 130 $KMeSO_4$, 8.5 NaCl, 5.0 HEPES, 0.5 EGTA, 4.0 MgATP, 0.3 NaGTP and with 285 mOsm (pH of 7.25 adjusted using KOH). In order to visualise neuronal morphology to identify the right cell type and to stimulate precisely a dendritic branch, either Alexa Fluor 594 or Alexa Fluor 488 (concentration 50µM, Thermo Fisher Scientific) was added to the patch pipette internal solution.

Whole-cell current clamp recording were made using a MultiClamp 700A amplifier (Axon Instruments). Immediately following the patching of the cell, a series of voltage steps (2 hyperpolarising and 6 depolarising) were given to obtain an indication of the health status and action potential threshold of the neuron before starting the stimulating experiments. The cell was then left around 10 minutes to allow the diffusion of the dye inside the cell membrane.

2.2.3 Live 2-photon imaging

The chosen neuronal cell body was patched and 2-photon imaging of the cell provided further confirmation of the cell type being targeted (Fig. 2.1B). The morphology of pyramidal cells and spiny stellate cells is distinctly different, as the former are much longer and exhibit the characteristic dendritic arbour (with basal and apical dendrites), while the latter have a much more radial dendritic arbour spanning a significantly smaller area.

Patched neurons were imaged using a Prairie Ultima 2-Photon laser scanning microscope (Prairie Technologies, Madison, WI) equipped with a 60X water immersion objective (Olympus, 1 NA). Imaging of neurons filled with Alexa Fluor 594 Hydrazide or Alexa Fluor 488 Hydrazide was performed using a 910 or 810 excitation wavelength, respectively (1 µm step, 1024X1024 pixels, 2 times line average).

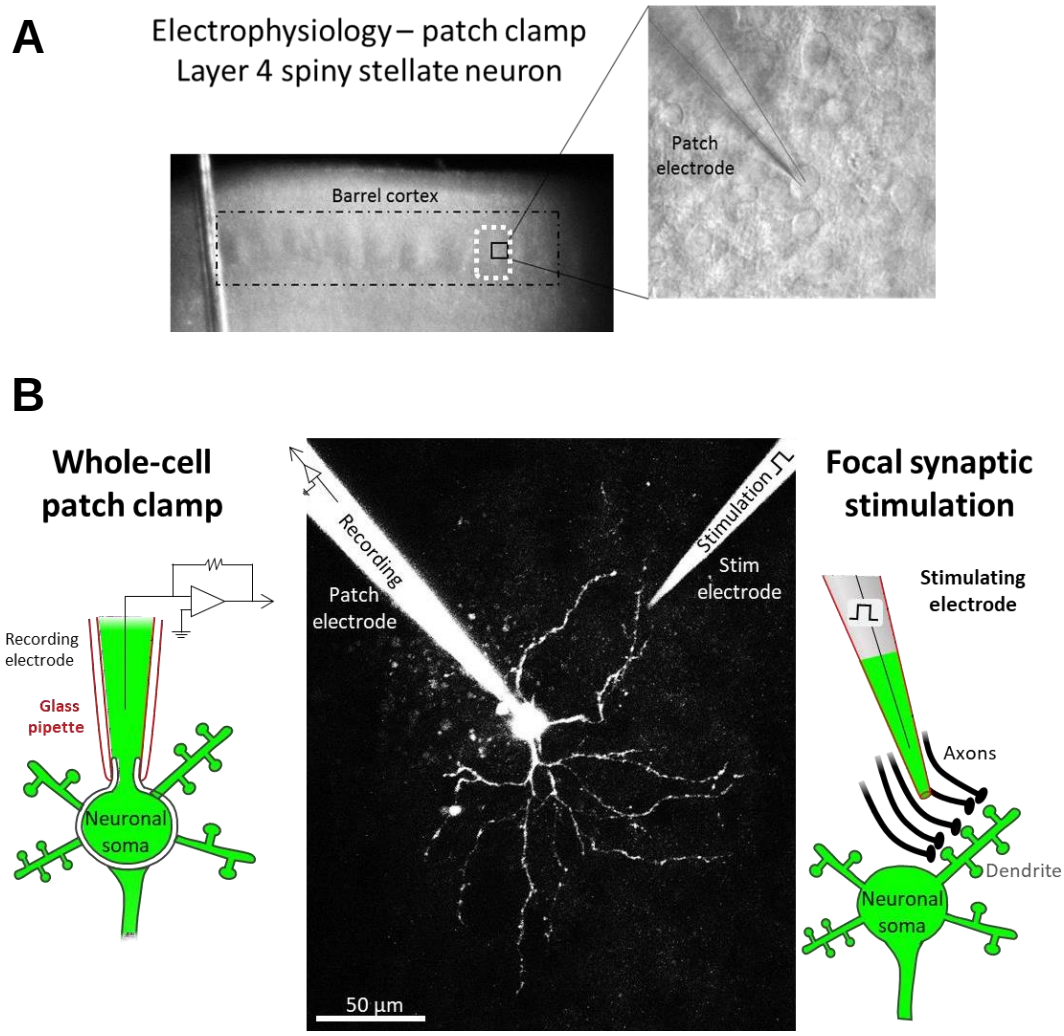

Figure 2. 1 Experimental procedure for eliciting dendritic spike

A. Brighfield image taken with a 4X objective lens showing a barrel cortex of an acutely dissected thalamocortical brain slice. The barrel field is highlighted inside the dotted line rectangle, white dotted line for single barrel. The zoomed in image shows a glass patch electrode attached to a L4 spiny stellate neurons. B. middle, maximum intensity projection 2-photon image of a spiny stellate neuron. A patch pipette, on the left of the image, has been used to fill the cell with Alexa Fluor 594 and to record electrical activity. A stimulation electrode, on the right of the image, is used for focal synaptic stimulations. On either side of the 2-photon image is a diagram showing whole-cell patch clamp and focal synaptic stimulation technique.

2.2.4 Focal synaptic stimulation

Focal synaptic stimulations were used to elicit dendritic spikes in the spiny stellate neurons of cortical layer 4 (Fig. 2.2 and 2.4, similar to Lavzin et al., 2012) in P7-P20 mice. Following whole-cell patch clamp of spiny stellate neurons, the cell was imaged and a suitable dendrite was chosen. The criteria for targeting the dendrite was the orientation, location and spatial relation to other dendrites of the patched cell; the selected dendrite was ideally located on the left side of the cell, as the stimulating electrode would approach the cell from that side of the objective; it was chosen so that it was deep enough to not be cut during slice preparation, to ensure preservation of the structural integrity of the cell, yet not too deep that it is difficult to image due to increased light scattering; finally, the dendrites preferentially targeted were relatively isolated from the rest of the dendritic branches to minimize the possibility of stimulating multiple dendrites, thus jeopardising the branch-specific effect of dendritic spike generation. The targeting of axonal projections innervating a single dendritic branch was achieved by stimulating in proximity of a chosen dendrite of the patched cell; electric pulses in the vicinity of an axon triggers glutamate release at the synapse and elicit a synaptic response which is supposedly local to the dendritic branch of choice. Care was taken to avoid direct stimulation of the dendrite (by monitoring the presence of a latency between the stimulus artefact and the change in membrane potential, reflective of the underlying synaptic transmission time). Stimulation was achieved using a monopolar electrode pulled from a patch glass pipette (similarly to the patch electrode) and filled with ACSF containing either Alexa 594 or Alexa 488 (50µM, Thermo Fisher Scientific). The stimulating electrode was connected to a Digitimer DS2A stimulation box (Digitimer Ltd.). 200 µs long square pulse stimulations were injected in trains of 5 stimulations at 0.2Hz. The intensity of the stimulations varied after each train of stimulations and the output was recorded and analysed. Intensities were varied in a pseudorandom non-incremental manner to limit the plasticity at the synapses and possibly mimic a more physiological pattern of inputs. Increasing the intensity putatively increases the number of fibres recruited to the dendrite, therefore providing a way to control the number of synapses being activated. The experiments were conducted in current clamp. Current was injected to hold the neuron at the desired resting membrane potential (Vm). In the control conditions, Vm was set at -60mV while in the hyperpolarised conditions Vm was held at -75 mV. The hyperpolarisation of the cell was used to investigate the effect of disengaging NMDARs. Furthermore, all focal synaptic stimulation experiments analysed were conducted in the presence of 50 µM pictrotoxin (PTX, Sigma-Aldrich) to block $GABA_A$

receptors and reduce interference of inhibitory responses in the electrophysiological traces.

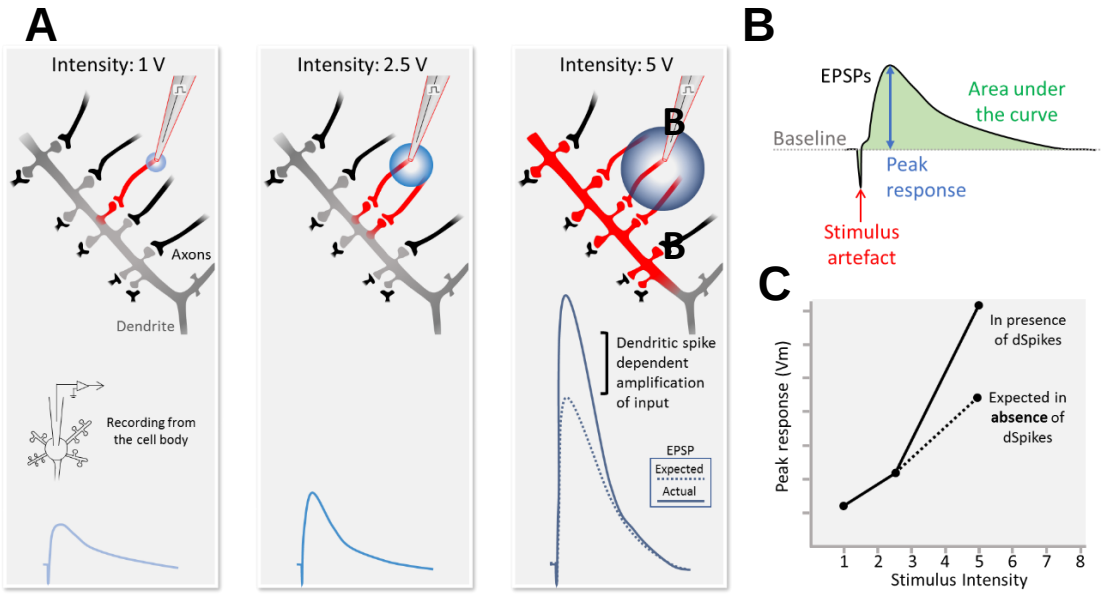

Figure 2. 2 Schematic of mechanisms of focal synaptic stimulation

A. shows a dendritic branch innervated by several axons. When a stimulating electrode is placed in proximity to the dendritic branch, it can stimulate the release of neurotransmitters from axons which synapse onto that dendritic branch. The resulting change in membrane potential can be recorded from the cell body, and an example is provided In the blue trace underneath the diagram. As the intensity increases, the sphere of action of the stimulation increases also, recruiting more and more fibres. A dendritic spike occurs when enough axons are activated on a dendrtitic branch and this leads to the activation of nearby synapses. This causes the membrane potential to leap up in a supralinear manner as shown by the difference between the expected (linear) and actual (supralinear) response. This is also shown in an example of an input/output curve for this experiment (C). B. shows a simplified response trace and the parameter being analysed in this study.

2.2.5 Analysis of dendritic stimulation data

The electrophysiological data were analysed using MATLAB (MathWorks, version R2018q). Traces containing action potentials were excluded from the analysis and the remaining subthreshold traces were normalised to the baseline (100 ms prior to the stimulus). The peaks of amplitudes of the response to the train of stimuli was then averaged for each stimulus intensity either between 2-20 ms after the stimulus (short window) or between 2-500 ms after the stimulus (long window). The results were plotted to construct an input/output curve at the different ages, for both the control and hyperpolarised conditions. The areas under the curve of the response were also

averaged at each stimulus intensity and it was plotted against the intensity of the stimulus.

The maximum response during short and long window, as well as the maximum area under the curve was calculated and compared between the two membrane potential conditions. For each cell, the maximum value of each parameter was selected, regardless of stimulus intensity and within a whole trial. The raw data was plotted and an average was calculated ($^{+}/_{-}$ SEM). This data from all ages investigated was combined together and a paired student's t-test was run using SPSS to test whether there is a significant difference in maximum response for the three parameters between experiments run with cells held at control and hyperpolarised resting membrane potential.

This same data was used to run a regression analysis to assess age-dependency of the maximum responses between P5-20. The plots were made in MATLAB (MathWorks, version R2018q) and a line of best fit was plotted using the polyfit and polyval in-built functions. Similar regression analysis (SPSS, IBM Statistics, version 24) was also run for the ratio of control/hyperpolarised values calculated for each cell. Plots of the ratio as a function of mouse age and best line of fit were created using MATLAB (MathWorks, version R2018q).

2.3 Results

2.3.1 Morphologies of L4 neurons

To investigate the presence of dendritic spikes in developing cortex, neuronal dendrites were stimulated and the membrane potential of layer 4 neurons was recorded using whole cell patch clamp in barrel cortex slices from mice aged P7-P20. These neurons were also filled with fluorescent dye from the patch pipette to allow 2-photon imaging of their morphology during recordings (Fig. 2.3 and 2.4). Most of the cells imaged (34/41 cells) exhibited the characteristic small cell bodies and symmetrical dendritic arbour, with dendrites spanning approximately the same distance from the cell body, in multiple directions. The rest of the imaged cells (7/41) had an apical dendrite extending towards the outer layers, which is characteristic of star pyramidal neurons which are also found in L4 barrels (Lübke et al., 2000; Staiger et al., 2004). Because barrel cortex spiny stellate and star pyramidal neurons have been shown to exhibit similar intrinsic properties (Cowan and Stricker, 2004; Feldmeyer et al., 1999; Schubert et al., 2003), the below analysis was carried out on both cell types.

Zooming in the dendrite reveals the presence of dendritic spines on the dendrites of both types of neurons from P7. Further analysis is required to quantify the increase of spines with age, but it is possible to qualitatively assess that the number of dendritic spines appears to increase with age, consistently with previous literature on the barrel cortex (Ashby and Isaac, 2011).

The cell bodies of spiny stellate cells in the L4 barrel cortex have been shown to be preferentially located on the barrel wall (Arnold et al., 2001; Egger et al., 2008). When fully mature, the dendrites of these neurons are projected into the barrel hollow where they are extensively innervated by thalamocortical afferents (Harris and Woolsey, 1983). The 2-photon images of patched neurons show that several neurons imaged exhibited this biased orientation of the dendrites towards one side, putatively the barrel hollow (Fig. 2.4). However, since the barrels were not labelled, it is only possible to postulate that this biased orientation is related the position of the neuron within a barrel.

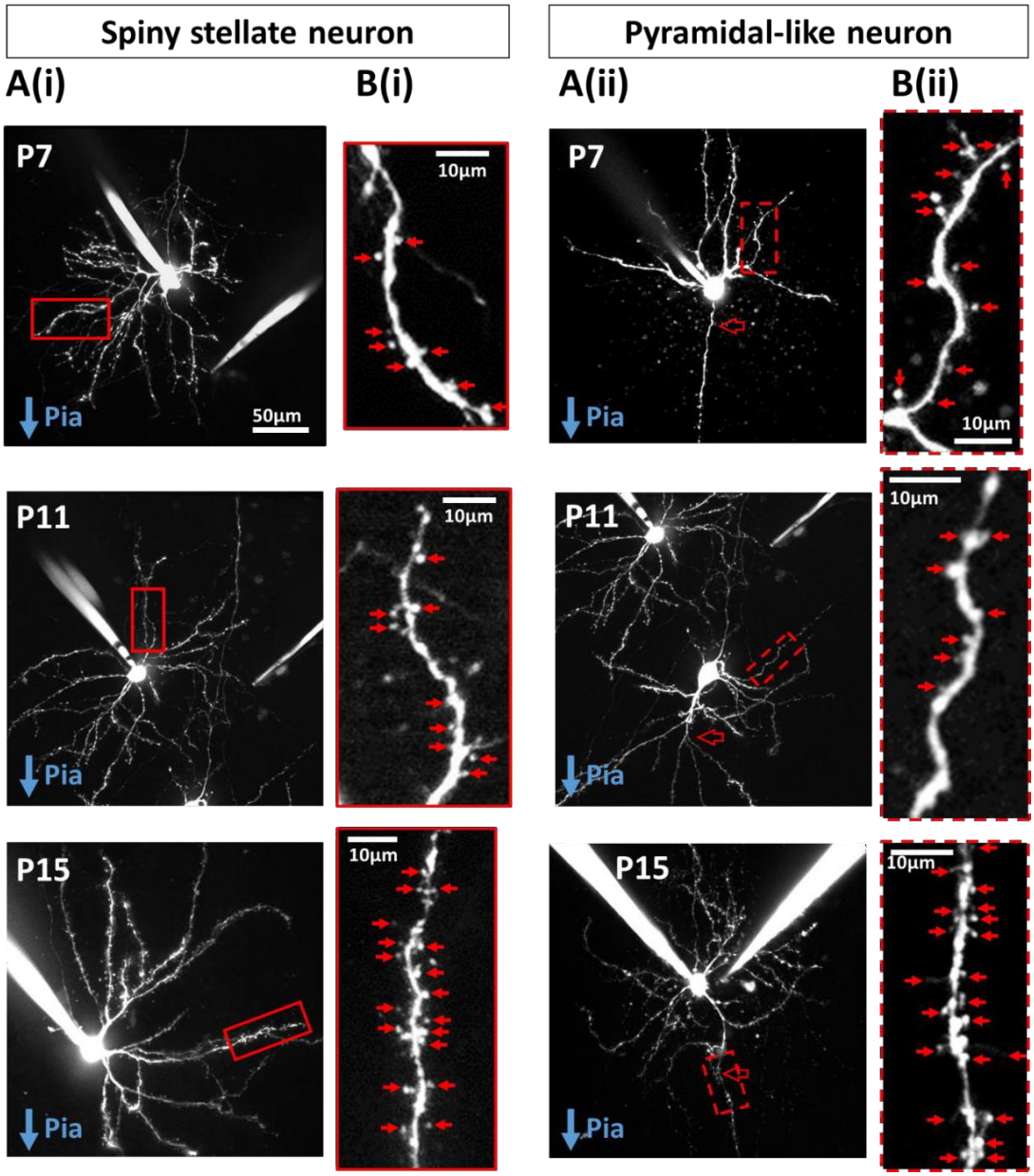

Figure 2. 3 Range of neuronal morphologies in L4

Maximum intensity projections of 2-photon image stacks showing neurons patched and filled with Alexa fluorescent dyes from 3 example ages, P7, P11 and P15. A(i) and A(ii): for each age, an example of a characteristic spiny stellate neuron and a pyramidal neuron is shown. The red hollow arrows in A(ii) show the apical dendrite that is present in pyramidal-like neurons, but not spiny stellate neurons. The light blue arrow indicates the direction where the pial surface is located. B(i) and B(ii): zoomed in images of single dendrites is shown next to each image. The red arrows indicate putative dendritic spines.

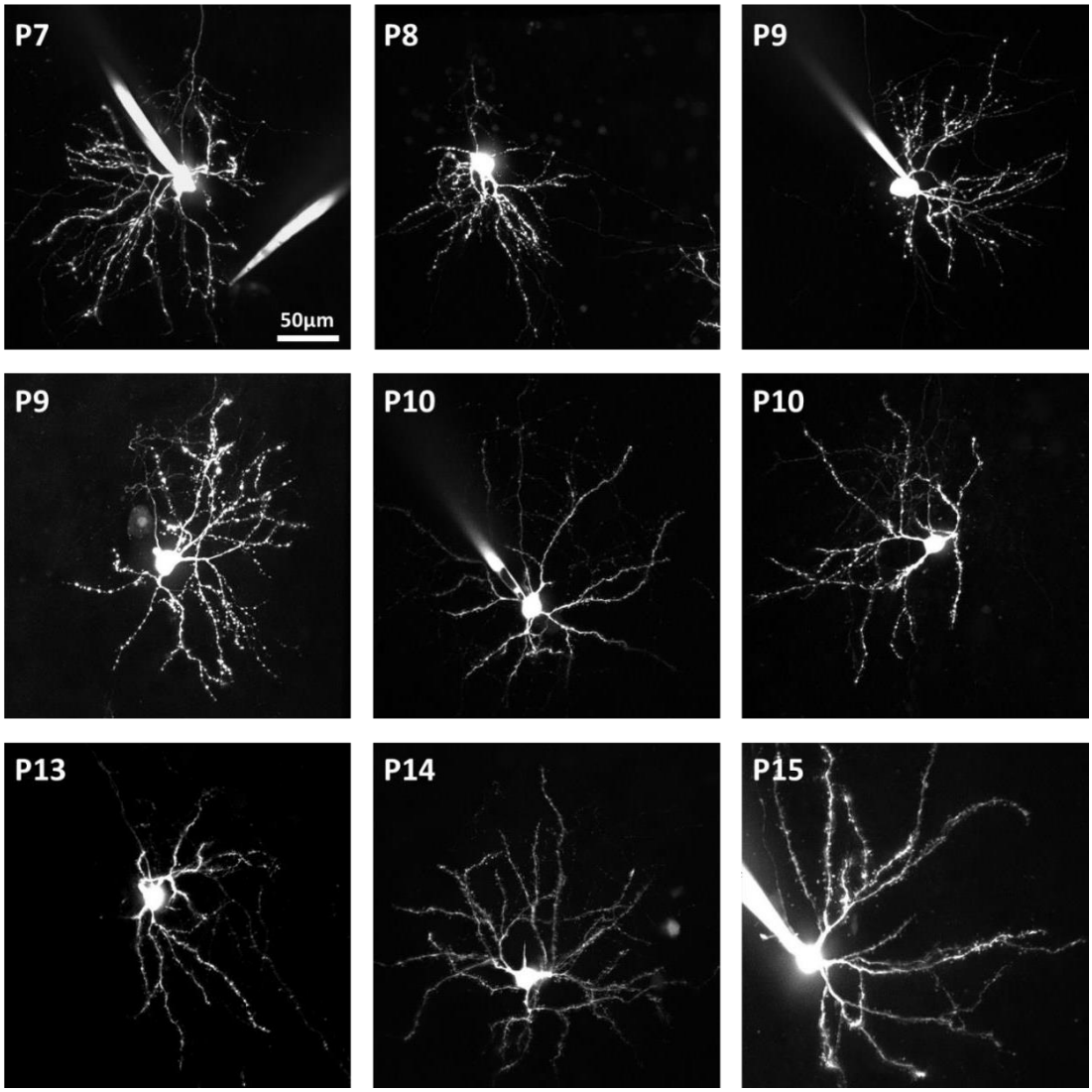

Figure 2. 4 Dendritic orientation of L4 spiny stellate neurons

2-photon images of L4 spiny stellate neurons from several ages (noted top left inside the image). A proportion of these neurons (4/6) exhibit a preferential orientation of the dendritic arbour towards one side of the image. All images are shown at the same scale.

2.3.2 Dendritic stimulation at different developmental ages

In order to elicit a dendritic spike, whole-cell patch clamp was used to record changes in the membrane potential of L4 barrel neurons in response to stimulations of axonal projections. The monopolar electrode was placed near (around 20-30 µm) a dendrite of the recorded cell in order to cause neurotransmitter release at the synapse and trigger a postsynaptic response. The response was anticipated to be almost exclusively due to glutamate release because $GABA_A$ receptors were blocked by the picrotoxin (PTX) included in the external solution. Care was taken to avoid direct stimulation of the dendrite by monitoring the presence of a latency of at least 2 ms between the stimulus artefact and the change in membrane potential, reflective of the underlying synaptic transmission time. The stimulations were given in trains of 5 pulses at 0.2Hz; Increasing the stimulus intensity putatively increases the number of fibres recruited to the dendrite, providing a way to control the number of synapses being activated. Therefore, to investigate the scaling of the excitatory postsynaptic potential (EPSP) size with different numbers of simultaneously activated inputs, the stimulus intensity was varied in a pseudorandom, non-incremental fashion.

The maximum intensity of the delivered stimulus in each experiment was increased until action potential generation (Fig. 2.5). The lowest intensity was that which clearly evoked no EPSPs at all. Recordings in which the cell spiked at every single stimulation within a train were discarded.

NMDA dendritic spikes are subthreshold events that, while they contribute to the depolarised state of the neuron, on their own do not usually trigger an action potential in the axon of the targeted neuron (Holthoff et al., 2004; Larkum et al., 2009; Major et al., 2008; Milojkovic et al., 2005; Oakley et al., 2001; Schiller et al., 2000);. The presence of action potentials in the response traces masks subthreshold events; therefore, onlythe traces that did not contain action potentials were analysed. Figure 2.8 shows traces from the same experiments before (Fig. 2.5A) and after (Fig. 2.5B) the removal of trials containing action potentials.

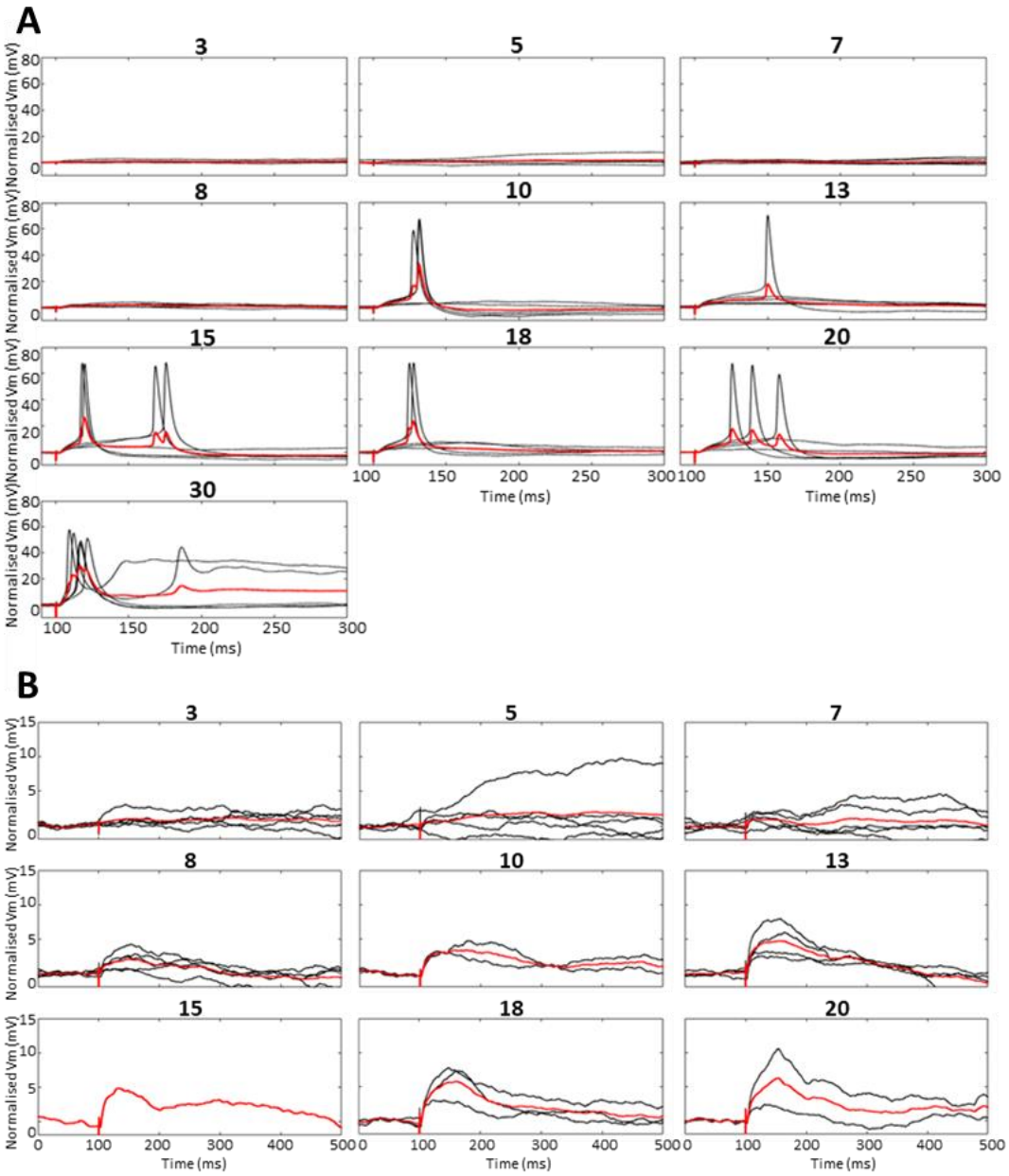

Figure 2. 5 Examples of somatic voltage recordings following focal synapti stimulations at different intensities

A. Example of traces from spiny stellate neurons being stimulated in thalamocortical brain slices from a P7 mouse. The number at the top of each graph indicates the stimulus intensity of the stimulation. The stimulus was given at 100 ms. In black are the single trials (5 stimulations at 0.2 Hz) while the overlaying trace in red is the mean of all the 5 traces. The traces are normalised to the mean baseline prior to the stimulus. B. The same example as in A after the removal of the traces containing action potentials, leaving subthreshold EPSPs only.

2.3.3 Average peak responses and areas under the curve following focal synaptic stimulation

In order to investigate the emergence of dendritic spikes during postnatal neuronal development, the experiments were conducted on P7-21 mice. This developmental period incapsulates the critical period of development of the spiny stellate neurons (Ashby and Isaac, 2001).

During the early stages of neuronal development, NMDARs are the main contributors to synaptic transmission, while AMPARs are inserted in the membrane later on (Barth and Malenka, 2001; Carmignoto and Vicini, 1992; Crair and Malenka, 1995; Daw et al., 2007; Feldman et al., 1998; Hestrin, 1992; Isaac et al., 1995, 1997; LoTurco et al., 1991; Monyer et al., 1994). These receptors are characterised by a large conductance, Na^+ and Ca^{2+} permeability and slow kinetics (Glasgow et al., 2015; Tong and Jahr, 1994). Because of the slow activation and opening duration of these receptors, the dendritic spike they support is very long lasting (up to 100 ms, Major et al., 2008). Previous literature has shown that NMDAR-mediated dendritic spikes can affect both the amplitude and the duration of the postsynaptic response, independently. Therefore, the parameters extracted from the electrophysiological recordings in the responses to focal synaptic stimulation were the average peak of the EPSP (both in the short, 2-20 ms, and long, 2-500 ms, window post-stimulus) and the area under the curve for the whole duration of the recording (2-500 ms post-stimulus). The area under the curve was used to measure differences in the duration and amplitudes of the responses, thus giving information about the shape and length of the trace, which might be underlying the NMDAR component.

L4 spiny stellate neurons have been previously reported to support NMDAR-mediated dendritic spikes in P15-20 mice (Lavzin et al., 2012). In order to investigate the requirement of NMDARs in dendritic spike generation, focal synaptic stimulation was carried out at normal voltage and then the neuron was hyperpolarised and the same set of stimuli was injected (Fig. 2.6). Hyperpolarisation of neurons reduces potential activation of NMDARs as it prevents voltage-dependent release of a magnesium block release, which therefore imposes a physical block to ionic influx via these ion channels (Mayer et al., 1984; Nowak et al., 1984). Hyperpolarizing the neuron by approximately 15 mV was previously shown to abolish NMDA-mediated dendritic spikes (Lavzin et al., 2012).

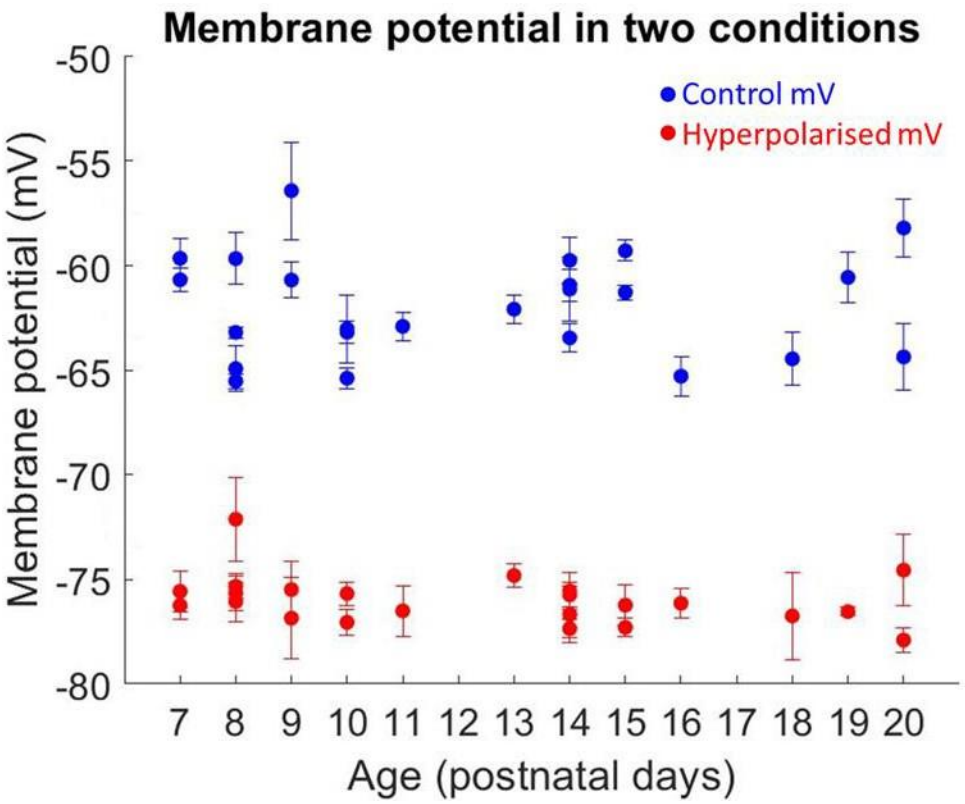

Figure 2. 6 Resting membrane potential in control and hyperpolarised conditions
Current injection in current clamp mode was used to hold the whole-cell patched cell at a specific membrane potential. In the control condition, the resting Vm was set at -60 mV (in blue) while in the hyperpolarised condition the cell was held at -75 mV. Cell resting membrane potential for each cell, averaged for each stimulation train, before stimulus, is shown. Error bars: S.E.M.

The average peak of the response to the stimulus is normalised to the baseline before the injection of current in all the graphs in Fig. 2.7. The data shown in this figure has been obtained by analysing the subthreshold-only traces. In all the recordings the dendrite was stimulated until the cell reached the threshold for action potential, but only subthreshold traces were analysed here.

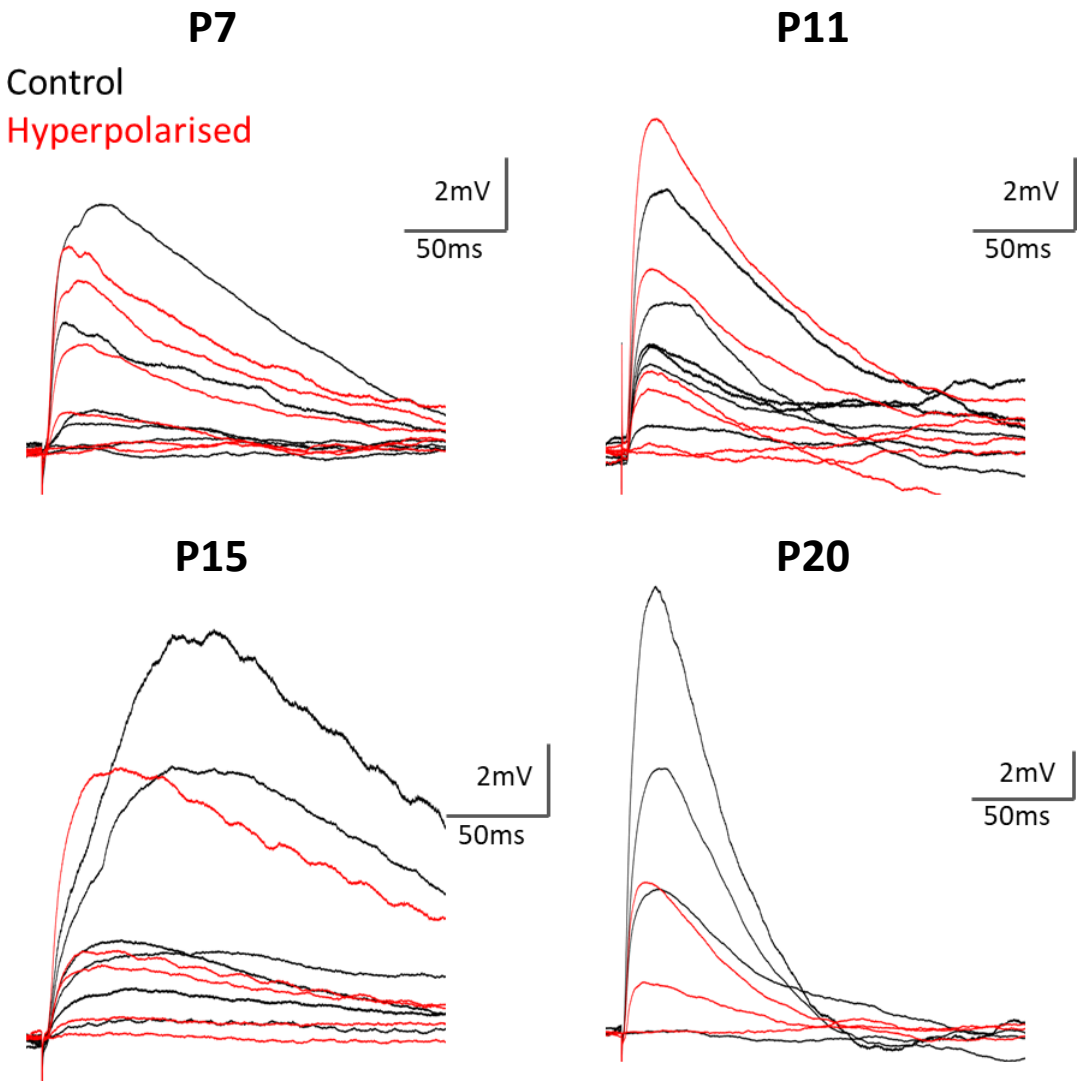

Figure 2. 7 Recording traces from a single cell in brain slices of selected ages following focal synaptic stimulation

Example traces from P7, P11, P15 and P20 pups. The responses from a single cell per age are shown overlaid. In black are the responses to the focal synaptic stimulations in the control resting Vm condition and in red the responses in the hyperpolarised condition.

Periodically throughout the recording session, the neuron was briefly imaged to ensure that the electrodes had not drifted from their original location; additionally, electrophysiological parameters, such as the amount of current being injected to keep the membrane potential at the desired value, were monitored as a measure of the health status of the neuron (leakiness). Aside from these imaging periods, 2-photon imaging was kept minimal to avoid phototoxic effects on the neurons.

The variability between each cell, dependent on various factors such as cell intrinsic differences and the proximity of the stimulating pipette to the dendrite, made it difficult

to average the data from different neurons. Therefore, results from single example trials from P7, P11, P15 and P20 mouse pups are shown in Fig 2.8.

The peak in the first window is indicative of fast-responsive currents (2-20 ms post stimulus), while the peak of the long window includes the peak value from the beginning of the short window and expanding until 500 ms post stimulus, thus including contributions from channels exhibiting both fast and slow kinetics. At all the examined ages, as the intensity of the stimulus increases there is an increase of the peak of the resulting EPSP in both the short and long window (Fig. 2.8). This shows how the amplitude of subthreshold EPSPs gets larger as putatively more fibres are recruited with increasing stimulations. The increase in amplitude can be observed in both control and hyperpolarised conditions. Similarly, the area under the curve becomes larger as the stimulus intensity increases, in both conditions and at all ages examined.

These results suggest that the stimulation close to the dendrite of the recorded cell is eliciting postsynaptic responses that become larger as the stimulus intensity increases.

A previous study by Lavzin and colleagues reported a NMDA-dependent supralinear response to increasing focal synaptic stimulation intensity (Lavzin et al., 2012). In the example shown in that paper, an approximately 5-fold increase in the postsynaptic output of the recorded neuron was obtained once a threshold of stimulation was reached. This nonlinear effect was completely abolished when NMDARs were pharmacologically blocked via superfusion of the brain slice with APV. The nonlinear effect (i.e. “jump" in response) resulting from the occurrence of a NMDA spike was distinctly obvious in their voltage recording traces and in the stimulus current-voltage relationship curves.

In the data presented in this study, no noticeable jump in the response to gradual increases of stimulus intensity was observed in the control or hyperpolarised condition. Instead, a gradual increase in the response was recorded. This was the case in all ages and animals looked at (P7-P21 for a total of 15 animals and 22 neurons).

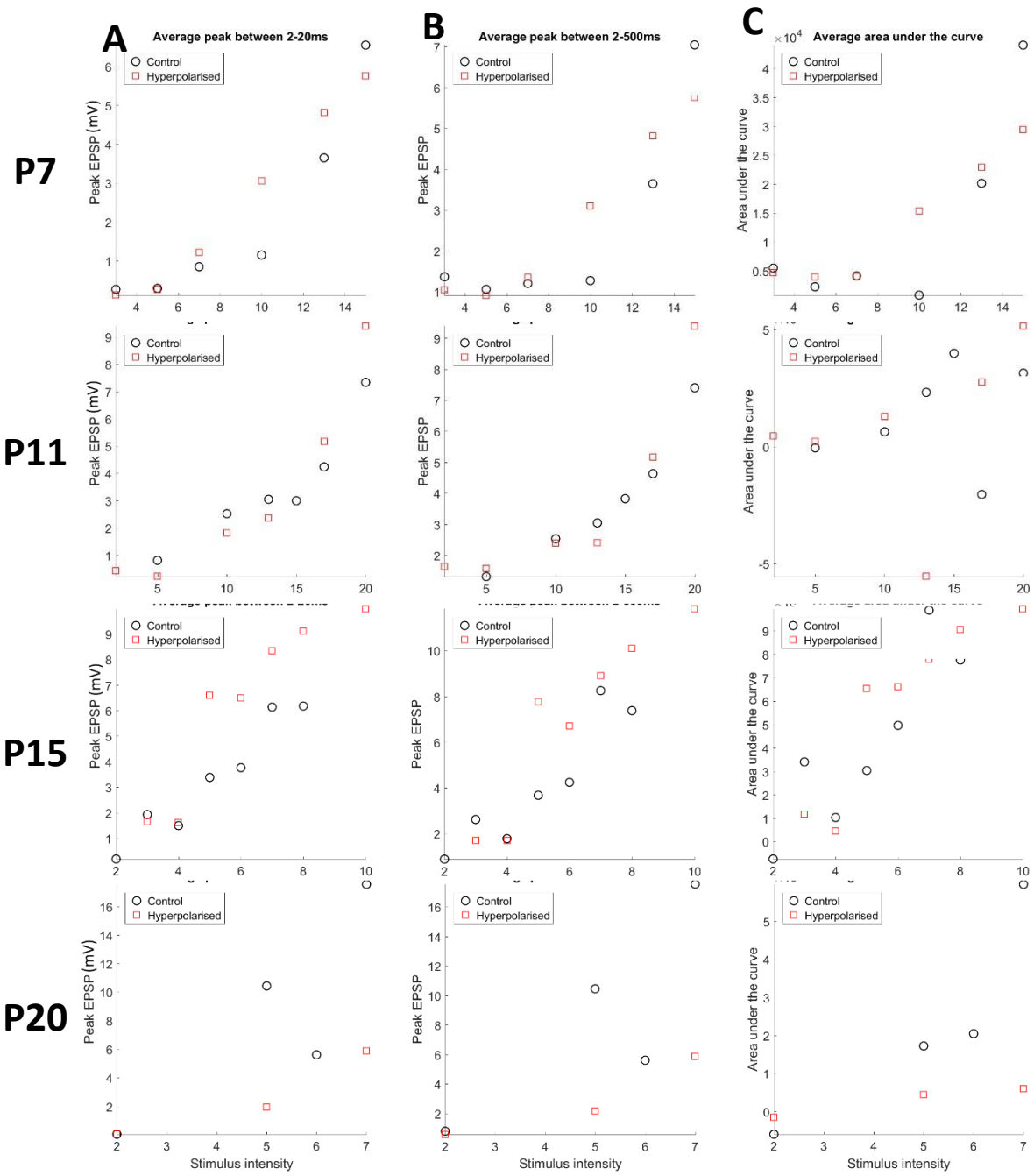

Figure 2. 8 Representative examples of parameters that were analysed for P7, P11, P15 and P20 animals

The relevant age can be seen on the left column of the figure. In all ages the average peak of the response between 2-20ms or 2-500ms and the average of the area under the curve was calculated and plotted. The black circles show the results in the control condition (membrane potential = -60mV), while the red squares indicate the results for the hyperpolarising condition (membrane potential = -75mV). The peak EPSP is normalised to the mean baseline prior to the stimulus. In all the examples shown the peak of the response increases as the stimulus increases in both the short and long time window (A and B). Similarly, stimulus dependent increase of the area under the curve can be observed (C).

2.3.3 The effects of disengaging NMDA receptors

In order to further explore the effect of the hyperpolarisation-dependent disengagement of NMDARs in response to focal synaptic stimulations, the maximum EPSP for each trial is plotted in Fig. 2.9. First, the response within the short window (2-200 ms post stimulus) was analysed. No statistically significant difference was detected in the maximum peak of the EPSP between the control and the hyperpolarised state of the cell. A similar result was found for the response during the long window (2-500 ms). On the other hand, the maximum value for the area under the curve is significantly reduced in the hyperpolarised state of the cell, compared with the control membrane potential. Because no statistically significant difference in the amplitude was detected, the difference in area under the curve is most likely due to a change in the duration of the EPSP. These results suggest that while hyperpolarising the cell, and therefore putatively blocking the action of NMDARs, shortens the duration of the EPSP, but has no significant effect on the amplitude of the response. This suggests that, overall, there is an NMDAR-component in the electrophysiological data acquired. In order to check this, NMDAR blockers such as APV should be used.

We then moved on to testing whether the value of the maximum EPSPs change with increasing developmental age of the mouse pups (Fig. 2.10). Regression analysis shows that there is a modest correlation between the maximum EPSPs recorded and age in both the short ($R^2 = 0.349$) and the long ($R^2 = 0.272$) window (Fig. 2.10A). The peaks of the responses for each cell increase from ~10 to ~15 mV between P7 and P20. On the other hand, non-statistically significant developmentally regulated changes were detected in the maximum of the area under the curve in response to focal synaptic stimulation. The same analysis was carried out for the responses following hyperpolarisation of the cell. A very weak correlation was found for the short and long window ($R^2 = 0.162$ and $R^2 = 0.105$, respectively), and for the area under the curve ($R^2 = 0.031$, Fig. 2.10B). These results suggest that hyperpolarising the cells influences developmental functional changes mediated by NMDAR activation.

Finally, in order to determine whether hyperpolarising the cell has an age-dependent effect on the three parameters investigated, a ratio of the control and hyperpolarised data was calculated, and regression analysis was carried out (Fig. 2.11). For both the maximum response in the short and long window, no statistically robust difference was observed across the ages investigated (P7-20). Similarly, the control/hyperpolarisation ratio of maximum area under the curve does not seem to be affected by the age of the animal.

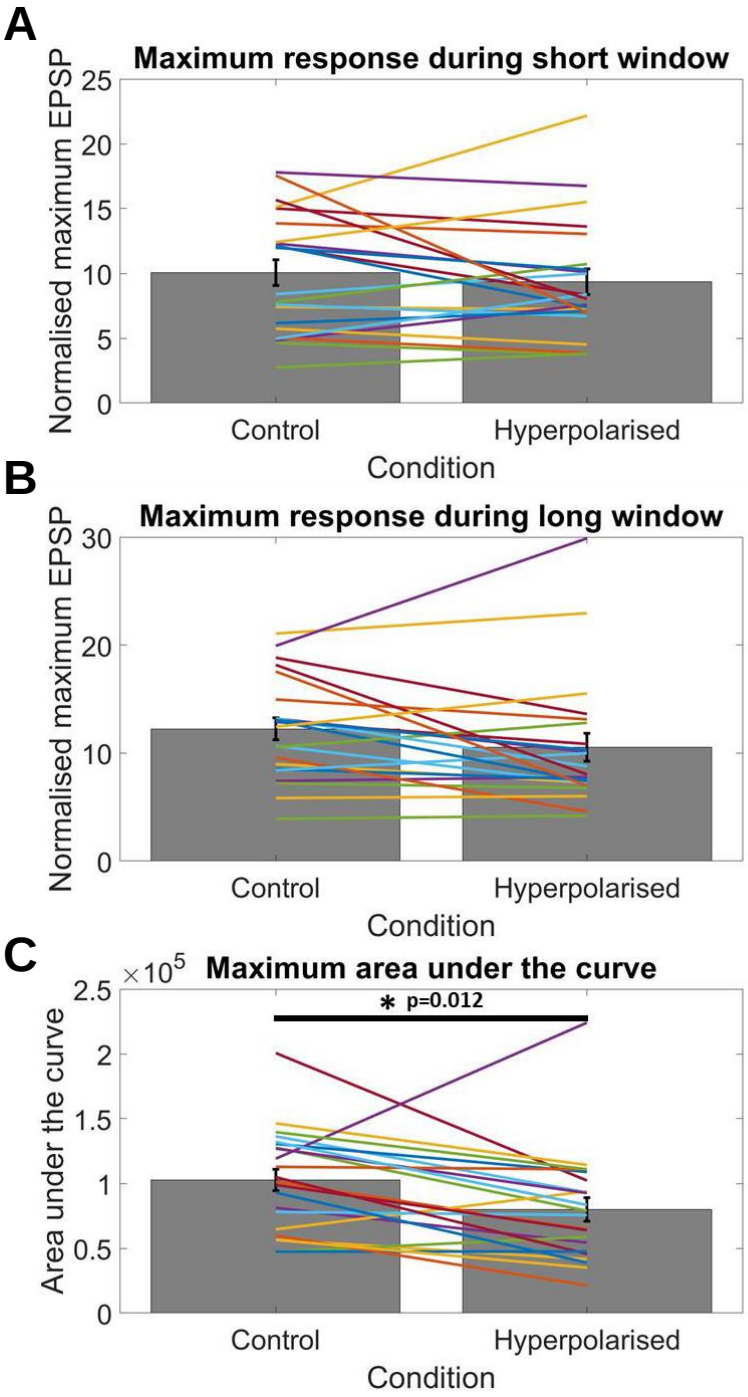

Figure 2. 9 Maximum responses in the control and hyperpolarised conditions
The peak of the EPSP for each trial is plotted for the short (A) and long (B) window and the maximum area under the curve (C). The bar plot shows the average of the maximum response for the two conditions (during control and hyperpolarised membrane potentials). Paired Student t-test was run. Error bar: SEM.

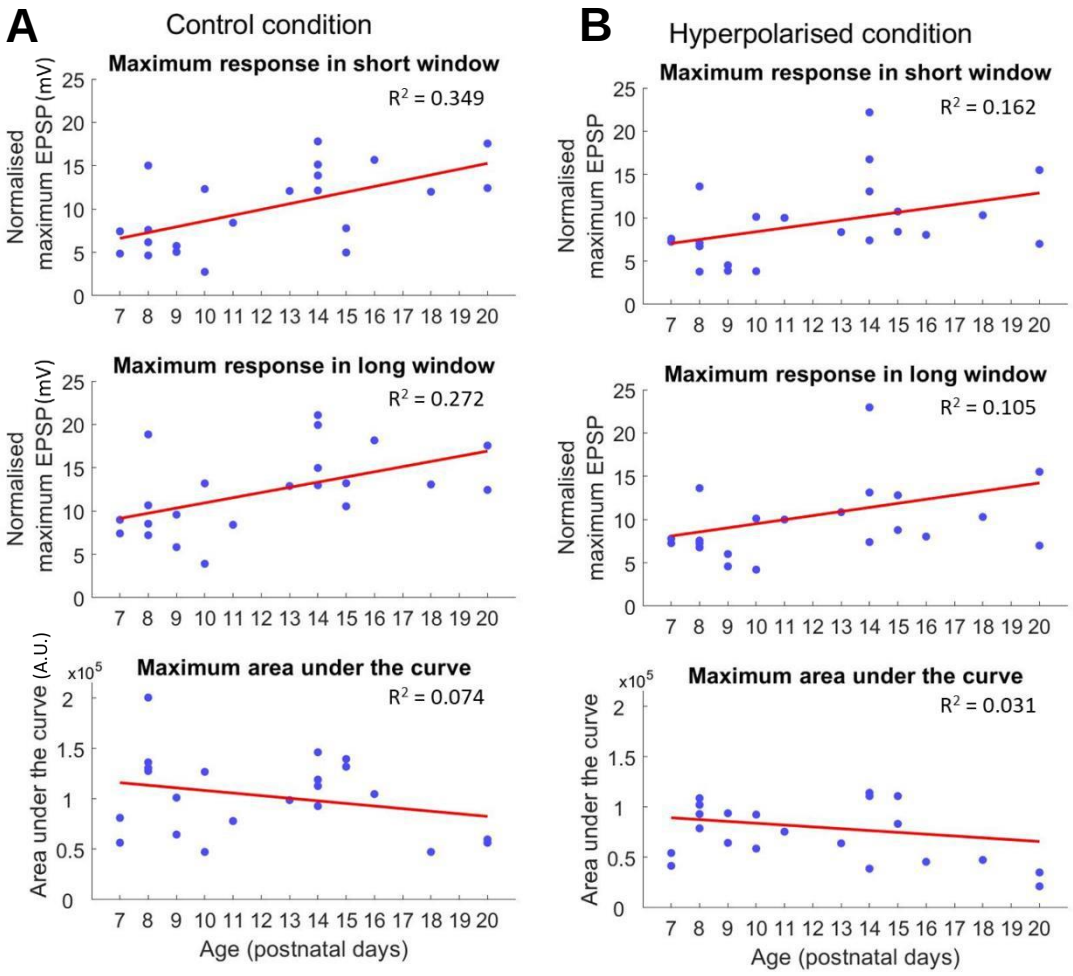

Figure 2.10 Age-dependent changes in maximum responses and area under the curve
For both the control (A) and the hyperpolarised (B) conditions, maximum EPSP for each cell is plotted against developmental age for the short and long window. Maximum area under the curve per trial is also shown. Red line shows the best fit line.

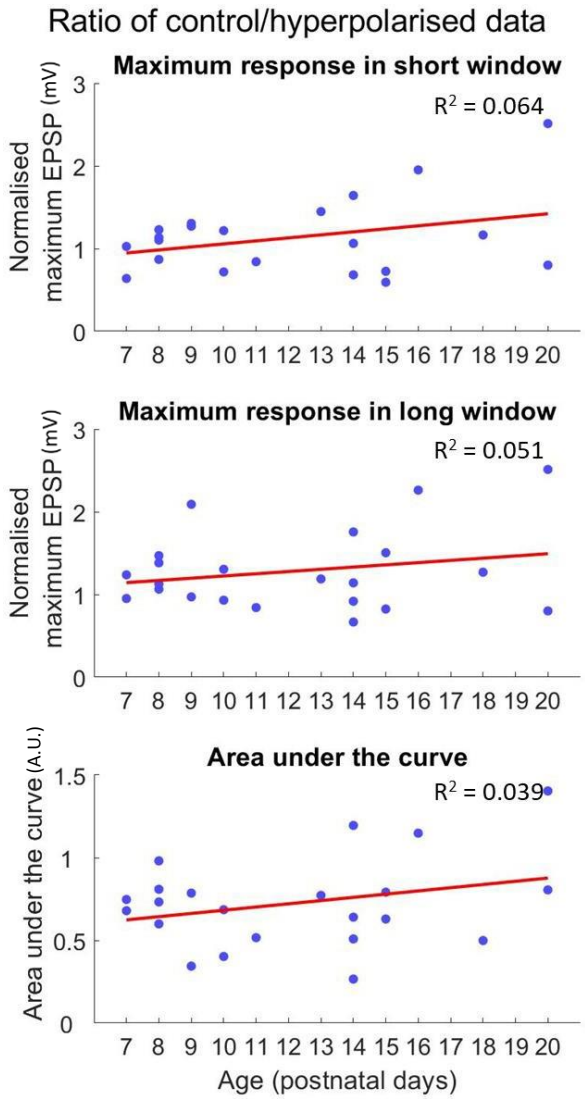

Figure 2. 11 Age-dependent changes in the ratio of control/hyperpolarised data
The ratio between control and hyperpolarised date for maximum EPSP for each cell is plotted against developmental age for the short and long window. Maximum area under the curve per trial is also shown. Red line shows the best fit line.

2.4 Discussion

2.4.1 Morphology of the L4 neurons of the developing barrel cortex

In the acute slice preparations, two main types of neuronal morphologies were observed by 2-photon imaging of fluorescent dye filled cells. The most prominent cell morphology exhibited radially extended dendrites and lacked an apical dendrite; these cells are morphologically similar to L4 spiny stellate cells. The other, rarer, type had a long apical dendrite that extended towards the more superficial cortical layers. These pyramidally-looking cells could be explained in a number of ways. They could be migrating pyramidal neurons that are passing through L4 to establish L2/3. However, the morphology of the imaged cells does not reflect the typical bipolar feature of migrating neuron (Noctor et al., 2004). Another option is that these neurons are spiny stellate neurons that have not retracted their apical dendrite yet. However, long term imaging studies reported that the retraction of the apical dendrite and dendritic refinement is close to completion by P5 (Mizuno et al., 2014; Nakazawa et al., 2018); as P7 is the youngest age of these experiments, and pyramidal-like neurons were imaged at various ages, including P15, it is unlikely that this can account for these observations. There is also a possibility that these cells are pyramidal neurons from L2/3 or L5 that have been patched by mistake, close to the border from L4. However, the morphology of L5 giant pyramidal cells and L2/3 cells is very recognizable, so while that is a possibility, it is unlikely. Finally, the most likely option is that the pyramidal-looking cells are L4 star pyramidal neurons, as these cells have been described to have an apical dendrite and sparsely populate the L4 barrels (Simons and Woolsey, 1984; White and DeAmicis, 1977). The incidence of these cells was low, so they were not excluded from subsequent analysis.

Spiny stellate neurons in the barrel cortex are oriented so that the cell bodies are preferentially located towards the periphery of the single barrel, while they project their dendrites towards the middle of the barrel (Simons and Woolsey, 1984; Steffen and Van der Loos, 1980; Woolsey et al., 1975). The biased orientation of spiny stellate neuron dendrites toward the centre of the barrel hollow has been proposed be optimal to sample the direct thalamocortical input (Arnold et al., 2001; Koralek et al., 1988). In this study, several, but not all, spiny stellate neurons extend their dendritic branches preferentially towards one side of the field of view. The development of this orientation is a dynamic process that has been reported to occur between P3 and P6 (Nakazawa et al., 2018). As no independent marker for the barrels has been used in these preparations, we can only speculate that the cell bodies of the spiny stellate neurons

align with the barrel walls and send their dendrites towards the middle of the barrel, consistently with previous literature (Arnold et al., 2001; Egger et al., 2008; Koralek et al., 1988; Nakazawa et al., 2018). Whilst the lack of biased dendritic orientation could be due to a delay in dendritic gross morphological refinement in the youngest pup imaged, it is unlikely to be the case in P14 brains. However, as barrels are 3D structures, the fact that we cannot see the orientation in the projected images does not exclude the fact that this is due to the point of view of the image acquisition, i.e. that the neurons are towards the surface or at the bottom of the barrel and projecting dendrites perpendicularly to the imaging planes.

2.4.2 Methodological differences with previously published method

Focal synaptic stimulation on the dendrites of developing spiny stellate neurons has previously been shown to elicit NMDAR-mediated dendritic spikes in P15-20 mice (Lavzin et al., 2012).

In the present study, the aim was to replicate these results and determine at what postnatal age dendritic spikes first emerge during neuronal development. Therefore, similarly to the method employed by Lavzin and colleagues, focal synaptic stimulation was used to trigger dendritic spiking in L4 spiny stellate cells in pups aged P7-P20. Unfortunately, in contrast to the observations reported in that paper, characteristic nonlinearity of dendritic spikes was not detected at any of the ages examined. The protocol was adapted from the Lavzin paper, but a few details differed slightly (Table 2 shows the similarities and difference between the two protocols).

The mouse lines used in the two studies were different. Lavzin and colleagues performed their dendritic stimulations in CD1 mice, an albino outbred stock, while the present experiments were conducted in brains from either PSD95-eGFP on a C57BL/6J background or wild type C57BL/6J mice. However, PSD95-eGFP knock-in mice show no electrophysiological difference from the control wild type mice (Zhu et al., 2018) and no nonlinearity was present in the wild type mice either; so this is unlikely to be the source of the discrepancy between the results. The reason for using the PSD95-eGFP for these experiments was because the plan was to eventually relate function (dendritic spikes) to structure (presence of PSD95 in specific dendritic branches).

Moreover, in the present study electrodes were pulled from glass capillaries and used for both whole-cell patch clamp and dendritic stimulation; this is a monopolar electrode, meaning that one pole is the electrode and the other pole is the ground

electrode in the bath. On the other hand, in the Lavzin paper, theta glass electrodes were used to deliver the focal synaptic stimulation; these glass electrodes are bipolar, containing two isolated channels, constituting the two poles, running along the length of the glass tube. The + and – poles are very close together and this conformation helps restricting the electric field, thus making it more local. Therefore, the differences in how focal the synaptic stimulation actually is could be the cause of the discrepancy; using a monopolar electrode producing a less local stimulation might mean that the neuron is being driven too much from the beginning, and therefore the dendritic spikes may already being occurring at the lower intensities, thus preventing the detection of the nonlinearity characteristic of the dendritic spikes.

The concentrations of the components for the intracellular solution and ACSF were also slightly different. The Alexa Fluor dyes used to visualise the neuron were of different wavelengths, but the same concentration was used in both studies; therefore, this is unlikely to have made a difference.

The recordings analysed only contained subthreshold traces, while traces containing action potentials were removed. The reason for the exclusion of traces containing somatic action potential was based on the assumption that dendritic spikes are subthreshold events; single dendritic spikes have been shown not to be sufficient to elicit a somatic action potential (Larkum et al., 2009; Lavzin et al., 2012; Milojkovic et al., 2005; Palmer et al., 2014; Polsky et al., 2004). In the reference paper, it is not mentioned if any adjustments to avoid somatic spiking were taken, and the NMDAR-mediate dendritic spikes presented in the figures did not have any overriding somatic spikes. There is, however, a possibility that in my preparation focal synaptic stimulation is triggering somatic action potentials quickly and this is masking underlying dendritic spiking activity.

The generation of dendritic spikes relies on the stimulation of synapses on a single dendritic branch, which triggers the local event. While care was taken in selecting a relatively spatially isolated dendritic branch, in a few instances, especially in older ages, this was rendered more difficult by the presence of sister dendrites around the stimulated dendrite. Furthermore, for the axons to be stimulated they need to be within the range of the electric field generated by the stimulating pipette (located close to the dendrite); however, there is no way of controlling the location on the dendrite (of the patched cell or other cells) where that axon makes synapses. This adds more confounding factors to the specificity of the targeting of a single dendritic branch, which is crucial for the subthreshold synaptic response of dendritic spikes. Additionally, the axonal density and innervation is likely to change over development

and this developmental shift may affect the results. Glutamate uncaging on visually-identified synapses on a single dendritic branch would be a way to more efficiently control the activation of synapses.

In general, the imprecision of stimulation range, the intrinsic cellular properties, and cell morphology might have added extra variability in the results presented in this study. The stimulation of more than one branch increases the risk of reaching threshold and driving an action potential, which then would make the detection of dendritic spikes more complicated. This may constitute an additional possible factor that may have influenced the results.

	Lavzin et al., 2012	*My protocol*
Mouse breed	CD1 mice, P15-20	C57BL/6J mice or PSD95-eGFP, P7-20
FSS protocol	1 stimulation	5 stimulations at 50 hz
FSS electrode	Theta electrode	Patching electrode (3-5 MΩ resistance)
Whole-cell patching electrode	Patching electrodes (6-10 MΩ)	Patching electrodes (3-5 MΩ)
Fluorescent dye	Alexa Fluor 633 (50 µM)	Alexa Fluor 594 or 488 (50 µM)
ACSF components (mM)	NaCl (125) $NaHCO_3$ (25) Glucose (25) NaH_2PO_4 (1.5) $CaCl_2$ (2) $MgCl_2$ (1)	NaCl (119) $NaHCO_3$ (26.5) D-Glucose (11) NaH_2PO_4 (1) $CaCl_2$ (2.5) $MgCl_2$ (1.3)
Intracellular solution composition (mM)	KGluconate (135) KCl (4) HEPES (10) Na2 phosphocreatine (10) GTP (0.3) Alexa and biocytin (0.05) pH 7.25 Osmolarity 285 mOsm	$KMeSO_4$ (130) NaCl (8.5) HEPES (10) NaGTP (0.3) EGTA(0.5) Alexa and biocytin (0.05) pH 7.25 Osmolarity 285 mOsm
NMDAR function block	APV or MK801	15mV hyperpolarisation

Table 2. Differences between the published and my protocol for dendritic spike generation
Differences in terms of mouse breed, focal synaptic stimulation (FSS) protocol and solutions are highlighted.

2.4.3 Dendritic spikes during development

Dendritic spikes occurring during development could lead to synaptic functional clustering that could potentially increase the computational efficiency of the processing of neuronal signals. *In vivo* studies showed that, during development, spontaneous activity preferentially activates synapses located nearby in CA3 pyramidal neuronal dendrites (Kleindienst et al., 2011) and in the visual system (Winnubst et al., 2015). This synchronicity between spatially close synapses was also found to be essential for synaptic regulation, as synapses asynchronous with respect to their neighbours became depressed (Winnubst et al., 2015). However, whilst the idea of developmentally regulated dendritic spikes as a mechanism to direct physical and functional synaptic clustering is extremely enticing, there is no conclusive evidence that this occurs in our model system yet. Furthermore, the electrophysiological and morphological nature of young immature neurons could mean that possibly NMDA spikes are not such a prevalent phenomenon, or they are not present at all, and this is the reason they could not be detected in our preparations.

2.4.4 Effects of hyperpolarising the membrane potential of L4 cells

Hyperpolarising the cell should reduce the activation of NMDARs by preventing the release of a voltage-dependent Mg^{+} block, which constitutes a physical block to ion entry through the channel (Nowak et al., 1984). However, hyperpolarisation should also increase the driving force for EPSP (as it places the Vm further from the reversal potential for AMPARs and NMDARs). The lack of dendritic spiking in these experiments may be due to the small engagement of NMDARs in these young neurons of the barrel cortex. However, comparisons between the kinetics of the maximum responses between the control (Vm maintained at 60mV) against the hyperpolarised (Vm maintained at 75 mV) condition suggested that the area under the curve, but not the amplitude, of the response is affected by the interference with NMDAR activation. A reduction in the area under the curve, but not the amplitude, of the postsynaptic response suggests that the EPSPs are longer in duration in the control condition. Therefore, decreasing the membrane potential of the cell by 15 mV is potentially affecting the slow, NMDAR-mediated component of EPSPs.

The fact that a significant NMDAR-dependent effect was detected in our preparation suggests that these receptors contribute to the EPSPs. However, since dendritic spikes were not observed using our analysis methods, the drive from the focal synaptic stimulations may just not be enough to trigger non-linear NMDAR-mediated dendritic events. A way to get around this problem and increase the activation of

NMDAR could be to do a sequence of 2 or more stimuli to try and test whether the resulting depolarising input is then sufficient to elicit dendritic spikes.

Furthermore, to achieve a more robust and reliable block of NMDARs, pharmacological blockers (e.g. the intracellular MK801 or the extracellular APV) can be used. This method would help ascertain the involvement of these receptors directly.

An age-dependent effect was also observed, by which the maximum EPSPs postsynaptic response increased with development. This is likely to reflect changes in the intrinsic properties of developing neurons. Fig. 2.7 shows the subthreshold EPSP responses from a single cell, in four brain slices from P7, P11, P15 and P20 mice. The responses at P20 appear considerably larger (note the difference in scale compared to traces from the other ages). This suggests that changes in dynamics and kinetics of ion channels underlying this response might be responsible for the developmentally regulated increase in the maximum EPSP observed in these cells.

2.4.5 Future experiments

The present study failed to replicate the previously published results showing NMDAR-mediated dendritic spikes in L4 neurons in P15-20 mice. In my hands, I could not elicit nonlinear responses to focal synaptic stimulation between P15-20 and in younger ages. A future experiment will be to elicit dendritic spike using a more spatially precise technique: photostimulation via glutamate uncaging. Glutamate uncaging allows to specifically target fluorescently identified dendritic spines by using 2-photon lasers to release glutamate from its chemical cage, at a specific location. This method has been previously used to trigger dendritic spiking in adult pyramidal neurons (Schiller et al., 2000). Similarly to focal synaptic stimulations, the aim is to increase the synaptic input until dendritic spike threshold is reached and a local nonlinear event occurs. This is achieved by uncaging glutamate on an increasing number of synapses, allowing a greater spatiotemporal control over synaptic input than was possible with focal synaptic stimulations. The downside of this method is that it is not clear that this pattern of activation would ever take place physiologically. However, it would inform us of whether regenerative nonlinear dendritic events are able to be supported by developing neurons.

Chapter 3: Developmentally regulated changes of PSD95 and SAP102 expression

3.1 PSD95 and SAP102

Members of the DLG subfamily of the MAGUK proteins form a protein network at the synapse which is extremely important for the correct transmission of neuronal signals. Whilst they share the main functional domains and all are involved to some degree in the recruitment, trafficking and/or scaffolding of receptors, these different proteins differ in terms of binding partners, subcellular localisation and orientation, dynamics and temporal expression during development.

This study focuses on two members of the MAGUK family of proteins: PSD95 and SAP102. PSD95 is a major component of the mature post-synaptic density of excitatory synapses (Cheng et al., 2006; Kennedy, 1997; MacGillavry et al., 2013; Nair et al., 2013; Sheng and Hoogenraad, 2007). and has been shown to promote synaptic maturation; on the other hand, SAP102 is a more dynamic and developmentally expressed protein that is involved in receptor trafficking at synapses (Elias et al., 2008; Sans et al., 2003; Washbourne et al., 2002).

Therefore, the comparison between the laminar expression of PSD95 and SAP102 provides a way to investigate changes in synapse maturation during brain development, as neurons in the layers develop and intracortical and long-range circuits. However, there are no studies that focus on a systematic interrogation of the presence of PSD95 or SAP102 in the cortical layers and how this might change at different stages of development, as the layers form and neuronal circuits are established and refined.

3.1.1 Aims:

1. Establish whether SAP102 and PSD95 follow a cortical layer-specific pattern of expression

2. Investigate whether the distribution of SAP102 and PSD95 changes over the course of development

3. Compare the temporal-spatial trajectory of SAP102 and PSD95

3.2 Methods

3.2.1 Mouse strains and breeding

All following procedures were conducted in accordance to the Animal Scientific Procedures Act 1986 (Home office, UK) and approved by the University of Bristol Animal Welfare and Ethics Review Board.

PSD95-eGFP and GKD mice (Fig. 3.1) were provided by Seth Grant (University of Edinburgh). In both mouse lines, a fluorophore was fused in-frame to the C-terminus of the wildtype protein, which was expressed under the endogenous promoter, using gene targeting (Zhu et al., 2018). In the PSD95-eGFP mice, PSD95 is fused to a single eGFP molecule (Broadhead et al., 2016). The GKD mice express endogenous PSD95 tagged with eGFP, endogenous SAP102 tagged with monomeric Kusabira Orange 2 (mKO2) and a tandem affinity purification (TAP)-tagged NR1 subunit3.

Adult mice from the two mouse colonies were kept in the same room on a 12/12 light/dark cycle. The cages contained the same enrichment consisting of a cardboard tube and nesting material (shredded paper). Groups of same sex siblings consisted of maximum 4 animals, to avoid overcrowding of the cages. Breeding mice were housed in cages as mating pairs or trios and checked daily for the presence of pups. Pups born on the same day were recorded as P0 and the pups were weaned 21 days post birth. All genotypes were maintained on a C57BL/6J background.

Breeding was devised and monitored to have a constant supply of 4-20 day old homozygous pups. At arrival, PSD95-eGFP original breeders were homozygous (PSD95eGFP/eGFP). On the other hand, the GKD mice were all homozygous for PSD95-eGFP and NR1 epitope but a mix of homozygous and hetero- and hemizygous for SAP102-mKO2 ($PSD95^{eGFP/+}$, $GRIN1^{TAP/+}$, $SAP102^{mKO2/+}$, $SAP102^{mKO2/X}$, $SAP102^{mKO2/\ Y}$). SAP102 is located on the X chromosome, therefore males can be hemizygous for SAP102-mKO2 or they are wildtype. The GKD mice were strategically paired in order to obtain SAP102 homozygous females and hemizygous males from one pair (homozygous female $PSD95^{eGFP/+}$, $GRIN1^{TAP/+}$, $SAP102^{mKO2/+}$ crossed with hemizygous male $PSD95^{eGFP/+}$, $GRIN1^{TAP/+}$, $SAP102^{mKO2/Y}$), and a mixture of homozygous, hemizygous and wild type (for SAP102) genotypes from a trio (2 heterozygous females $PSD95^{eGFP/+}$, $GRIN1^{TAP/+}$, $SAP102^{mKO2/X}$ crossed with hemizygous male $PSD95^{eGFP/+}$, $GRIN1^{TAP/+}$, $SAP102^{mKO2/Y}$). Pups born within a day were checked for fluorescence using a flashlight paired with a set of coloured glass goggles (Nightsea, USA). The

fluorescence across the whole brain was bright enough to be detected on the dissected brain at any age (Fig. 3.2) and through the thin skull and meninges at younger ages.

Table 2 shows the exact number of brain slices and animals used for the experiments with the PSD95-eGFP and GKD mice.

	PSD95-eGFP		**GKD**	
Postnatal day	*Number of animals*	*Number of slices*	*Number of animals*	*Number of slices*
4	3	10	2	4
5	3	10	2	5
6	3	6	3	6
7	4	12	1	3
8	3	10	3	8
9	3	8	2	8
10	2	6	2	6
11	3	11	3	8
12	3	7	0	0
13	2	11	1	2
14	3	10	1	3
15	2	7	2	5
16	1	2	0	0
17	2	5	2	7
18	2	7	1	4
19	0	0	2	2
20	0	0	2	2

Table 3. Summary of animal numbers used for imaging experiments

For each postnatal day examined, a list of n numbers of animals and slices imaged for each mouse line are indicated.

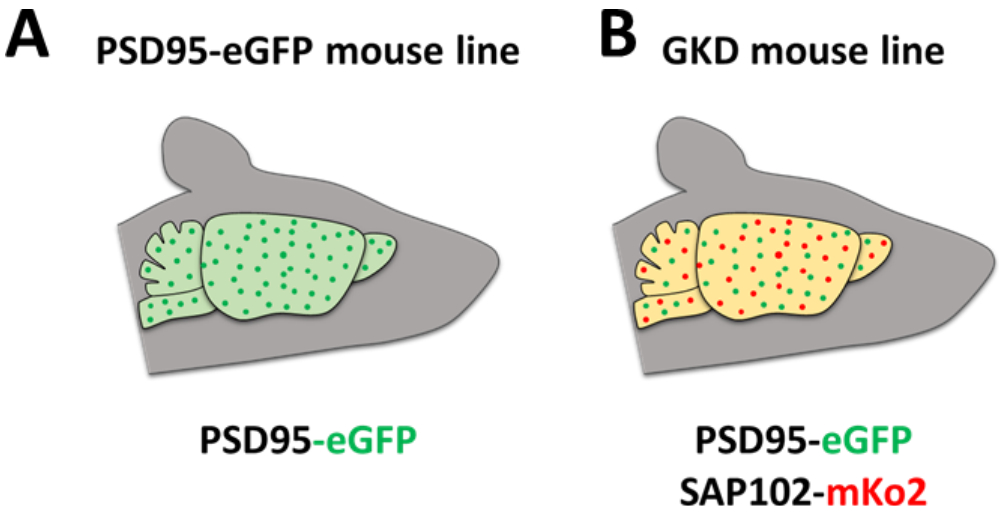

Figure 3. 1 The two mouse lines used for this study
A. In PSD95-eGFP mouse brains endogenous PSD95 is tagged with eGFP at the C-terminus. B. GKD mice express eGFP-tagged PSD95 and mKO2-tagged SAP102, allowing dual imaging of these proteins in the same slice preparations.

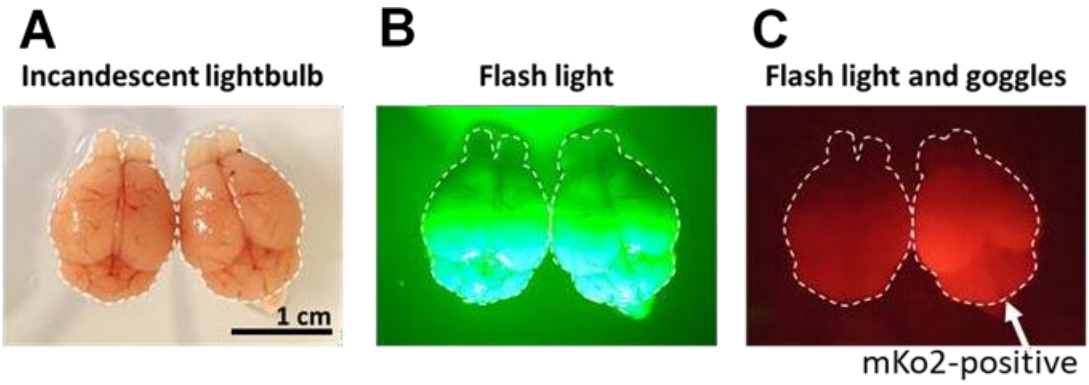

Figure 3. 2 Assessment of genotype using flashlight and goggles
Dissected brains from a P10 mouse observed under a lightbulb (A), a flashlight (B) and through goggles (C). The brain on the left in all the pictures is SAP102-mKO2 negative, while in the brain on the right SAP102-mKO2 is expressed.

3.2.2 Live 2-Photon imaging on thalamocortical PSD95-eGFP brain slices

Thalamocortical brain slices containing the barrel cortex were obtained from PSD95-eGFP mice between P5 and P20 as described in the previous chapter and in (Agmon and Connors, 1991, Fig. 3.3A). The tissue was left to rest at room temperature for 30-45 minutes and it was then imaged with an upright Prairie Ultima 2-Photon laser scanning microscope (Prairie Technologies, Madison, WI). Low magnification images of the barrel cortex were acquired using a 16X objective (Nikon, 0.8 NA). This objective allowed the capturing of cortical layers 1-5A at all the ages investigated, without the need to adjust to account for the growth of the tissue. High magnification images of the single barrels were obtained using a 60X water-immersion objective (Olympus, 1 NA). The settings of the 2-photon laser microscope (laser wavelength, power and gain) were kept constant throughout the study. PSD95-eGFP was excited using a 2-photon excitation wavelength of 910, using a MaiTai Ti-Sapphire tuneable laser (Spectra Physics), controlled through a Pockels cell (Thorlabs) and detected using a gallium arsenide phosphide (GaAsP) detector. The acquisition was controlled by the Prairie Software. Barrel structures in cortical L4 were identified by brighfield imaging using a 4X objective (Olympus, 0.1 NA). The thalamocortical section was then held in place in the perfused bath using a harp. 2-photon cortical z-stacks of 50-100 slices were acquired with a 60X immersion objective lens (1 µm step, 1024X1024 pixels, 2 times line average).

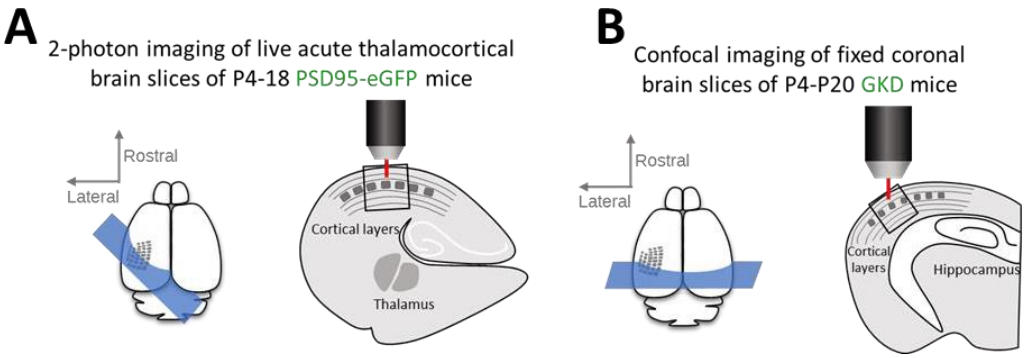

Figure 3. 1 Brain slice preparations for 2-photon and confocal imaging
A. PSD95 -eGFP mouse brains were sectioned to obtain thalamocortical slices, which were live imaged using a 2-photon microscope. B. GKD mouse brains were fixed and coronal sections were obtained. After mounting, they were imaged using a confocal microscope.

3.2.3 Coronal sectioning

GKD mouse brains were dissected in ice cold dissecting solution and drop fixed in 4% paraformaldehyde overnight. The brains were washed 3 times in phosphate buffer solution (PBS, VWR international) and stored at 4°C until needed. In preparation for sectioning, the brains were kept in a 30% sucrose solution for at least 1 day to cryoprotect the tissue. On the sectioning day, after embedding in optimal cutting temperature compound (OCT, Agar Scientific), the brain was sliced using a freezing microtome (Reichert) to obtain cortical brain slices (Fig. 3.3B). Individual slices were collected in a 90 well plate and kept in PBS at 4°C until either mounted or stained with antibodies.

3.2.4 Immunohistochemistry

The brain sections were collected using a thin brush and gently placed in a well of 6 well plate containing 2ml of block solution containing 0.3% triton-100X (Sigma-Aldrich) and 3% bovine serum albumin (BSA, Fisher) in equal parts. A maximum of 4 slices per well was established as optimal in order to avoid the sticking together of tissue due to overcrowding. After blocking for 1 hour on a rotating table at room temperature, the block solution was removed and the slices were incubated with 1.5 ml of complexin3 rabbit primary antibody in block solution (1:1000, Synaptic systems) overnight, on a rotating table at 4°C. After the incubation time, the tissue was washed 3 times for 15 minutes with 0.3% triton-100X solution (Sigma-Aldrich) and it was then incubated in the dark with 1.5 ml of block solution containing Alexa 633-conjugated goat anti-rabbit secondary antibody (1:500, Invitrogen) for 2 hours on a rotating table at room temperature. Slices were then washed with 0.3% triton-100X 3 times and were then mounted on superfrost slides (Thermo Scientific). The slides were left to dry at room temperature for either 30 minutes or overnight and mounting was finished by applying a couple of drops (~10 µl) of Vectashield hard mount medium containing DAPI (Vectorlabs) and a coverslip was gently lowered to the slide to minimise bubble entrapment. The slides were stored flat at 4°C until imaging. All this procedure was carried out minimising the exposure to light of the brain slices, to prevent bleaching of fluorophores.

3.2.5 Confocal imaging of coronal sections of fixed P4-20 GKD mice.

Confocal imaging was carried out with a Leica SP8 laser scanning microscope using a dry 10X (Leica, 0.4 NA) for the low magnification images and an oil-immersion 63X (Leica, 1.4 NA) for the higher magnification images. The settings for image acquisition were as specified in Fig. 3.4. 50 µm stack images were acquired (1 µm step size, 1024X1024 pixels resolution).

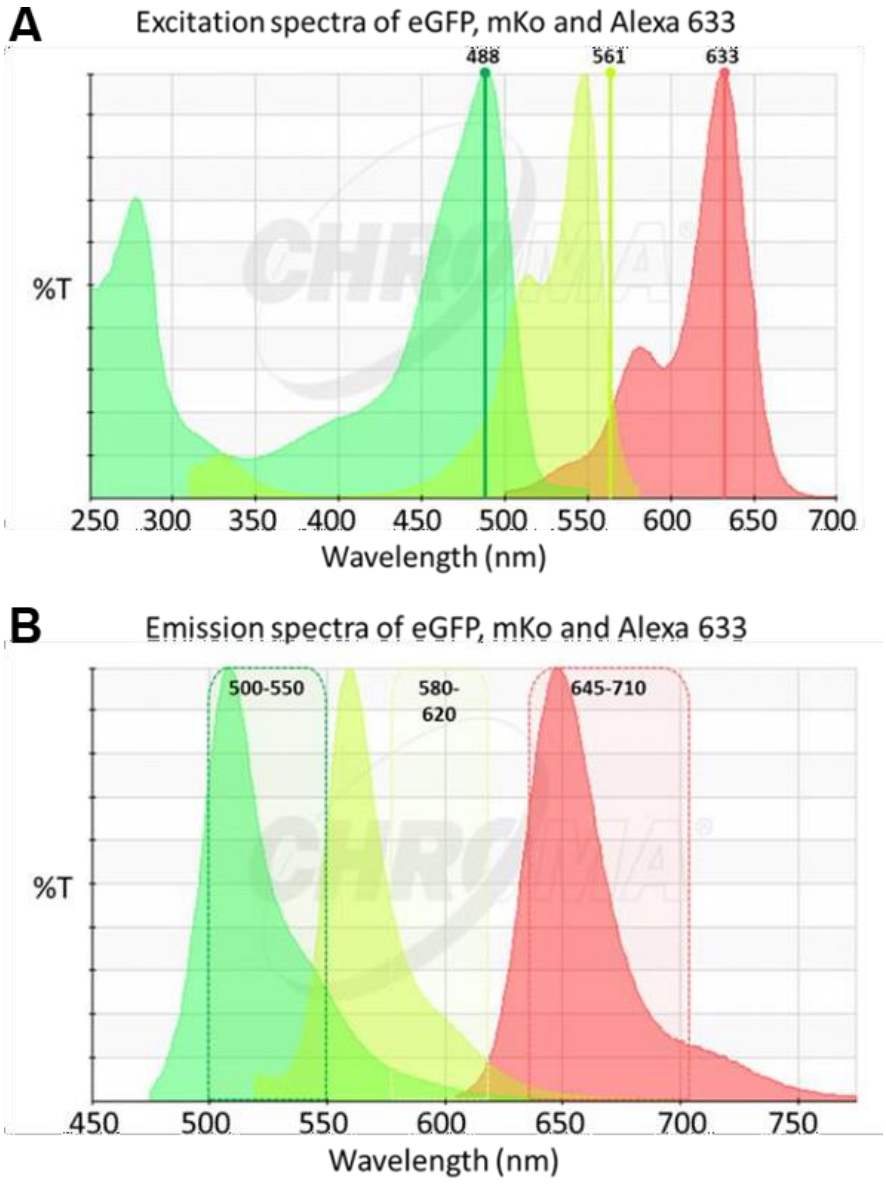

Figure 3. 2 Confocal spectra for imaging of SAP102, PSD95 and Alexa Fluor 633

Excitation (A) and emission spectra for eGFP, mKO2 and Alexa 633, and confocal settings used to image them. %T = percentage of transmission. Adapted from Chroma Technology corp. Spectra Viewer.

3.2.6 Distinguishing cortical layers based on anatomical landmarks

Cortical layers can be distinguished using specific anatomical landmarks, which are visible in PSD95-eGFP expressing brain sections (Fig. 3.5). Layer 1 is identifiable by its adjacency to the pial surface and the noticeably scarce presence of neuronal cell bodies. Layer 4 is recognisable by the presence of barrel structures within the barrel field of the primary somatosensory area. PSD95 is present in abundance inside the barrel edges and its levels are greatly reduced in the septa between the barrels. These anatomical landmarks were present from the earliest age that was examined (P4) and were clearly visible in bright field, 2-photon and confocal images. Layer 2/3 is defined by being flanked by layer 1 and layer 4. Finally, layer 5A is defined as the layer located just deeper of the barrels in layer 4. The layers deeper of layer 5A, layer 5B and layer 6 were not distinguishable by imaging PSD95 only, therefore the following analysis focused on the area between layer 1 and layer 5A only.

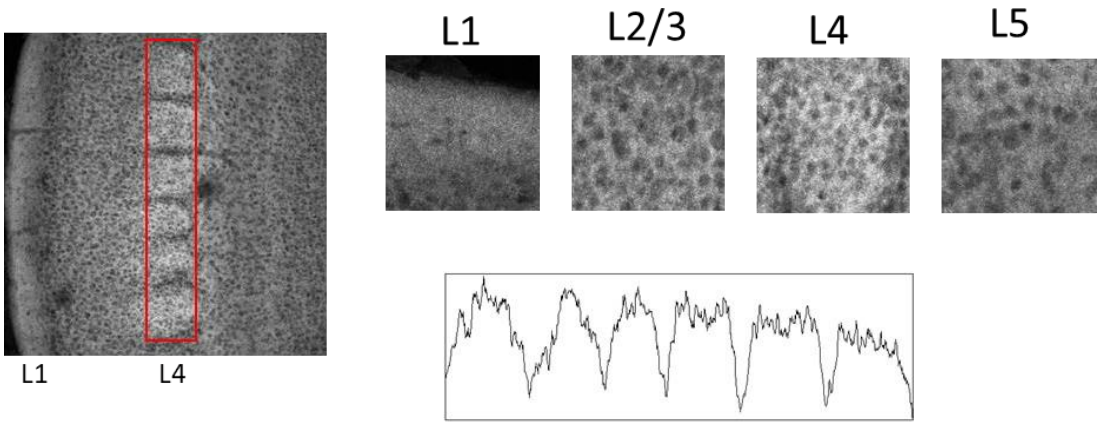

Figure 3. 3 Method to define cortical layers

2-photon images of the cortex of a P10 mouse. High magnification images show the different layers. L1 is clearly recognizable as it mostly lacks cell bodies and it's adjacent to edge of the slice. L4 contains the barrel structures (red rectangle on image and plot of the profile of fluorescence intensity). L2/3 is formed of highly dense pyramidal neurons and is in between L1 and L4. Finally, layer 5A is situated just deeper of L4.

3.2.7 Image analysis with ImageJ

Confocal images were analysed using ImageJ to extract the values of the intensity of fluorescence (Fig. 3.6 for experimental workflow). After performing a projection of the 50-frames image stacks according to the maximum intensity, the whole imaging field was selected and a plot profile function in ImageJ was run to calculate the average pixel intensity across the whole field of view. For each image, the distance of the pia (coinciding with the beginning of L1), the bottom of L4 (as identified by the top of the barrel field) and the boundary between L4 and L5 (as assessed by bottom of the barrel field) from the left edge of the image (pixels) was noted down and used to normalise the data. These values and all the values of the plot profile function were stored in a structure in MATLAB, ready for further analysis.

3.2.8 Analysis of plot profiles with MATLAB

Firstly, the raw data for both the distance and the intensity values of each plot profile was normalised. The distance (X) was normalised by using the values for the location of the pia ($X_{minimum}$) and the L4/L5 boundary ($X_{maximum}$) using the formula:

$$X_{normalised} = [X - X_{minimum}] / (X_{maximum} - X_{minimum})$$

This important step allows a comparison of the expression of the proteins of interest in the same layers at different timepoints by compensating for the expansion of the tissue during developmental growth. By maintaining the distance between L1 and the beginning of L5 we are then able to make meaningful comments on the relative expression of these proteins in the different layers and compare it between ages.

Secondly, the raw intensity (Y) was also normalised to the maximum intensity (usually in Layer 1) using the following formula:

$$Y_{normalised} = [Y - Y_{minimum}] / (Y_{maximum} - Y_{minimum})$$

Even though the settings used to acquire the confocal images were kept exactly the same for all the images acquired, this further normalisation helped compensating for any changes in lasers which were out of our control and regardless of the total level of fluorescence. Furthermore, this normalisation is pivotal to compare the fluorescence of the two fluorophore-tagged proteins at different timepoints as it normalises for changes in expression level by providing a relative measure of intensity across the cortical layers.

Finally, the normalised intensity data was binned in a consistent manner for all the data to provide smoother curves to analyse and facilitate averaging of profiles.

The plot profiles were plotted against each other across all the timepoints and comparisons between the levels of the three proteins across the different layers and how this changes during development was analysed.

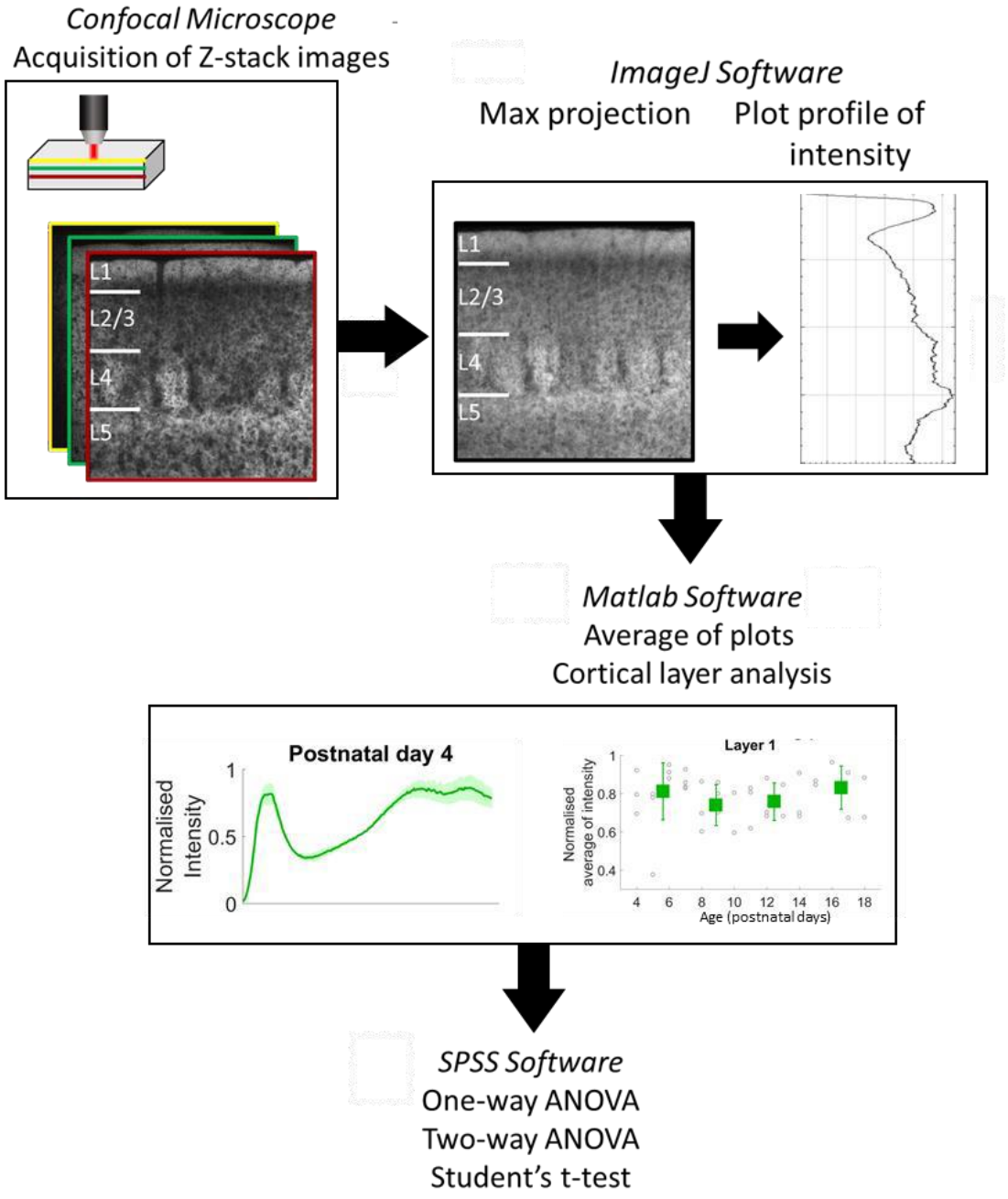

Figure 3. 4 Experimental workflow
Images of the cortex were acquired using either a 2-photon or confocal microscope. Following maximum intensity projection of the z-stacks using ImageJ, the plots of the intensity were averaged by animal for each age using Matlab. SPSS was used to perform statistical tests such as one- and two-way ANOVAs and t-tests.

3.2.9 Peaks of fluorescence in different ages

In order to further quantify the data and unpick the contribution to the fluorescence in the different cortical layers, small consistent sections of the fluorescence curve in each of the cortical layers were extracted and averaged together (Fig. 3.7). The areas selected was based on the manual image-based identification of the layers, based on anatomical landmarks. Following normalisation and binning, the x value for the pia was set at 0, while the boundary between L4 and L5A was set at 1. The areas of the data representative from each layer were isolated using the binned normalised distance value as a reference; L1 fluorescence values were selected just deeper of the pial surface (between 0.05 and 0.15), while L4 values were chosen between 0.8 and 0.95, 0.05 pixels before the L4/L5 boundary. L5 values were taken between 1 and 1.15. Finally, data for layer 2/3 was identified as the middle values in between the pial value (0) and the layer4/layer5A boundary (1), at 0.4 and 0.55. This measure unfortunately does not allow for a distinction between cortical layer 2 and layer 3, which is not easily achieved by our imaging paradigms, but it provides an objective manner to select these layers without relying on the imaging alone. The mean of the range of these fluorescence values and the standard errors of the means were calculated. Throughout the analysis of the fluorescence across the different layers, the curvature of the cortex was not taken into account. The profile of fluorescence was extracted for the whole imaging frame, and the above method of analysing a small portion within the layers helped balancing against areas from neighbouring layers crossing the borders.

The fluorescence in layer 1 consisted of a much narrower peak, compared to the other layers. This meant that the mean value did not appear to be representative of the actual intensity of fluorescence, but rather it fell lower. For this reason, a slightly different approach was adopted to calculate the mean peaks of fluorescence in this area. A larger area was selected starting from the pia (0 – 0.2), the maximum intensity value of this selected region was found and an average of 7 binned values on either side was calculated. This method results into a more accurate calculation of the average peak of layer 1.

3.2.10 Area under the curve

The raw fluorescence data was used to calculate the area under the curve. This parameter was computed using the “trapz” function in MATLAB (MathWorks, version R2018q). This function uses the trapezoidal method, which consists of breaking down the area into smaller trapezoids, thus approximating the integration of the area.

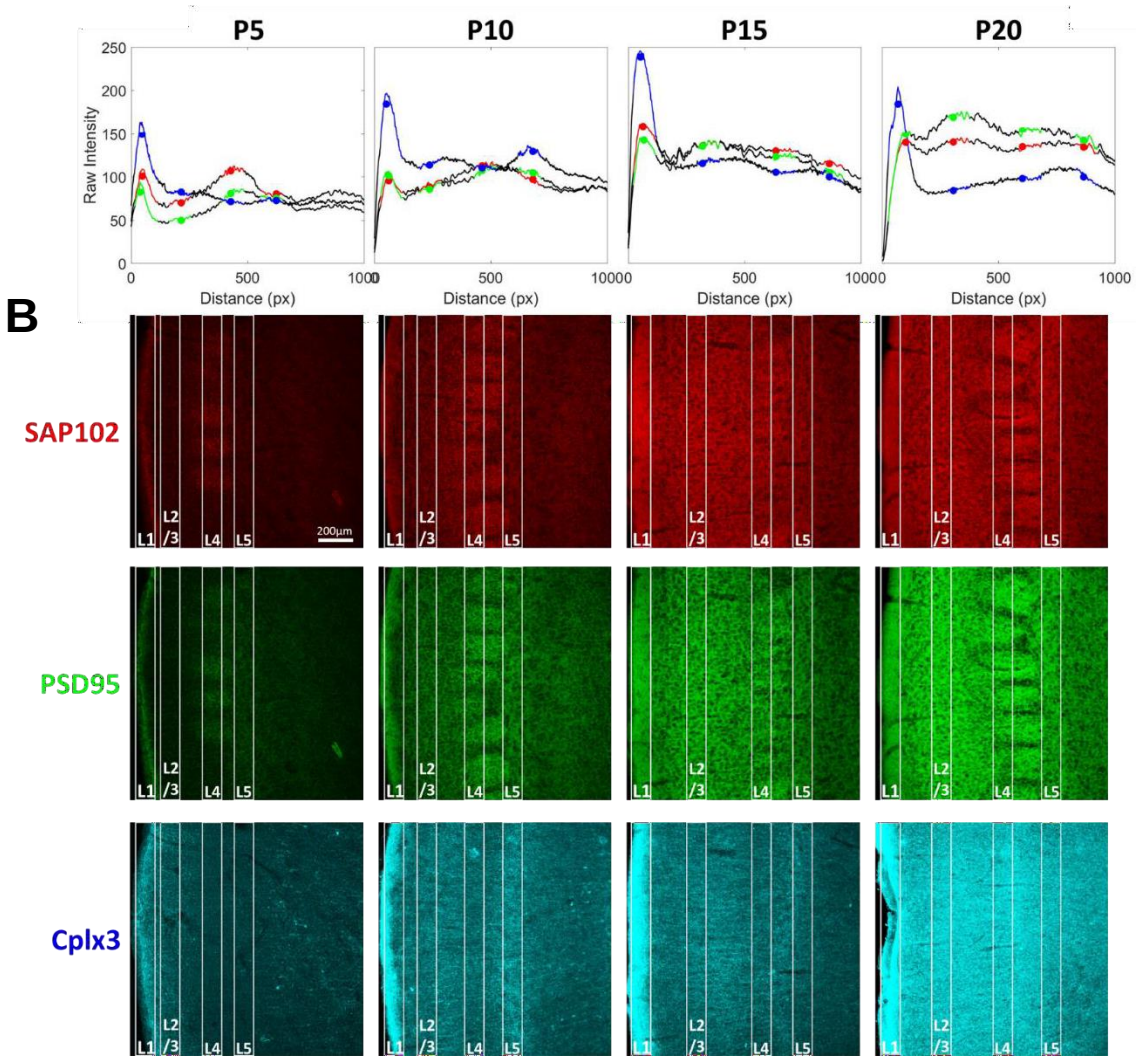

Figure 3. 5 Layer by layer analysis method

A. Plot profiles of intensity of fluorescence for example ages to show how the layers were selected in an objective manner for each analysis. The overlaid dot is the average for each layer (blue for Cplx3, red for SAP102 and green for PSD95).

B. shows the correspondent area of the image frame that was averaged.

3.2.11 Fluorescent puncta and colocalization analysis

The analysis of fluorescent puncta and the co-localisation between PSD95 and Cplx3 was achieved by running a custom Fiji macro (Stephen Cross, University of Bristol) on the high magnification confocal images acquired with 63X objective (Fig. 3.8). After thresholding the images (threshold multiplier 0.8), regions of interest were automatically drawn around the fluorescent puncta across the whole imaging field (minimum punctum area set to 0.01µm^2). For both the PSD95 and Cplx3 channel the density, area, intensity of puncta in each layer were calculated. The extracted parameters were then averaged for the whole image at all ages. Puncta colocalization was defined as any PSD95-eGFP punctum that overlapped for at least 25% of its area with Cplx3 puncta. This data was then plugged into Matlab to obtain averages and further analysis.

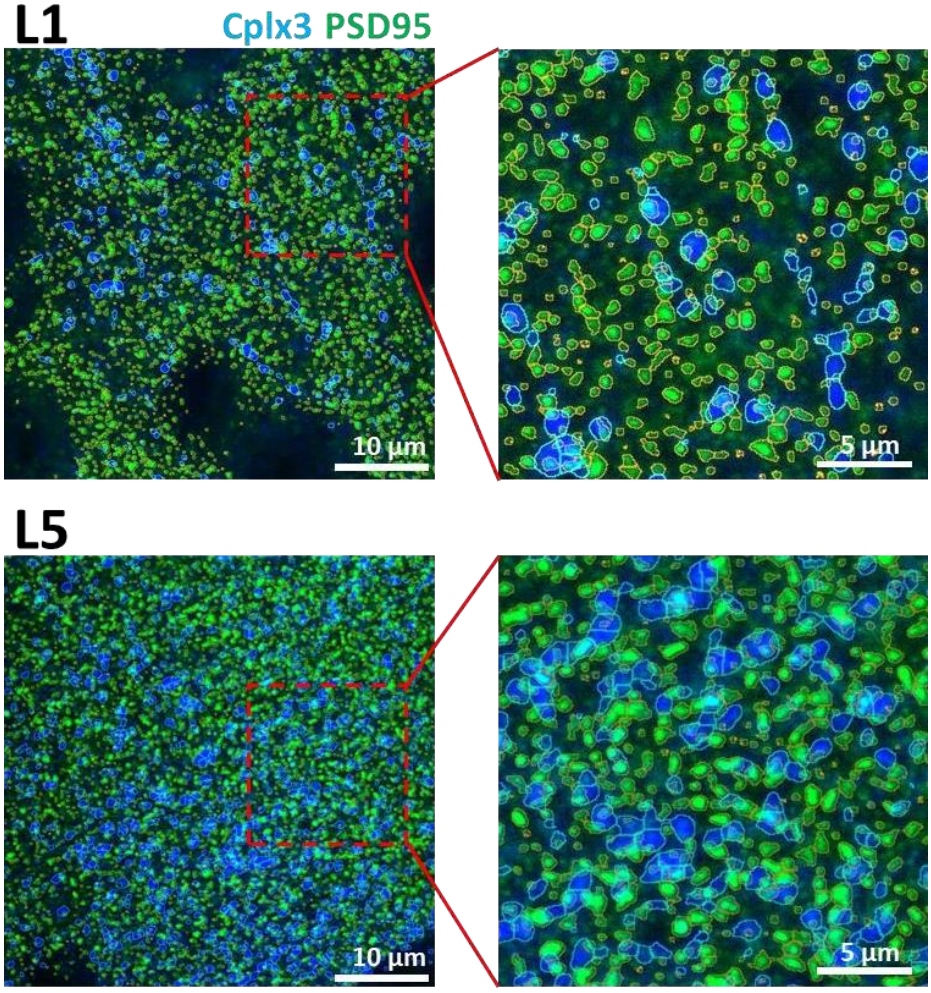

Figure 3. 6 Puncta analysis method

Single plane confocal images from L1 and L5 acquired with a 63X objective and 4X zoom. The zoomed in view shows the regions of interest that were identified by the ImageJ plug-in and used to extract information about puncta density, intensity and area and colocalization.

3.2.12 Statistical analysis and age-grouping

All statistical analysis was run on age-grouped data using the SPSS software. Whilst the data acquisition and the averages were carried out on a daily basis, grouping of the postnatal days was employed in order to account for natural variability in actual hours of birth (mice were checked for pups once a day, leading to 12-24 hours of imprecision) and to test differences between comparable sizes of animal numbers. The ages were grouped in a way to encapsulate reported critical periods of this somatosensory system: P4-7 (critical periods of thalamic inputs into L4, Barth and Malenka, 2001; Crair and Malenka, 1995), P8-10 (critical periods of spiny stellate cells in L4, Ashby and Isaac, 2011), P11-14 (critical periods of projections from L4 to L2/3, Lendvai et al., 2000; Maravall et al., 2004; Stern et al., 2001), P15-17 (critical periods for horizontal connections in L2/3, Wen and Barth, 2011) and finally the last timepoint P18-20.

When testing the changes of intensity of fluorescence of single fluorophores over development, a one-way ANOVA with Bonferroni *post hoc* test was run. When comparing the expression of the two proteins over time a two-way ANOVA was run to test for significance, and if the output showed significant interaction between the independent factors then multiple t-tests with Bonferroni correction were run to establish which elements were statistically significant. The new alpha value was 0.0125 for the 4 age groups of the 2-photon imaging and 0.01 for the 5 age groups of the confocal imaging.

3.3 Results

3.3.1 Developmental profile of PSD95

To assess developmental changes of the spatial expression pattern of PSD95-eGFP, 2-photon live imaging of thalamocortical PSD95-eGFP brain slices during the first 3 postnatal weeks was performed. Since the genetic tagging of PSD95 allows quantitative analysis of the anatomical distribution of this protein, layer-specific developmental profile of expression of PSD95-eGFP was constructed between P4 and P18.

The barrels in L4 were clearly visible both with the brightfield and 2photon imaging of the eGFP-tagged protein as early as P4 and until the last age imaged (P18, Fig. 3.9). The localisation of this cortical layer was instrumental to define the boundaries to the more superficial L2/3 and the deeper L5.

3.3.1.1 PSD95-eGFP appears as precisely distributed puncta

Live 2-photon imaging of thalamocortical brain slices revealed that PSD95-eGFP is distributed throughout the neocortex as fluorescent puncta (Fig. 3.10). In the cortical plate, the cell bodies are noticeable for the lack of fluorescence, as they appear as black circles. A closer look into the barrel-containing layer 4 shows how the puncta are preferentially located within the barrel boundaries, and as the brain grows and develops, the PSD95-defined barrel structures increase in size and the number of puncta appears to increase.

In order to explore the localisation of PSD95-eGFP puncta within the neuron, few individual neurons were patched and filled with Alexa Fluor 594 hydrazyde and 2-photon imaging was conducted (Fig. 3.11). Dual imaging of the dye filled neuron and PSD95-eGFP shows that PSD95-eGFP is found in some but not all dendritic spines during development. Despite the high fluorescence intensity within the L4 barrels, it proved to be difficult to identify PSD95-eGFP proteins in dendritic spines of spiny stellate neurons. The overlap between this protein and dendritic spines was most prominent in more mature looking spines, usually belonging to pyramidal neurons. These observations were mostly qualitative, more experiments will be required to further characterise the expression of PSD95 in spines and related morphology to function with functional studies.

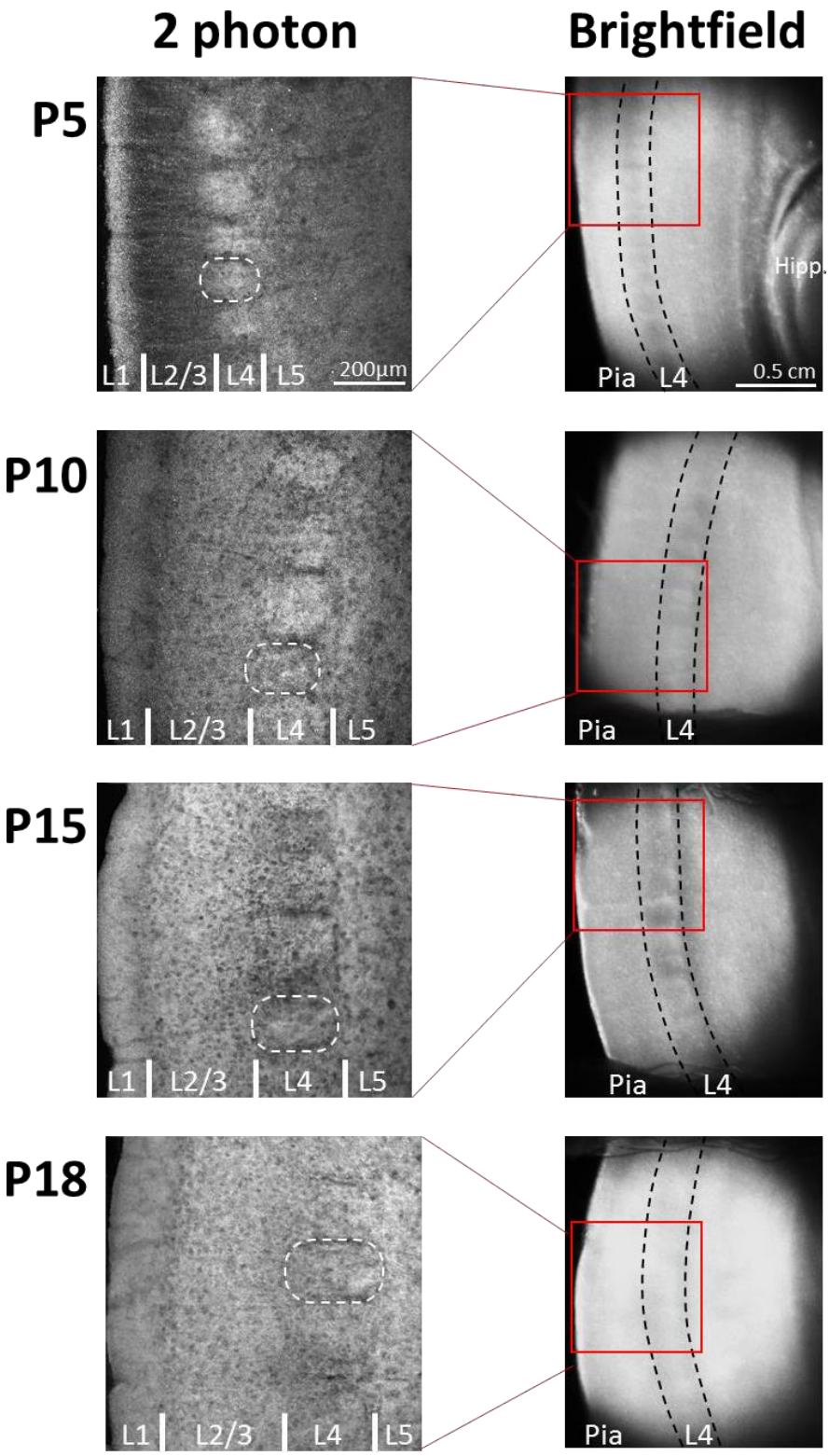

Figure 3. 7 2-photon imaging of the PSD95-eGFP brains

Example ages of cortical plates imaged and analyses. Images on the left show 2-photon images; the barrels are distinguishable in all ages examined (white dashed circles). On the right, brighfield images of the same thalamocortical slices. Scalebar same throughout.

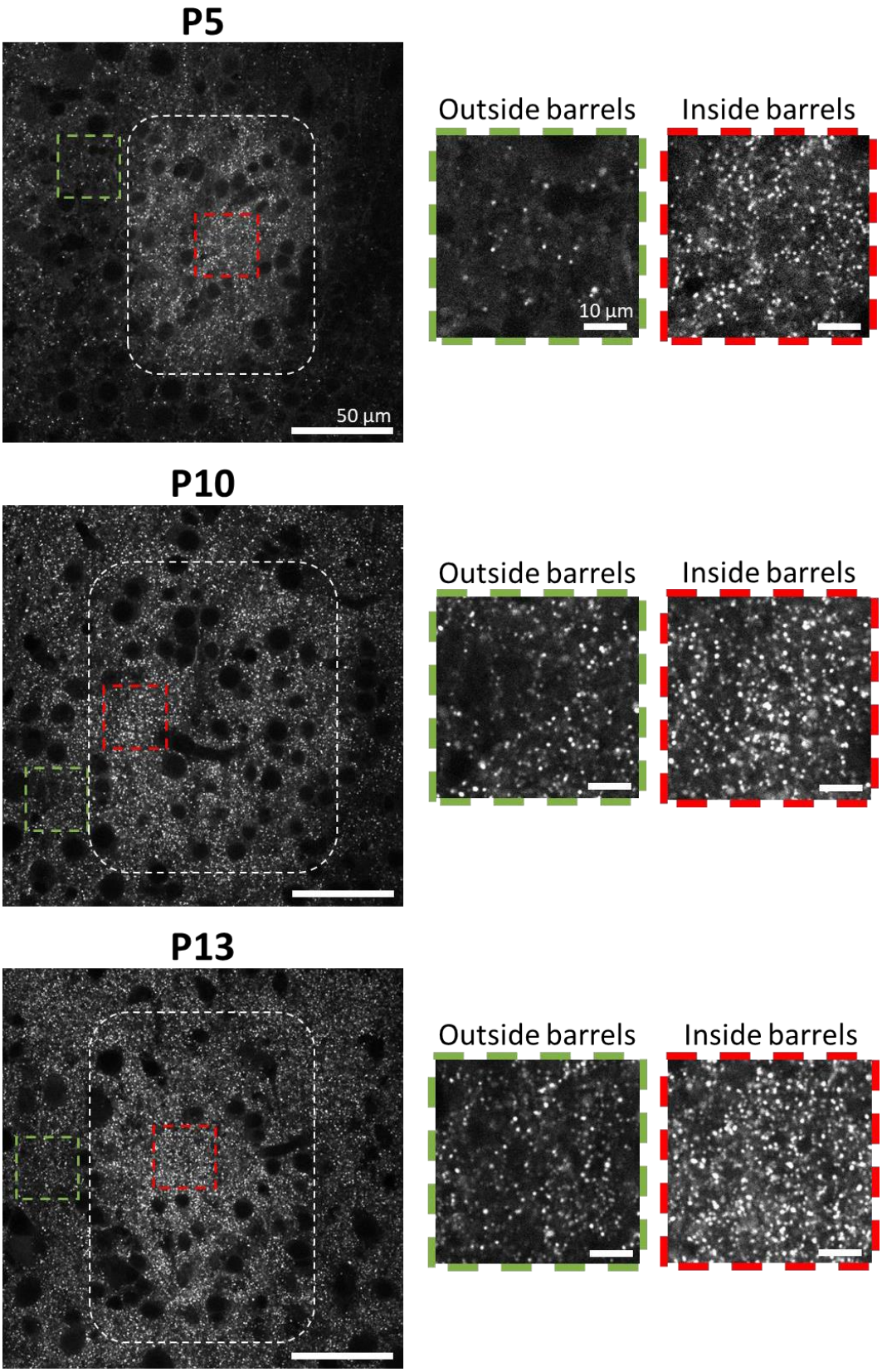

Figure 3. 8 PSD95-eGFP appears as puncta

2-photon images of the PSD95-eGFP mouse thalamocortical brain slices, showing barrels in L4 (white dashed circles). Images at the side show higher magnification sections to show that eGFP puncta increases over time and is mostly present within barrel hollows, rather than in the septa.

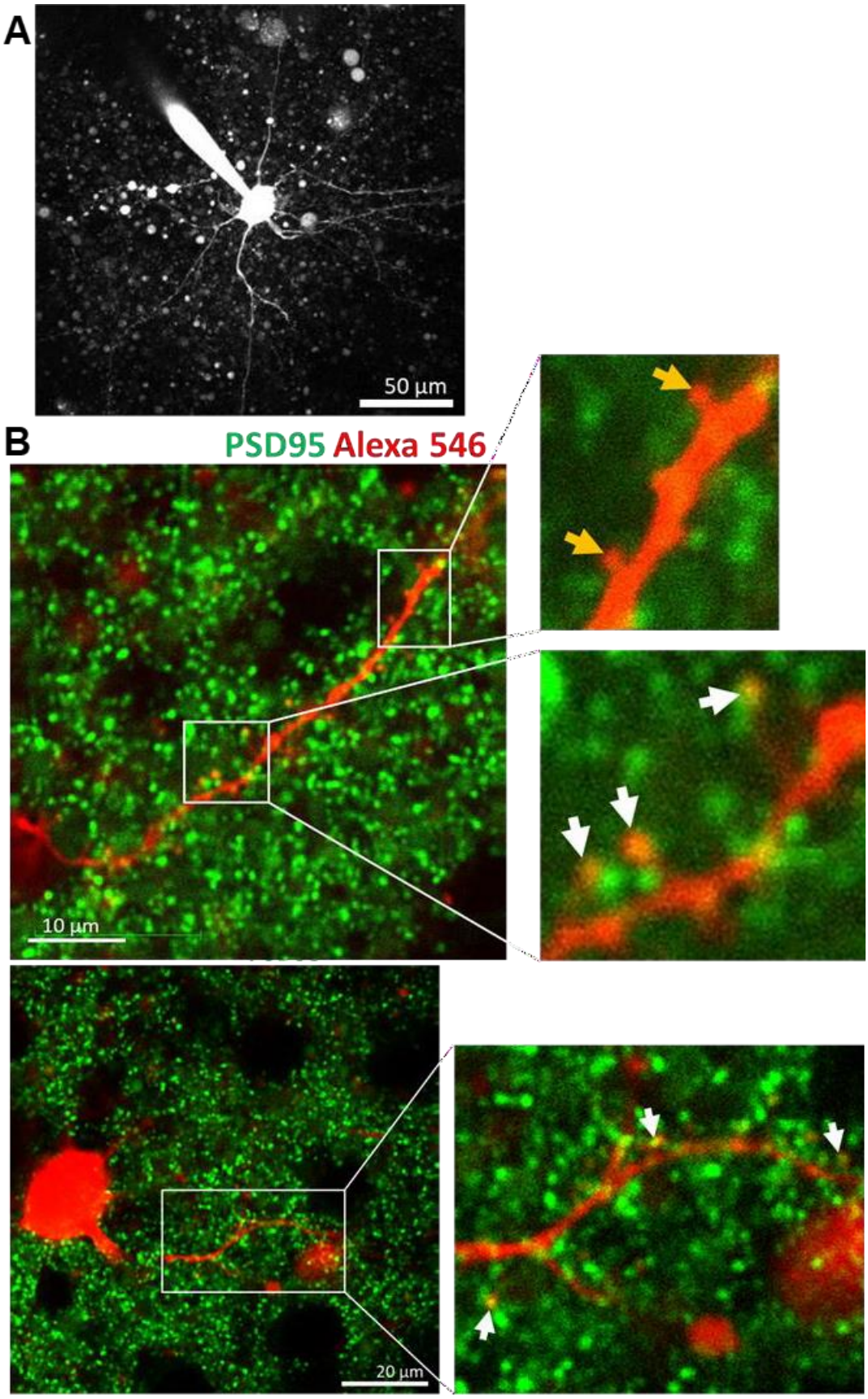

Figure 3. 9 Subcellular localisation of PSD95-Egfp

A. 2-photon maximum projections of PSD95-eGFP and an Alexa 594-filled cortical neuron from a P14 mouse. B. shows zoomed in images of dendrites and spines. White arrows show colocalization of PSD95-eGFP onto individual spines, while the yellow arrows show spines lacking PSD95-eGFP.

3.3.1.2 Laminar expression of PSD95-eGFP is developmentally regulated

In order to compare the expression of PSD95-eGFP in cortical layers during brain development, barrel cortices between P4 and P18 were fixed and the profiles of fluorescence across the field of view were analysed (Fig. 3.12).

The profiles of fluorescence were normalised to the maximum value, which was usually within L1. Sections of the profile plots representing L1, L2/3, L4 and L5A were averaged in order to investigate if the proportional (rather than absolute) intensity of the separate layers changed over development. Our results show that the expression of PSD95 follows a layer-specific distribution, which is developmentally regulated (Fig. 3.13).

The analysis of the 2-photon images shows that the relative levels of PSD95-eGFP in L1 are high from P4, the first time point examined. Whilst the high relative proportion of L1 remains constant during the 2 postnatal weeks investigated, the proportional intensity of fluorescence in L2/3, L4 and L5A undergoes a significant change in relative expression over time. The normalised PSD95-eGFP levels significantly increase in L2/3, sharply increasing between P4-7 and P11-14, reaching a stable level of expression from P15 onwards. On the other hand, the relative fluorescence intensity in L4 and L5A is stable between P4 and P15 and then significantly declines between P15 and P18. This result shows that there is a layer-specific enrichment of PSD95 and this changes as the brain grows and neuronal circuits refine.

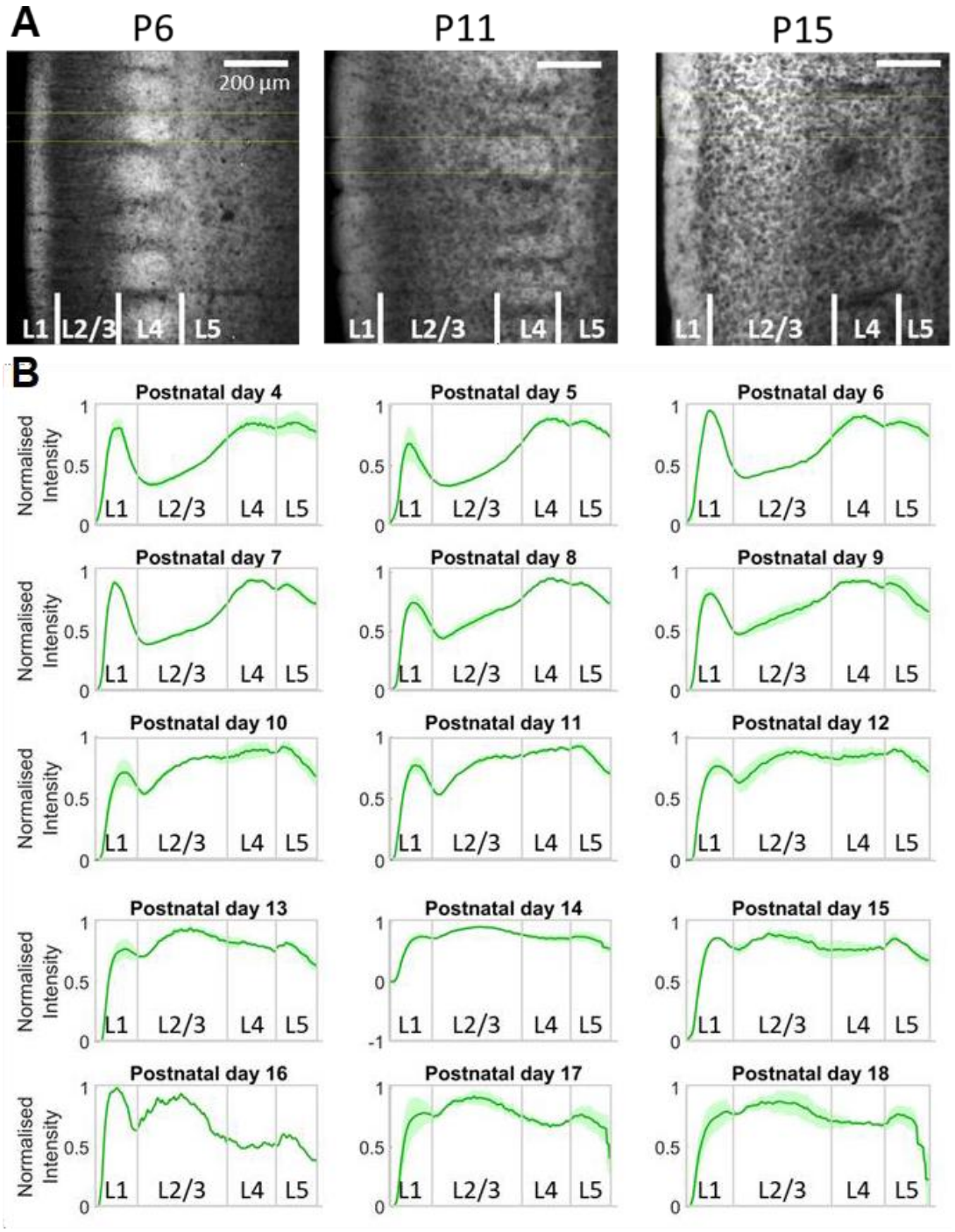

Figure 3. 10 Day-by-day analysis of profile of intensity of PSD95-eGFP

A. 2-photon images of example time points. Underneath is the plot profile of intensity for L4, showing the barrel structures. B. Averages of normalised plot of the intensity of the fluorescence for each postnatal day. Plots were normalised to the maximum intensity and the distance between L1 and L4 was normalised as well. In dark green is the average, in light green is the +/- SEM for each data point. Number of animals, number of slices: P4(3,10), P5(3,10), P6(3,6), P7(4,12), P8(3,10), P9(3,8), P10(2,6), P11(3,11), P12(3,7), P13(2,11), P14(3,10), P15(2,7), P16(1,2), P17(2,5), P18(2,7).

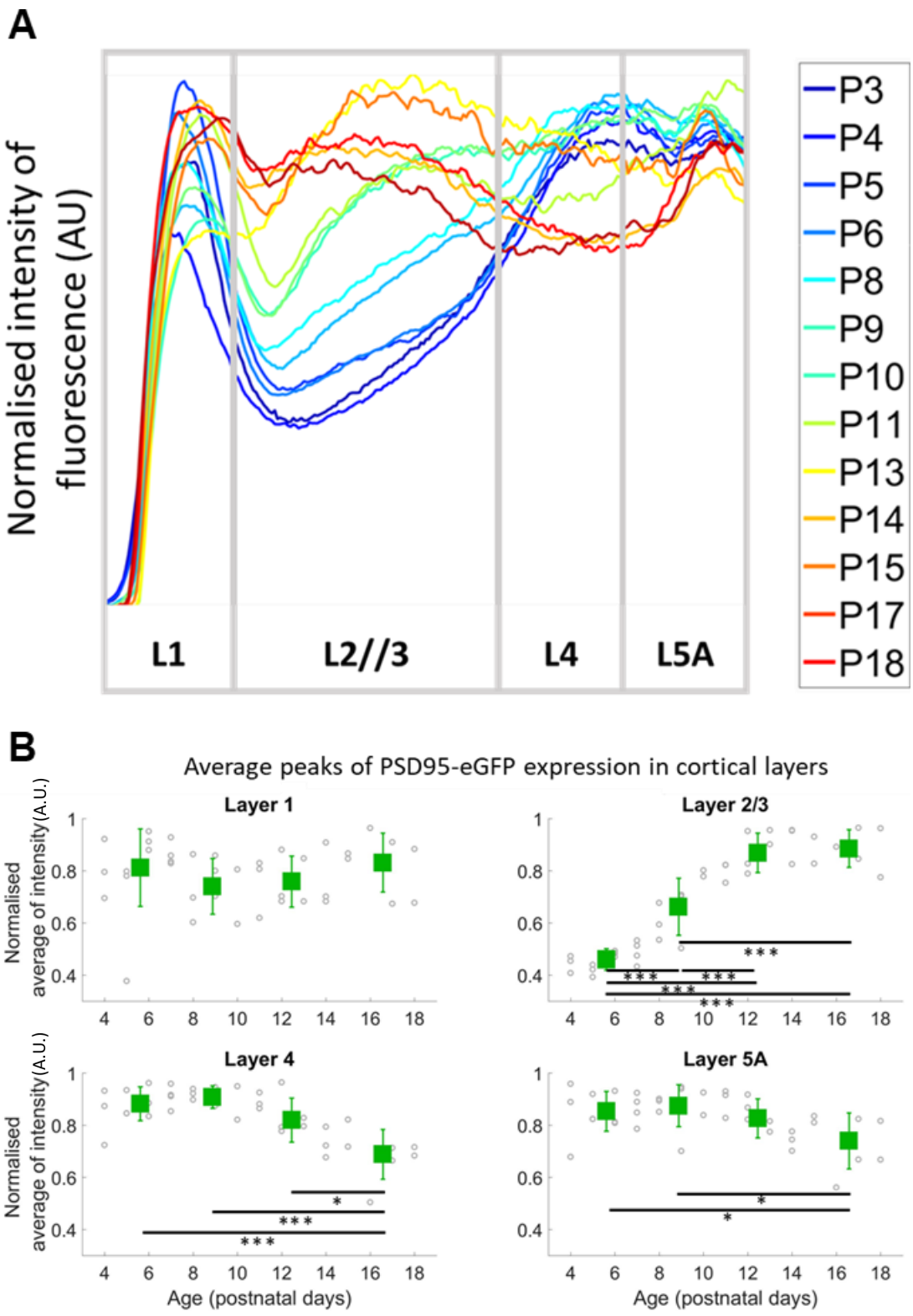

Figure 3. 11 Laminar profile of expression of PSD95-eGFP

A. PSD95-eGFP follows a layer-specific profile of expression in all layers except L1 where intensities remain constant. B. Averages of normalised data in grey open circles and averaged of the age groups in green filled squares. Error bars represent SEM. Number of animals, number of slices: P4(3,10), P5(3,10), P6(3,6), P7(4,12), P8(3,10), P9(3,8), P10(2,6), P11(3,11), P12(3,7), P13(2,11), P14(3,10), P15(2,7), P16(1,2), P17(2,5), P18(2,7). Statistical test: one-way ANOVA and Bonferroni post-hoc. * p<0.05 ** p<0.01 *** p<0.001.

3.3.2 PSD95 and SAP102

The analysis of the spatiotemporal expression of PSD95-eGFP in my previous experiments revealed that this protein is enriched in specific cortical layers and this pattern of expression changes over development. In the interest of understanding the sequence of events that occurs during brain and synaptic development, the cortical distribution of PSD95 and SAP102 during development was compared by imaging PSD95-eGFP and SAP102-mKO2 using the GKD mice pups.

3.3.2.*1 Confocal imaging of GKD mice*

After breeding to achieve the correct PSD95$^{eGFP/+}$/SAP102$^{mKO2/+}$ genotype, confocal images of coronal fixed brain sections were acquired. 2-photon imaging of live tissue was not to be suitable for the characterisation of SAP102 because we were not able to image the mKO2 fluorophore with sufficient brightness while minimizing bleaching.

Confocal imaging of fixed coronal brain slices shows that both proteins appear as fluorescent puncta across the tissue (Fig. 3.14).

As it was the case in the PSD95-eGFP mouse line, in the GKD mice both PSD95-eGFP and SAP102 proteins show a high barrel hollow-low septa distribution that allows the identification of the L4 barrels. This enables the detection of the layer boundaries at all the ages examined.

High magnification single confocal images of the cortex show a difference in the punctate distribution of SAP102-mKO2 and PSD95-eGFP. Whilst individual puncta can mostly be resolved, SAP102 puncta appear diffuse, while PSD95 appears in much more discrete clusters (Fig. 3.14A and B). Furthermore, the image with merged channels shows that there is not a complete overlap between these two proteins (Fig. 3.14C). The subcellular distribution of SAP102 and PSD95 is also distinct. Superimposing the images from the two channels also shows that, in neuronal cell bodies, SAP102-puncta are present in the cytoplasm, but excluded from the putative nucleus, while PSD95 is completely absent in both the putative nucleus and the whole cell body (Fig.15B). This is consistent with previous reports that PSD95 is mainly synaptic, while SAP102, while also enriched at glutamatergic PSDs, it is also cytoplasmic (El-Husseini et al., 2000; Müller et al., 1996; Sans et al., 2005; Zheng et al., 2010).

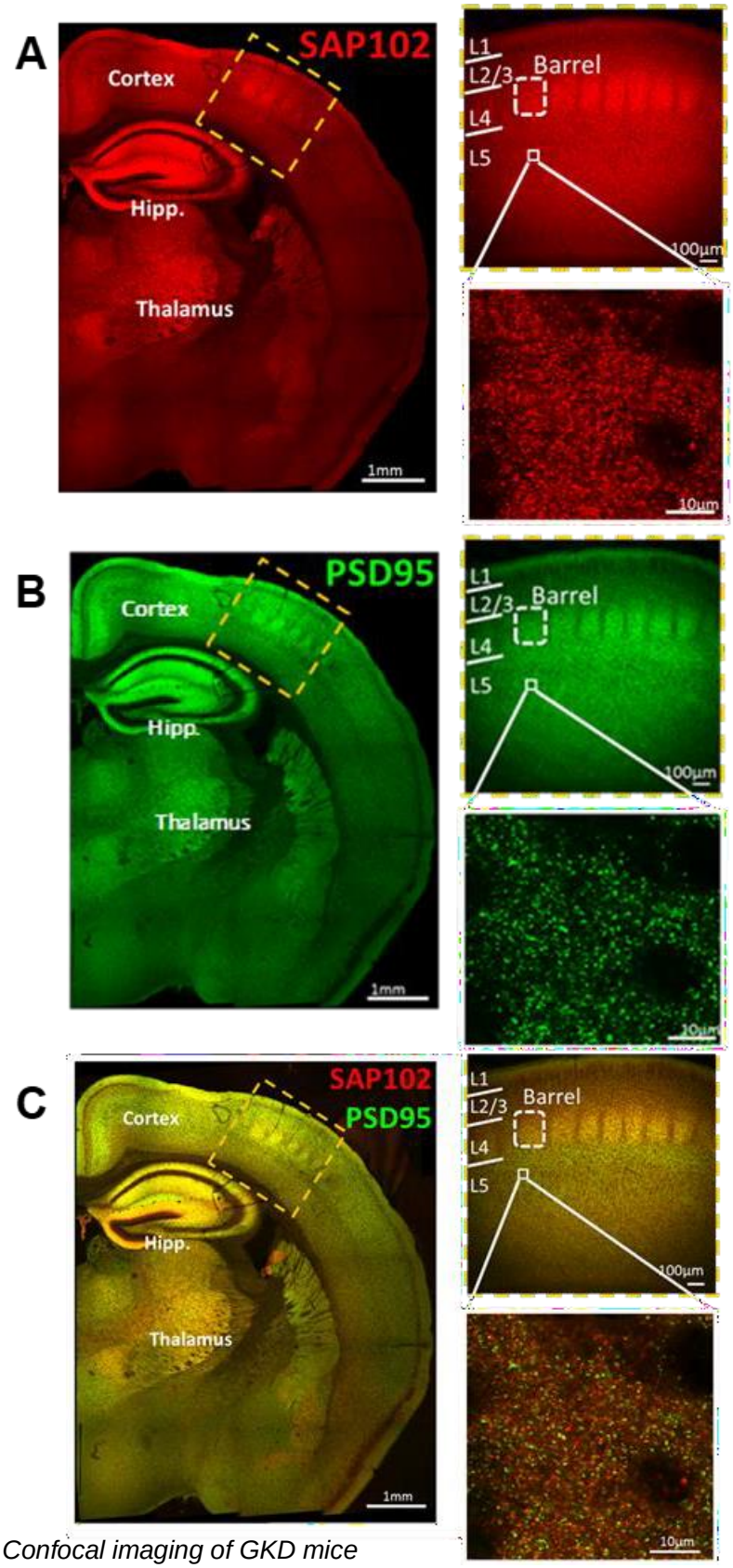

Figure 3. 12 Confocal imaging of GKD mice

Coronal sections of GDK mouse shows SAP102 (A), PSD95 (B) and a merged channel image (C) of a P15 mouse. Higher magnification images for both proteins and merged channels are found on right panels, showing the barrels (white dashed circle). Hipp, hippocampus.

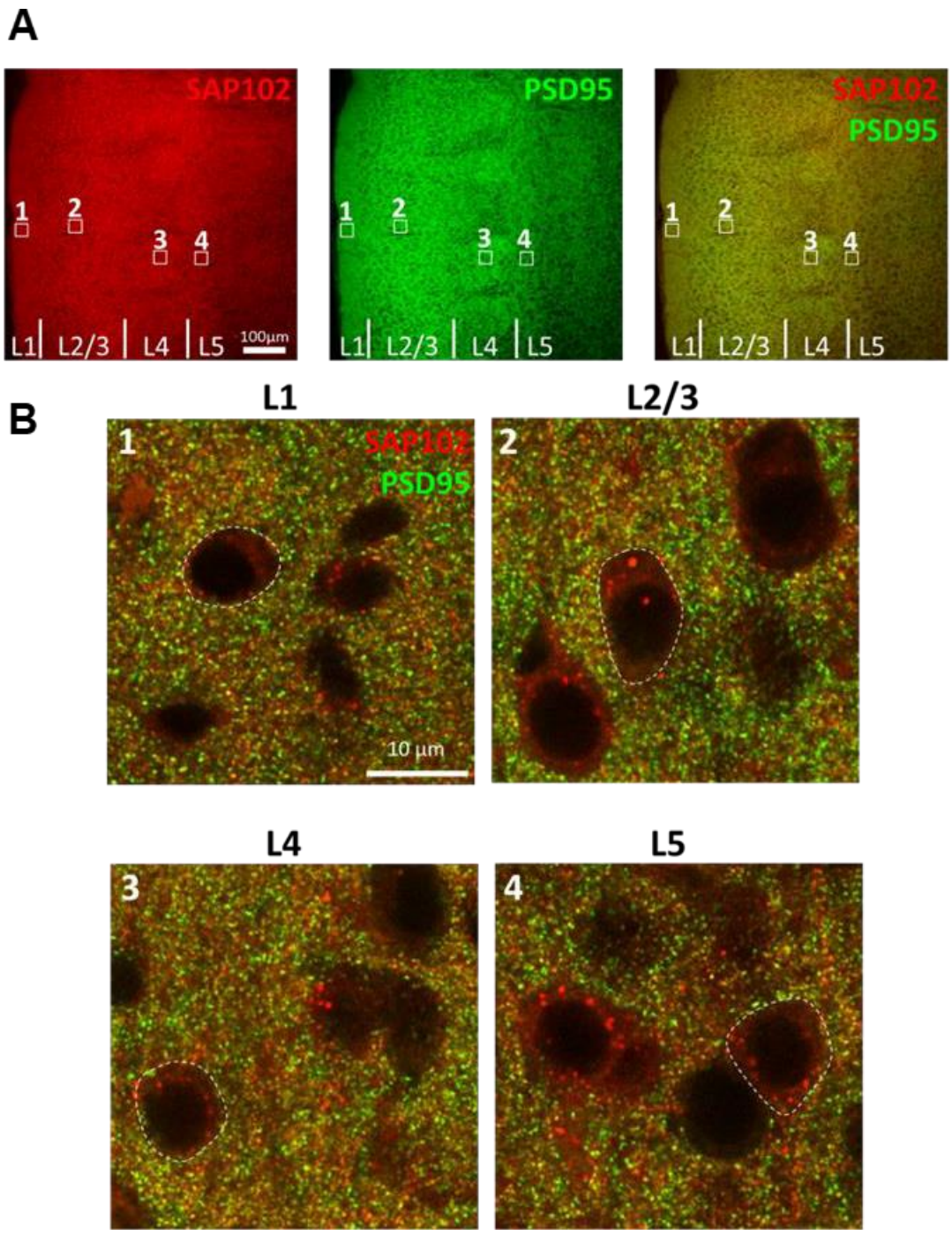

Figure 3. 13 Subcellular localisation of SAP102-mKO2 and PSD95-eGFP

Confocal images of a P15 GKD mouse. Low magnification images are shown in A, and zoomed in images for each layer are shown in B. White dashed line marks the boundaries of cell bodies that contain SAP102-MKO2 puncta but lack PSD95-eGFP.

3.3.2.3 The size of cortical layers during development

As the mouse pup grows and develops, the whole organism is expanding in size as well as refining the function of its components. The brain, and specifically the neocortex, is no exception to this process. Using the cortical anatomical landmarks of the pial surface (at the edge of the coronal brain slice) and the lower and upper edges of the barrels in L4, the change in dimensions of the distance from the edge of the brain slice to L2/3 and the width of L4 was quantified (Fig. 3.16). The outer-most layers of the GKD mouse neocortex undergo a significant expansion, doubling in size (from an average of 300 µm in P3 animals, to an average of 600 µm in P20 mice). This increase in size appears to be a gradual until it plateaus in the older animals. Layer 4 is about half the size of L1 and 2/3 in the first time point and also undergoes a physical expansion, reaching 260 µm in width. L1 and L2/3 expand by almost 400 µm, while the size of L4 increases by 150 µm. Regression analysis shows a strong age-related prediction for the size of L1 and 2/3 (R^2=0.692, fig. 3.16B) and a weaker prediction for L4 (R^2=0.302, fig. 3.16C).

Qualitative observations of the confocal imaging suggest that the expansion of L2/3 is what is mostly contributing to the L1-2/3 increase in size. It is important to note that the area of the barrel cortex that the brain sections images were acquired from was not kept constant. Previous studies have shown that cortical depth and laminar organization of the single barrels can vary across the murine vibrissal cortex (Egger et al., 2012). The cortices included in this analysis contained visible barrel structures, but the part of the barrel cortex being examined was not noted down. Nevertheless, despite this inherent variability, the growth of the neocortex follows a clear upward and gradual trend which plateaus between P10-15.

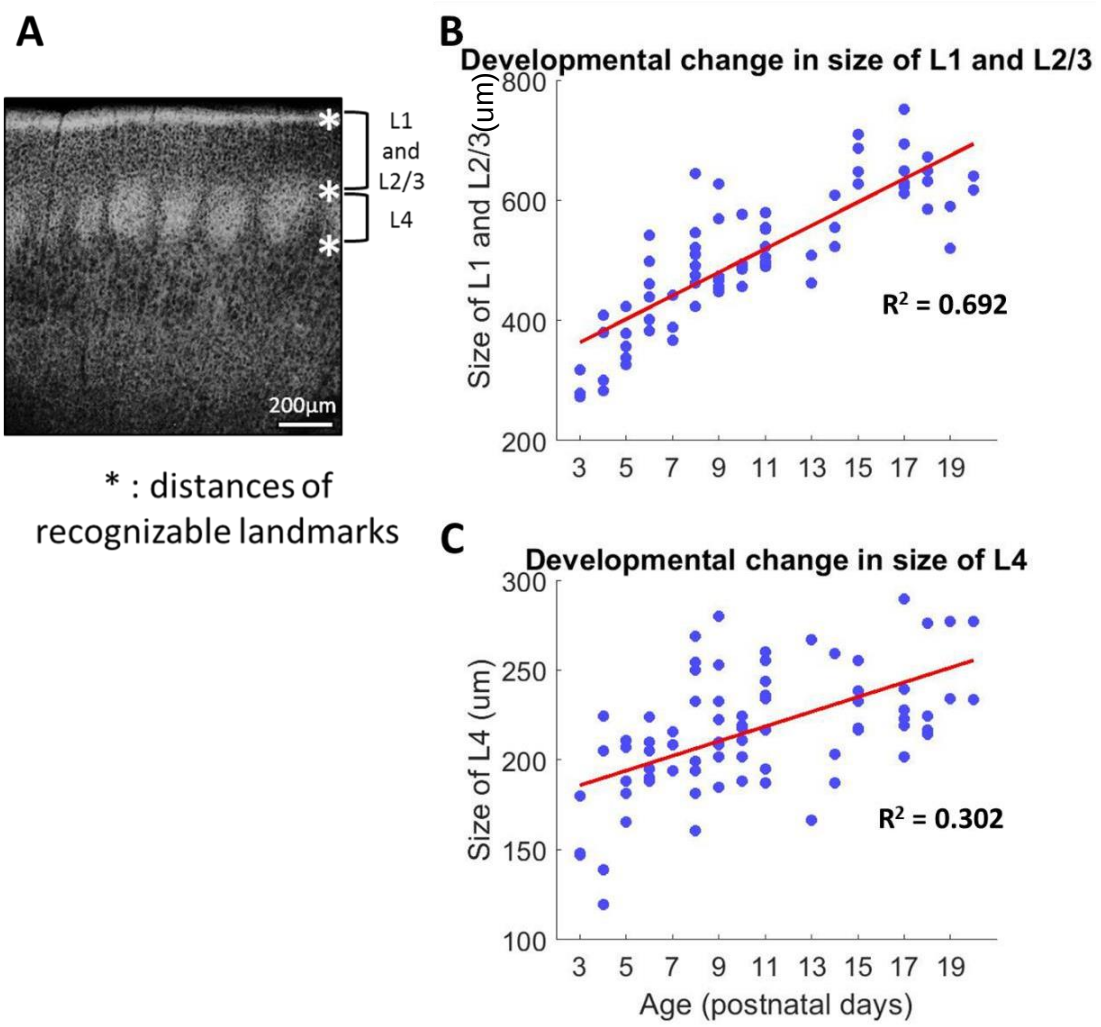

Figure 3. 14 Changes in the size of the cortical layers in the first 3 postnatal weeks
A shows the anatomical landmarks used to determine layer size in each image. B and C shows the linear fit used for the regression analysis for L1-3 and L4, respectively. Number of animals, number of slices: P4(2,4), P5(2,5), P6(3,6), P7(1,3), P8(3,8), P9(2,8), P10(2,6), P11(3,8), P13(1,2), P14(1,3), P15(2,5), P17(2,7), P18(1,4), P19 (2,2), P20(2,2).

3.3.2.2 Comparison between PSD95 expression in PSD95-eGFP and GKD mice

As a first step in characterising the expression of SAP102 and PSD95 during early postnatal development of the GKD mice, it was important to assess whether the layer-specific developmental trajectory of PSD95-eGFP was similar in the two genotypes (PSD95-eGFP and GKD) and using the two different imaging methods (2-photon live imaging of thalamocortical brain slices vs. confocal imaging of fixed coronal sections, Fig. 3.17). The age-grouped analysis showed there was no significant difference between the layer-specific relative expression of PSD95-eGFP between the two genotypes. It was therefore concluded that the developmentally regulated laminar enrichment of this protein is independent of the imaging modality and is not affected by the presence of another fluorophore-tagged protein (SAP102-mKO2).

The developmental profiles of fluorescence of PSD95-eGFP and SAP102-mKO2 in the GKD mouse brain cortex were then examined in order to compare the pattern of expression of two proteins (Fig. 3.18 and Fig. 3.19).

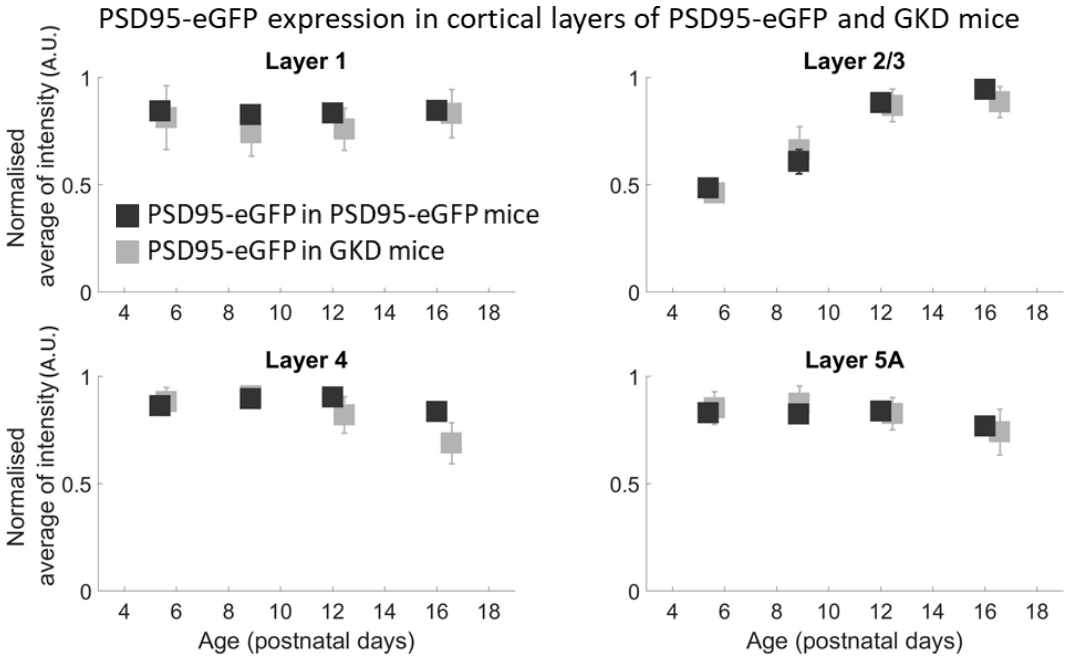

Figure 3. 15 Comparison of layer-specific developmental expression between the two genotypes and imaging methods

Layer analysis of confocal (in black) and 2-photon (in grey) imaging of PSD95-eGFP in the GDK and PSD95-eGFP mouse line, respectively. Filled squares represent the age-grouped averages of the normalised intensity at different time points during development. The error bar is the SEM. There was no significant difference between the two genotypes in any of the layers and ages analysed. 2-photon number of animals, number of slices: P4(3,10), P5(3,10), P6(3,6), P7(4,12), P8(3,10), P9(3,8), P10(2,6), P11(3,11), P12(3,7), P13(2,11), P14(3,10), P15(2,7), P16(1,2), P17(2,5), P18(2,7). Confocal number of animals, number of slices: P4(2,4), P5(2,5), P6(3,6), P7(1,3), P8(3,8), P9(2,8), P10(2,6), P11(3,8), P13(1,2), P14(1,3), P15(2,5), P17(2,7), P18(1,4), P19 (2,2), P20(2,2).Statistical test: repeated paired t-test with Bonferroni correction. * p<0.05 ** p<0.01 *** p<0.001.

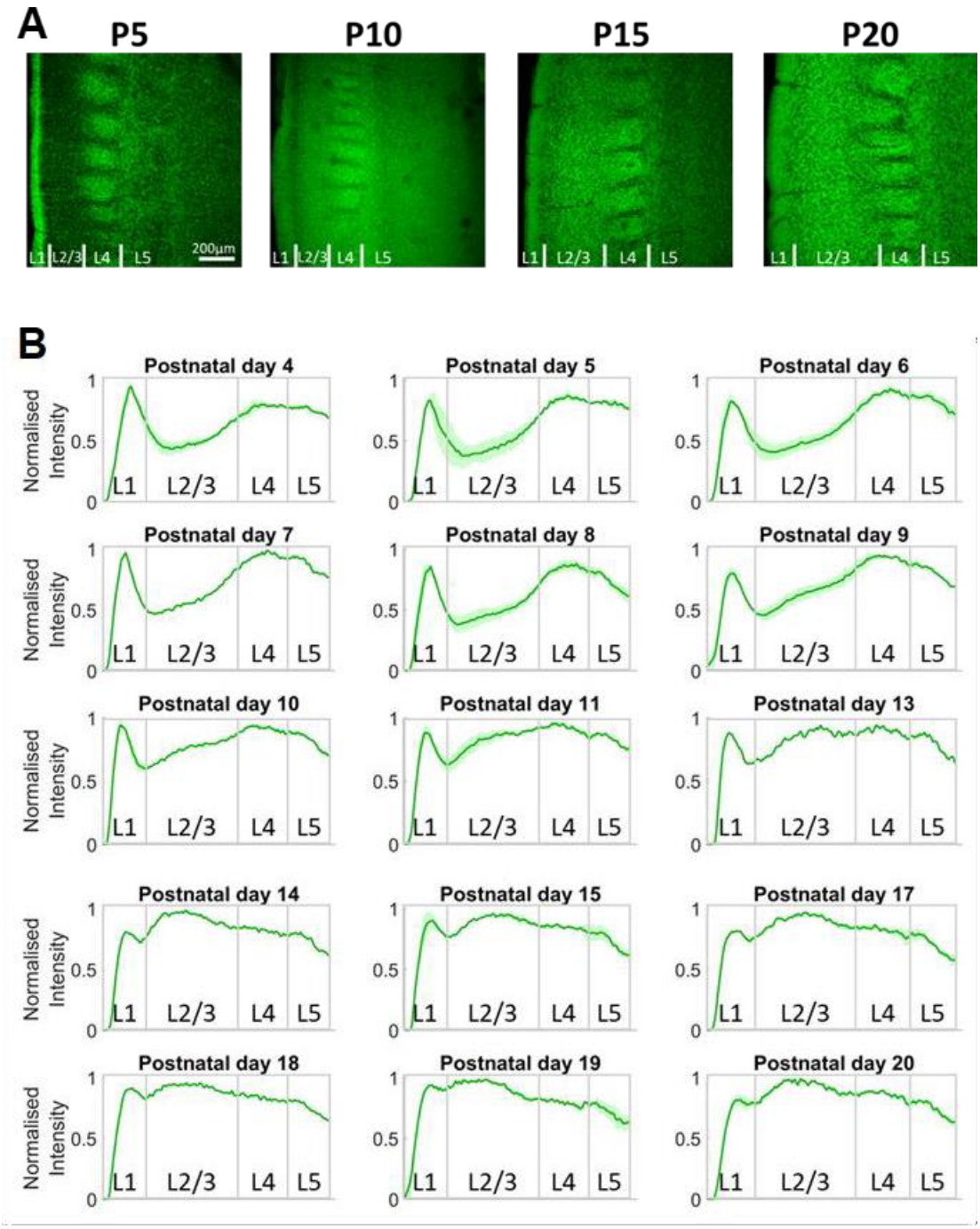

Figure 3. 16 Day-by-day analysis of profile of intensity of PSD95-eGFP in the GKD mice
A. Confocal images of example time points. B. Averages of normalised plot of the intensity of the fluorescence for each postnatal day. Plots were normalised to the maximum intensity and the distance between L1 and L4 was normalised as well. In dark green is the average, in light green is the +/- SEM for each data point. Number of animals, number of slices: P4(2,4), P5(2,5), P6(3,6), P7(1,3), P8(3,8), P9(2,8), P10(2,6), P11(3,8), P13(1,2), P14(1,3), P15(2,5), P17(2,7), P18(1,4), P19 (2,2), P20(2,2).

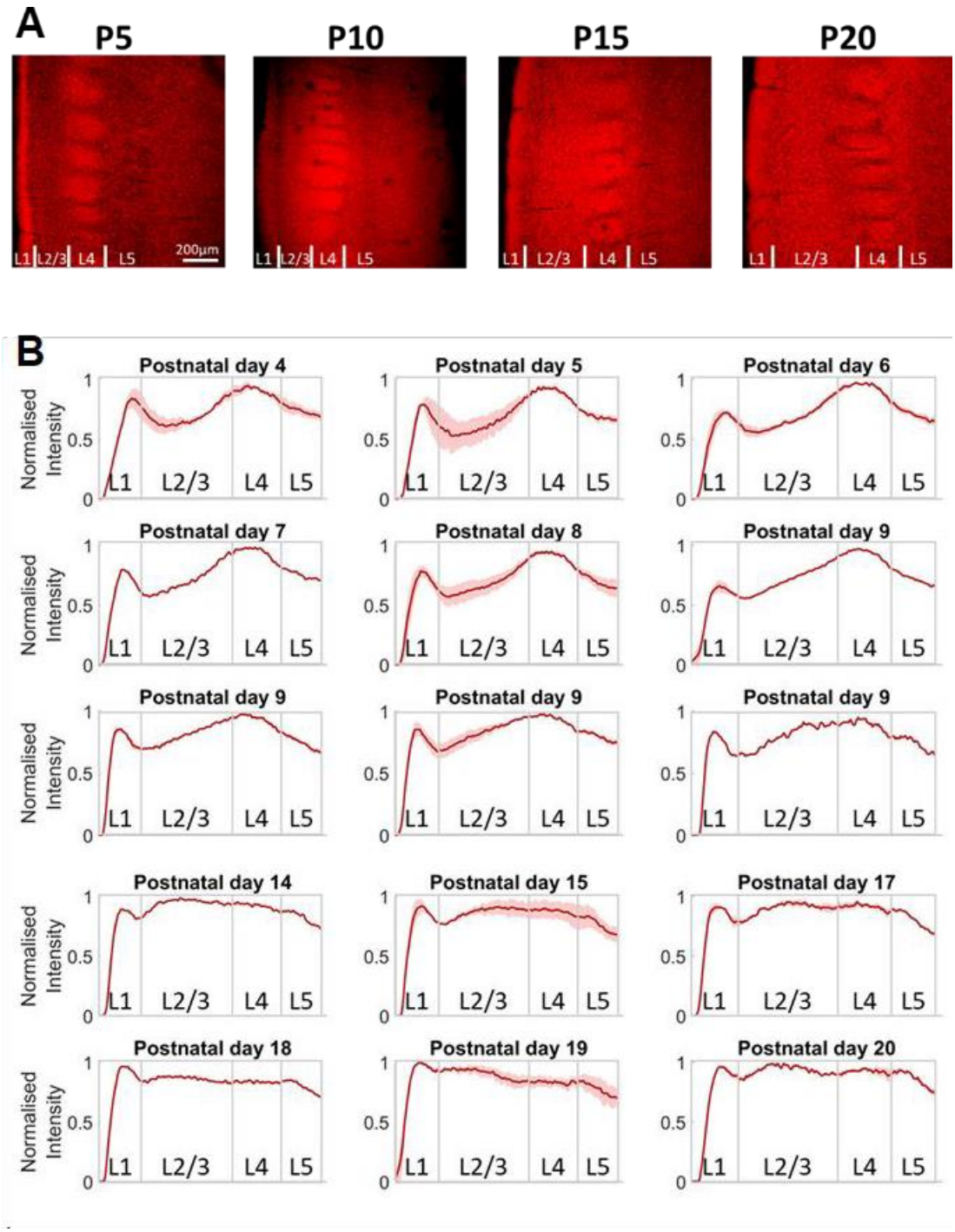

Figure 3. 17 Day-by-day analysis of profile of intensity of SAP102-mKO2 in the GKD mice
A. Confocal images of example time points. B. Averages of normalised plot of the intensity of the fluorescence for each postnatal day. Plots were normalised to the maximum intensity and the distance between L1 and L4 was normalised as well. In red is the average, in pink is the +/- SEM for each data point. Number of animals, number of slices: P4(2,4), P5(2,5), P6(3,6), P7(1,3), P8(3,8), P9(2,8), P10(2,6), P11(3,8), P13(1,2), P14(1,3), P15(2,5), P17(2,7), P18(1,4), P19 (2,2), P20(2,2).

3.3.2.4 The expression of both MAGUKs increases over time

Many different laboratories have quantified the presence of PSD95 and SAP102 in whole brain or cortical lysates using western blotting or immunohistochemistry, and have shown that the expression of both proteins increases during the development of animals. In order to assess whether this increase also occurs in the barrel cortex of the GKD brains, the area under the curve of raw intensity profiles from L1 to L4 was calculated at the different developmental time points (Fig 3.20). Importantly, the imaging settings of the confocal microscope were kept consistent between imaging sessions, in order to be able to compare data across the developmental ages. Using the raw (not normalised) data, the area under the curve was calculated between L1 and L4/5 boundary. For both proteins, the area under the curve between L1 and L4 of the raw intensity of fluorescence significantly increases over time. Obviously, as previously shown, the brain cortex is also physically enlarging; were the protein amount staying stable, the intensity would be diluted down as the cortex grows. Therefore, the increase of the areas under the curve in the growing cortical layers suggest that the expression of SAP102 and PSD95 exhibits a significant developmentally regulated increase during the first 3 postnatal weeks.

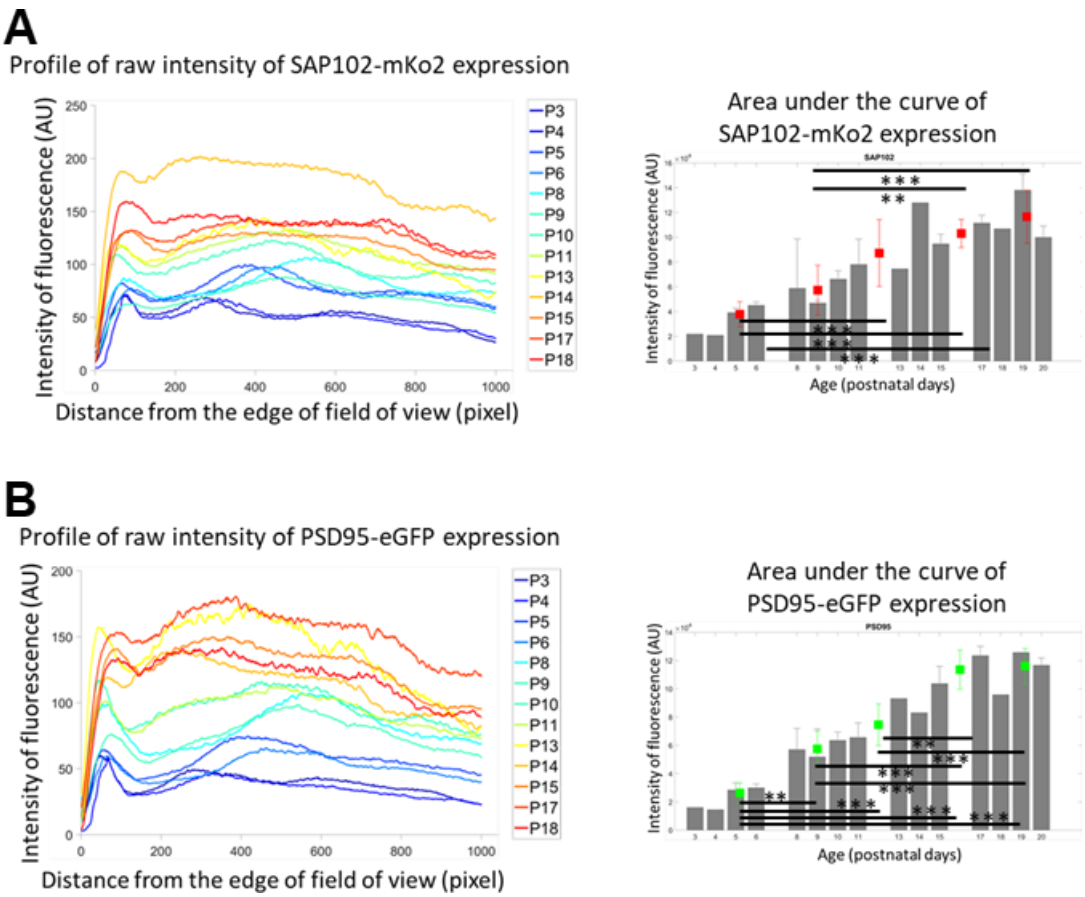

Figure 3. 18 Area under the curve of the raw intensity of profile across the different time points

The raw intensity between L1 and the deeper edge of L4 was averaged by animal and then by age and plotted for SAP102 (A) and PSD95 (B). Statistical analysis showed a significant increase in the area under the curve over time. Number of animals, number of slices: P4(2,4), P5(2,5), P6(3,6), P7(1,3), P8(3,8), P9(2,8), P10(2,6), P11(3,8), P13(1,2), P14(1,3), P15(2,5), P17(2,7), P18(1,4), P19 (2,2), P20(2,2).Statistical test: one-way ANOVA and Bonferroni post-hoc. * $p<0.05$ ** $p<0.01$ *** $p<0.001$.

3.3.2.5 Layer-specific, developmentally regulated distribution of MAGUKs

Since the confocal imaging settings were kept constant for all the ages investigated, the raw fluorescence of SAP102-mKO2 and PSD95-eGFP was analysed (Fig 3.21).

For both proteins, the levels of expression in every layer significantly increase over the course of the first 3 postnatal weeks.

In L1 and L4, the levels of SAP102-mKO2 fluorescence significantly increase between P4-7 compared to P18-20. In layer 2/3, levels increase from P11-14 and then remain stable. Similarly, fluorescent levels in L5A increase from P11-14 and then plateau.

The laminar expression of PSD95-eGFP over development follows a similar trajectory. The expression of this protein in L1 significantly increases around P11-14 and then it plateaus. Similarly, in L2/3 the levels of fluorescence gradually increase from P8-10 until P15; after this time points no significant increase is observed until P20. The expression within L4 significantly increases from P4-7 to P8-10, P11-14 and P15-17. After P11-14 the levels reach stability. Finally, in L5A a significant increase in PSD95-eGFP fluorescence is observed between P4-7 to P11-14 and then the levels remain stable.

By dividing the value of the fluorescence intensity in the final timepoint (P18-20) by the fluorescence value at the earlies age-group investigated (P4-7), we can assess by how much the expression of the two protein increases over time. The raw levels of fluorescence of SAP102-mKO2 approximately double in each layer (fold changes between the first and last age group (in A.U.): L1 = 2.18, L2/3 = 2.6, L4 = 1.7, L5A = 2.07). On the other hand, the expression of PSD95-eGFP increases by slightly more in L1, 4 and 5A (fold changes between the first and last age group (in A.U.): L1 = 2.18, L2/3 = 2.6, L4 = 1.7, L5A = 2.07) and it exhibits a 4-fold enrichment in L2/3 (fold change between the first and last age group (in A.U.): L4 = 4.40).

This general laminar increase of expression is consistent with the increase of the total level of fluorescence in the whole field of view imaged shown in our previous analysis. Interestingly, for both SAP102-mKO2 and PSD95-eGFP, the intensity of the relative expression of the two MAGUKs is not statistically significantly different between the two last timepoint, suggesting the expression peaks around P15. Additionally, the distribution of both PSD95 and SAP102 suggests that the most pronounced developmental increase occurs in L2/3.

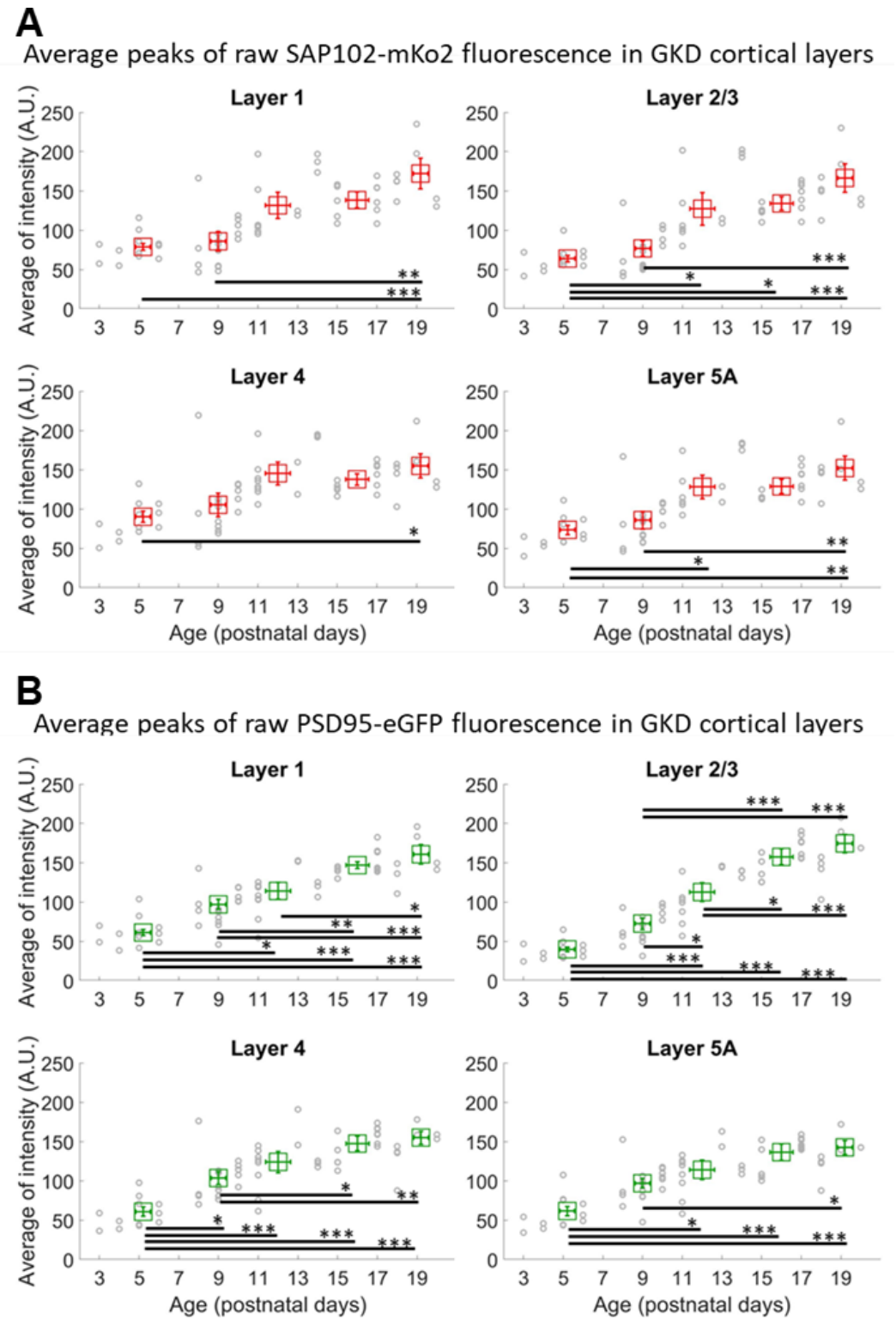

Figure 3. 19 Laminar analysis of the changes in raw expression of PSD95-eGFP and SAP102-mKO2

Raw data for each brain slice imaged in grey open circles and averages by animal for the age groups in red squares (SAP102, B) or green squares (PSD95, B). Error bars represent SEM, vertical for intensity and horizontal for age group. Number of animals, number of slices: P4(2,4), P5(2,5), P6(3,6), P7(1,3), P8(3,8), P9(2,8), P10(2,6), P11(3,8), P13(1,2), P14(1,3), P15(2,5), P17(2,7), P18(1,4), P19 (2,2), P20(2,2).Statistical test: one-way ANOVA and Bonferroni post-hoc. * $p<0.05$ ** $p<0.01$ *** $p<0.001$.

3.3.2.6 Comparison between the two MAGUKs PSD95 and SAP102

Since literature has shown that these proteins have a specifically different developmental profile (SAP102 levels rising before PSD95), and since PSD95 is a marker for mature synapses, we then moved onto assessing the difference between the expression of these two MAGUKs by comparing the normalised intensity over time.

The direct comparison of the raw intensities of PSD95-eGFP and SAP102-mKO2 is not possible because they are tagged with two different fluorophores requiring distinct settings to optimise image acquisition. In order to compare the laminar distribution of these two MAGUKs and how it changes over time, the intensity of fluorescence was normalised to the maximum value and normalising the distance between L1 and L4/L5 boundary allows a closer look to the relative contribution of each layer compared to the maximum intensity of fluorescence at the different timepoints (Fig. 3.22 and 3.23).

Qualitatively, in P5 slices, the mean fluorescence profiles of relative laminar expression of PSD95 and SAP102 appears to be differentially distributed across the cortical layers (Fig. 3.22A). The relative expression of SAP102 is higher than the expression of PSD95 in L2/3, while the relative proportion of L5A appears higher in PSD95 than SAP102. This difference in relative distribution appears to attenuate in older animals where the shape of the profile of intensity follows a more similar laminar pattern (Fig. 3.22B).

In the case of SAP102, the relative expression in L1 is stable until P11-14, then significantly increases around these postnatal days, and finally stabilises again (Fig. 3.23). The expression in L2/3 exhibits the most prominent developmental increase of proportional fluorescence. The levels significantly increase from P8-10, then again to P11-14 and then remain stable. SAP102-mKO2 relative fluorescence in L4 is stable throughout early postnatal development, and L5A exhibits a slight increase in relative fluorescence intensity between P4-7 and P18-20.

In contrast, the relative layer-specific expression of PSD95-eGFP does not significantly change during development in L1, L4 and L5. The expression of this protein, however, undergoes a nearly 2-fold enrichment of the relative amount in L2/3 from the end of the 1st postnatal week until the end of the 3rd again (Fig. 3.23). The levels are statistically stable until P11-14 when a significant increase in relative fluorescence occurs. The levels of expression of this PSD95-eGFP then reaches a plateau.

The comparison between the normalised intensity of fluorescence for SAP102-mKO2 and PSD95-eGFP shows no significant difference in both L1 and L4 at any ages examined. On the other hand, SAP102 was significantly more enriched in L2/3 than PSD95 between P4-7, and this relative difference disappeared as PSD95 levels increase at later time points. L5A showed the opposite trend of relative expression of the two proteins; the relative enrichment of PSD95-eGFP in L5A was higher than that of SAP102 between P4-7, while from P8 onwards the two proteins were relatively distributed at the same level in this layer. This suggests that earlier on, in L2/3, the fluorescence of SAP102 are higher than the levels of PSD95 and the opposite in L5A.

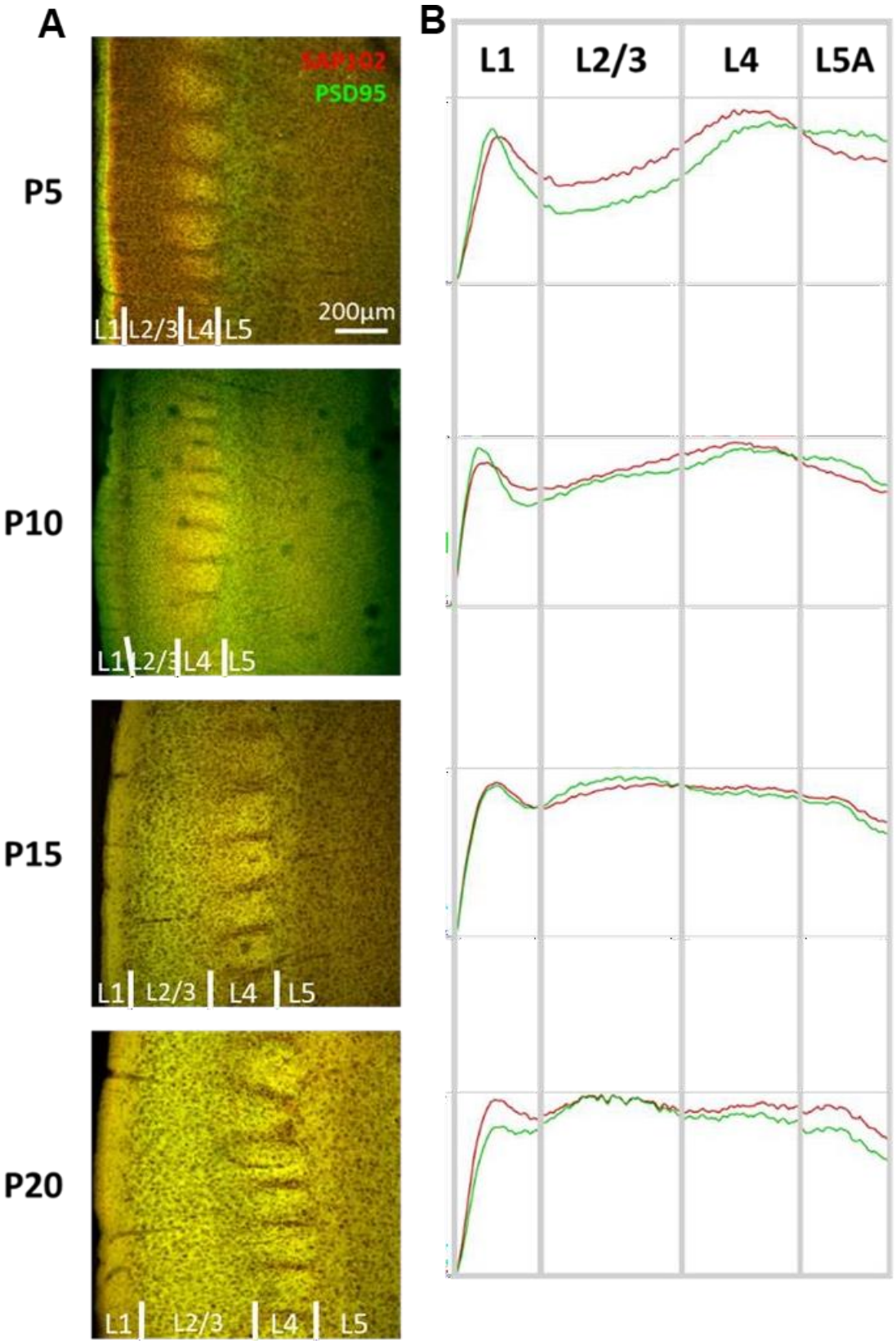

Figure 3. 20 Comparison of the laminar expression of the two MAGUKs

A. shows representative maximum projected confocal images of the barrel cortex at different ages. B. shows overlaid plot profiles of fluorescence of SAP102 and PSD95 across the barrel field.

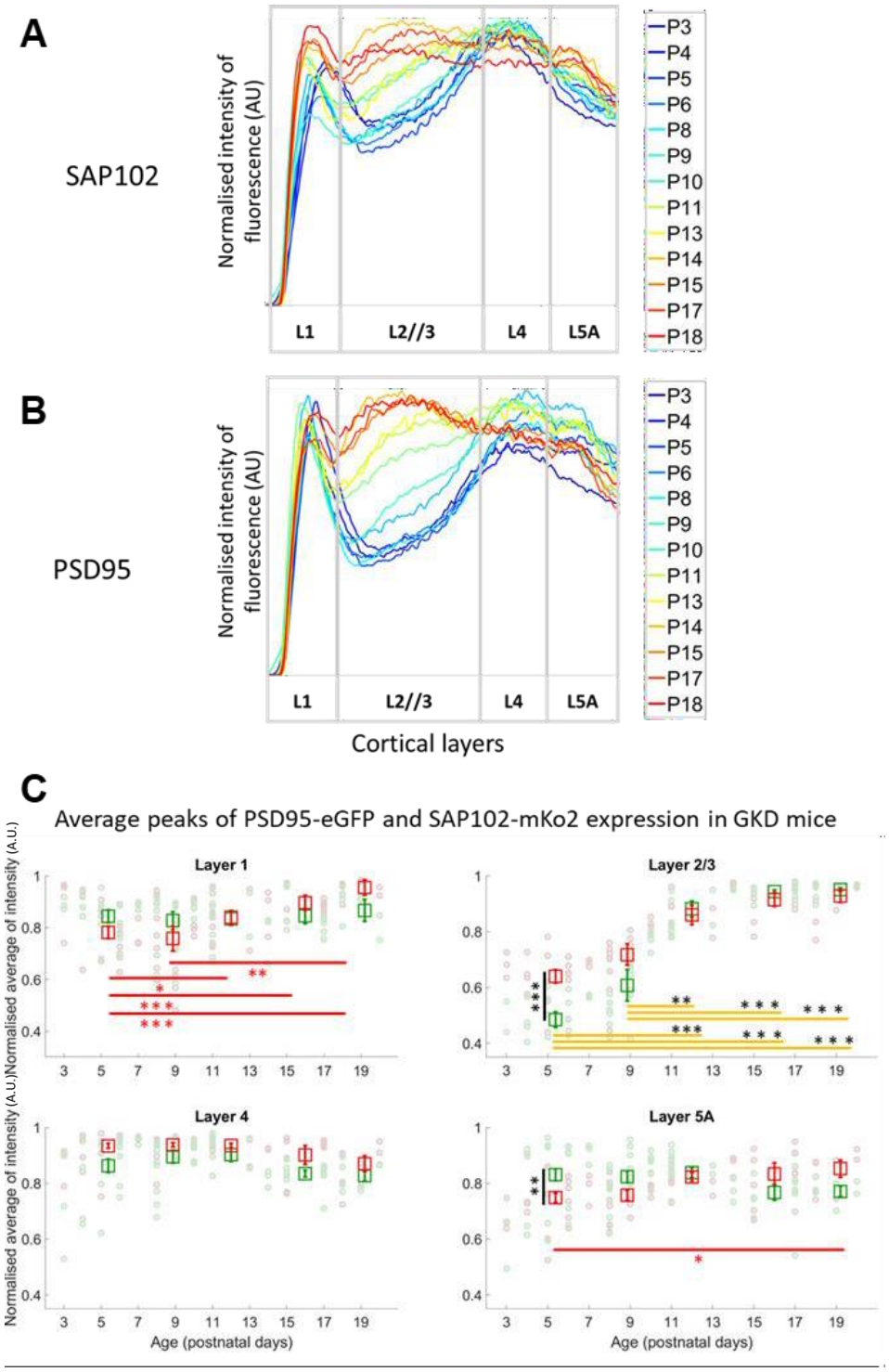

Figure 3. 21 Laminar profiles of expression of the two MAGUKs

A and B. Plot profiles of intensity for SAP102 (A) and PSD95 (B). Ages are color coded from coldest (youngest) to warmest (oldest). C. Normalised laminar expression of PSD95 (green) and SAP102 (red). Normalised data for each animal in circles (green for PSD95 and red for SAP102) and averages by animal for the age groups in green squares (PSD95) or red squares (SAP102). Statistical significance for SAP102 in red, for both PSD95 and SAP102 in yellow and the difference between the two proteins is in black. Error bars represent SEM. Number of animals, number of slices: P4(2,4), P5(2,5), P6(3,6), P7(1,3), P8(3,8), P9(2,8), P10(2,6), P11(3,8), P13(1,2), P14(1,3), P15(2,5), P17(2,7), P18(1,4), P19 (2,2), P20(2,2).Statistical test: repeated paired t-test with Bonferroni correction. * p<0.05 ** p<0.01 *** p<0.001.

3.3.2.7 Layer 5 expression of MAGUKs is differentially regulated during development

The comparison between PSD95 and SAP102 across the cortical layers revealed an interesting, previously unreported, enrichment of PSD95-eGFP expression in L5A early on during development (P4-7). PSD95-eGFP forms a fluorescent band located just below the barrels of L4, in putative L5A, from the earliest timepoint (P4) until the oldest age (P20). On the other hand, SAP102-mKO2 does not appear to be as enriched in L5A until after P10. In order to further quantify these observations, a ratio of L5 to L4 fluorescence was calculated using both the normalised and the raw data (Fig. 3.24).

While the L5/L4 ratio of the normalised fluorescence of PSD95-eGFP remains stable over time, the ratio of normalised SAP102-mKO2 fluorescence significantly increases over time, from P4-10 to P18-20 (Fig. 3.24A). The ratio of fluorescence in the two layers is significantly higher for PSD95 over SAP102 between P4 and P14; after this age the difference disappears as the L5/L4 ratio of SAP102-mKO2 reaches PSD95 level.

Measurement of the raw fluorescence intensity shows slightly different results (Fig. 3.24B). While the L5/L4 ratio of SAP102-mKO2 increases over time, the ratio of PSD95-eGFP fluorescence is shown to decline over time between P4-7 and P11-20. The comparison between the two MAGUKs shows that the fluorescence L5/L4 ratio is significantly higher for PSD95-eGFP between P4 and P10; from P11 until P18 there is no significant difference between the L5/L4 ratio of PSD95-eGFP and SAP102-mKO2; finally from P18-20 the ratio of L5/L4 is significantly higher for SAP102-mKO2 than for PSD95-eGFP.

The confocal imaging suggests that L5A PSD95-eGFP fluorescence is higher than the L5A fluorescence of SAP102-mKO2 (Figs. 3.18, 3.19, 3.22). Furthermore, the raw data shows that the raw intensity of both proteins in L4 and in L5 increases over time (Fig. 3.21). We therefore conclude that the increase in the L5/L4 ratio of SAP102 intensity is due to a developmentally regulated enrichment in L5A, which is already present from early postnatal ages in the case of PSD95.

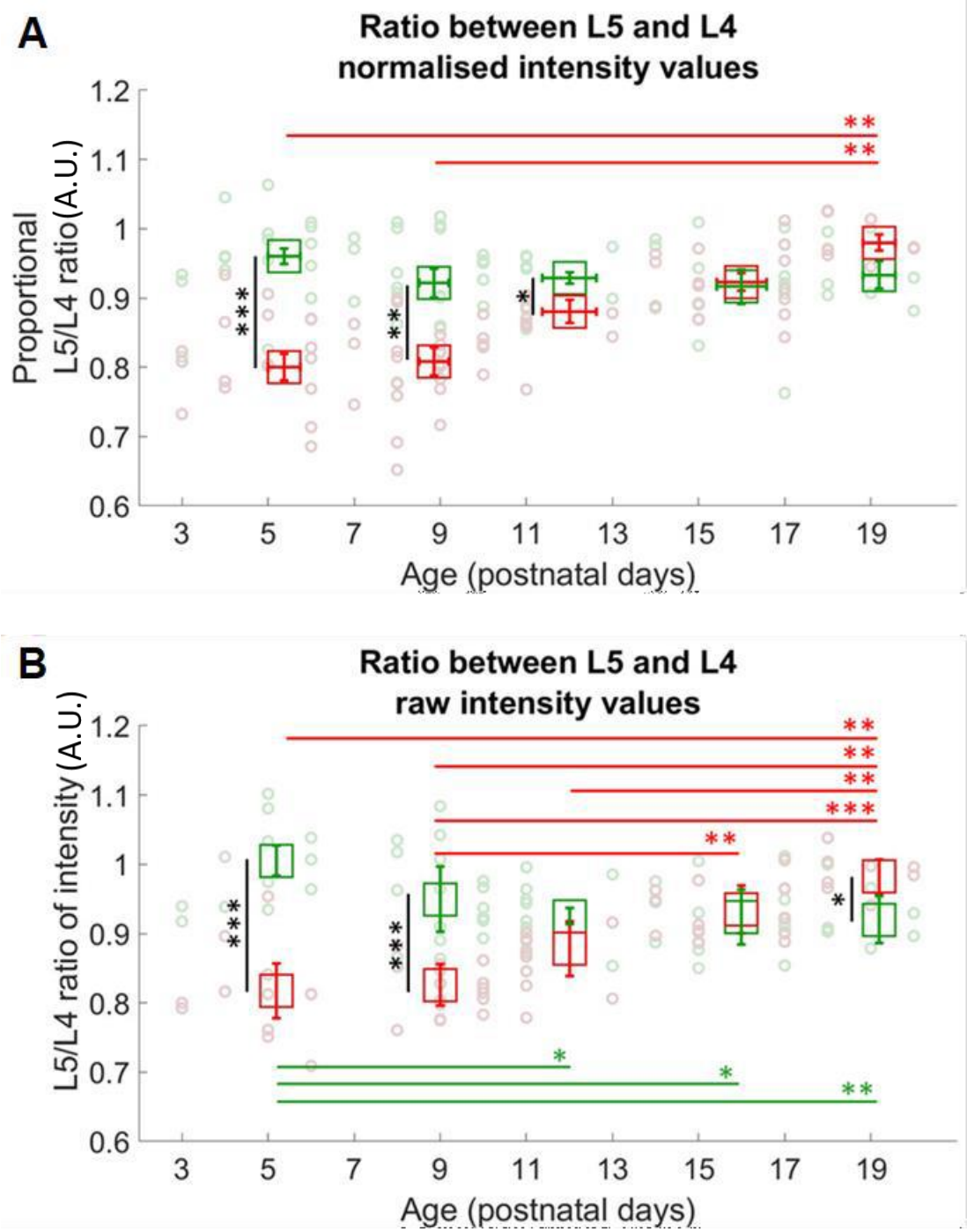

Figure 3. 22 Developmental changes of the ratio of L5 to L4 for the two MAGUKs

A. L5-to-L4 ratio of normalised expression of SAP102 (red) and PSD95 (green). Averages for each brain slice in circles and averages by age group in green squares (PSD95) or red squares (SAP102). B. L5-to-L4 ratio of raw expression of SAP102 (red) and PSD95 (green). Averages for each brain slice in circles and averages by age group in green squares (PSD95) or red squares (SAP102). Statistical significance for SAP102 in red, for both PSD95 and SAP102 in yellow and the difference between the two proteins is in black. Error bars represent SEM. Number of animals, number of slices: P4(2,4), P5(2,5), P6(3,6), P7(1,3), P8(3,8), P9(2,8), P10(2,6), P11(3,8), P13(1,2), P14(1,3), P15(2,5), P17(2,7), P18(1,4), P19 (2,2), P20(2,2).Statistical test: repeated paired t-test with Bonferroni correction. * $p<0.05$ ** $p<0.01$ *** $p<0.001$.

3.3.3 Developmental profile of Complexin 3-positive subplate neurons

Our results suggest that PSD95, but not SAP102, is specifically slightly enriched in L5A from very early on in postnatal mouse brain development. PSD95 is a marker for mature synapses and Lambert and colleagues have shown that it is the last MAGUK to accumulate at nascent synapses, which further supports the notion of the involvement of this postsynaptic scaffolding protein in relatively mature synapses (Lambert et al., 2017). Therefore, the presence of PSD95-eGFP in L5A before an increase in SAP102-mKO2 was very perplexing and might suggest that a subpopulation of synapses in this layer is part of an early-developed circuit. The next step was to investigate a potential presynaptic partner: a subpopulation of subplate neurons expressing the protein Cplx3.

Subplate neurons are among the first neurons to be generated and they have been shown to be crucial for thalamocortical pathfinding and correct circuit development. Recently, Viswanathan et al. showed that Cplx3-positive subplate neurons send their projections to L5A and L1 as early as P8; this population is shown to largely disappear by P21 (Viswanathan et al., 2017, Ferrer et al., 1990; Price et al., 1997; Rakic and Zecevic, 2000). As Cplx3 is a presynaptically located SNARE-complex regulator, this marker can be used to test whether this subpopulation of subplate neurons can constitute a presynaptic partner to the L5A synapses enriched with PSD95-eGFP.

3.3.3.1 Developmental expression of Cplx3

Immunohistochemistry was performed to stain for Cplx3 in the GKD mouse brains and compare the laminar distribution of genetically tagged PSD95-eGFP, SAP102-mKO2 and antibody-labelled Cplx3-Alexa633.

Firstly, primary and secondary controls were conducted on fixed GKD coronal slices of barrel cortex (Fig. 3.25). For the primary antibody control, the brain slice was incubated with the primary antibody only, whilst keeping all the other components and timing of the staining consistent with the immunostaining protocol (Fig. 3.25A); this ensured that there was no auto-fluorescence in the tissue that would contribute to Cplx3-Alexa Fluor 633 signal. The secondary antibody control consisted of incubating the brain tissue with secondary antibody Alexa 633 in the absence of a primary antibody (Fig. 3.25B); this control was used to test for non-specific binding of Alexa 633. In both cases, the fluorescence in the 633 channel was non-existent or negligible. It was therefore concluded that these antibodies are an efficient and accurate method

to detect Cplx3 in these brain slices. Additionally, the fluorescence of PSD95-eGFP and SAP102-mKO2 did not appear to be affected by the immunohistochemical procedure and no bleed through from these channels was observed, even in older aged (P15), where the expression of the MAGUKs is relatively high.

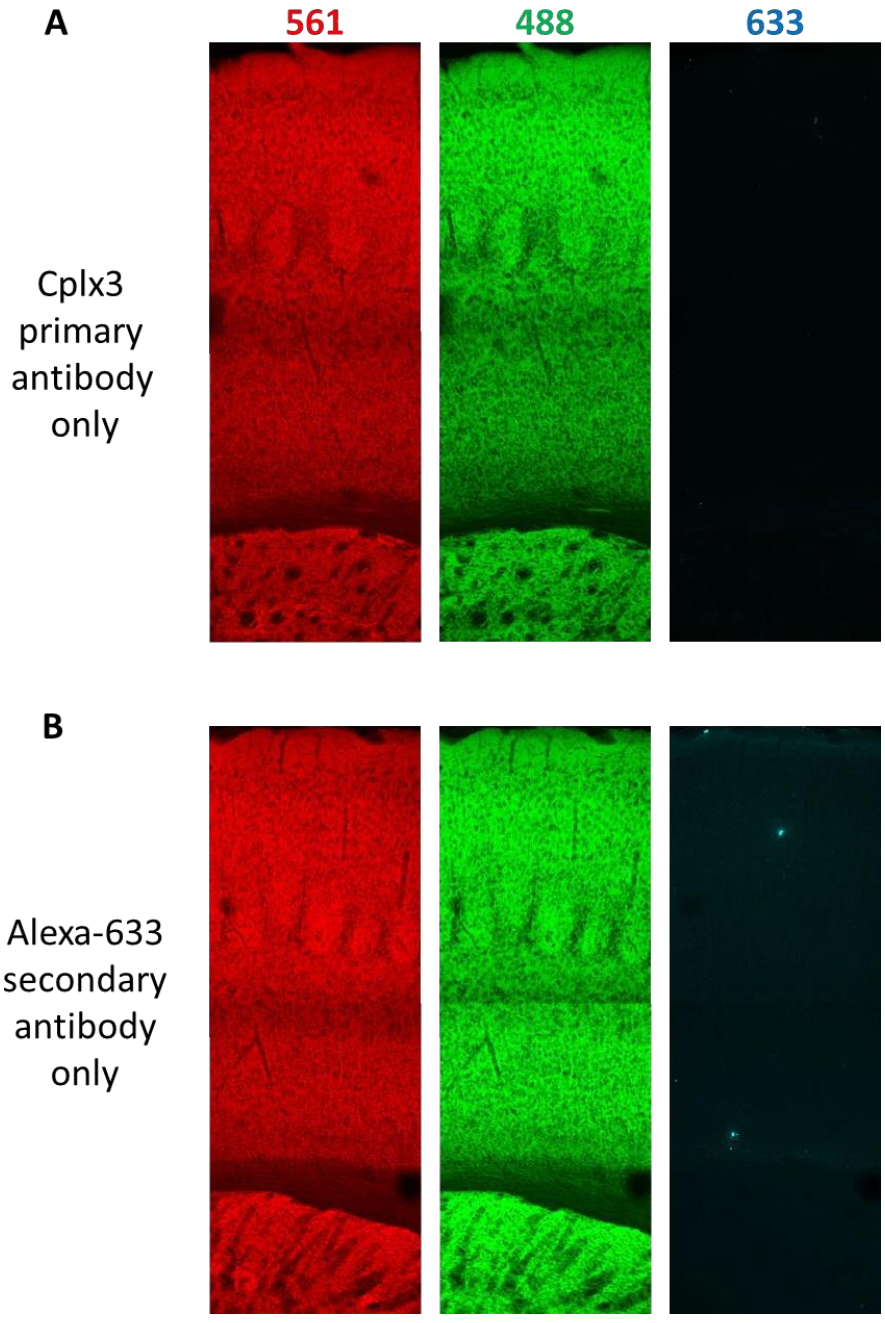

Figure 3. 23 Antibody controls for Cplx3 immunostaining
Following incubation with both primary only (A) and secondary only (B) negligible fluorescence can be seen in the 633 imaging channel.

Confocal images of the whole coronal section of a P15 mouse shows that this protein is enriched in selected areas of the brain, including specific hippocampal areas and the cortex (Fig. 3.26). Consistently with previous reports, fluorescence can be observed in the cell bodies of neurons in the subplate layer, located below the cortical plate. A sparse population of Cplx3-positive neuronal cell bodies can also be noticed scattered in L6 and L5 (Fig. 3.26, red inserts). Whilst Cplx3 acts at the presynaptic terminal, the immature form of this protein, retained in the endoplasmic reticulum, is likely responsible for the cell body labelling. Cplx3 fluorescent puncta are present across the cortical plate, but they are absent from the barrel hollows. High magnification images show that Cplx3 appears as fluorescent puncta, putatively in the presynaptic terminals of SP neurons. Cplx3-positive neuronal cell bodies were observed in the subplate at all ages examined (from P4 to P20, Fig. 3.27).

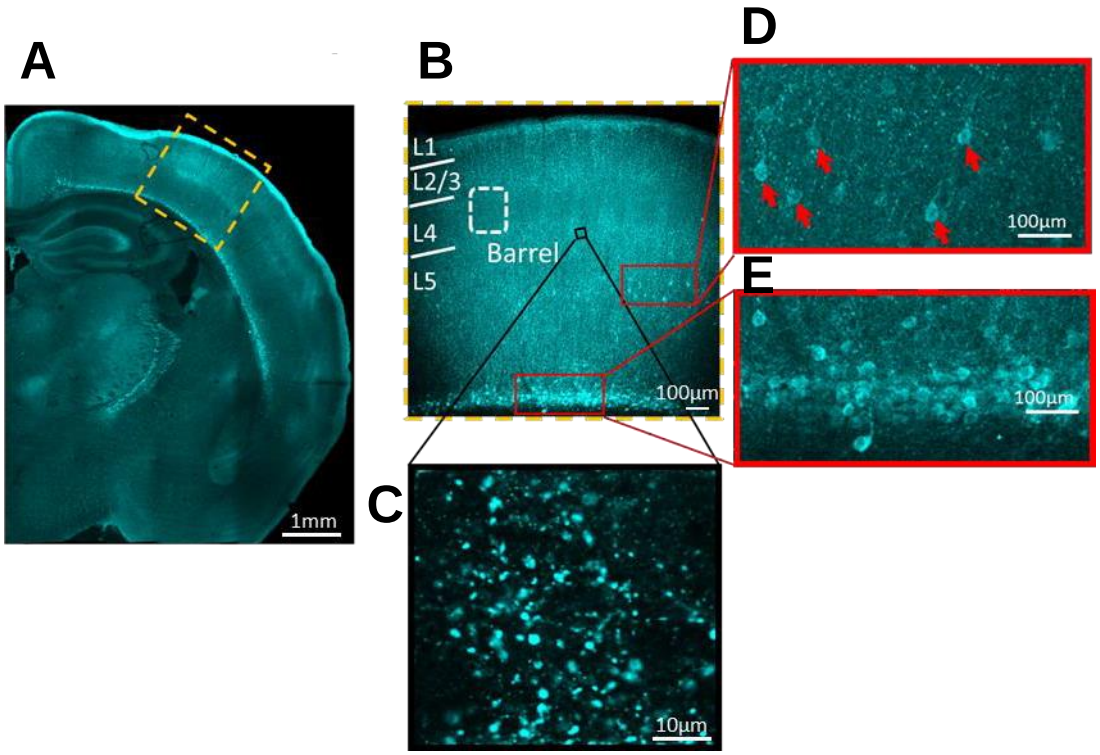

Figure 3. 24 Confocal imaging of coronal sections showing Cplx3 staining
Example of a P15 mouse brain slice stained for Cplx3. A. The cortical image shows Cplx3+ neurons located in the subplate area, below the cortical plate (E). B. Staining is present in L1,L2/3 and 5, but absent from the barrels (white dashed circles). C. A high magnification image shows Cplx3 punctate pattern. D. Some sparse cell bodies can also be noticed in L5 (red arrows in red insert).

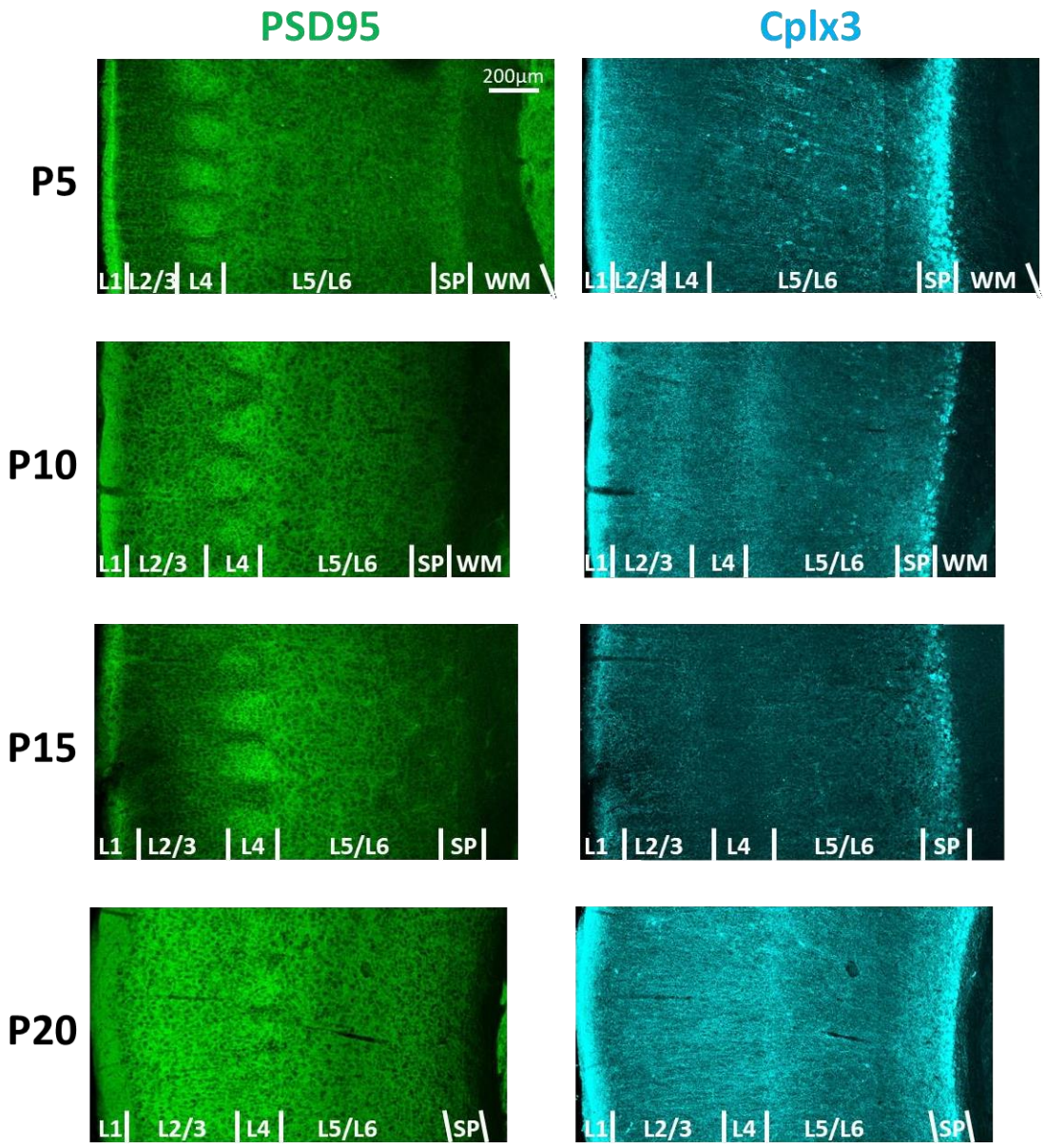

Figure 3. 25 Example confocal images of the cortical plate and subplate

Images of GKD mice stained for Cplx3 show that the subplate is present at every age that was examined. PSD95 on the left and Cplx3 on the right. Cplx3 is absent from barrels in L4 (identified by imaging PSD95). SP, subplate; WM, white matter.

In order to assess whether the expression of the protein changes in the cortical plate with increasing developmental age, the area under the curve of L1-L4 intensity was calculated. The raw intensity of Cplx3 fluorescence is stable from P4 to P14 (as statistically assessed) and then significantly increases at P15. From P15 until P20 its expression is stable (Fig. 3.28).

Layer-specific analysis of normalised fluorescence intensity shows that there is no significant change in Cpxl3 expression between P4 and P20 in any of the layers interrogated (Fig. 3.29). This suggests the cortical expression of Cplx3 rises after P15 without changing its relative distribution in L1-5A, i.e. Cplx3 preferential enrichment in specific layers does not change during development. It is important to notice that the level of expression is reflective of the presynaptic terminals innervating the cortical layers, while the fluorescent somas contained in the subplate were entirely excluded from this analysis, as they were located deeper than the image acquired with the 10x objective.

In a similar manner to the expression of the MAGUK proteins, the levels of Cplx3 in layer 1 are high from the earliest timepoint imaged (P4). Moreover, at all examined ages, Cplx3 is consistently mostly absent from the barrels, but enriched in a band just below the barrels, in putative L5A.

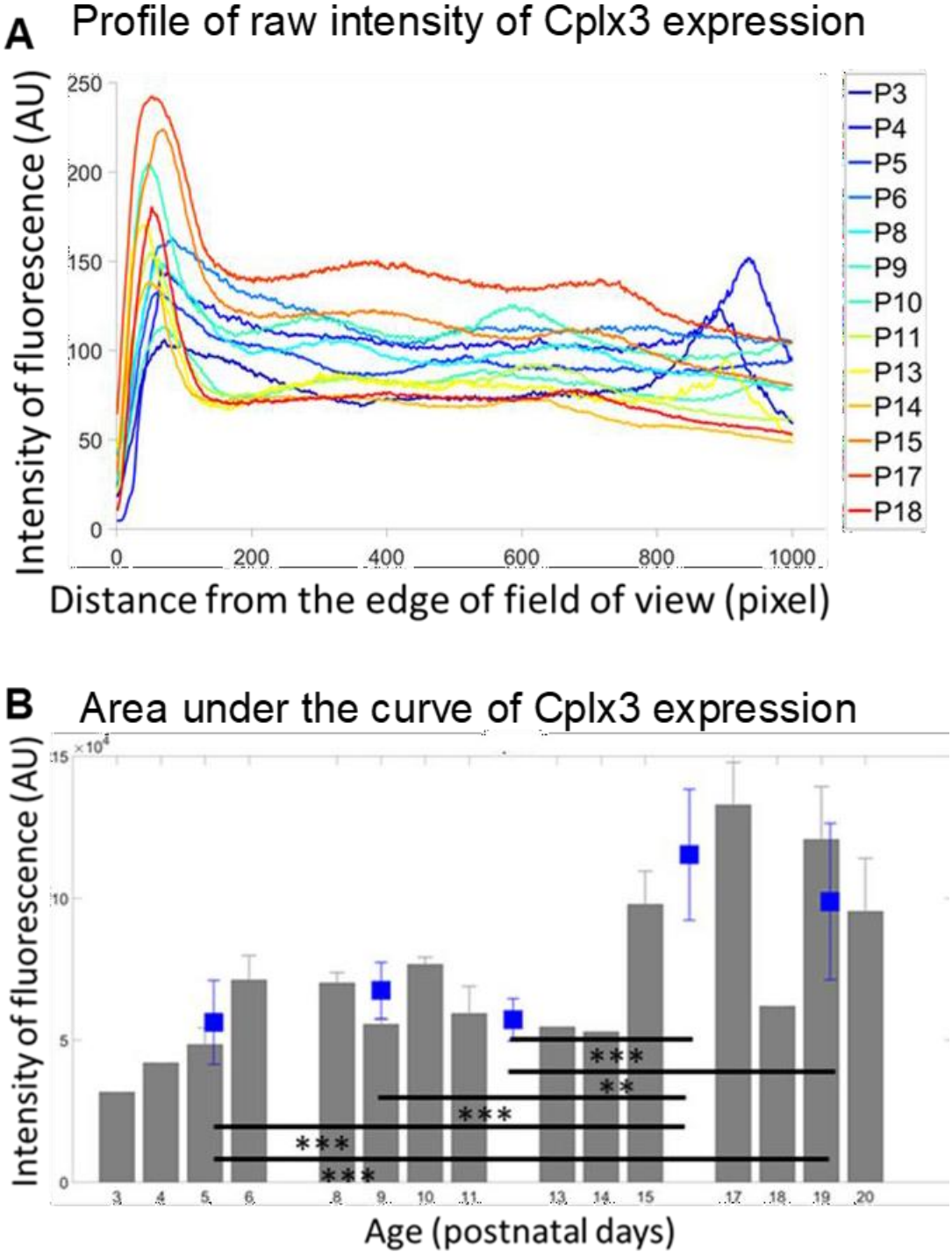

Figure 3. 26 Area under the curve of the raw intensity of Cplx3

A. plot profiles of raw fluorescence of Cplx3 stained with AlexaFluor 633. Ages are color coded from coldest (youngest) to warmest (oldest). B. area under the curve of expression of Cplx3 over development. Grey bars show average for each postnatal age, blue squares show the averages for each age group. Error bars: S.E.M. Number of animals, number of slices: P4(2,4), P5(2,5), P6(3,6), P7(1,3), P8(3,8), P9(2,8), P10(2,6), P11(3,8), P13(1,2), P14(1,3), P15(2,5), P17(2,7), P18(1,4), P19 (2,2), P20(2,2). Statistical test: one-way ANOVA and Bonferroni post-hoc. * $p<0.05$ ** $p<0.01$ *** $p<0.001$.

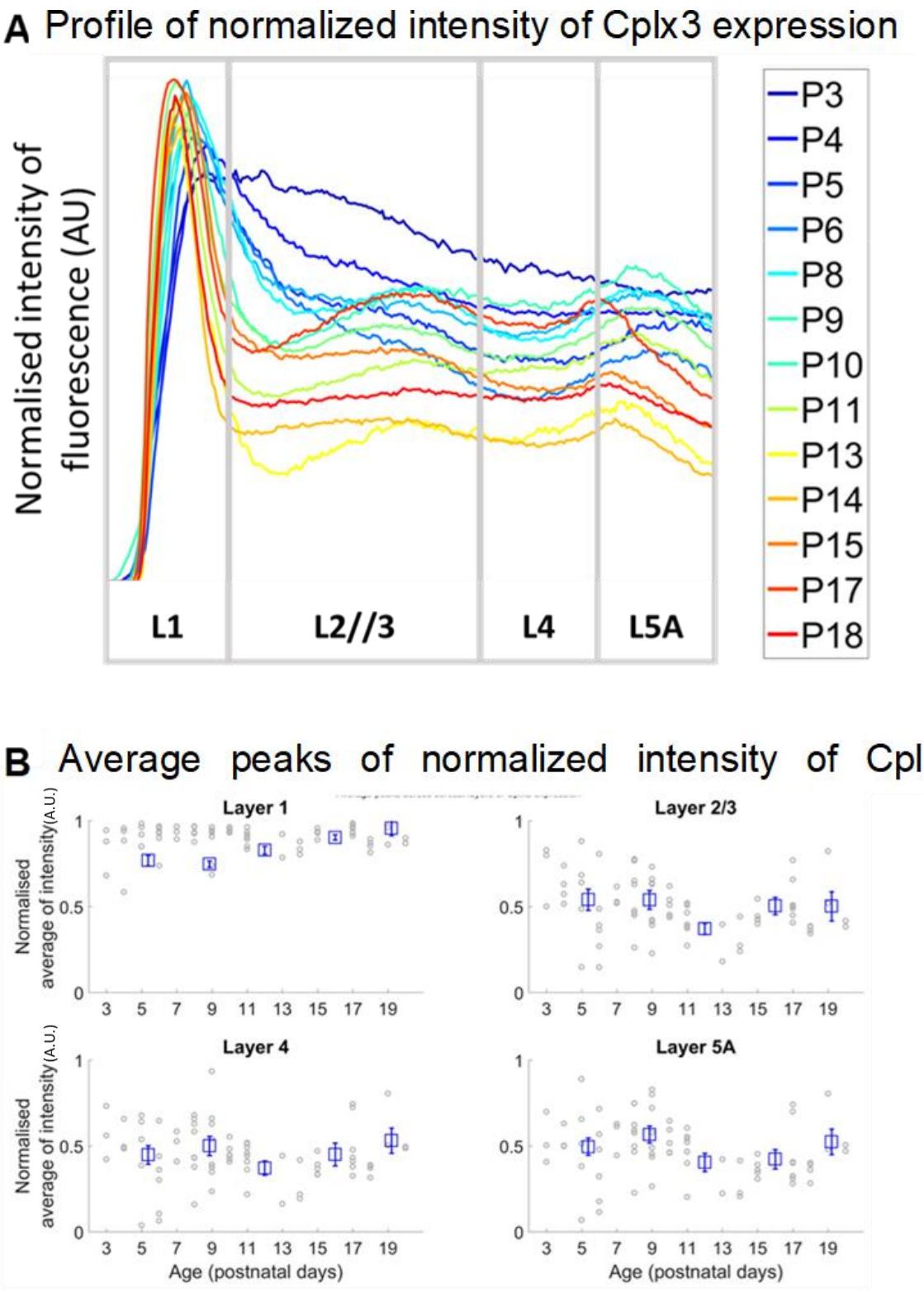

Figure 3. 27 Normalised intensity of Cplx3 in the GKD animals

A. Plot profiles of normalised intensity for Cplx3-Alexa Fluor 633. Ages are color coded from coldest (youngest) to warmest (oldest). B. Normalised laminar expression of Cplx3. Normalised data for each animal in circles and averages by animal for the age groups in squares.No statistical significance was found for any of the layers. Error bars represent SEM. Number of animals, number of slices: P4(2,4), P5(2,5), P6(3,6), P7(1,3), P8(3,8), P9(2,8), P10(2,6), P11(3,8), P13(1,2), P14(1,3), P15(2,5), P17(2,7), P18(1,4), P19 (2,2), P20(2,2).Statistical test: one-way ANOVA and Bonferroni post-hoc. * p<0.05 ** p<0.01 *** p<0.001.

3.3.3.2 Analysis of PSD95-eGFP and Cplx3 puncta characteristics

Layer 5A shows a consistent enrichment of PSD95 from early on, while SAP102 levels are seen to rise towards the middle of the 2nd postnatal week of life of the mouse. Furthermore, the expression pattern of Cplx3 suggests that the SP neurons containing this presynaptic protein are projecting to L1, L2/3 as well as L5A. As previously discussed, PSD95 is mainly postsynaptic, while Cplx3 is mainly presynaptic, therefore the question arises: are the subplate neurons projecting and making contacts directly to PSD95-containing synapses in layer 5?

In order to address this question, high magnification confocal images of L1 and L5 from coronal brain slices of the GKD mice were acquired (Fig 3.30). Firstly, we examined the protein density, size and intensity of the PSD95-eGFP and Cplx3 puncta. Because the size of the PSD is related to amounts of PSD95 and glutamate receptors and therefore synaptic strength (Holtmaat and Svoboda, 2009; Matsuzaki et al., 2004; Patterson and Yasuda, 2011; Takumi et al., 1999), this measure gives us an indication of the developmental change in strength of synapses.

In both L1 and L5A, the density of PSD95-eGFP puncta significantly increases from P8-10 until P15-17 (Fig. 3.31). In L1, the intensity and area of these puncta also increases with developmental age, from P4-10 until P18-20. In L5 PSD95-eGFP puncta increase in intensity between P4-10 and P15-17, while the area does not significantly change over development.

In L1, Cplx3-positive puncta decrease in both density and intensity between P4-7 and P8-10 (Fig. 3.32); From P11-14 the density significantly increases and stabilises, while the intensity does not change further. The area of Cplx3 puncta in this superficial layer also decreases between P4-7 and P8-10.

In L5, no developmentally regulated change in the density or intensity of Cplx3-postive puncta, but the area significantly decreases between P4-7 and P11-14.

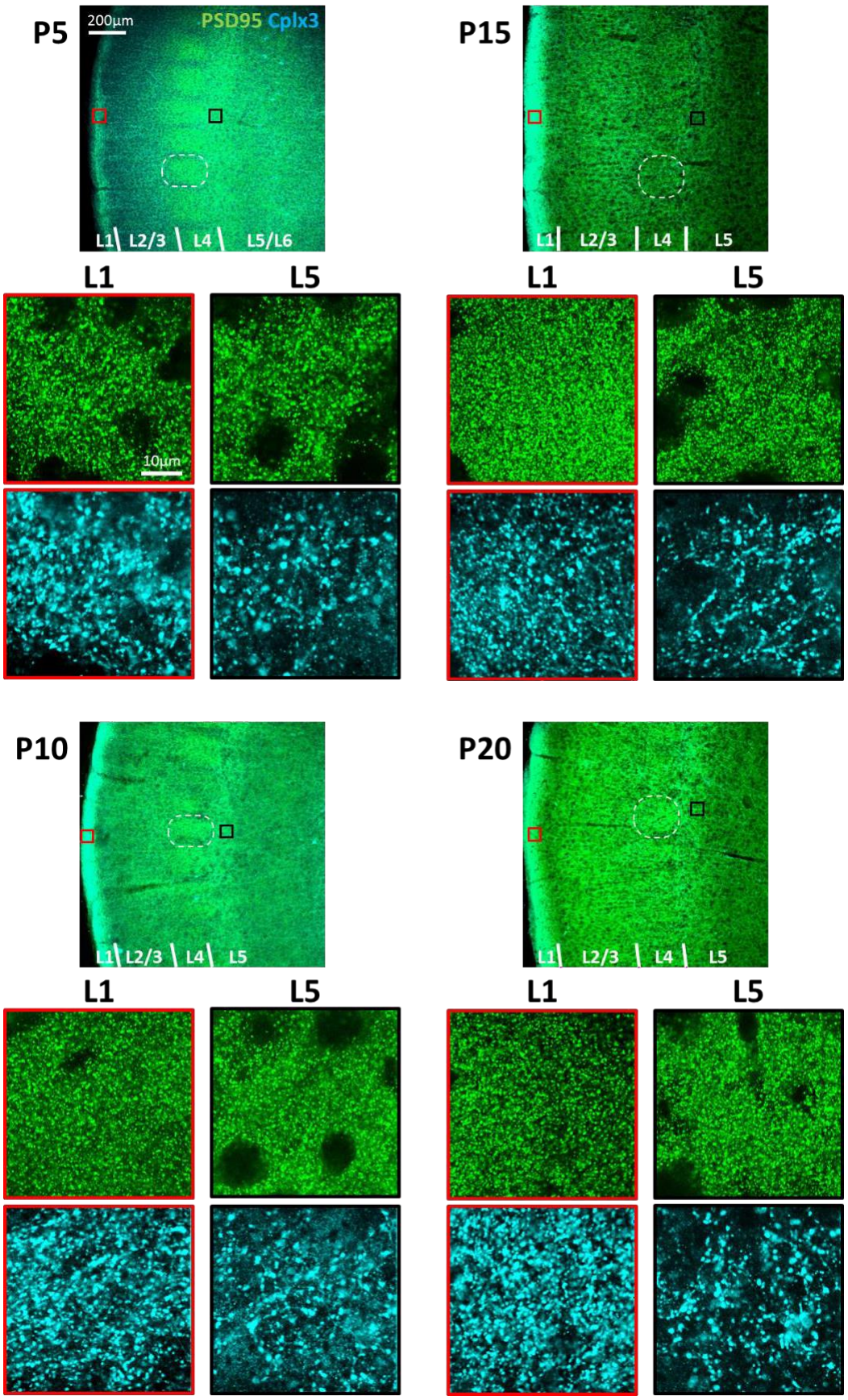

Figure 3. 28 High magnification images of L1 and L5A

Confocal imaging of PSD95-eGFP and Cplx3 in the GKD mice at specific postnatal ages. Barrels are highlighted in the white dashed circles. Zoomed in images show cortical portions from L1 (red) and L5A (black).

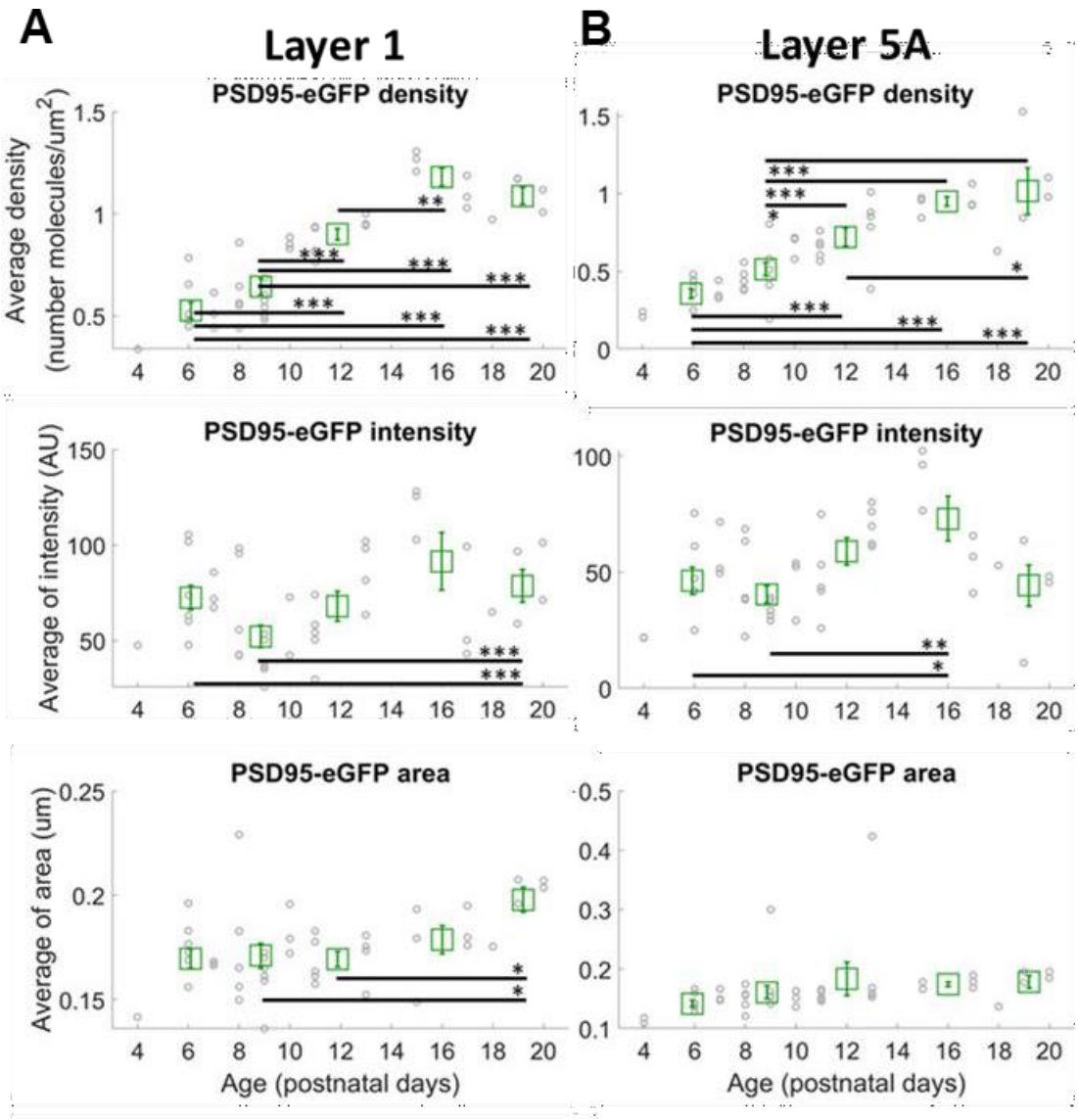

Figure 3. 29 PSD95-eGFP puncta analysis in L1 and L5A

Puncta parameters analysed were puncta density, intensity and area for Layer 1 (A) and L5A (B). Averages from single animals shown in gray cicles and averages in green squares. Error bars represent S.E.M. Number of animals, number of slices: P4(2,4), P5(2,5), P6(3,6), P7(1,3), P8(3,8), P9(2,8), P10(2,6), P11(3,8), P13(1,2), P14(1,3), P15(2,5), P17(2,7), P18(1,4), P19 (2,2), P20(2,2).Statistical test: one-way ANOVA and Bonferroni post-hoc. * $p<0.05$ ** $p<0.01$ *** $p<0.001$.

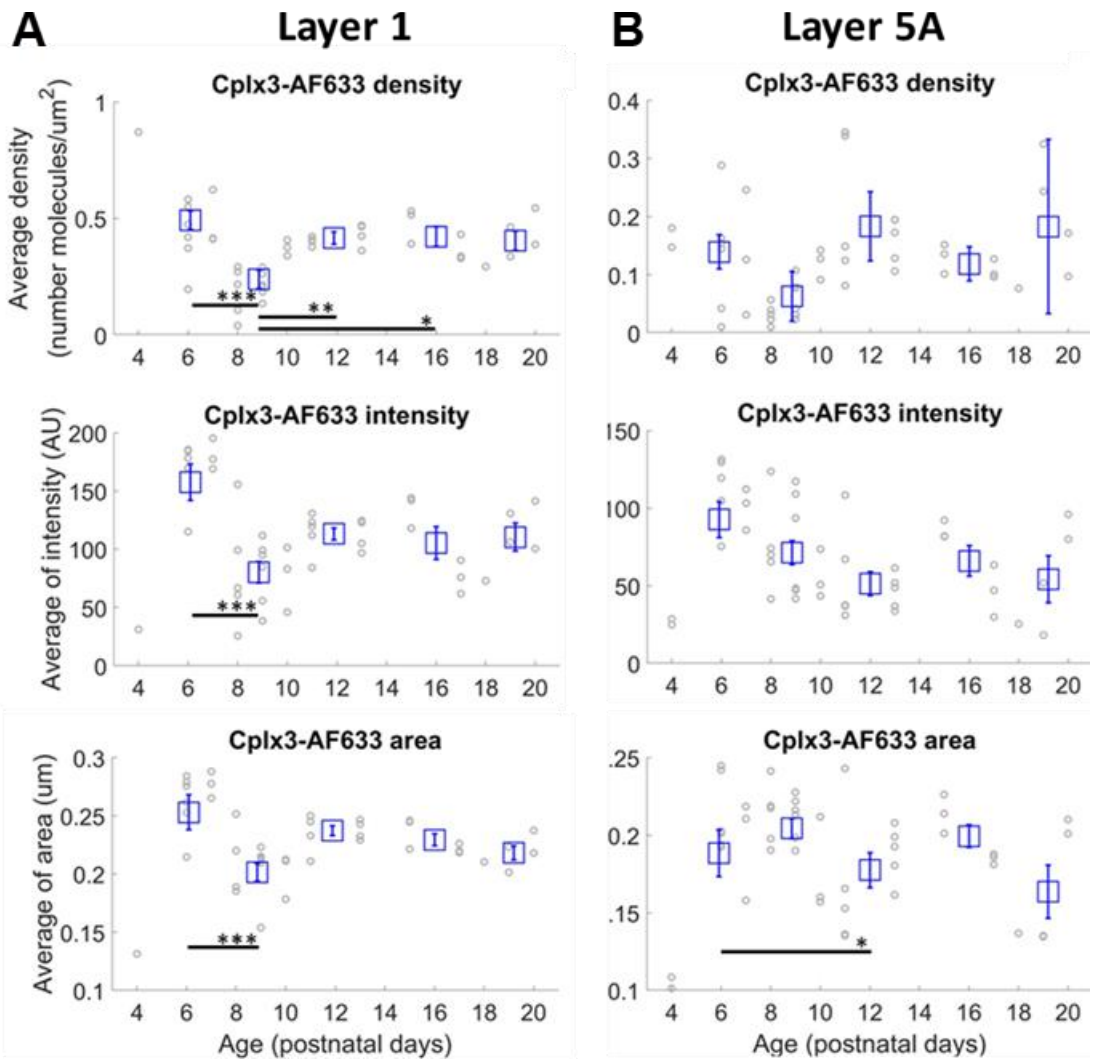

Figure 3. 30 Cplx3 puncta analysis in L1 and L5A

Puncta parameters analysed were puncta density, intensity and area for Layer 1 (A) and L5A (B). Averages from single animals shown in gray cicles and averages in blue squares. Error bars represent S.E.M. Number of animals, number of slices: P4(2,4), P5(2,5), P6(3,6), P7(1,3), P8(3,8), P9(2,8), P10(2,6), P11(3,8), P13(1,2), P14(1,3), P15(2,5), P17(2,7), P18(1,4), P19 (2,2), P20(2,2).Statistical test: one-way ANOVA and Bonferroni post-hoc. * p<0.05 ** p<0.01 *** p<0.001.

3.3.3.3 Co-localization analysis to investigate L5 enrichment

To assess the colocalization of the presynaptic Cplx3 and postsynaptic protein PSD95, a custom ImageJ macro was used to draw regions of interest around each puncta and calculate the percentage of overlap between the two proteins (colocalization percentage) and the area that they overlap by (colocalization area) in L1 and L5A (Fig. 3.33 and 3.34).

Both L1 and L5A exhibited a developmental increase in the percentage of puncta exhibiting an overlap. In fact, an increase in the percentage of PSD95-eGFP puncta that co-localise with Cplx3 between P4-10 and P11-21 was observed in both layers. The overlapping area of PSD95 onto Cplx3 peaked around P8-10 and remained stable in L1 and decreased significantly in L5.

The relatively low level of colocalization between PSD95 and Cplx3, suggests that the subplate might not be the only presynaptic partner for the PSD95-containing synapses in L5A.

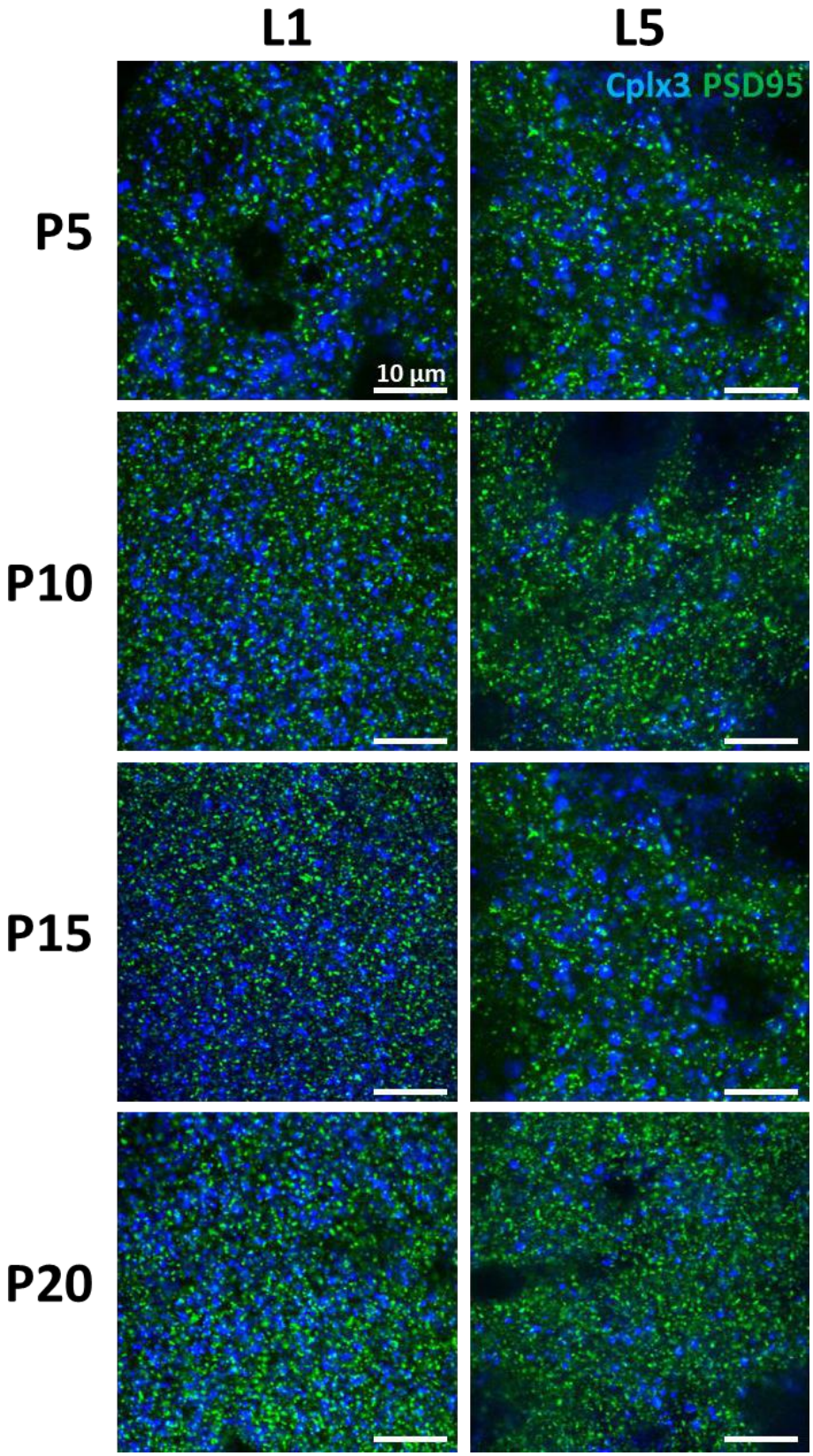

Figure 3. 31 High magnification images of PSD95 and Cpx3 puncta
Single confocal images from L1 and L5A GKD mice barrel cortex stained for Cplx3 at different postnatal ages.

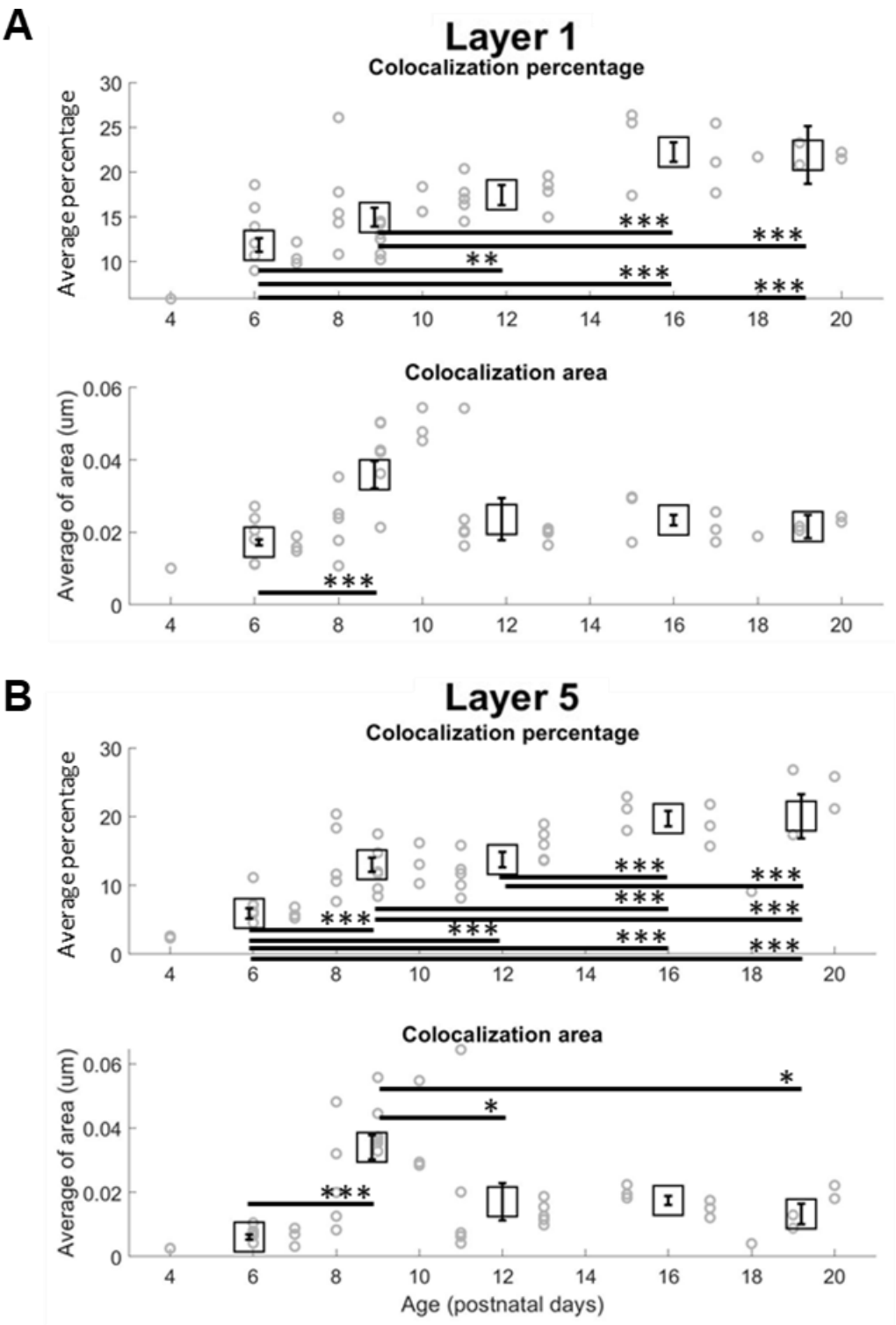

Figure 3. 32 PSD95-eGFP and Cplx3 puncta colocalisation in L1 and L5
Colocalisation percentages and areas for L1 (A) and L5A (B) is plotted as a function of postnatal day. Averages from single animals shown in gray cicles and averages in black squares. Error bars represent S.E.M. Number of animals, number of slices: P4(2,4), P5(2,5), P6(3,6), P7(1,3), P8(3,8), P9(2,8), P10(2,6), P11(3,8), P13(1,2), P14(1,3), P15(2,5), P17(2,7), P18(1,4), P19 (2,2), P20(2,2).Statistical test: one-way ANOVA and Bonferroni post-hoc. * p<0.05 ** p<0.01 *** p<0.001.

3.4 Discussion

This study provides evidence for a developmentally regulated, layer-specific expression of SAP102 and PSD95. Furthermore, it reveals an interesting developmental pattern whereby in L5A, the levels of PSD95 are high early in development.

A substantial amount of evidence suggests that PSD95 and SAP102 assume complementary but distinct roles during synapse formation and maturation: PSD95 promotes synaptic stability in mature synapses, while SAP102 is important during early trafficking of receptors to the developing synapse (Elias et al., 2008; Sans et al., 2003; Washbourne et al., 2002). We can therefore extrapolate our results about the relative distributions of these two MAGUKs and speculate about the functional sequential development of the cortical layers of the early postnatal mouse barrel cortex.

3.4.1 Methodological considerations

3.4.1.1 Genetic labelling

The visualisation of cellular proteins has been pivotal to further our understanding of the complex cellular machines and mechanisms underlying cell functions. Immunolabelling is a widely used technique that allows the visual detection of proteins via antibody binding. However, one of the main drawbacks of this technique is that it requires the fixation and permeabilization of the tissue to allow antibody binding. This method, therefore, imposes limitations on the investigation of protein dynamics as it is incompatible with live cell imaging.

An alternative approach is to tag the target protein with fluorophores (Chalfie et al., 1994; Cubitt et al., 1995). While this allows the live imaging of protein dynamics, the tagged proteins are usually overexpressed in the tissue and this perturbation can have effects on what is being studied. For example, many studies have shown that over expressing PSD95 and SAP102 leads in changes in number and size of dendritic spines, electrophysiological parameters and plasticity (Béïque and Andrade, 2003; Ehrlich and Malinow, 2004; El-Husseini et al., 2000; Stein et al., 2003).

In order avoid confounding effects due to contingent overexpression, the investigation of changes in expression of SAP102 and PSD95 in the barrel cortex during development was achieved by imaging the brains from 2 knock-in mouse lines. In these mice, gene targeting was used to make sure every single copy of the endogenous proteins is tagged with a fluorescent protein (eGFP for PSD95 and

mKO2 for SAP102) and that this tagged protein is expressed under the endogenous promoter (Zhu et al., 2018). The 1:1 stochiometric ratio of the protein to the monomeric fluorophores means that measuring parameters like the size of fluorescent puncta or the brightness accurately reflects actual changes in the proteins that have been tagged. Therefore, this technique allows for quantitative analysis of the MAGUK proteins whilst avoiding their overexpression, which, especially the case of PSD95 and SAP102, has been shown to cause undesirable morphological and functional effect (El-Husseini et al., 2000).

The introduction of proteins tagged with fluorescent molecules into the cells, however, may lead to undesired effects on protein function, targeting and folding, even when the fluorophores are relatively small and chemically inert (eGFP is 32.7 kDa and mKO2 is 24.5 kDa). For example, even though largely no overt toxicity has been detected when using GFP (Brazelton and Blau, 2005), some studies have reported induction of apoptosis and oxidative stress related to the expression of this protein (Ganini et al., 2017; Liu et al., 1999). In the PSD95-eGFP and GKD mice, a comparison between mice expressing fluorescently tagged PSD95 and SAP102 and endogenous proteins in wild type mice was carried out to examine potential negative effects of the fusion of the two proteins (Zhu et al., 2018). No abnormality was found in terms of global and regional expression levels of the proteins, subcellular targeting to the postsynaptic density or electrophysiological properties. Furthermore, general animal development, body weight and behaviour were reported to be normal. Therefore, as far as it has been investigated, in this double knock-in mouse line the tagging of the two MAGUKs and NR1 subunit does not lead to overt effects (Zhu et al., 2018).

One of the limitations of a global labelling technique, however, is that it prevents cell-type specific and high-contrast investigations. Both SAP102 and PSD95 are part of protein complexes putatively present in synaptic structure of all neuronal cell types. Therefore, in adult brains both proteins are extremely concentrated, and this makes investigating their localisation in individual neurons more complex.

Therefore, genetic tagging of the MAGUK proteins has the clear advantages over immunohistochemical and transfection methods that it allows to extract quantitative measures of the proteins and explore protein dynamics with live imaging, without encountering potentially deleterious effects of over expression of the proteins. While the live imaging aspect was not thoroughly exploited in this study, it would certainly be very interesting to follow this avenue by, for example, combining electrophysiology and calcium imaging with the imaging of PSD95-eGFP.

3.4.1.2 Identification of cortical layers

The aim of the present study was to identify developmental patterns of expression of SAP102 and PSD95 in the cortical layers of the barrel cortex. The layers were distinguished by imaging the fluorescence and discerning patterns of distributions and relating it to what is known about the cellular composition of each layer. Therefore, L1 was identified by the fact that it is the outermost layer and contains very few cell bodies (which were visible as round silhouettes lacking fluorescence). The layer 4 barrels were also clearly noticeable because of the enrichment in the barrel hollows, rather than the septa. Finally, L2/3 was defined as the area between L1 and L4, and L5A was the area just deeper from the barrel containing L4.

This method does exhibit a certain circularity, because in order to study changes in fluorescence in cortical layers we define these cortical layers using the patterns of fluorescence in the tissue. Another way to approach this and increase the subjectivity of the layer detection process would be to use independent markers. The labelling of various transcription factors has been used to label cortical layers, as they are expressed in waves during the development of the cortex (Mukhtar and Taylor, 2018). While retaining some level of laminar specificity, most of these transcription factors are expressed in several layers or cell types. For example, Cux1 preferentially labels superficial layers (L2-4), while FoxP2 is preferentially expressed in deeper layers (L5-6). The barrels of the barrel cortex can also be specifically labelled using cytochrome oxidase, Nissl stain and markers for thalamocortical afferents, such as VGlut1 and SERT (Ballester-Rosado et al., 2016; Crandall et al., 2017; Li et al., 2013; Sehara et al., 2010). These methods to label specific layers and laminar structures could be employed to provide an objective way to identify layers and also give an independent view of layer development.

3.4.1.3 Puncta analysis

High magnification single plane confocal images were analysed to extract information about fluorescent puncta size, density and intensity over development. One important consideration is that my previous images show that PSD95 is completely absent from cell bodies. In this analysis, the cell bodies have not been excluded from the analysis, and this may have a significant impact on our quantification of the density of these puncta, especially in L5A which contains more cell bodies than L1.

3.4.2 Developmentally regulated laminar distribution of proteins

Neurons in different cortical layers exhibit different ontogenetic age, morphology, connectivity and molecular profiles; they are denominated according to which layer hosts their cell body (e.g.: L2/3 neurons). However, the axonal and dendritic projections which are crucial for synaptic function usually span multiple if not all cortical layers. It is therefore crucial, when examining differences in laminar distribution of neuronal proteins, to take into account all neuronal compartments and their locations across the whole width of the neocortex, as functionally the areas affected by neurons are greatly bigger than the area where the cell body is located.

As previously discussed, PSD95 is a marker for mature synapses, as corroborated by studies showing its expression increases with age (Sans et al., 2000; Song et al., 1999). Larger dendritic spines contain bigger PSDs (Arellano et al., 2007; Harris et al., 1992; Harris and Stevens, 1989) and larger PSDs contain more AMPA and NMDA receptors (Katz et al., 2009; Noguchi et al., 2005; Nusser et al., 1998); therefore, PSD area positively correlates with synaptic strength (Holtmaat and Svoboda, 2009; Matsuzaki et al., 2004; Patterson and Yasuda, 2011; Takumi et al., 1999). PSD95 is the major component of the PSD and is thought to provide “slots” for AMPA receptors to bind to (Ehrlich and Malinow, 2004; Schnell et al., 2002; Stein et al., 2003). As receptors move in and out of the synapse, they can bind to these “slots”. PSD95 is thought to affect the number of glutamate receptors, and therefore synaptic strength, through this mechanism. Therefore, the levels of this protein can be used as a proxy for the maturation state of synapses in the different layers. On the other hand, the interpretation of the presence of SAP102 is a little bit more complicated, as this protein is highly dynamic and present in the cytoplasm, as well as in synapses (El-Husseini et al., 2000; Müller et al., 1996; Sans et al., 2005; Zheng et al., 2010).

Studies in the hippocampus have shown that in newly formed synapses MAGUKs are accumulated in an asynchronous and sequential fashion (Lambert et al., 2017). SAP102 is the first MAGUK to enrich and reach mature levels compared to neighbouring spines (within 1.5 hours), followed by SAP97 and PSD93 and finally PSD95, corroborating that this protein is specifically enriched in more functionally mature synapses. Therefore, our prediction was that on the larger scale of the cortical plate our two fluorescently tagged proteins would follow a similar temporal order, with SAP102 being enriched first and PSD95 levels ramping up subsequently (Lambert et al., 2017).

While it is true that this protein is the first MAGUK to be accumulated at newly born synapses and its levels are higher than the other MAGUKs early on, the expression of SAP102 increases developmentally, suggesting it plays a role throughout life, rather than being simply developmental.

In order to study the developmental trajectory of these two MAGUKs, developmental profiles of expression were constructed for SAP102 and PSD95. The laminar specific distribution of these proteins highlighted an interesting pattern in L5A, which prompted the investigation of the expression patterns of Cplx3 SP axonal terminal in that layer. Throughout the study, the raw data is shown to measure the amount of fluorescently-labelled proteins in specific layers; in order to compare laminar distribution between different proteins, the normalised data was analysed. The normalisation informs us of the relative contribution of the fluorescence from different layers, rather than the absolute value of fluorescence intensity.

3.4.2.1 Subcellular localisation

SAP102-mKO2 and PSD95-eGFP puncta appear to have a different characteristics and subcellular localisation. SAP102-mKO2 puncta appear much more diffuse, while PSD95-eGFP puncta appear as discrete clusters. Additionally, dual channel images show that while PSD95-eGFP is absent from both cell bodies and putatively the nucleus, SAP102-mKO2 is present in the cell body, but absent from the putative nucleus as well, suggesting this protein is expressed throughout the cytoplasm. Confirmation would be provided by DAPI staining of nuclei. These observations are consistent with the knowledge that SAP102 is a highly mobile cytoplasmic protein that is present in axons, cell bodies and dendrites, while PSD95 is specifically enriched at the post synapse (Chen et al., 2011; El-Husseini et al., 2000; Kennedy, 1997; MacGillavry et al., 2013; Müller et al., 1996; Nair et al., 2013; Sans et al., 2005; Sheng and Hoogenraad, 2007; Zheng et al., 2010).

Most puncta seem to be either SAP102 or PSD95, not a lot of overlap is obvious from my confocal images. This is consistent with data suggesting that they form distinct complexes (Frank and Grant, 2017; Frank et al., 2016). My colocalization analysis focused on PSD95 and Cplx3 solely; this is because the diffuse staining specific to SAP102-mKO2 made it difficult for the ImageJ macro to identify puncta reliably. Therefore, we can only speculate and make qualitative observations on the differential synaptic localisation of these two proteins.

3.4.2.2 Cplx3-positive subplate neurons

The barrel cortex circuits in the adult are extremely well characterised. L5A is specifically targeted by the POM nucleus of the thalamus (which also sends its axons to L1) and the primary motor cortex (Ahissar and Kleinfeld, 2003; Bureau et al., 2006; Chmielowska et al., 1989; Kim and Ebner, 1999; Koralek et al., 1988; Lu and Lin, 1993). However, because PSD95-eGFP is present from such an early age, it was speculated that early developmental circuits may be involved. One such essential early neural loops is the thalamus-subplate-L4 circuit. This connection is essential to allow the thalamocortical connections to reach their correct cortical targets (mainly L4 for VPM nucleus and L5 and L1 for POM nucleus).

Cplx3 is a presynaptic SNARE complex regulator. In the retina, it is involved in fast synaptic transmission at ribbon synapses (Reim et al., 2005). This proteins is also a subplate marker as it labels a subpopulation of these cells located between the white matter and L6 (Hoerder-Suabedissen et al., 2013, 2009). It has been reported to be expressed in glutamatergic subplate cell bodies and axonal terminals from early postnatal stages to adulthood, with its expression peaking around P8 (Hoerder-Suabedissen et al., 2013, 2009). While most of subplate markers show that the subplate terminals project to L4 from early postnatal ages, Cplx3 has been shown to be absent from L4 barrels and to be enriched in L1 and L5A (Viswanathan et al., 2017).

In order to investigate the possibility that PSD95-enriched synapses in L5A forming synapses with Cplx3-positive subplate axonal terminals, two complementary approaches can be used.: an imaging-based method by which the analysis of co-localisation of the proteins provides a measure of their possible interaction, and a functional-based method, whereby functional connectivity is tested between the subplate neurons and the layer 5 pyramidal neurons via paired stimulation. As there is little information about the connection probabilities of these two types of neurons, time constraints called for the employment of an imaging-based approach.

3.4.2.3 Laminar expression

From the earliest time points that were examined, PSD95, SAP102 and Cplx3 were significantly enriched in L1. This layers contains a sparsely distributed population of interneurons (Bradford et al., 1977; Lee et al., 2015; Schuman et al., 2019) and, primarily during early development, is populated with Cajal-Retzius neurons (Cajal, 1995). Similarly to subplate neurons, Cajal-Retzius cells are among the first neurons to be generated during development (Marín-Padilla, 1998). However, these neurons

are only present transiently and disappear by P11 in the mouse cortex (Portera-Cailliau et al., 2005). Subplate neurons have been reported to send their projections to this marginal zone, and to retract their axonal terminals to L4 by P7 (Hoerder-Suabedissen and Molnár, 2012; Piñon et al., 2009).

Due to the transient nature and scarce density of the Cajal-Retzius cells in the developing L1, it is unlikely that the fluorescent band observed in correspondence to this layer is solely due to glutamatergic PSD in these cells; furthermore, no significant decrease, but rather an increase can be detected around P11, when these cells cease to be present; this suggests that while Cajal-Retzius may express some PSD95 and SAP102, a great portion of the fluorescence proteins detected must be contained in the postsynaptic compartments of other cells.

This superficial layer is also densely populated with apical dendrites from L2/3 and L5 pyramidal neurons, probably substantially contribute to the postsynaptic compartments containing the MAGUKs imaged in this study.

During the first 3 postnatal weeks, the fluorescence of the two MAGUKs undergoes the greatest developmentally regulated increase in L2/3. This layer is also physically significantly expanding over the course of this time period. The concomitant increase in size and in fluorescence suggests that even more protein is being added in order to make this value larger, as if the number of puncta was the same but the layer was growing, the apparent density would decrease. Whilst the expression of both proteins of interest increases in L2/3, comparing the two MAGUKs led to discover that SAP102 is present at higher levels than PSD95 in the first week, and subsequently levels of PSD95 match up with those of SAP102.

The intensity of L4 appears to significantly increase in the confocal images of the GKD mice, whilst the proportional fluorescence remains stable over time. Since the mouse barrel septa are relatively small, this data has been obtained by analysing fluorescence across the whole field of view, regardless of single barrel boundary. However, further analysis focusing on the L4 barrel hollows vs. septa might provide further information on the expression of these proteins over development. For example, septal-specific distribution has been previously shown for Cplx3-SPN axonal terminals (Viswanathan et al., 2017).

The developmental pattern of expression in L5A is extremely intriguing, as PSD95 expression appears to be higher specifically in the area of the tissue before SAP102 expression increases. This is unexpected, as SAP102 has previously been reported to be expressed in abundance before PSD95. In order to investigate further what is

synapsing with the PSD95-containing postsynaptic compartment in this layer, immunohistochemistry for Cplx3 was performed on the GKD mice. This presynaptic protein, in fact, had been previously reported to be specifically enriched in L1 and L5 (Viswanathan et al., 2017). Our imaging and analysis suggest that only about 10-20% of PSD95 puncta colocalize with Cplx3 in L1 and 5-20% in L5. However, it is unclear whether all Cplx3 SPNs contain this protein at their presynaptic sites, so the Cplx3 axonal terminals may be underreported in this study. Both PSD95 and presynaptic Cplx3 appears to increase over development. Concomitantly, there is an increase of the numbers of PSD95 puncta, while the numbers of Cplx3 puncta remains mostly stable over the time period analysed. This suggests that more synapses are maturing and being enriched with PSD95 and this may lead to the increase in overlap between Cplx3 and PSD95.

Additionally to Cplx3 SPNs, there might be other presynaptic partners that are making contact with putative PSD95-eGFP containing synapses. In L5A, similarly to L1, the colocalization between postsynaptic L1 and L5A are both recipients of thalamocortical innervation from the POM (Ahissar and Kleinfeld, 2003; Bureau et al., 2006; Chmielowska et al., 1989; Kim and Ebner, 1999; Koralek et al., 1988; Lu and Lin, 1993), therefore, it is a possibility that the developmental trajectory of synaptic maturation in this layer is related to the POM pathway development. It would be very interesting to stain for these neurons and assess the developmental pattern alongside that of PSD95, SAP102, and Cplx3.

3.4.2.4 Developmental regulation

Our results suggest that the levels of SAP102, PSD95 and Cplx3 increase during the first two postnatal weeks and that their expression plateaus from P15 onwards.

The fluorescence intensity of PSD95-eGFP in L4 significantly increase between P4-8 and P11-14, suggesting these synapses are becoming more mature during this time. P4-8 is the critical period for thalamocortical inputs to L4 (Barth and Malenka, 2001; Crair and Malenka, 1995) and between P9-11 synapses in this layer undergo an extensive period of synaptogenesis (Ashby and Isaac, 2011), so it would make sense for synapses to start maturing and accumulating PSD95 around this time.

The critical period for L4 to L2/3 connections is slightly later, between P10-14 P14 (Lendvai et al., 2000; Maravall et al., 2004; Shoykhet et al., 2005; Stern et al., 2001), and the intralaminar connections in this layer mature even later (P14-17, Wen and Barth, 2011). Indeed, in this layer, the relative intensity of SAP102 is higher that PSD95 between P4-7; additionally, a significant spike in PSD95 raw expression can

be observed around P11-14 and the levels continue to rise until P17 when the expression profile plateaus.

Therefore, the observed changes in SAP102 and PSD95 expression align with the idea that synapses are maturing at particular times, slightly different between layers.

Consistently with previous reports of Cplx3 expression, in the GKD mice this protein was highly expressed in L1 and L5A, but absent from L4 barrels at all postnatal ages investigated. Our results, furthermore, suggest that the expression of this protein is stable until approximately P11 and then peaks around the end of the 2nd postnatal week, slightly later than was shown in previous studies.

3.4.3 Future studies

The use of the GKD knock-in mouse line and my results offer the scope for many prospective studies to understand synaptic and network changes occurring during early postnatal development.

In terms of expanding our understanding of MAGUKs, the following experiments can be carried out; It would be interesting to construct developmental profiles of laminar expression of other proteins. For example, as changes in MAGUKs are thought to occur simultaneously with the developmental switch of NR2B to NR2A, staining for specific NMDAR subunits and looking at their relative enrichment over time compared with the MAGUKs could provide insight into structural-functional synaptic development.

Subcellular localisation suggested that PSD95 is specifically enriched in some synapses, so a further experiment would be to combine 2P imaging to characterise PSD95 content in dendritic spines and perform glutamate uncaging; by specifically targeting PSD95-enriched vs. PSD95-depleted dendrites, it would be possible to investigate changes (if any) in electrophysiological properties e.g. AMPA-to-NMDA ratio, EPSP kinetics characteristic of NMDAR subunit (and relate this to the developmental switch); this would allow to collect information about the relationship between the presence of this mature marker and mature electrophysiologic signature.

Further experiments can be conducted to explore the relationship between the Cplx3-positive subplate neurons and L5A. For example, paired recordings between SP and L5A would help elucidate whether they are functionally connected. Also exploring the spatiotemporal pattern of thalamocortical inputs in relation to PSD95-eGFP and Cplx3 expression in L5A via immunohistochemistry, neuronal retrograde labelling or crosses with thalamic reporter lines would further our understanding of the temporal sequence

of thalamocortical and subplate innervations of L5A and relate it to neuronal maturation using SAP102 and PSD95 as proxies.

Finally, it would be very interesting to investigate changes in MAGUKs following manipulation of the development of the barrel cortex via experience-deprivation experiments (either infraorbital nerve severing or whisker trimming/ablatio) or genetic approaches (for example on genetically silenced models such as in the conditional Snap 25 knock-out mouse line, Hoerder-Suabedissen et al., 2019; Korrell et al., 2019).

Chapter 4: General discussion and conclusion

The first 3 weeks of neocortical development are rich in synaptic and network changes; synapses are added and eliminated, neuronal proteins are trafficked around and are developmentally regulated, and many functional switches occur. Changes in the structure and the function in the developing neuronal network are closely linked to and all work towards the refinement of the neural circuit to give rise to a fully mature and operational brain. We know that this is important because when aspects of this finely tuned developmental mechanisms go wrong, it can lead to neurodevelopmental disorders. For example, aberrant expression of the two proteins investigated during my PhD have been implicated in several neurodevelopmental disorders, such as autism spectrum disorder and schizophrenia. Whilst the contributing factors to these disorders is most likely multifactorial, and it is difficult to disentangle cause and effect, understanding how brain development occurs normally is crucial to understand what happens when process goes wrong.

The focus of this research was to investigate whether dendritic spikes can occur early in development and to construct a developmental profile of the laminar distribution of SAP102 and PSD95 during the first 3 postnatal weeks of life of mouse pups.

Dendritic spikes have been shown to play an active role during synaptic plasticity, both instructing it and being affected by it. Therefore, it is speculated that these events may be important during synaptic development, a period of extreme and widespread plasticity that crucially relies on synaptic activity. However, to date only one study has shown nonlinear activity in the developing L4 spiny stellate neurons (Lavzin et al., 2012). In these studies, P15-20 brain slices were probed for dendritic spikes and NMDA-dependent regenerative activity was elicited using focal synaptic stimulation.

I attempted to replicate these results in the same animal model and cell type, and using a very similar approach, in the same age range and earlier in order to map out how early on dendritic spikes could be elicited; the developmental angle was taken to try and unpick at what point during development barrel cortex neurons express the synaptic machinery necessary to support these events.

However, in contrast to the data shown in the Lavzin paper (Lavzin et al., 2012), the lack of overt nonlinearity in my responses suggests that dendritic spikes either were not elicited because of technical difficulties, or they simply are not a prominent feature

of immature neurons. This negative result was consistent both at very young ages (P7-15), and during the 3rd postnatal week.

The focus of my PhD then moved onto investigating sequential synaptic development in the cortical layers of the mouse barrel cortex, using PSD95 and SAP102 as a proxy for mature and developing synapses, respectively. The developmental profile of expression was constructed by confocal imaging of the PSD95-eGFP and GKD mouse cortices. This approach revealed a precise and robust developmental pattern of expression of these two MAGUKs in the different cortical layers. The levels of both PSD95 and SAP102 increased with developmental age. Whilst levels of both proteins were high in L1 and L4, compared to the rest of the layers, the levels in L2/3 doubled or quadrupled over the three postnatal weeks. L5A exhibited an interesting pattern, by which PSD95 was present in a band just deeper of L4 from early on, while levels of SAP102 increased over postnatal development. Further investigation revealed that Cplx3 subplate neurons project to this area from the first to the third postnatal week; therefore, neurons from this early-born layer might be responsible for at least a portion of the maturing synapses in cortical L5A.

The dendritic spike experiments were carried out in L4 spiny stellate neurons, the main cell type in the L4 barrels, between the second and third postnatal week. The developmental expression of PSD95 shows that this protein is enriched in this area from early on, but its expression peaks around the end of the second postnatal week. This suggests that synaptic maturation, as inferred from the presence of PSD95, occurs around then. As, in my hands, dendritic spikes were not elicited between P7 and P20, this suggests that more mature mechanism may be required to elicit dendritic spikes in these cells.

Main results

In conclusion these were my main results:

1. Between P7-20, focal synaptic stimulation causes no obvious nonlinearity in subthreshold EPSPs in response to increasing stimulus intensity.

2. Hyperpolarisation-induced block of NMDARs causes a decrease in duration of the postsynaptic response, suggesting these receptors are contributing to the depolarised state of the neuron in these young cells.

3. SAP102 and PSD95 follow a developmentally regulated, lamina specific pattern of distribution in the barrel neocortex.

4. PSD95 is specifically enriched in L5A early on, before SAP102 levels increase, and this layer receives innervation from Cplx3^{+} subplate neurons.

Future directions

The PSD95-eGFP and GKD mice are a powerful tool to investigate neuronal development. A major advantage of a knock-in mouse line is the ability to live image the tagged proteins, without needing to fix or process the sample in any way. This provides a way to investigate functional changes related to the presence of that protein in particular locations.

Preliminary experiments where I have patched and filled the neuron with Alexa fluorescence dyes to visualise the structure, have suggested that PSD95 is found in several mature looking (mushroom shaped, rather than filopodia) synapses, but not all. Therefore, it would be extremely interesting to specifically select dendrites containing a large number of PSD95-eGFP proteins in their dendritic spines and perform glutamate uncaging on these spines to try eliciting dendritic spikes. Then compare these results with the stimulation of dendrites mostly lacking PSD95-eGFP. In order to do so, a more thorough characterisation of the subcellular localisation of PSD95-eGFP in the different cortical neurons, at different developmental stages, would be required.

Bibliography

Ackman, J.B., Burbridge, T.J., Crair, M.C., 2012. Retinal waves coordinate patterned activity throughout the developing visual system. Nature 490, 219–225. https://doi.org/10.1038/nature11529

Agmon, A., Connors, B.W., 1991. Thalamocortical responses of mouse somatosensory (barrel) cortex in vitro. Neuroscience 41, 365–379.

Agmon, A., Yang, L.T., O'Dowd, D.K., Jones, E.G., 1993. Organized growth of thalamocortical axons from the deep tier of terminations into layer IV of developing mouse barrel cortex. J. Neurosci. Off. J. Soc. Neurosci. 13, 5365–5382.

Ahissar, E., Kleinfeld, D., 2003. Closed-loop Neuronal Computations: Focus on Vibrissa Somatosensation in Rat. Cereb. Cortex 13, 53–62. https://doi.org/10.1093/cercor/13.1.53

Ahissar, E., Sosnik, R., Bagdasarian, K., Haidarliu, S., 2001. Temporal frequency of whisker movement. II. Laminar organization of cortical representations. J. Neurophysiol. 86, 354–367. https://doi.org/10.1152/jn.2001.86.1.354

Akhmetshina, D., Nasretdinov, A., Zakharov, A., Valeeva, G., Khazipov, R., 2016. The Nature of the Sensory Input to the Neonatal Rat Barrel Cortex. J. Neurosci. Off. J. Soc. Neurosci. 36, 9922–9932. https://doi.org/10.1523/JNEUROSCI.1781-16.2016

Al-Hallaq, R.A., Yasuda, R.P., Wolfe, B.B., 2001. Enrichment of N-methyl-D-aspartate NR1 splice variants and synaptic proteins in rat postsynaptic densities. J. Neurochem. 77, 110–119. https://doi.org/10.1046/j.1471-4159.2001.t01-1-00210.x

Allendoerfer, K.L., Shatz, C.J., 1994. The subplate, a transient neocortical structure: its role in the development of connections between thalamus and cortex. Annu. Rev. Neurosci. 17, 185–218. https://doi.org/10.1146/annurev.ne.17.030194.001153

Allene, C., Cossart, R., 2010. Early NMDA receptor-driven waves of activity in the developing neocortex: physiological or pathological network oscillations? J. Physiol. 588, 83–91. https://doi.org/10.1113/jphysiol.2009.178798

Alloway, K.D., Zhang, M., Chakrabarti, S., 2004. Septal columns in rodent barrel cortex: functional circuits for modulating whisking behavior. J. Comp. Neurol. 480, 299–309. https://doi.org/10.1002/cne.20339

Amitai, Y., Friedman, A., Connors, B.W., Gutnick, M.J., 1993. Regenerative activity in apical dendrites of pyramidal cells in neocortex. Cereb. Cortex N. Y. N 1991 3, 26–38. https://doi.org/10.1093/cercor/3.1.26

Anderson, S., Mione, M., Yun, K., Rubenstein, J.L., 1999. Differential origins of neocortical projection and local circuit neurons: role of Dlx genes in neocortical interneuronogenesis. Cereb Cortex 9, 646–654.

Anderson, S.A., Marin, O., Horn, C., Jennings, K., Rubenstein, J.L., 2001. Distinct cortical migrations from the medial and lateral ganglionic eminences. Development.

Angevine, J.B., Sidman, R.L., 1961. Autoradiographic study of cell migration during histogenesis of cerebral cortex in the mouse. Nature 192, 766–768. https://doi.org/10.1038/192766b0

Antic, S.D., Zhou, W.-L., Moore, A.R., Short, S.M., Ikonomu, K.D., 2010. The decade of the dendritic NMDA spike. J. Neurosci. Res. 88, 2991–3001. https://doi.org/10.1002/jnr.22444

Antón-Bolaños, N., Espinosa, A., López-Bendito, G., 2018. Developmental interactions between thalamus and cortex: a true love reciprocal story. Curr. Opin. Neurobiol. 52, 33–41. https://doi.org/10.1016/j.conb.2018.04.018

Antonini, A., Shatz, C.J., 1990. Relation Between Putative Transmitter Phenotypes and Connectivity of Subplate Neurons During Cerebral Cortical Development. Eur. J. Neurosci. 2, 744–761. https://doi.org/10.1111/j.1460-9568.1990.tb00465.x

Arakawa, H., Erzurumlu, R.S., 2015. Role of whiskers in sensorimotor development of C57BL/6 mice. Behav. Brain Res. 287, 146–155. https://doi.org/10.1016/j.bbr.2015.03.040

Araya, R., Eisenthal, K.B., Yuste, R., 2006. Dendritic spines linearize the summation of excitatory potentials. Proc. Natl. Acad. Sci. U. S. A. 103, 18799–18804. https://doi.org/10.1073/pnas.0609225103

Archie, K.A., Mel, B.W., 2000. A model for intradendritic computation of binocular disparity. Nat. Neurosci. 3, 54–63. https://doi.org/10.1038/71125

Arellano, J.I., Benavides-Piccione, R., Defelipe, J., Yuste, R., 2007. Ultrastructure of dendritic spines: correlation between synaptic and spine morphologies. Front. Neurosci. 1, 131–143. https://doi.org/10.3389/neuro.01.1.1.010.2007

Armstrong-James, M., Fox, K., 1987. Spatiotemporal convergence and divergence in the rat S1 “barrel” cortex. J. Comp. Neurol. 263, 265–281. https://doi.org/10.1002/cne.902630209

Arnold, P.B., Li, C.X., Waters, R.S., 2001. Thalamocortical arbors extend beyond single cortical barrels: an in vivo intracellular tracing study in rat. Exp. Brain Res. 136, 152–168. https://doi.org/10.1007/s002210000570

Ashby, M.C., Isaac, J.T.R., 2011. Maturation of a Recurrent Excitatory Neocortical Circuit by Experience-Dependent Unsilencing of Newly Formed Dendritic Spines. Neuron 70, 510–521. https://doi.org/10.1016/j.neuron.2011.02.057

Audette, N.J., Urban-Ciecko, J., Matsushita, M., Barth, A.L., 2018. POm Thalamocortical Input Drives Layer-Specific Microcircuits in Somatosensory Cortex. Cereb. Cortex N. Y. N 1991 28, 1312–1328. https://doi.org/10.1093/cercor/bhx044

Auladell, C., Pérez-Sust, P., Supèr, H., Soriano, E., 2000. The early development of thalamocortical and corticothalamic projections in the mouse. Anat. Embryol. (Berl.) 201, 169–179. https://doi.org/10.1007/pl00008238

Azevedo, F.A.C., Carvalho, L.R.B., Grinberg, L.T., Farfel, J.M., Ferretti, R.E.L., Leite, R.E.P., Filho, W.J., Lent, R., Herculano-Houzel, S., 2009. Equal numbers of neuronal and nonneuronal cells make the human brain an isometrically scaled-up primate brain. J. Comp. Neurol. 513, 532–541. https://doi.org/10.1002/cne.21974

Ballester-Rosado, C.J., Sun, H., Huang, J.-Y., Lu, H.-C., 2016. mGluR5 Exerts Cell-Autonomous Influences on the Functional and Anatomical Development of Layer IV Cortical Neurons in the Mouse Primary Somatosensory Cortex. J. Neurosci. 36, 8802–8814. https://doi.org/10.1523/JNEUROSCI.1224-16.2016

Bard, L., Sainlos, M., Bouchet, D., Cousins, S., Mikasova, L., Breillat, C., Stephenson, F.A., Imperiali, B., Choquet, D., Groc, L., 2010. Dynamic and specific interaction between synaptic NR2-NMDA receptor and PDZ proteins. Proc. Natl. Acad. Sci. U. S. A. 107, 19561–19566. https://doi.org/10.1073/pnas.1002690107

Barrow, S.L., Constable, J.R., Clark, E., El-Sabeawy, F., McAllister, A.K., Washbourne, P., 2009. Neuroligin1: a cell adhesion molecule that recruits PSD-95 and NMDA receptors by distinct mechanisms during synaptogenesis. Neural Develop. 4, 17. https://doi.org/10.1186/1749-8104-4-17

Barth, A.L., Malenka, R.C., 2001. NMDAR EPSC kinetics do not regulate the critical period for LTP at thalamocortical synapses. Nat. Neurosci. 4, 235–236. https://doi.org/10.1038/85070

Bartlett, T.E., Bannister, N.J., Collett, V.J., Dargan, S.L., Massey, P.V., Bortolotto, Z.A., Fitzjohn, S.M., Bashir, Z.I., Collingridge, G.L., Lodge, D., 2007. Differential roles of NR2A and NR2B-containing NMDA receptors in LTP and LTD in the CA1 region of two-week old rat hippocampus. Neuropharmacology 52, 60–70. https://doi.org/10.1016/j.neuropharm.2006.07.013

Bats, C., Groc, L., Choquet, D., 2007. The interaction between Stargazin and PSD-95 regulates AMPA receptor surface trafficking. Neuron 53, 719–734. https://doi.org/10.1016/j.neuron.2007.01.030

Bavelier, D., Levi, D.M., Li, R.W., Dan, Y., Hensch, T.K., 2010. Removing brakes on adult brain plasticity: from molecular to behavioral interventions. J. Neurosci. Off. J. Soc. Neurosci. 30, 14964–14971. https://doi.org/10.1523/JNEUROSCI.4812-10.2010

Béïque, J.-C., Andrade, R., 2003. PSD-95 regulates synaptic transmission and plasticity in rat cerebral cortex. J. Physiol. 546, 859–867. https://doi.org/10.1113/jphysiol.2002.031369

Béïque, J.-C., Lin, D.-T., Kang, M.-G., Aizawa, H., Takamiya, K., Huganir, R.L., 2006. Synapse-specific regulation of AMPA receptor function by PSD-95. Proc. Natl. Acad. Sci. U. S. A. 103, 19535–19540. https://doi.org/10.1073/pnas.0608492103

Bender, K.J., Rangel, J., Feldman, D.E., 2003. Development of Columnar Topography in the Excitatory Layer 4 to Layer 2/3 Projection in Rat Barrel Cortex. J. Neurosci. 23, 8759–8770. https://doi.org/10.1523/JNEUROSCI.23-25-08759.2003

Bentivoglio, M., Mazzarello, P., 1999. The history of radial glia. Brain Res Bull 49, 305–315.

Berger, T., Larkum, M.E., Lüscher, H.R., 2001. High I(h) channel density in the distal apical dendrite of layer V pyramidal cells increases bidirectional attenuation of EPSPs. J. Neurophysiol. 85, 855–868. https://doi.org/10.1152/jn.2001.85.2.855

Binshtok, A.M., Fleidervish, I.A., Sprengel, R., Gutnick, M.J., 2006. NMDA Receptors in Layer 4 Spiny Stellate Cells of the Mouse Barrel Cortex Contain the NR2C Subunit. J. Neurosci. 26, 708–715. https://doi.org/10.1523/JNEUROSCI.4409-05.2006

Bloss, E.B., Cembrowski, M.S., Karsh, B., Colonell, J., Fetter, R.D., Spruston, N., 2018. Single excitatory axons form clustered synapses onto CA1 pyramidal cell dendrites. Nat. Neurosci. 21, 353–363. https://doi.org/10.1038/s41593-018-0084-6

Blue, M.E., Parnavelas, J.G., 1983. The formation and maturation of synapses in the visual cortex of the rat. I. Qualitative analysis. J. Neurocytol. 12, 599–616. https://doi.org/10.1007/BF01181526

Boon, J., Clarke, E., Kessaris, N., Goffinet, A., Molnár, Z., Hoerder-Suabedissen, A., 2019. Long-range projections from sparse populations of GABAergic neurons in murine subplate. J. Comp. Neurol. 527, 1610–1620. https://doi.org/10.1002/cne.24592

Bradford, R., Parnavels, J.G., Lieberman, A.R., 1977. Neurons in layer I of the developing occipital cortex of the rat. J. Comp. Neurol. 176, 121–132. https://doi.org/10.1002/cne.901760108

Branco, T., Häusser, M., 2011. Synaptic Integration Gradients in Single Cortical Pyramidal Cell Dendrites. Neuron 69, 885–892. https://doi.org/10.1016/j.neuron.2011.02.006

Branco, T., Häusser, M., 2010. The single dendritic branch as a fundamental functional unit in the nervous system. Curr. Opin. Neurobiol., Signalling mechanisms 20, 494–502. https://doi.org/10.1016/j.conb.2010.07.009

Brandalise, F., Carta, S., Helmchen, F., Lisman, J., Gerber, U., 2016. Dendritic NMDA spikes are necessary for timing-dependent associative LTP in CA3 pyramidal cells. Nat. Commun. 7, 13480. https://doi.org/10.1038/ncomms13480

Brazelton, T.R., Blau, H.M., 2005. Optimizing techniques for tracking transplanted stem cells in vivo. Stem Cells Dayt. Ohio 23, 1251–1265. https://doi.org/10.1634/stemcells.2005-0149

Brecht, M., Roth, A., Sakmann, B., 2003. Dynamic receptive fields of reconstructed pyramidal cells in layers 3 and 2 of rat somatosensory barrel cortex. J. Physiol. 553, 243–265. https://doi.org/10.1113/jphysiol.2003.044222

Bresler, T., Ramati, Y., Zamorano, P.L., Zhai, R., Garner, C.C., Ziv, N.E., 2001. The dynamics of SAP90/PSD-95 recruitment to new synaptic junctions. Mol. Cell. Neurosci. 18, 149–167. https://doi.org/10.1006/mcne.2001.1012

Broadhead, M.J., Horrocks, M.H., Zhu, F., Muresan, L., Benavides-Piccione, R., DeFelipe, J., Fricker, D., Kopanitsa, M.V., Duncan, R.R., Klenerman, D., Komiyama, N.H., Lee, S.F., Grant, S.G.N., 2016. PSD95 nanoclusters are postsynaptic building blocks in hippocampus circuits. Sci. Rep. 6. https://doi.org/10.1038/srep24626

Brown, K.N., Chen, S., Han, Z., Lu, C.H., Tan, X., Zhang, X.J., Ding, L., Lopez-Cruz, A., Saur, D., Anderson, S.A., Huang, K., Shi, S.H., 2011. Clonal production and organization of inhibitory interneurons in the neocortex. Science 334, 480–486.

Bruno, R.M., Khatri, V., Land, P.W., Simons, D.J., 2003. Thalamocortical angular tuning domains within individual barrels of rat somatosensory cortex. J. Neurosci. Off. J. Soc. Neurosci. 23, 9565–9574.

Bureau, I., Shepherd, G.M.G., Svoboda, K., 2004. Precise Development of Functional and Anatomical Columns in the Neocortex. Neuron 42, 789–801. https://doi.org/10.1016/j.neuron.2004.05.002

Bureau, I., von Saint Paul, F., Svoboda, K., 2006. Interdigitated paralemniscal and lemniscal pathways in the mouse barrel cortex. PLoS Biol. 4, e382. https://doi.org/10.1371/journal.pbio.0040382

Burns, M.E., Augustine, G.J., 1995. Synaptic structure and function: Dynamic organization yields architectural precision. Cell 83, 187–194. https://doi.org/10.1016/0092-8674(95)90160-4

Bustos, F.J., Varela-Nallar, L., Campos, M., Henriquez, B., Phillips, M., Opazo, C., Aguayo, L.G., Montecino, M., Constantine-Paton, M., Inestrosa, N.C., Zundert, B. van, 2014. PSD95 Suppresses Dendritic Arbor Development in Mature Hippocampal Neurons by Occluding the Clustering of NR2B-NMDA Receptors. PLOS ONE 9, e94037. https://doi.org/10.1371/journal.pone.0094037

Bystron, I., Blakemore, C., Rakic, P., 2008. Development of the human cerebral cortex: Boulder Committee revisited. Nat. Rev. Neurosci. 9, 110–122. https://doi.org/10.1038/nrn2252

Cai, C., Li, H., Rivera, C., Keinänen, K., 2006. Interaction between SAP97 and PSD-95, Two Maguk Proteins Involved in Synaptic Trafficking of AMPA Receptors. J. Biol. Chem. 281, 4267–4273. https://doi.org/10.1074/jbc.M505886200

Cameron, R.S., Rakic, P., 1991. Glial cell lineage in the cerebral cortex: a review and synthesis. Glia.

Campbell, K., Götz, M., 2002. Radial glia: multi-purpose cells for vertebrate brain development. Trends Neurosci. 25, 235–238. https://doi.org/10.1016/S0166-2236(02)02156-2

Cane, M., Maco, B., Knott, G., Holtmaat, A., 2014. The relationship between PSD-95 clustering and spine stability in vivo. J. Neurosci. Off. J. Soc. Neurosci. 34, 2075–2086. https://doi.org/10.1523/JNEUROSCI.3353-13.2014

Cang, J., Feldheim, D.A., 2013. Developmental mechanisms of topographic map formation and alignment. Annu. Rev. Neurosci. 36, 51–77. https://doi.org/10.1146/annurev-neuro-062012-170341

Carmignoto, G., Vicini, S., 1992. Activity-dependent decrease in NMDA receptor responses during development of the visual cortex. Science 258, 1007–1011. https://doi.org/10.1126/science.1279803

Catalano, S.M., Robertson, R.T., Killackey, H.P., 1991. Early ingrowth of thalamocortical afferents to the neocortex of the prenatal rat. Proc. Natl. Acad. Sci. U. S. A. 88, 2999–3003. https://doi.org/10.1073/pnas.88.8.2999

Catalano, S.M., Shatz, C.J., 1998. Activity-dependent cortical target selection by thalamic axons. Science 281, 559–562. https://doi.org/10.1126/science.281.5376.559

Caviness, V.S., Rakic, P., 1978. Mechanisms of cortical development: a view from mutations in mice. Annu. Rev. Neurosci. 1, 297–326. https://doi.org/10.1146/annurev.ne.01.030178.001501

Chakrabarti, S., Alloway, K.D., 2006. Differential origin of projections from SI barrel cortex to the whisker representations in SII and MI. J. Comp. Neurol. 498, 624–636. https://doi.org/10.1002/cne.21052

Chalfie, M., Tu, Y., Euskirchen, G., Ward, W.W., Prasher, D.C., 1994. Green fluorescent protein as a marker for gene expression. Science 263, 802–805. https://doi.org/10.1126/science.8303295

Chapin, J.K., Lin, C.S., 1984. Mapping the body representation in the SI cortex of anesthetized and awake rats. J. Comp. Neurol. 229, 199–213. https://doi.org/10.1002/cne.902290206

Chen, B.-S., Thomas, E.V., Sanz-Clemente, A., Roche, K.W., 2011. NMDA Receptor-Dependent Regulation of Dendritic Spine Morphology by SAP102 Splice Variants. J. Neurosci. 31, 89–96. https://doi.org/10.1523/JNEUROSCI.1034-10.2011

Chen, C.-C., Bajnath, A., Brumberg, J.C., 2015. The impact of development and sensory deprivation on dendritic protrusions in the mouse barrel cortex. Cereb. Cortex N. Y. N 1991 25, 1638–1653. https://doi.org/10.1093/cercor/bht415

Chen, H., Epstein, J., Stern, E., 2010. Neural plasticity after acquired brain injury: evidence from functional neuroimaging. PM R 2, S306-312. https://doi.org/10.1016/j.pmrj.2010.10.006

Chen, J.L., Villa, K.L., Cha, J.W., So, P.T.C., Kubota, Y., Nedivi, E., 2012. Clustered Dynamics of Inhibitory Synapses and Dendritic Spines in the Adult Neocortex. Neuron 74, 361–373. https://doi.org/10.1016/j.neuron.2012.02.030

Chen, Xiaowei, Leischner, U., Rochefort, N.L., Nelken, I., Konnerth, A., 2011. Functional mapping of single spines in cortical neurons in vivo. Nature 475, 501–505. https://doi.org/10.1038/nature10193

Chen, Xiaobing, Nelson, C.D., Li, X., Winters, C.A., Azzam, R., Sousa, A.A., Leapman, R.D., Gainer, H., Sheng, M., Reese, T.S., 2011. PSD-95 is required to sustain the molecular organization of the postsynaptic density. J. Neurosci. Off. J. Soc. Neurosci. 31, 6329–6338. https://doi.org/10.1523/JNEUROSCI.5968-10.2011

Cheng, D., Hoogenraad, C.C., Rush, J., Ramm, E., Schlager, M.A., Duong, D.M., Xu, P., Wijayawardana, S.R., Hanfelt, J., Nakagawa, T., Sheng, M., Peng, J., 2006. Relative and absolute quantification of postsynaptic density proteome isolated from rat forebrain and cerebellum. Mol. Cell. Proteomics MCP 5, 1158–1170. https://doi.org/10.1074/mcp.D500009-MCP200

Chittajallu, R., Isaac, J.T.R., 2010. Emergence of cortical inhibition by coordinated sensory-driven plasticity at distinct synaptic loci. Nat. Neurosci. 13, 1240–1248. https://doi.org/10.1038/nn.2639

Chmielowska, J., Carvell, G.E., Simons, D.J., 1989. Spatial organization of thalamocortical and corticothalamic projection systems in the rat SmI barrel cortex. J. Comp. Neurol. 285, 325–338. https://doi.org/10.1002/cne.902850304

Clancy, B., Silva-Filho, M., Friedlander, M.J., 2001. Structure and projections of white matter neurons in the postnatal rat visual cortex. J. Comp. Neurol. 434, 233–252. https://doi.org/10.1002/cne.1174

Clause, A., Kim, G., Sonntag, M., Weisz, C.J.C., Vetter, D.E., Rűbsamen, R., Kandler, K., 2014. The Precise Temporal Pattern of Prehearing Spontaneous Activity Is Necessary for Tonotopic Map Refinement. Neuron 82, 822–835. https://doi.org/10.1016/j.neuron.2014.04.001

Colbert, C.M., Magee, J.C., Hoffman, D.A., Johnston, D., 1997. Slow recovery from inactivation of Na+ channels underlies the activity-dependent attenuation of dendritic action potentials in hippocampal CA1 pyramidal neurons. J. Neurosci. Off. J. Soc. Neurosci. 17, 6512–6521.

Collins, M.O., Husi, H., Yu, L., Brandon, J.M., Anderson, C.N.G., Blackstock, W.P., Choudhary, J.S., Grant, S.G.N., 2006. Molecular characterization and comparison of the components and multiprotein complexes in the postsynaptic proteome. J. Neurochem. 97 Suppl 1, 16–23. https://doi.org/10.1111/j.1471-4159.2005.03507.x

Colonnier, M., 1968. Synaptic patterns on different cell types in the different laminae of the cat visual cortex. An electron microscope study. Brain Res. 9, 268–287. https://doi.org/10.1016/0006-8993(68)90234-5

Connors, B.W., Gutnick, M.J., 1990. Intrinsic firing patterns of diverse neocortical neurons. Trends Neurosci. 13, 99–104. https://doi.org/10.1016/0166-2236(90)90185-d

Costa, N.M. da, Martin, K.A.C., 2011. How Thalamus Connects to Spiny Stellate Cells in the Cat's Visual Cortex. J. Neurosci. 31, 2925–2937. https://doi.org/10.1523/JNEUROSCI.5961-10.2011

Cowan, A.I., Stricker, C., 2004. Functional connectivity in layer IV local excitatory circuits of rat somatosensory cortex. J. Neurophysiol. 92, 2137–2150. https://doi.org/10.1152/jn.01262.2003

Craig, A.M., Graf, E.R., Linhoff, M.W., 2006. How to build a central synapse: clues from cell culture. Trends Neurosci. 29, 8–20. https://doi.org/10.1016/j.tins.2005.11.002

Crair, M.C., Malenka, R.C., 1995. A critical period for long-term potentiation at thalamocortical synapses. Nature 375, 325–328. https://doi.org/10.1038/375325a0

Crandall, S.R., Patrick, S.L., Cruikshank, S.J., Connors, B.W., 2017. Infrabarrels Are Layer 6 Circuit Modules in the Barrel Cortex that Link Long-Range Inputs and Outputs. Cell Rep. 21, 3065–3078. https://doi.org/10.1016/j.celrep.2017.11.049

Craven, S.E., El-Husseini, A.E., Bredt, D.S., 1999. Synaptic targeting of the postsynaptic density protein PSD-95 mediated by lipid and protein motifs. Neuron 22, 497–509. https://doi.org/10.1016/s0896-6273(00)80705-9

Cubitt, A.B., Heim, R., Adams, S.R., Boyd, A.E., Gross, L.A., Tsien, R.Y., 1995. Understanding, improving and using green fluorescent proteins. Trends Biochem. Sci. 20, 448–455. https://doi.org/10.1016/s0968-0004(00)89099-4

D'Arcangelo, G., 2001. The role of the Reelin pathway in cortical development. Symp Soc Exp Biol.

Daw, M.I., Ashby, M.C., Isaac, J.T.R., 2007. Coordinated developmental recruitment of latent fast spiking interneurons in layer IV barrel cortex. Nat. Neurosci. 10, 453–461. https://doi.org/10.1038/nn1866

de Bartolomeis, A., Buonaguro, E.F., Iasevoli, F., Tomasetti, C., 2014. The emerging role of dopamine–glutamate interaction and of the postsynaptic density in bipolar disorder pathophysiology: Implications for treatment. J. Psychopharmacol. (Oxf.) 28, 505–526. https://doi.org/10.1177/0269881114523864

De Carlos, J.A., O'Leary, D.D., 1992. Growth and targeting of subplate axons and establishment of major cortical pathways. J. Neurosci. Off. J. Soc. Neurosci. 12, 1194–1211.

De Felipe, J., Marco, P., Fairén, A., Jones, E.G., 1997. Inhibitory synaptogenesis in mouse somatosensory cortex. Cereb. Cortex N. Y. N 1991 7, 619–634. https://doi.org/10.1093/cercor/7.7.619

Dingledine, R., Borges, K., Bowie, D., Traynelis, S.F., 1999. The glutamate receptor ion channels. Pharmacol. Rev. 51, 7–61.

Donoghue, J.P., Parham, C., 1983. Afferent connections of the lateral agranular field of the rat motor cortex. J. Comp. Neurol. 217, 390–404. https://doi.org/10.1002/cne.902170404

Drakew, A., Deller, T., Heimrich, B., Gebhardt, C., Del Turco, D., Tielsch, A., Förster, E., Herz, J., Frotscher, M., 2002. Dentate granule cells in reeler mutants and VLDLR and ApoER2 knockout mice. Exp. Neurol. 176, 12–24. https://doi.org/10.1006/exnr.2002.7918

Dufour, A., Rollenhagen, A., Sätzler, K., Lübke, J.H.R., 2016. Development of Synaptic Boutons in Layer 4 of the Barrel Field of the Rat Somatosensory Cortex: A Quantitative Analysis. Cereb. Cortex 26, 838–854. https://doi.org/10.1093/cercor/bhv270

Dupont, E., Hanganu, I.L., Kilb, W., Hirsch, S., Luhmann, H.J., 2006. Rapid developmental switch in the mechanisms driving early cortical columnar networks. Nature 439, 79–83. https://doi.org/10.1038/nature04264

Durham, D., Woolsey, T.A., 1984. Effects of neonatal whisker lesions on mouse central trigeminal pathways. J. Comp. Neurol. 223, 424–447. https://doi.org/10.1002/cne.902230308

Egger, R., Narayanan, R.T., Helmstaedter, M., Kock, C.P.J. de, Oberlaender, M., 2012. 3D Reconstruction and Standardization of the Rat Vibrissal Cortex for Precise Registration of Single Neuron Morphology. PLOS Comput. Biol. 8, e1002837. https://doi.org/10.1371/journal.pcbi.1002837

Egger, V., Nevian, T., Bruno, R.M., 2008. Subcolumnar dendritic and axonal organization of spiny stellate and star pyramid neurons within a barrel in rat somatosensory cortex. Cereb. Cortex N. Y. N 1991 18, 876–889. https://doi.org/10.1093/cercor/bhm126

Ehrlich, I., Klein, M., Rumpel, S., Malinow, R., 2007. PSD-95 is required for activity-driven synapse stabilization. Proc. Natl. Acad. Sci. U. S. A. 104, 4176–4181. https://doi.org/10.1073/pnas.0609307104

Ehrlich, I., Malinow, R., 2004. Postsynaptic density 95 controls AMPA receptor incorporation during long-term potentiation and experience-driven synaptic plasticity. J. Neurosci. Off. J. Soc. Neurosci. 24, 916–927. https://doi.org/10.1523/JNEUROSCI.4733-03.2004

El-Husseini, A.E.-D., Schnell, E., Chetkovich, D.M., Nicoll, R.A., Bredt, D.S., 2000. PSD-95 Involvement in Maturation of Excitatory Synapses. Science 290, 1364–1368. https://doi.org/10.1126/science.290.5495.1364

Elias, G.M., Elias, L. a. B., Apostolides, P.F., Kriegstein, A.R., Nicoll, R.A., 2008. Differential trafficking of AMPA and NMDA receptors by SAP102 and PSD-95 underlies synapse development. Proc. Natl. Acad. Sci. U. S. A. 105, 20953–20958. https://doi.org/10.1073/pnas.0811025106

Elias, G.M., Funke, L., Stein, V., Grant, S.G., Bredt, D.S., Nicoll, R.A., 2006. Synapse-specific and developmentally regulated targeting of AMPA receptors by a family of MAGUK scaffolding proteins. Neuron 52, 307–320. https://doi.org/10.1016/j.neuron.2006.09.012

Erzurumlu, R.S., Chen, Z.-F., Jacquin, M.F., 2006. Molecular determinants of the face map development in the trigeminal brainstem. Anat. Rec. A. Discov. Mol. Cell. Evol. Biol. 288A, 121–134. https://doi.org/10.1002/ar.a.20285

Erzurumlu, R.S., Jhaveri, S., 1990. Thalamic axons confer a blueprint of the sensory periphery onto the developing rat somatosensory cortex. Brain Res. Dev. Brain Res. 56, 229–234. https://doi.org/10.1016/0165-3806(90)90087-f

Erzurumlu, R.S., Killackey, H.P., 1982. Critical and sensitive periods in neurobiology. Curr. Top. Dev. Biol. 17, 207–240.

Espinosa, J.S., Wheeler, D.G., Tsien, R.W., Luo, L., 2009. Uncoupling dendrite growth and patterning: single-cell knockout analysis of NMDA receptor 2B. Neuron 62, 205–217. https://doi.org/10.1016/j.neuron.2009.03.006

Estebanez, L., El Boustani, S., Destexhe, A., Shulz, D.E., 2012. Correlated input reveals coexisting coding schemes in a sensory cortex. Nat. Neurosci. 15, 1691–1699. https://doi.org/10.1038/nn.3258

Fagiolini, M., Hensch, T.K., 2000. Inhibitory threshold for critical-period activation in primary visual cortex. Nature 404, 183–186. https://doi.org/10.1038/35004582

Fairen, A., Cobas, A., Fonseca, M., 1986. Times of generation of glutamic acid decarboxylase immunoreactive neurons in mouse somatosensory cortex. J Comp Neurol 251, 67–83.

Feldman, D.E., Nicoll, R.A., Malenka, R.C., Isaac, J.T., 1998. Long-term depression at thalamocortical synapses in developing rat somatosensory cortex. Neuron 21, 347–357. https://doi.org/10.1016/s0896-6273(00)80544-9

Feldmeyer, D., Egger, V., Lubke, J., Sakmann, B., 1999. Reliable synaptic connections between pairs of excitatory layer 4 neurones within a single “barrel” of developing rat somatosensory cortex. J. Physiol. 521 Pt 1, 169–190. https://doi.org/10.1111/j.1469-7793.1999.00169.x

Feldmeyer, D., Lübke, J., Silver, R.A., Sakmann, B., 2002. Synaptic connections between layer 4 spiny neurone-layer 2/3 pyramidal cell pairs in juvenile rat barrel cortex: physiology and anatomy of interlaminar signalling within a cortical column. J. Physiol. 538, 803–822. https://doi.org/10.1113/jphysiol.2001.012959

Feldmeyer, D., Roth, A., Sakmann, B., 2005. Monosynaptic connections between pairs of spiny stellate cells in layer 4 and pyramidal cells in layer 5A indicate that lemniscal and paralemniscal afferent pathways converge in the infragranular somatosensory cortex. J. Neurosci. Off. J. Soc. Neurosci. 25, 3423–3431. https://doi.org/10.1523/JNEUROSCI.5227-04.2005

Feller, M.B., Wellis, D.P., Stellwagen, D., Werblin, F.S., Shatz, C.J., 1996. Requirement for cholinergic synaptic transmission in the propagation of spontaneous retinal waves. Science 272, 1182–1187. https://doi.org/10.1126/science.272.5265.1182

Ferezou, I., Bolea, S., Petersen, C.C.H., 2006. Visualizing the cortical representation of whisker touch: voltage-sensitive dye imaging in freely moving mice. Neuron 50, 617–629. https://doi.org/10.1016/j.neuron.2006.03.043

Ferrer, I., Bernet, E., Soriano, E., del Rio, T., Fonseca, M., 1990. Naturally occurring cell death in the cerebral cortex of the rat and removal of dead cells by transitory phagocytes. Neuroscience 39, 451–458. https://doi.org/10.1016/0306-4522(90)90281-8

Forster, E., Tielsch, A., Saum, B., Weiss, K.H., Johanssen, C., Graus-Porta, D., Muller, U., Reelin, F.M., 2002. Disabled 1, and beta 1 integrins are required for the formation of the radial glial scaffold, in: the hippocampus. Proc Natl Acad Sci. pp. 13178–13183.

Fortin, D.A., Tillo, S.E., Yang, G., Rah, J.-C., Melander, J.B., Bai, S., Soler-Cedeño, O., Qin, M., Zemelman, B.V., Guo, C., Mao, T., Zhong, H., 2014. Live Imaging of Endogenous PSD-95 Using ENABLED: A Conditional Strategy to Fluorescently Label Endogenous Proteins. J. Neurosci. 34, 16698–16712. https://doi.org/10.1523/JNEUROSCI.3888-14.2014

Frank, R.A., Grant, S.G., 2017. Supramolecular organization of NMDA receptors and the postsynaptic density. Curr. Opin. Neurobiol. 45, 139–147. https://doi.org/10.1016/j.conb.2017.05.019

Frank, R.A.W., Komiyama, N.H., Ryan, T.J., Zhu, F., O'Dell, T.J., Grant, S.G.N., 2016. NMDA receptors are selectively partitioned into complexes and supercomplexes during synapse maturation. Nat. Commun. 7, 11264. https://doi.org/10.1038/ncomms11264

Friauf, E., Shatz, C.J., 1991. Changing patterns of synaptic input to subplate and cortical plate during development of visual cortex. J. Neurophysiol. 66, 2059–2071. https://doi.org/10.1152/jn.1991.66.6.2059

Friedlander, M.J., Torres-Reveron, J., 2009. The changing roles of neurons in the cortical subplate. Front. Neuroanat. 3. https://doi.org/10.3389/neuro.05.015.2009

Friedman, H.V., Bresler, T., Garner, C.C., Ziv, N.E., 2000. Assembly of new individual excitatory synapses: time course and temporal order of synaptic molecule recruitment. Neuron 27, 57–69. https://doi.org/10.1016/s0896-6273(00)00009-x

Fu, M., Yu, X., Lu, J., Zuo, Y., 2012. REPETITIVE MOTOR LEARNING INDUCES COORDINATED FORMATION OF CLUSTERED DENDRITIC SPINES IN VIVO. Nature 483, 92–95. https://doi.org/10.1038/nature10844

Fujita, I., Tanaka, K., Ito, M., Cheng, K., 1992. Columns for visual features of objects in monkey inferotemporal cortex. Nature 360, 343–346. https://doi.org/10.1038/360343a0

Fukata, M., Fukata, Y., Adesnik, H., Nicoll, R.A., Bredt, D.S., 2004. Identification of PSD-95 palmitoylating enzymes. Neuron 44, 987–996. https://doi.org/10.1016/j.neuron.2004.12.005

Fukata, Y., Dimitrov, A., Boncompain, G., Vielemeyer, O., Perez, F., Fukata, M., 2013. Local palmitoylation cycles define activity-regulated postsynaptic subdomains. J. Cell Biol. 202, 145–161. https://doi.org/10.1083/jcb.201302071

Fukaya, M., Ueda, H., Yamauchi, K., Inoue, Y., Watanabe, M., 1999. Distinct spatiotemporal expression of mRNAs for the PSD-95/SAP90 protein family in the mouse brain. Neurosci. Res. 33, 111–118. https://doi.org/10.1016/S0168-0102(98)00120-5

Funahashi, R., Maruyama, T., Yoshimura, Y., Komatsu, Y., 2013. Silent synapses persist into adulthood in layer 2/3 pyramidal neurons of visual cortex in dark-reared mice. J. Neurophysiol. 109, 2064–2076. https://doi.org/10.1152/jn.00912.2012

Furuta, T., Deschênes, M., Kaneko, T., 2011. Anisotropic Distribution of Thalamocortical Boutons in Barrels. J. Neurosci. 31, 6432–6439. https://doi.org/10.1523/JNEUROSCI.6154-10.2011

Gambino, F., Pagès, S., Kehayas, V., Baptista, D., Tatti, R., Carleton, A., Holtmaat, A., 2014. Sensory-evoked LTP driven by dendritic plateau potentials in vivo. Nature 515, 116–119. https://doi.org/10.1038/nature13664

Gandhi, R.M., Kogan, C.S., Messier, C., MacLeod, L.S., 2014. Visual–spatial learning impairments are associated with hippocampal PSD-95 protein dysregulation in a mouse model of fragile X syndrome. Neuroreport 25, 255–261. https://doi.org/10.1097/WNR.0000000000000087

Ganini, D., Leinisch, F., Kumar, A., Jiang, J., Tokar, E.J., Malone, C.C., Petrovich, R.M., Mason, R.P., 2017. Fluorescent proteins such as eGFP lead to catalytic oxidative stress in cells. Redox Biol. 12, 462–468. https://doi.org/10.1016/j.redox.2017.03.002

García-Moreno, F., López-Mascaraque, L., De Carlos, J.A., 2007. Origins and migratory routes of murine Cajal-Retzius cells. J. Comp. Neurol. 500, 419–432. https://doi.org/10.1002/cne.21128

Gardoni, F., Marcello, E., Di Luca, M., 2009. Postsynaptic density-membrane associated guanylate kinase proteins (PSD-MAGUKs) and their role in CNS disorders. Neuroscience 158, 324–333. https://doi.org/10.1016/j.neuroscience.2008.07.068

Garner, C.C., Waites, C.L., Ziv, N.E., 2006. Synapse development: still looking for the forest, still lost in the trees. Cell Tissue Res. 326, 249–262. https://doi.org/10.1007/s00441-006-0278-1

Gelman, D., Griveau, A., Dehorter, N., Teissier, A., Varela, C., Pla, R., Pierani, A., Marín, O., 2011. A wide diversity of cortical GABAergic interneurons derives from the embryonic preoptic area. J. Neurosci. Off. J. Soc. Neurosci. 31, 16570–16580. https://doi.org/10.1523/JNEUROSCI.4068-11.2011

Gerrow, K., Romorini, S., Nabi, S.M., Colicos, M.A., Sala, C., El-Husseini, A., 2006. A preformed complex of postsynaptic proteins is involved in excitatory synapse development. Neuron 49, 547–562. https://doi.org/10.1016/j.neuron.2006.01.015

Gezelius, H., López-Bendito, G., 2017. Thalamic neuronal specification and early circuit formation. Dev. Neurobiol. 77, 830–843. https://doi.org/10.1002/dneu.22460

Ghosh, A., Antonini, A., McConnell, S.K., Shatz, C.J., 1990. Requirement for subplate neurons in the formation of thalamocortical connections. Nature 347, 179–181. https://doi.org/10.1038/347179a0

Ghosh, A., Shatz, C.J., 1992. Involvement of subplate neurons in the formation of ocular dominance columns. Science 255, 1441–1443. https://doi.org/10.1126/science.1542795

Glasgow, N.G., Retchless, B.S., Johnson, J.W., 2015. Molecular bases of NMDA receptor subtype-dependent properties. J. Physiol. 593, 83–95. https://doi.org/10.1113/jphysiol.2014.273763

Golding, N.L., Spruston, N., 1998. Dendritic sodium spikes are variable triggers of axonal action potentials in hippocampal CA1 pyramidal neurons. Neuron 21, 1189–1200. https://doi.org/10.1016/s0896-6273(00)80635-2

Golding, N.L., Staff, N.P., Spruston, N., 2002. Dendritic spikes as a mechanism for cooperative long-term potentiation. Nature 418, 326–331. https://doi.org/10.1038/nature00854

Gollo, L.L., Kinouchi, O., Copelli, M., 2009. Active dendrites enhance neuronal dynamic range. PLoS Comput. Biol. 5, e1000402. https://doi.org/10.1371/journal.pcbi.1000402

Götz, M., Huttner, W.B., 2005. The cell biology of neurogenesis. Nat. Rev. Mol. Cell Biol. 6, 777–788. https://doi.org/10.1038/nrm1739

Grant, R.A., Mitchinson, B., Prescott, T.J., 2012. The development of whisker control in rats in relation to locomotion. Dev. Psychobiol. 54, 151–168. https://doi.org/10.1002/dev.20591

Gray, N.W., Weimer, R.M., Bureau, I., Svoboda, K., 2006. Rapid Redistribution of Synaptic PSD-95 in the Neocortex In Vivo. PLOS Biol. 4, e370. https://doi.org/10.1371/journal.pbio.0040370

Grutzendler, J., Kasthuri, N., Gan, W.-B., 2002. Long-term dendritic spine stability in the adult cortex. Nature 420, 812–816. https://doi.org/10.1038/nature01276

Guo, C., Peng, J., Zhang, Y., Li, A., Li, Y., Yuan, J., Xu, X., Ren, M., Gong, H., Chen, S., 2017. Single-axon level morphological analysis of corticofugal projection neurons in mouse barrel field. Sci. Rep. 7. https://doi.org/10.1038/s41598-017-03000-8

Han, K.-S., Cooke, S.F., Xu, W., 2017. Experience-Dependent Equilibration of AMPAR-Mediated Synaptic Transmission during the Critical Period. Cell Rep. 18, 892–904. https://doi.org/10.1016/j.celrep.2016.12.084

Hanganu, I.L., Kilb, W., Luhmann, H.J., 2002. Functional Synaptic Projections onto Subplate Neurons in Neonatal Rat Somatosensory Cortex. J. Neurosci. 22, 7165–7176. https://doi.org/10.1523/JNEUROSCI.22-16-07165.2002

Hanganu, I.L., Kilb, W., Luhmann, H.J., 2001. Spontaneous Synaptic Activity of Subplate Neurons in Neonatal Rat Somatosensory Cortex. Cereb. Cortex 11, 400–410. https://doi.org/10.1093/cercor/11.5.400

Harnett, M.T., Magee, J.C., Williams, S.R., 2015. Distribution and function of HCN channels in the apical dendritic tuft of neocortical pyramidal neurons. J. Neurosci. Off. J. Soc. Neurosci. 35, 1024–1037. https://doi.org/10.1523/JNEUROSCI.2813-14.2015

Harris, K.M., Jensen, F.E., Tsao, B., 1992. Three-dimensional structure of dendritic spines and synapses in rat hippocampus (CA1) at postnatal day 15 and adult ages: implications for the maturation of synaptic physiology and long-term potentiation [published erratum appears in J Neurosci 1992 Aug;12(8):following table of contents]. J. Neurosci. 12, 2685–2705. https://doi.org/10.1523/JNEUROSCI.12-07-02685.1992

Harris, K.M., Stevens, J.K., 1989. Dendritic spines of CA 1 pyramidal cells in the rat hippocampus: serial electron microscopy with reference to their biophysical characteristics. J. Neurosci. Off. J. Soc. Neurosci. 9, 2982–2997.

Harris, R.M., Woolsey, T.A., 1983. Computer-assisted analyses of barrel neuron axons and their putative synaptic contacts. J. Comp. Neurol. 220, 63–79. https://doi.org/10.1002/cne.902200107

Helmchen, F., Svoboda, K., Denk, W., Tank, D.W., 1999. In vivo dendritic calcium dynamics in deep-layer cortical pyramidal neurons. Nat. Neurosci. 2, 989–996. https://doi.org/10.1038/14788

Hestrin, S., 1992. Developmental regulation of NMDA receptor-mediated synaptic currents at a central synapse. Nature 357, 686–689. https://doi.org/10.1038/357686a0

Hevner, R.F., Zecevic, N., 2006. Pioneer Neurons and Interneurons in the Developing Subplate: Molecular Markers, Cell Birthdays, and Neurotransmitters, in: Erzurumlu, R., Guido, W., Molnár, Z. (Eds.), Development and Plasticity in Sensory Thalamus and Cortex. Springer US, Boston, MA, pp. 1–18. https://doi.org/10.1007/978-0-387-38607-2_1

Higashi, S., Hioki, K., Kurotani, T., Kasim, N., Molnár, Z., 2005. Functional thalamocortical synapse reorganization from subplate to layer IV during postnatal development in the reeler-like mutant rat (shaking rat Kawasaki). J. Neurosci. Off. J. Soc. Neurosci. 25, 1395–1406. https://doi.org/10.1523/JNEUROSCI.4023-04.2005

Higashi, S., Molnár, Z., Kurotani, T., Toyama, K., 2002. Prenatal development of neural excitation in rat thalamocortical projections studied by optical recording. Neuroscience 115, 1231–1246. https://doi.org/10.1016/s0306-4522(02)00418-9

Hoerder-Suabedissen, A., Korrell, K.V., Hayashi, S., Jeans, A., Ramirez, D.M.O., Grant, E., Christian, H.C., Kavalali, E.T., Wilson, M.C., Molnár, Z., 2019. Cell-Specific Loss of SNAP25 from Cortical Projection Neurons Allows Normal Development but Causes Subsequent Neurodegeneration. Cereb. Cortex N. Y. N 1991 29, 2148–2159. https://doi.org/10.1093/cercor/bhy127

Hoerder-Suabedissen, A., Molnár, Z., 2012. Morphology of mouse subplate cells with identified projection targets changes with age. J. Comp. Neurol. 520, 174–185. https://doi.org/10.1002/cne.22725

Hoerder-Suabedissen, A., Oeschger, F.M., Krishnan, M.L., Belgard, T.G., Wang, W.Z., Lee, S., Webber, C., Petretto, E., Edwards, A.D., Molnár, Z., 2013. Expression profiling of mouse subplate reveals a dynamic gene network and disease association with autism and schizophrenia. Proc. Natl. Acad. Sci. U. S. A. 110, 3555–3560. https://doi.org/10.1073/pnas.1218510110

Hoerder-Suabedissen, A., Wang, W.Z., Lee, S., Davies, K.E., Goffinet, A.M., Rakić, S., Parnavelas, J., Reim, K., Nicolić, M., Paulsen, O., Molnár, Z., 2009. Novel markers reveal subpopulations of subplate neurons in the murine cerebral cortex. Cereb. Cortex N. Y. N 1991 19, 1738–1750. https://doi.org/10.1093/cercor/bhn195

Hofer, S.B., Mrsic-Flogel, T.D., Bonhoeffer, T., Hübener, M., 2009. Experience leaves a lasting structural trace in cortical circuits. Nature 457, 313–317. https://doi.org/10.1038/nature07487

Hoffer, Z.S., Hoover, J.E., Alloway, K.D., 2003. Sensorimotor corticocortical projections from rat barrel cortex have an anisotropic organization that facilitates integration of inputs from whiskers in the same row. J. Comp. Neurol. 466, 525–544. https://doi.org/10.1002/cne.10895

Hoffman, D.A., Magee, J.C., Colbert, C.M., Johnston, D., 1997. K+ channel regulation of signal propagation in dendrites of hippocampal pyramidal neurons. Nature 387, 869–875. https://doi.org/10.1038/43119

Hollmann, M., Heinemann, S., 1994. Cloned glutamate receptors. Annu. Rev. Neurosci. 17, 31–108. https://doi.org/10.1146/annurev.ne.17.030194.000335

Holthoff, K., Kovalchuk, Y., Yuste, R., Konnerth, A., 2004. Single-shock LTD by local dendritic spikes in pyramidal neurons of mouse visual cortex. J. Physiol. 560, 27–36. https://doi.org/10.1113/jphysiol.2004.072678

Holtmaat, A., Svoboda, K., 2009. Experience-dependent structural synaptic plasticity in the mammalian brain. Nat. Rev. Neurosci. 10, 647–658. https://doi.org/10.1038/nrn2699

Holtmaat, A., Wilbrecht, L., Knott, G.W., Welker, E., Svoboda, K., 2006. Experience-dependent and cell-type-specific spine growth in the neocortex. Nature 441, 979–983. https://doi.org/10.1038/nature04783

Hubel, D.H., Wiesel, T.N., 1963. Shape and arrangement of columns in cat's striate cortex. J. Physiol. 165, 559-568.2.

Isaac, J.T., Nicoll, R.A., Malenka, R.C., 1995. Evidence for silent synapses: implications for the expression of LTP. Neuron 15, 427–434. https://doi.org/10.1016/0896-6273(95)90046-2

Isaac, J.T.R., Crair, M.C., Nicoll, R.A., Malenka, R.C., 1997. Silent Synapses during Development of Thalamocortical Inputs. Neuron 18, 269–280. https://doi.org/10.1016/S0896-6273(00)80267-6

Iwasato, T., Datwani, A., Wolf, A.M., Nishiyama, H., Taguchi, Y., Tonegawa, S., Knöpfel, T., Erzurumlu, R.S., Itohara, S., 2000. Cortex-restricted disruption of NMDAR1 impairs neuronal patterns in the barrel cortex. Nature 406, 726–731. https://doi.org/10.1038/35021059

Jacobs, E.C., Campagnoni, C., Kampf, K., Reyes, S.D., Kalra, V., Handley, V., Xie, Y.-Y., Hong-Hu, Y., Spreur, V., Fisher, R.S., Campagnoni, A.T., 2007. Visualization of corticofugal projections during early cortical development in a τ-GFP-transgenic mouse: Formation of early cortical circuitry. Eur. J. Neurosci. 25, 17–30. https://doi.org/10.1111/j.1460-9568.2006.05258.x

Jeanmonod, D., Rice, F.L., Van der Loos, H., 1981. Mouse somatosensory cortex: alterations in the barrelfield following receptor injury at different early postnatal ages. Neuroscience 6, 1503–1535. https://doi.org/10.1016/0306-4522(81)90222-0

Jensen, K.F., Killackey, H.P., 1987. Terminal arbors of axons projecting to the somatosensory cortex of the adult rat. I. The normal morphology of specific thalamocortical afferents. J. Neurosci. Off. J. Soc. Neurosci. 7, 3529–3543.

Jeyifous, O., Lin, E.I., Chen, X., Antinone, S.E., Mastro, R., Drisdel, R., Reese, T.S., Green, W.N., 2016. Palmitoylation regulates glutamate receptor distributions in postsynaptic densities through control of PSD95 conformation and orientation. Proc. Natl. Acad. Sci. U. S. A. 113, E8482–E8491. https://doi.org/10.1073/pnas.1612963113

Jia, H., Varga, Z., Sakmann, B., Konnerth, A., 2014. Linear integration of spine Ca2+ signals in layer 4 cortical neurons in vivo. Proc. Natl. Acad. Sci. U. S. A. 111, 9277–9282. https://doi.org/10.1073/pnas.1408525111

Jimenez, D., Lopez-Mascaraque, L.M., Valverde, F., 2002. De Carlos JA. Tangential migration in neocortical development. Dev Biol.

Johnston, D., Narayanan, R., 2008. Active dendrites: colorful wings of the mysterious butterflies. Trends Neurosci. 31, 309–316. https://doi.org/10.1016/j.tins.2008.03.004

Jung, H.Y., Mickus, T., Spruston, N., 1997. Prolonged sodium channel inactivation contributes to dendritic action potential attenuation in hippocampal pyramidal neurons. J. Neurosci. Off. J. Soc. Neurosci. 17, 6639–6646.

Kaizuka, T., Takumi, T., 2018. Postsynaptic density proteins and their involvement in neurodevelopmental disorders. J. Biochem. (Tokyo) 163, 447–455. https://doi.org/10.1093/jb/mvy022

Kampa, B.M., Letzkus, J.J., Stuart, G.J., 2007. Dendritic mechanisms controlling spike-timing-dependent synaptic plasticity. Trends Neurosci. 30, 456–463. https://doi.org/10.1016/j.tins.2007.06.010

Kandler, K., Clause, A., Noh, J., 2009. Tonotopic reorganization of developing auditory brainstem circuits. Nat. Neurosci. 12, 711–717. https://doi.org/10.1038/nn.2332

Kanold, P.O., Deng, R., Meng, X., 2019. The Integrative Function of Silent Synapses on Subplate Neurons in Cortical Development and Dysfunction. Front. Neuroanat. 13, 41. https://doi.org/10.3389/fnana.2019.00041

Kanold, P.O., Kara, P., Reid, R.C., Shatz, C.J., 2003. Role of subplate neurons in functional maturation of visual cortical columns. Science 301, 521–525. https://doi.org/10.1126/science.1084152

Kanold, P.O., Luhmann, H.J., 2010. The subplate and early cortical circuits. Annu. Rev. Neurosci. 33, 23–48. https://doi.org/10.1146/annurev-neuro-060909-153244

Kanold, P.O., Nelken, I., Polley, D.B., 2014. Local versus global scales of organization in auditory cortex. Trends Neurosci. 37, 502–510. https://doi.org/10.1016/j.tins.2014.06.003

Kanold, P.O., Shatz, C.J., 2006. Subplate neurons regulate maturation of cortical inhibition and outcome of ocular dominance plasticity. Neuron 51, 627–638. https://doi.org/10.1016/j.neuron.2006.07.008

Katz, Y., Menon, V., Nicholson, D.A., Geinisman, Y., Kath, W.L., Spruston, N., 2009. Synapse Distribution Suggests a Two-Stage Model of Dendritic Integration in CA1 Pyramidal Neurons. Neuron 63, 171–177. https://doi.org/10.1016/j.neuron.2009.06.023

Kawashima, N., Takamiya, K., Sun, J., Kitabatake, A., Sobue, K., 1997. Differential expression of isoforms of PSD-95 binding protein (GKAP/SAPAP1) during rat brain development. FEBS Lett. 418, 301–304. https://doi.org/10.1016/s0014-5793(97)01399-9

Keck, T., Mrsic-Flogel, T.D., Vaz Afonso, M., Eysel, U.T., Bonhoeffer, T., Hübener, M., 2008. Massive restructuring of neuronal circuits during functional reorganization of adult visual cortex. Nat. Neurosci. 11, 1162–1167. https://doi.org/10.1038/nn.2181

Kelly, P.T., Vernon, P., 1985. Changes in the subcellular distribution of calmodulin-kinase II during brain development. Brain Res. 350, 211–224. https://doi.org/10.1016/0165-3806(85)90265-2

Kennedy, M.B., 2000. Signal-processing machines at the postsynaptic density. Science 290, 750–754. https://doi.org/10.1126/science.290.5492.750

Kennedy, M.B., 1997. The postsynaptic density at glutamatergic synapses. Trends Neurosci. 20, 264–268. https://doi.org/10.1016/s0166-2236(96)01033-8

Kerchner, G.A., Nicoll, R.A., 2008. Silent synapses and the emergence of a postsynaptic mechanism for LTP. Nat. Rev. Neurosci. 9, 813–825. https://doi.org/10.1038/nrn2501

Khazipov, R., Luhmann, H.J., 2006. Early patterns of electrical activity in the developing cerebral cortex of humans and rodents. Trends Neurosci. 29, 414–418. https://doi.org/10.1016/j.tins.2006.05.007

Kilb, W., 2012. Development of the GABAergic system from birth to adolescence. Neurosci. Rev. J. Bringing Neurobiol. Neurol. Psychiatry 18, 613–630. https://doi.org/10.1177/1073858411422114

Kilb, W., Hanganu, I.L., Okabe, A., Sava, B.A., Shimizu-Okabe, C., Fukuda, A., Luhmann, H.J., 2008. Glycine receptors mediate excitation of subplate neurons in neonatal rat cerebral cortex. J. Neurophysiol. 100, 698–707. https://doi.org/10.1152/jn.00657.2007

Kim, E., Sheng, M., 2004. PDZ domain proteins of synapses. Nat. Rev. Neurosci. 5, 771–781. https://doi.org/10.1038/nrn1517

Kim, H.G., Connors, B.W., 1993. Apical dendrites of the neocortex: correlation between sodium- and calcium-dependent spiking and pyramidal cell morphology. J. Neurosci. 13, 5301–5311.

Kim, S., Kim, Y., Lee, S.-H., Ho, W.-K., 2018. Dendritic spikes in hippocampal granule cells are necessary for long-term potentiation at the perforant path synapse. eLife 7, e35269. https://doi.org/10.7554/eLife.35269

Kim, U., Ebner, F.F., 1999. Barrels and septa: separate circuits in rat barrels field cortex. J. Comp. Neurol. 408, 489–505.

Kiritani, T., Wickersham, I.R., Seung, H.S., Shepherd, G.M.G., 2012. Hierarchical connectivity and connection-specific dynamics in the corticospinal-corticostriatal microcircuit in mouse motor cortex. J. Neurosci. Off. J. Soc. Neurosci.32, 4992–5001. https://doi.org/10.1523/JNEUROSCI.4759-11.2012

Kirkby, L., Sack, G., Firl, A., Feller, M.B., 2013. A role for correlated spontaneous activity in the assembly of neural circuits. Neuron 80, 1129–1144. https://doi.org/10.1016/j.neuron.2013.10.030

Kleindienst, T., Winnubst, J., Roth-Alpermann, C., Bonhoeffer, T., Lohmann, C., 2011. Activity-dependent clustering of functional synaptic inputs on developing hippocampal dendrites. Neuron 72, 1012–1024. https://doi.org/10.1016/j.neuron.2011.10.015

Koelbl, C., Helmstaedter, M., Lübke, J., Feldmeyer, D., 2015. A barrel-related interneuron in layer 4 of rat somatosensory cortex with a high intrabarrel connectivity. Cereb. Cortex N. Y. N 1991 25, 713–725. https://doi.org/10.1093/cercor/bht263

Kondo, S., Al-Hasani, H., Hoerder-Suabedissen, A., Wang, W.Z., Molnár, Z., 2015. Secretory function in subplate neurons during cortical development. Front. Neurosci. 9. https://doi.org/10.3389/fnins.2015.00100

Koralek, K.A., Jensen, K.F., Killackey, H.P., 1988. Evidence for two complementary patterns of thalamic input to the rat somatosensory cortex. Brain Res. 463, 346–351. https://doi.org/10.1016/0006-8993(88)90408-8

Korrell, K.V., Disser, J., Parley, K., Vadisiute, A., Requena-Komuro, M.-C., Fodder, H., Pollart, C., Knott, G., Molnár, Z., Hoerder-Suabedissen, A., 2019. Differential effect on myelination through abolition of activity-dependent synaptic vesicle release or reduction of overall electrical activity of selected cortical projections in the mouse. J. Anat. 235, 452–467. https://doi.org/10.1111/joa.12974

Kostović, I., Judaš, M., Sedmak, G., 2011. Developmental history of the subplate zone, subplate neurons and interstitial white matter neurons: relevance for schizophrenia. Int. J. Dev. Neurosci. Off. J. Int. Soc. Dev. Neurosci. 29, 193–205. https://doi.org/10.1016/j.ijdevneu.2010.09.005

Kostovic, I., Rakic, P., 1990. Developmental history of the transient subplate zone in the visual and somatosensory cortex of the macaque monkey and human brain. J. Comp. Neurol. 297, 441–470. https://doi.org/10.1002/cne.902970309

Kriegstein, A., Alvarez-Buylla, A., 2009. The glial nature of embryonic and adult neural stem cells. Annu Rev Neurosci.

Kriegstein, A.R., Gotz, M., 2003. Radial glia diversity: a matter of cell fate. Glia.

Laaris, N., Keller, A., 2002. Functional Independence of Layer IV Barrels. J. Neurophysiol. 87, 1028–1034.

Lambert, J.T., Hill, T.C., Park, D.K., Culp, J.H., Zito, K., 2017. Protracted and asynchronous accumulation of PSD95-family MAGUKs during maturation of nascent dendritic spines. Dev. Neurobiol. 77, 1161–1174. https://doi.org/10.1002/dneu.22503

Landers, M., Haidarliu, S., Philip Zeigler, H., 2006. Development of rodent macrovibrissae: effects of neonatal whisker denervation and bilateral neonatal enucleation. Somatosens. Mot. Res. 23, 11–17. https://doi.org/10.1080/08990220600700784

Larkum, M.E., Nevian, T., Sandler, M., Polsky, A., Schiller, J., 2009. Synaptic integration in tuft dendrites of layer 5 pyramidal neurons: a new unifying principle. Science 325, 756–760. https://doi.org/10.1126/science.1171958

Larkum, M.E., Zhu, J.J., 2002. Signaling of layer 1 and whisker-evoked Ca2+ and Na+ action potentials in distal and terminal dendrites of rat neocortical pyramidal neurons in vitro and in vivo. J. Neurosci. Off. J. Soc. Neurosci. 22, 6991–7005. https://doi.org/20026717

Larkum, M.E., Zhu, J.J., Sakmann, B., 1999. A new cellular mechanism for coupling inputs arriving at different cortical layers. Nature 398, 338–341. https://doi.org/10.1038/18686

Larsen, D.D., Callaway, E.M., 2006. Development of layer-specific axonal arborizations in mouse primary somatosensory cortex. J. Comp. Neurol. 494, 398–414. https://doi.org/10.1002/cne.20754

Lau, C.G., Takeuchi, K., Rodenas-Ruano, A., Takayasu, Y., Murphy, J., Bennett, M.V.L., Zukin, R.S., 2009. Regulation of NMDA receptor Ca2+ signalling and synaptic plasticity. Biochem. Soc. Trans. 37, 1369–1374. https://doi.org/10.1042/BST0371369

Lavdas, A.A., Grigoriou, M., Pachnis, V., Parnavelas, J.G., 1999. The medial ganglionic eminence gives rise to a population of early neurons in the developing cerebral cortex. J. Neurosci. Off. J. Soc. Neurosci. 19, 7881–7888.

Lavzin, M., Rapoport, S., Polsky, A., Garion, L., Schiller, J., 2012. Nonlinear dendritic processing determines angular tuning of barrel cortex neurons in vivo. Nature 490, 397–401. https://doi.org/10.1038/nature11451

Lee, A.J., Wang, G., Jiang, X., Johnson, S.M., Hoang, E.T., Lanté, F., Stornetta, R.L., Beenhakker, M.P., Shen, Y., Julius Zhu, J., 2015. Canonical Organization of Layer 1 Neuron-Led Cortical Inhibitory and Disinhibitory Interneuronal Circuits. Cereb. Cortex N. Y. N 1991 25, 2114–2126. https://doi.org/10.1093/cercor/bhu020

Lefort, S., Tomm, C., Floyd Sarria, J.-C., Petersen, C.C.H., 2009. The excitatory neuronal network of the C2 barrel column in mouse primary somatosensory cortex. Neuron 61, 301–316. https://doi.org/10.1016/j.neuron.2008.12.020

Lendvai, B., Stern, E.A., Chen, B., Svoboda, K., 2000. Experience-dependent plasticity of dendritic spines in the developing rat barrel cortex in vivo. Nature 404, 876–881. https://doi.org/10.1038/35009107

Levitt, P., Rakic, P., 1980. Immunoperoxidase localization of glial fibrillary acidic protein in radial glial cells and astrocytes of the developing rhesus monkey brain. J Comp Neurol 193, 815–840.

Li, H., Fertuzinhos, S., Mohns, E., Hnasko, T.S., Verhage, M., Edwards, R., Sestan, N., Crair, M.C., 2013. Laminar and columnar development of barrel cortex relies on thalamocortical neurotransmission. Neuron 79, 970–986. https://doi.org/10.1016/j.neuron.2013.06.043

Lichtman, J.W., Colman, H., 2000. Synapse elimination and indelible memory. Neuron 25, 269–278. https://doi.org/10.1016/s0896-6273(00)80893-4

Lim, S., Naisbitt, S., Yoon, J., Hwang, J.I., Suh, P.G., Sheng, M., Kim, E., 1999. Characterization of the Shank family of synaptic proteins. Multiple genes, alternative splicing, and differential expression in brain and development. J. Biol. Chem. 274, 29510–29518. https://doi.org/10.1074/jbc.274.41.29510

Liu, H.S., Jan, M.S., Chou, C.K., Chen, P.H., Ke, N.J., 1999. Is green fluorescent protein toxic to the living cells? Biochem. Biophys. Res. Commun. 260, 712–717. https://doi.org/10.1006/bbrc.1999.0954

Liu, M., Shi, R., Hwang, H., Han, K.S., Wong, M.H., Ren, X., Lewis, L.D., Brown, E.N., Xu, W., 2018. SAP102 regulates synaptic AMPAR function through a CNIH-2-dependent mechanism. J. Neurophysiol. 120, 1578–1586. https://doi.org/10.1152/jn.00731.2017

Llinás, R., Sugimori, M., 2012. Probing the functional properties of mammalian dendrites. 1980. Cerebellum Lond. Engl. 11, 612–628.

Lohmann, C., Kessels, H.W., 2014. The developmental stages of synaptic plasticity. J. Physiol. 592, 13–31. https://doi.org/10.1113/jphysiol.2012.235119

López-Bendito, G., Cautinat, A., Sánchez, J.A., Bielle, F., Flames, N., Garratt, A.N., Talmage, D.A., Role, L.W., Charnay, P., Marín, O., Garel, S., 2006. Tangential neuronal migration controls axon guidance: a role for neuregulin-1 in thalamocortical axon navigation. Cell 125, 127–142. https://doi.org/10.1016/j.cell.2006.01.042

López-Bendito, G., Molnár, Z., 2003. Thalamocortical development: how are we going to get there? Nat. Rev. Neurosci. 4, 276–289. https://doi.org/10.1038/nrn1075

López-Bendito, G., Sturgess, K., Erdélyi, F., Szabó, G., Molnár, Z., Paulsen, O., 2004. Preferential origin and layer destination of GAD65-GFP cortical interneurons. Cereb. Cortex N. Y. N 1991 14, 1122–1133. https://doi.org/10.1093/cercor/bhh072

Losonczy, A., Magee, J.C., 2006. Integrative properties of radial oblique dendrites in hippocampal CA1 pyramidal neurons. Neuron 50, 291–307. https://doi.org/10.1016/j.neuron.2006.03.016

LoTurco, J.J., Blanton, M.G., Kriegstein, A.R., 1991. Initial expression and endogenous activation of NMDA channels in early neocortical development. J. Neurosci. Off. J. Soc. Neurosci. 11, 792–799.

Lu, S.M., Lin, R.C., 1993. Thalamic afferents of the rat barrel cortex: a light- and electron-microscopic study using Phaseolus vulgaris leucoagglutinin as an anterograde tracer. Somatosens. Mot. Res. 10, 1–16. https://doi.org/10.3109/08990229309028819

Lübke, J., Egger, V., Sakmann, B., Feldmeyer, D., 2000. Columnar Organization of Dendrites and Axons of Single and Synaptically Coupled Excitatory Spiny Neurons in Layer 4 of the Rat Barrel Cortex. J. Neurosci. 20, 5300–5311. https://doi.org/10.1523/JNEUROSCI.20-14-05300.2000

Luhmann, H.J., Reiprich, R.A., Hanganu, I., Kilb, W., 2000. Cellular physiology of the neonatal rat cerebral cortex: intrinsic membrane properties, sodium and calcium currents. J. Neurosci. Res. 62, 574–584. https://doi.org/10.1002/1097-4547(20001115)62:4<574::AID-JNR12>3.0.CO;2-0

MacGillavry, H.D., Song, Y., Raghavachari, S., Blanpied, T.A., 2013. Nanoscale scaffolding domains within the postsynaptic density concentrate synaptic

AMPA receptors. Neuron 78, 615–622. https://doi.org/10.1016/j.neuron.2013.03.009

Magdaleno, S., Keshvara, L., Curran, T., 2002. Rescue of ataxia and preplate splitting by ectopic expression of Reelin in reeler mice. Neuron.

Magee, J.C., 1998. Dendritic hyperpolarization-activated currents modify the integrative properties of hippocampal CA1 pyramidal neurons. J. Neurosci. Off. J. Soc. Neurosci. 18, 7613–7624.

Magee, J.C., Johnston, D., 1995. Characterization of single voltage-gated Na+ and Ca2+ channels in apical dendrites of rat CA1 pyramidal neurons. J. Physiol. 487, 67–90. https://doi.org/10.1113/jphysiol.1995.sp020862

Major, G., Polsky, A., Denk, W., Schiller, J., Tank, D.W., 2008. Spatiotemporally Graded NMDA Spike/Plateau Potentials in Basal Dendrites of Neocortical Pyramidal Neurons. J. Neurophysiol. 99, 2584–2601. https://doi.org/10.1152/jn.00011.2008

Malinow, R., Mainen, Z.F., Hayashi, Y., 2000. LTP mechanisms: from silence to four-lane traffic. Curr. Opin. Neurobiol. 10, 352–357.

Manns, I.D., Sakmann, B., Brecht, M., 2004. Sub- and suprathreshold receptive field properties of pyramidal neurones in layers 5A and 5B of rat somatosensory barrel cortex. J. Physiol. 556, 601–622. https://doi.org/10.1113/jphysiol.2003.053132

Maravall, M., Stern, E.A., Svoboda, K., 2004. Development of intrinsic properties and excitability of layer 2/3 pyramidal neurons during a critical period for sensory maps in rat barrel cortex. J. Neurophysiol. 92, 144–156. https://doi.org/10.1152/jn.00598.2003

Marín, O., 2013. Cellular and molecular mechanisms controlling the migration of neocortical interneurons. Eur. J. Neurosci. 38, 2019–2029. https://doi.org/10.1111/ejn.12225

Marrs, G.S., Green, S.H., Dailey, M.E., 2001. Rapid formation and remodeling of postsynaptic densities in developing dendrites. Nat. Neurosci. 4, 1006–1013. https://doi.org/10.1038/nn717

Massey, P.V., Johnson, B.E., Moult, P.R., Auberson, Y.P., Brown, M.W., Molnar, E., Collingridge, G.L., Bashir, Z.I., 2004. Differential roles of NR2A and NR2B-containing NMDA receptors in cortical long-term potentiation and long-term depression. J. Neurosci. Off. J. Soc. Neurosci. 24, 7821–7828. https://doi.org/10.1523/JNEUROSCI.1697-04.2004

Matsuzaki, M., Honkura, N., Ellis-Davies, G.C.R., Kasai, H., 2004. Structural basis of long-term potentiation in single dendritic spines. Nature 429, 761–766. https://doi.org/10.1038/nature02617

Mayer, M.L., Westbrook, G.L., Guthrie, P.B., 1984. Voltage-dependent block by Mg2+ of NMDA responses in spinal cord neurones. Nature 309, 261–263. https://doi.org/10.1038/309261a0

McConnell, S.K., Ghosh, A., Shatz, C.J., 1994. Subplate pioneers and the formation of descending connections from cerebral cortex. J. Neurosci. Off. J. Soc. Neurosci. 14, 1892–1907.

Meister, M., Wong, R.O., Baylor, D.A., Shatz, C.J., 1991. Synchronous bursts of action potentials in ganglion cells of the developing mammalian retina. Science 252, 939–943. https://doi.org/10.1126/science.2035024

Meng, X., Kao, J.P.Y., Kanold, P.O., 2014. Differential signaling to subplate neurons by spatially specific silent synapses in developing auditory cortex. J. Neurosci. Off. J. Soc. Neurosci. 34, 8855–8864. https://doi.org/10.1523/JNEUROSCI.0233-14.2014

Miller, M.W., 1985. Cogeneration of retrogradely labeled corticocortical projection and GABAimmunoreactive local circuit neurons in cerebral cortex. Brain Res 355, 187–192.

Milojkovic, B.A., Radojicic, M.S., Antic, S.D., 2005. A Strict Correlation between Dendritic and Somatic Plateau Depolarizations in the Rat Prefrontal Cortex Pyramidal Neurons. J. Neurosci. 25, 3940–3951. https://doi.org/10.1523/JNEUROSCI.5314-04.2005

Miyata, T., Kawaguchi, A., Okano, H., Ogawa, M., 2001. Asymmetric inheritance of radial glial fibers by cortical neurons. Neuron.

Miyoshi, G., Hjerling-Leffler, J., Karayannis, T., Sousa, V.H., Butt, S.J., Battiste, J., Johnson, J.E., Machold, R.P., Fishell, G., 2010. Genetic fate mapping reveals that the caudal ganglionic eminence produces a large and diverse population of superficial cortical interneurons. J Neurosci 30, 1582–1594.

Mizuno, H., Ikezoe, K., Nakazawa, S., Sato, T., Kitamura, K., Iwasato, T., 2018. Patchwork-Type Spontaneous Activity in Neonatal Barrel Cortex Layer 4 Transmitted via Thalamocortical Projections. Cell Rep. 22, 123–135. https://doi.org/10.1016/j.celrep.2017.12.012

Mizuno, H., Luo, W., Tarusawa, E., Saito, Y.M., Sato, T., Yoshimura, Y., Itohara, S., Iwasato, T., 2014. NMDAR-Regulated Dynamics of Layer 4 Neuronal Dendrites during Thalamocortical Reorganization in Neonates. Neuron 82, 365–379. https://doi.org/10.1016/j.neuron.2014.02.026

Mo, C., Petrof, I., Viaene, A.N., Sherman, S.M., 2017. Synaptic properties of the lemniscal and paralemniscal pathways to the mouse somatosensory thalamus. Proc. Natl. Acad. Sci. 114, E6212–E6221. https://doi.org/10.1073/pnas.1703222114

Molnár, Z., Adams, R., Blakemore, C., 1998a. Mechanisms Underlying the Early Establishment of Thalamocortical Connections in the Rat. J. Neurosci. 18, 5723–5745. https://doi.org/10.1523/JNEUROSCI.18-15-05723.1998

Molnár, Z., Adams, R., Goffinet, A., Blakemore, C., 1998b. The Role of the First Postmitotic Cortical Cells in the Development of Thalamocortical Innervation in the ReelerMouse. J. Neurosci. 18, 5746–5765. https://doi.org/10.1523/JNEUROSCI.18-15-05746.1998

Molnár, Z., Blakemore, C., 1995. How do thalamic axons find their way to the cortex? Trends Neurosci. 18, 389–397. https://doi.org/10.1016/0166-2236(95)93935-Q

Montgomery, J.M., Zamorano, P.L., Garner, C.C., 2004. MAGUKs in synapse assembly and function: an emerging view. Cell. Mol. Life Sci. CMLS 61, 911–929. https://doi.org/10.1007/s00018-003-3364-5

Monyer, H., Burnashev, N., Laurie, D.J., Sakmann, B., Seeburg, P.H., 1994. Developmental and regional expression in the rat brain and functional properties of four NMDA receptors. Neuron 12, 529–540. https://doi.org/10.1016/0896-6273(94)90210-0

Morest, D.K., 1970. A study of neurogenesis in the forebrain of opossum pouch.

Mountcastle, V.B., 1957. Modality and topographic properties of single neurons of cat's somatic sensory cortex. J. Neurophysiol. 20, 408–434. https://doi.org/10.1152/jn.1957.20.4.408

Mukhtar, T., Taylor, V., 2018. Untangling Cortical Complexity During Development. J. Exp. Neurosci. 12, 1179069518759332. https://doi.org/10.1177/1179069518759332

Müller, B.M., Kistner, U., Kindler, S., Chung, W.J., Kuhlendahl, S., Fenster, S.D., Lau, L.F., Veh, R.W., Huganir, R.L., Gundelfinger, E.D., Garner, C.C., 1996. SAP102, a novel postsynaptic protein that interacts with NMDA receptor complexes in vivo. Neuron 17, 255–265. https://doi.org/10.1016/s0896-6273(00)80157-9

Murata, Y., Constantine-Paton, M., 2013. Postsynaptic Density Scaffold SAP102 Regulates Cortical Synapse Development through EphB and PAK Signaling Pathway. J. Neurosci. 33, 5040–5052. https://doi.org/10.1523/JNEUROSCI.2896-12.2013

Myakhar, O., Unichenko, P., Kirischuk, S., 2011. GABAergic projections from the subplate to Cajal-Retzius cells in the neocortex. Neuroreport 22, 525–529. https://doi.org/10.1097/WNR.0b013e32834888a4

Nadarajah, B., Brunstrom, J.E., Grutzendler, J., Wong, R.O., Pearlman, A.L., 2001. Two modes of radial migration in early development of the cerebral cortex. Nat Neurosci.

Nadarajah, B., Parnavelas, J.G., 2002. Modes of neuronal migration in the developing cerebral cortex. Nat Rev Neurosci.

Nair, D., Hosy, E., Petersen, J.D., Constals, A., Giannone, G., Choquet, D., Sibarita, J.-B., 2013. Super-resolution imaging reveals that AMPA receptors inside synapses are dynamically organized in nanodomains regulated by PSD95. J. Neurosci. Off. J. Soc. Neurosci. 33, 13204–13224. https://doi.org/10.1523/JNEUROSCI.2381-12.2013

Nakazawa, S., Mizuno, H., Iwasato, T., 2018. Differential dynamics of cortical neuron dendritic trees revealed by long-term in vivo imaging in neonates. Nat. Commun. 9, 1–15. https://doi.org/10.1038/s41467-018-05563-0

Nery, S., Fishell, G., Corbin, J.G., 2002. The caudal ganglionic eminence is a source of distinct cortical and subcortical cell populations. Nat. Neurosci. 5, 1279–1287. https://doi.org/10.1038/nn971

Nevian, T., Larkum, M.E., Polsky, A., Schiller, J., 2007. Properties of basal dendrites of layer 5 pyramidal neurons: a direct patch-clamp recording study. Nat. Neurosci. 10, 206–214. https://doi.org/10.1038/nn1826

Nicoll, R.A., Malenka, R.C., 1999. Expression mechanisms underlying NMDA receptor-dependent long-term potentiation. Ann. N. Y. Acad. Sci. 868, 515–525. https://doi.org/10.1111/j.1749-6632.1999.tb11320.x

Niculescu, D., Michaelsen-Preusse, K., Güner, Ü., van Dorland, R., Wierenga, C.J., Lohmann, C., 2018. A BDNF-Mediated Push-Pull Plasticity Mechanism for Synaptic Clustering. Cell Rep. 24, 2063–2074. https://doi.org/10.1016/j.celrep.2018.07.073

Nimchinsky, E.A., Sabatini, B.L., Svoboda, K., 2002. Structure and function of dendritic spines. Annu. Rev. Physiol. 64, 313–353. https://doi.org/10.1146/annurev.physiol.64.081501.160008

Noctor, S.C., Flint, A.C., Weissman, T.A., Dammerman, R.S., Kriegstein, A.R., 2001. Neurons derived from radial glial cells establish radial units in neocortex. Nature.

Noctor, S.C., Martinez-Cerdeno, V., Ivic, L., Kriegstein, A.R., 2004. Cortical neurons arise in symmetric and asymmetric division zones and migrate through specific phases. Nat Neurosci.

Noguchi, J., Matsuzaki, M., Ellis-Davies, G.C.R., Kasai, H., 2005. Spine-neck geometry determines NMDA receptor-dependent Ca2+ signaling in dendrites. Neuron 46, 609–622. https://doi.org/10.1016/j.neuron.2005.03.015

Noritake, J., Fukata, Y., Iwanaga, T., Hosomi, N., Tsutsumi, R., Matsuda, N., Tani, H., Iwanari, H., Mochizuki, Y., Kodama, T., Matsuura, Y., Bredt, D.S., Hamakubo, T., Fukata, M., 2009. Mobile DHHC palmitoylating enzyme mediates activity-sensitive synaptic targeting of PSD-95. J. Cell Biol. 186, 147–160. https://doi.org/10.1083/jcb.200903101

Nowak, L., Bregestovski, P., Ascher, P., Herbet, A., Prochiantz, A., 1984. Magnesium gates glutamate-activated channels in mouse central neurones. Nature 307, 462–465. https://doi.org/10.1038/307462a0

Nusser, Z., Lujan, R., Laube, G., Roberts, J.D., Molnar, E., Somogyi, P., 1998. Cell type and pathway dependence of synaptic AMPA receptor number and variability in the hippocampus. Neuron 21, 545–559. https://doi.org/10.1016/s0896-6273(00)80565-6

Oakley, J.C., Schwindt, P.C., Crill, W.E., 2001. Dendritic calcium spikes in layer 5 pyramidal neurons amplify and limit transmission of ligand-gated dendritic current to soma. J. Neurophysiol. 86, 514–527. https://doi.org/10.1152/jn.2001.86.1.514

Oberlaender, M., de Kock, C.P.J., Bruno, R.M., Ramirez, A., Meyer, H.S., Dercksen, V.J., Helmstaedter, M., Sakmann, B., 2012. Cell type-specific three-dimensional structure of thalamocortical circuits in a column of rat vibrissal

cortex. Cereb. Cortex N. Y. N 1991 22, 2375–2391. https://doi.org/10.1093/cercor/bhr317

Ogawa, M., Miyata, T., Nakajima, K., Yagyu, K., Seike, M., Ikenaka, K., Yamamoto, H., Mikoshiba, K., 1995. The reeler gene-associated antigen on Cajal-Retzius neurons is a crucial molecule for laminar organization of cortical neurons. Neuron.

Okabe, S., Kim, H.D., Miwa, A., Kuriu, T., Okado, H., 1999. Continual remodeling of postsynaptic density and its regulation by synaptic activity. Nat. Neurosci. 2, 804–811. https://doi.org/10.1038/12175

Okabe, S., Urushido, T., Konno, D., Okado, H., Sobue, K., 2001. Rapid Redistribution of the Postsynaptic Density Protein PSD-Zip45 (Homer 1c) and Its Differential Regulation by NMDA Receptors and Calcium Channels. J. Neurosci. 21, 9561–9571. https://doi.org/10.1523/JNEUROSCI.21-24-09561.2001

O'Leary, D.D.M., Chou, S.-J., Sahara, S., 2007. Area patterning of the mammalian cortex. Neuron 56, 252–269. https://doi.org/10.1016/j.neuron.2007.10.010

Opazo, P., Sainlos, M., Choquet, D., 2012. Regulation of AMPA receptor surface diffusion by PSD-95 slots. Curr. Opin. Neurobiol. 22, 453–460. https://doi.org/10.1016/j.conb.2011.10.010

Palmer, L.M., 2014. Dendritic integration in pyramidal neurons during network activity and disease. Brain Res. Bull. 103, 2–10. https://doi.org/10.1016/j.brainresbull.2013.09.010

Palmer, L.M., Shai, A.S., Reeve, J.E., Anderson, H.L., Paulsen, O., Larkum, M.E., 2014. NMDA spikes enhance action potential generation during sensory input. Nat. Neurosci. 17, 383–390. https://doi.org/10.1038/nn.3646

Patterson, M., Yasuda, R., 2011. Signalling pathways underlying structural plasticity of dendritic spines. Br. J. Pharmacol. 163, 1626–1638. https://doi.org/10.1111/j.1476-5381.2011.01328.x

Peron, S.P., Freeman, J., Iyer, V., Guo, C., Svoboda, K., 2015. A Cellular Resolution Map of Barrel Cortex Activity during Tactile Behavior. Neuron 86, 783–799. https://doi.org/10.1016/j.neuron.2015.03.027

Petersen, C.C., Sakmann, B., 2001. Functionally independent columns of rat somatosensory barrel cortex revealed with voltage-sensitive dye imaging. J. Neurosci. Off. J. Soc. Neurosci. 21, 8435–8446.

Phillips, G.R., Huang, J.K., Wang, Y., Tanaka, H., Shapiro, L., Zhang, W., Shan, W.-S., Arndt, K., Frank, M., Gordon, R.E., Gawinowicz, M.A., Zhao, Y., Colman, D.R., 2001. The Presynaptic Particle Web: Ultrastructure, Composition, Dissolution, and Reconstitution. Neuron 32, 63–77. https://doi.org/10.1016/S0896-6273(01)00450-0

Pierret, T., Lavallée, P., Deschênes, M., 2000. Parallel Streams for the Relay of Vibrissal Information through Thalamic Barreloids. J. Neurosci. 20, 7455–7462. https://doi.org/10.1523/JNEUROSCI.20-19-07455.2000

Piñon, M.C., Jethwa, A., Jacobs, E., Campagnoni, A., Molnár, Z., 2009. Dynamic integration of subplate neurons into the cortical barrel field circuitry during

postnatal development in the Golli-tau-eGFP (GTE) mouse. J. Physiol. 587, 1903–1915. https://doi.org/10.1113/jphysiol.2008.167767

Pockberger, H., 1991. Electrophysiological and morphological properties of rat motor cortex neurons in vivo. Brain Res. 539, 181–190. https://doi.org/10.1016/0006-8993(91)91619-c

Poirazi, P., Mel, B.W., 2001. Impact of active dendrites and structural plasticity on the memory capacity of neural tissue. Neuron 29, 779–796. https://doi.org/10.1016/s0896-6273(01)00252-5

Polleux, F., Whitford, K.L., Dijkhuizen, P.A., Vitalis, T., Ghosh, A., 2002. Control of cortical interneuron migration by neurotrophins and PI3-kinase signaling. Dev. Camb. Engl. 129, 3147–3160.

Polsky, A., Mel, B.W., Schiller, J., 2004. Computational subunits in thin dendrites of pyramidal cells. Nat. Neurosci. 7, 621–627. https://doi.org/10.1038/nn1253

Portera-Cailliau, C., Weimer, R.M., De Paola, V., Caroni, P., Svoboda, K., 2005. Diverse modes of axon elaboration in the developing neocortex. PLoS Biol. 3, e272. https://doi.org/10.1371/journal.pbio.0030272

Prange, O., Murphy, T.H., 2001. Modular Transport of Postsynaptic Density-95 Clusters and Association with Stable Spine Precursors during Early Development of Cortical Neurons. J. Neurosci. 21, 9325–9333. https://doi.org/10.1523/JNEUROSCI.21-23-09325.2001

Price, D.J., Aslam, S., Tasker, L., Gillies, K., 1997. Fates of the earliest generated cells in the developing murine neocortex. J. Comp. Neurol. 377, 414–422. https://doi.org/10.1002/(SICI)1096-9861(19970120)377:3<414::AID-CNE8>3.0.CO;2-5

Rakic, P., 1988. Specification of cerebral cortical areas. Science.

Rakic, S., Zecevic, N., 2000. Programmed cell death in the developing human telencephalon. Eur. J. Neurosci. 12, 2721–2734. https://doi.org/10.1046/j.1460-9568.2000.00153.x

Rao, A., Kim, E., Sheng, M., Craig, A.M., 1998. Heterogeneity in the Molecular Composition of Excitatory Postsynaptic Sites during Development of Hippocampal Neurons in Culture. J. Neurosci. 18, 1217–1229. https://doi.org/10.1523/JNEUROSCI.18-04-01217.1998

Rebsam, A., Seif, I., Gaspar, P., 2002. Refinement of thalamocortical arbors and emergence of barrel domains in the primary somatosensory cortex: a study of normal and monoamine oxidase a knock-out mice. J. Neurosci. Off. J. Soc. Neurosci. 22, 8541–8552.

Reep, R.L., 2000. Cortical layer VII and persistent subplate cells in mammalian brains. Brain. Behav. Evol. 56, 212–234. https://doi.org/10.1159/000047206

Reim, K., Wegmeyer, H., Brandstätter, J.H., Xue, M., Rosenmund, C., Dresbach, T., Hofmann, K., Brose, N., 2005. Structurally and functionally unique complexins at retinal ribbon synapses. J. Cell Biol. 169, 669–680. https://doi.org/10.1083/jcb.200502115

Reyes, A., Sakmann, B., 1999. Developmental switch in the short-term modification of unitary EPSPs evoked in layer 2/3 and layer 5 pyramidal neurons of rat neocortex. J. Neurosci. Off. J. Soc. Neurosci. 19, 3827–3835.

Rhodes, P., 2006. The properties and implications of NMDA spikes in neocortical pyramidal cells. J. Neurosci. Off. J. Soc. Neurosci. 26, 6704–6715. https://doi.org/10.1523/JNEUROSCI.3791-05.2006

Rio, J.A.D., Soriano, E., Ferrer, I., 1992. Development of GABA-immunoreactivity in the neocortex of the mouse. J. Comp. Neurol. 326, 501–526. https://doi.org/10.1002/cne.903260403

Robertson, R.T., Annis, C.M., Baratta, J., Haraldson, S., Ingeman, J., Kageyama, G.H., Kimm, E., Yu, J., 2000. Do subplate neurons comprise a transient population of cells in developing neocortex of rats? J. Comp. Neurol. 426, 632–650. https://doi.org/10.1002/1096-9861(20001030)426:4<632::AID-CNE10>3.0.CO;2-4

Rumpel, S., Hatt, H., Gottmann, K., 1998. Silent synapses in the developing rat visual cortex: evidence for postsynaptic expression of synaptic plasticity. J. Neurosci. Off. J. Soc. Neurosci. 18, 8863–8874.

Rumpel, S., Kattenstroth, G., Gottmann, K., 2004. Silent synapses in the immature visual cortex: layer-specific developmental regulation. J. Neurophysiol. 91, 1097–1101. https://doi.org/10.1152/jn.00443.2003

Sans, N., Petralia, R.S., Wang, Y.-X., Blahos, J., Hell, J.W., Wenthold, R.J., 2000. A Developmental Change in NMDA Receptor-Associated Proteins at Hippocampal Synapses. J. Neurosci. 20, 1260–1271.

Sans, N., Prybylowski, K., Petralia, R.S., Chang, K., Wang, Y.-X., Racca, C., Vicini, S., Wenthold, R.J., 2003. NMDA receptor trafficking through an interaction between PDZ proteins and the exocyst complex. Nat. Cell Biol. 5, 520–530. https://doi.org/10.1038/ncb990

Sans, N., Wang, P.Y., Du, Q., Petralia, R.S., Wang, Y.-X., Nakka, S., Blumer, J.B., Macara, I.G., Wenthold, R.J., 2005. mPins modulates PSD-95 and SAP102 trafficking and influences NMDA receptor surface expression. Nat. Cell Biol. 7, 1179–1190. https://doi.org/10.1038/ncb1325

Scheiffele, P., 2003. Cell-cell signaling during synapse formation in the CNS. Annu. Rev. Neurosci. 26, 485–508. https://doi.org/10.1146/annurev.neuro.26.043002.094940

Schikorski, T., Stevens, C.F., 1997. Quantitative Ultrastructural Analysis of Hippocampal Excitatory Synapses. J. Neurosci. 17, 5858–5867. https://doi.org/10.1523/JNEUROSCI.17-15-05858.1997

Schiller, J., Major, G., Koester, H.J., Schiller, Y., 2000. NMDA spikes in basal dendrites of cortical pyramidal neurons. Nature 404, 285–289. https://doi.org/10.1038/35005094

Schiller, Jackie, Schiller, Y., 2001. NMDA receptor-mediated dendritic spikes and coincident signal amplification. Curr. Opin. Neurobiol. 11, 343–348. https://doi.org/10.1016/S0959-4388(00)00217-8

Schiller, J., Schiller, Y., Stuart, G., Sakmann, B., 1997. Calcium action potentials restricted to distal apical dendrites of rat neocortical pyramidal neurons. J. Physiol. 505, 605–616.

Schnell, E., Sizemore, M., Karimzadegan, S., Chen, L., Bredt, D.S., Nicoll, R.A., 2002. Direct interactions between PSD-95 and stargazin control synaptic AMPA receptor number. Proc. Natl. Acad. Sci. 99, 13902–13907. https://doi.org/10.1073/pnas.172511199

Schubert, D., Kötter, R., Zilles, K., Luhmann, H.J., Staiger, J.F., 2003. Cell type-specific circuits of cortical layer IV spiny neurons. J. Neurosci. Off. J. Soc. Neurosci. 23, 2961–2970.

Schuman, B., Machold, R.P., Hashikawa, Y., Fuzik, J., Fishell, G.J., Rudy, B., 2019. Four Unique Interneuron Populations Reside in Neocortical Layer 1. J. Neurosci. Off. J. Soc. Neurosci. 39, 125–139. https://doi.org/10.1523/JNEUROSCI.1613-18.2018

Sehara, K., Kawasaki, H., 2011. Neuronal circuits with whisker-related patterns. Mol. Neurobiol. 43, 155–162. https://doi.org/10.1007/s12035-011-8170-8

Sehara, K., Toda, T., Iwai, L., Wakimoto, M., Tanno, K., Matsubayashi, Y., Kawasaki, H., 2010. Whisker-Related Axonal Patterns and Plasticity of Layer 2/3 Neurons in the Mouse Barrel Cortex. J. Neurosci. 30, 3082–3092. https://doi.org/10.1523/JNEUROSCI.6096-09.2010

Senft, S.L., Woolsey, T.A., 1991. Mouse barrel cortex viewed as Dirichlet domains. Cereb. Cortex N. Y. N 1991 1, 348–363. https://doi.org/10.1093/cercor/1.4.348

Sepulveda, F.J., Bustos, F.J., Inostroza, E., Zúñiga, F.A., Neve, R.L., Montecino, M., van Zundert, B., 2010. Differential roles of NMDA Receptor Subtypes NR2A and NR2B in dendritic branch development and requirement of RasGRF1. J. Neurophysiol. 103, 1758–1770. https://doi.org/10.1152/jn.00823.2009

Sheng, M., Hoogenraad, C.C., 2007. The postsynaptic architecture of excitatory synapses: a more quantitative view. Annu. Rev. Biochem. 76, 823–847. https://doi.org/10.1146/annurev.biochem.76.060805.160029

Shimogori, T., Banuchi, V., Ng, H.Y., Strauss, J.B., Grove, E.A., 2004. Embryonic signaling centers expressing BMP, WNT and FGF proteins interact to pattern the cerebral cortex. Dev. Camb. Engl. 131, 5639–5647. https://doi.org/10.1242/dev.01428

Shoykhet, M., Land, P.W., Simons, D.J., 2005. Whisker trimming begun at birth or on postnatal day 12 affects excitatory and inhibitory receptive fields of layer IV barrel neurons. J. Neurophysiol. 94, 3987–3995. https://doi.org/10.1152/jn.00569.2005

Sidman, R.L., Rakic, P., 1973. Neuronal migration, with special reference to developing human brain: a review. Brain Res. 62, 1–35. https://doi.org/10.1016/0006-8993(73)90617-3

Simons, D.J., 1985. Temporal and spatial integration in the rat SI vibrissa cortex. J. Neurophysiol. 54, 615–635. https://doi.org/10.1152/jn.1985.54.3.615

Simons, D.J., Carvell, G.E., 1989. Thalamocortical response transformation in the rat vibrissa/barrel system. J. Neurophysiol. 61, 311–330. https://doi.org/10.1152/jn.1989.61.2.311

Simons, D.J., Woolsey, T.A., 1984. Morphology of Golgi-Cox-impregnated barrel neurons in rat SmI cortex. J. Comp. Neurol. 230, 119–132. https://doi.org/10.1002/cne.902300111

Sjöström, P.J., Turrigiano, G.G., Nelson, S.B., 2001. Rate, Timing, and Cooperativity Jointly Determine Cortical Synaptic Plasticity. Neuron 32, 1149–1164. https://doi.org/10.1016/S0896-6273(01)00542-6

Smart, I.H.M., Dehay, C., Giroud, P., Berland, M., Kennedy, H., 2002. Unique morphological features of the proliferative zones and postmitotic compartments of the neural epithelium giving rise to striate and extrastriate cortex in the monkey. Cereb. Cortex N. Y. N 1991 12, 37–53. https://doi.org/10.1093/cercor/12.1.37

Smith, S.L., Smith, I.T., Branco, T., Häusser, M., 2013. Dendritic spikes enhance stimulus selectivity in cortical neurons in vivo. Nature 503, 115–120. https://doi.org/10.1038/nature12600

Song, J.Y., Ichtchenko, K., Südhof, T.C., Brose, N., 1999. Neuroligin 1 is a postsynaptic cell-adhesion molecule of excitatory synapses. Proc. Natl. Acad. Sci. U. S. A. 96, 1100–1105. https://doi.org/10.1073/pnas.96.3.1100

Spruston, N., 2008. Pyramidal neurons: dendritic structure and synaptic integration. Nat. Rev. Neurosci. 9, 206–221. https://doi.org/10.1038/nrn2286

Spruston, N., Schiller, Y., Stuart, G., Sakmann, B., 1995. Activity-dependent action potential invasion and calcium influx into hippocampal CA1 dendrites. Science 268, 297–300. https://doi.org/10.1126/science.7716524

Staiger, J.F., Flagmeyer, I., Schubert, D., Zilles, K., Kötter, R., Luhmann, H.J., 2004. Functional diversity of layer IV spiny neurons in rat somatosensory cortex: quantitative morphology of electrophysiologically characterized and biocytin labeled cells. Cereb. Cortex N. Y. N 1991 14, 690–701. https://doi.org/10.1093/cercor/bhh029

Steffen, H., Van der Loos, H., 1980. Early lesions of mouse vibrissal follicles: Their influence on dendrite orientation in the cortical barrelfield. Exp. Brain Res. 40, 419–431. https://doi.org/10.1007/BF00236150

Stein, V., House, D.R.C., Bredt, D.S., Nicoll, R.A., 2003. Postsynaptic density-95 mimics and occludes hippocampal long-term potentiation and enhances long-term depression. J. Neurosci. Off. J. Soc. Neurosci. 23, 5503–5506.

Steiner, P., Higley, M.J., Xu, W., Czervionke, B.L., Malenka, R.C., Sabatini, B.L., 2008. Destabilization of the Postsynaptic Density by PSD-95 Serine 73 Phosphorylation Inhibits Spine Growth and Synaptic Plasticity. Neuron 60, 788–802. https://doi.org/10.1016/j.neuron.2008.10.014

Stern, E.A., Maravall, M., Svoboda, K., 2001. Rapid development and plasticity of layer 2/3 maps in rat barrel cortex in vivo. Neuron 31, 305–315. https://doi.org/10.1016/s0896-6273(01)00360-9

Stuart, G., Schiller, J., Sakmann, B., 1997. Action potential initiation and propagation in rat neocortical pyramidal neurons. J. Physiol. 505 (Pt 3), 617–632. https://doi.org/10.1111/j.1469-7793.1997.617ba.x

Stuart, G., Spruston, N., 1998. Determinants of voltage attenuation in neocortical pyramidal neuron dendrites. J. Neurosci. Off. J. Soc. Neurosci. 18, 3501–3510.

Stuart, G.J., Sakmann, B., 1994. Active propagation of somatic action potentials into neocortical pyramidal cell dendrites. Nature 367, 69–72. https://doi.org/10.1038/367069a0

Suarez-Sola, M.L., GonzalezDelgado, F.J., Pueyo-Morlans, M., Medina-Bolivar, C., HernandezAcosta, N.C., Gonzalez-Gomez, M., Meyer, G., 2009. Neurons in the white matter of the adult human neocortex. Front. Neuroanat. 3. https://doi.org/10.3389/neuro.05.007.2009

Sudhof, T.C., 2004. The synaptic vesicle cycle. Annu. Rev. Neurosci. 27, 509–547. https://doi.org/10.1146/annurev.neuro.26.041002.131412

Sullivan, R.M., Landers, M.S., Flemming, J., Vaught, C., Young, T.A., Jonathan Polan, H., 2003. Characterizing the functional significance of the neonatal rat vibrissae prior to the onset of whisking. Somatosens. Mot. Res. 20, 157–162. https://doi.org/10.1080/0899022031000105190

Sun, Q., Srinivas, K.V., Sotayo, A., Siegelbaum, S.A., 2014. Dendritic Na+ spikes enable cortical input to drive action potential output from hippocampal CA2 pyramidal neurons. eLife 3. https://doi.org/10.7554/eLife.04551

Sur, M., Rubenstein, J.L.R., 2005. Patterning and plasticity of the cerebral cortex. Science 310, 805–810. https://doi.org/10.1126/science.1112070

Takahashi, H., Magee, J.C., 2009. Pathway interactions and synaptic plasticity in the dendritic tuft regions of CA1 pyramidal neurons. Neuron 62, 102–111. https://doi.org/10.1016/j.neuron.2009.03.007

Takahashi, N., Kitamura, K., Matsuo, N., Mayford, M., Kano, M., Matsuki, N., Ikegaya, Y., 2012. Locally synchronized synaptic inputs. Science 335, 353–356. https://doi.org/10.1126/science.1210362

Takahashi, N., Oertner, T.G., Hegemann, P., Larkum, M.E., 2016. Active cortical dendrites modulate perception. Science 354, 1587–1590. https://doi.org/10.1126/science.aah6066

Takahashi, T., Goto, T., Miyama, S., Nowakowski, R.S., Caviness, V.S., 1999. Sequence of neuron origin and neocortical laminar fate: relation to cell cycle of origin in the developing murine cerebral wall. J. Neurosci. Off. J. Soc. Neurosci. 19, 10357–10371.

Takumi, Y., Ramírez-León, V., Laake, P., Rinvik, E., Ottersen, O.P., 1999. Different modes of expression of AMPA and NMDA receptors in hippocampal synapses. Nat. Neurosci. 2, 618–624. https://doi.org/10.1038/10172

Tan, S.S., Kalloniatis, M., Sturm, K., Tam, P.P., Reese, B.E., 1998. Faulkner-Jones B. Separate progenitors for radial and tangential cell dispersion during development of the cerebral neocortex. Neuron.

Tanaka, D.H., Mikami, S., Nagasawa, T., Miyazaki, J., Nakajima, K., Murakami, F., 2010. CXCR4 is required for proper regional and laminar distribution of cortical somatostatin-, calretinin-, and neuropeptide Y-expressing GABAergic interneurons. Cereb Cortex 20, 2810–2817.

Tarpey, P., Parnau, J., Blow, M., Woffendin, H., Bignell, G., Cox, C., Cox, J., Davies, H., Edkins, S., Holden, S., Korny, A., Mallya, U., Moon, J., O'Meara, S., Parker, A., Stephens, P., Stevens, C., Teague, J., Donnelly, A., Mangelsdorf, M., Mulley, J., Partington, M., Turner, G., Stevenson, R., Schwartz, C., Young, I., Easton, D., Bobrow, M., Futreal, P.A., Stratton, M.R., Gecz, J., Wooster, R., Raymond, F.L., 2004. Mutations in the DLG3 Gene Cause Nonsyndromic X-Linked Mental Retardation. Am. J. Hum. Genet. 75, 318–324.

Tarusawa, E., Sanbo, M., Okayama, A., Miyashita, T., Kitsukawa, T., Hirayama, T., Hirabayashi, T., Hasegawa, S., Kaneko, R., Toyoda, S., Kobayashi, T., Kato-Itoh, M., Nakauchi, H., Hirabayashi, M., Yagi, T., Yoshimura, Y., 2016. Establishment of high reciprocal connectivity between clonal cortical neurons is regulated by the Dnmt3b DNA methyltransferase and clustered protocadherins. BMC Biol. 14, 103. https://doi.org/10.1186/s12915-016-0326-6

Tiriac, A., Uitermarkt, B.D., Fanning, A.S., Sokoloff, G., Blumberg, M.S., 2012. Rapid whisker movements in sleeping newborn rats. Curr. Biol. CB 22, 2075–2080. https://doi.org/10.1016/j.cub.2012.09.009

Tolner, E.A., Sheikh, A., Yukin, A.Y., Kaila, K., Kanold, P.O., 2012. Subplate neurons promote spindle bursts and thalamocortical patterning in the neonatal rat somatosensory cortex. J. Neurosci. Off. J. Soc. Neurosci. 32, 692–702. https://doi.org/10.1523/JNEUROSCI.1538-11.2012

Tong, G., Jahr, C.E., 1994. Regulation of glycine-insensitive desensitization of the NMDA receptor in outside-out patches. J. Neurophysiol. 72, 754–761. https://doi.org/10.1152/jn.1994.72.2.754

Topinka, J.R., Bredt, D.S., 1998. N-terminal palmitoylation of PSD-95 regulates association with cell membranes and interaction with K+ channel Kv1.4. Neuron 20, 125–134. https://doi.org/10.1016/s0896-6273(00)80440-7

Torborg, C.L., Feller, M.B., 2005. Spontaneous patterned retinal activity and the refinement of retinal projections. Prog. Neurobiol. 76, 213–235. https://doi.org/10.1016/j.pneurobio.2005.09.002

Trachtenberg, J.T., Chen, B.E., Knott, G.W., Feng, G., Sanes, J.R., Welker, E., Svoboda, K., 2002. Long-term in vivo imaging of experience-dependent synaptic plasticity in adult cortex. Nature 420, 788–794. https://doi.org/10.1038/nature01273

Tritsch, N.X., Bergles, D.E., 2010. Developmental Regulation of Spontaneous Activity in the Mammalian Cochlea. J. Neurosci. 30, 1539–1550. https://doi.org/10.1523/JNEUROSCI.3875-09.2010

Tropea, D., Majewska, A.K., Garcia, R., Sur, M., 2010. Structural Dynamics of Synapses in Vivo Correlate with Functional Changes during Experience-Dependent Plasticity in Visual Cortex. J. Neurosci. 30, 11086–11095. https://doi.org/10.1523/JNEUROSCI.1661-10.2010

Valcanis, H., Tan, S.-S., 2003. Layer specification of transplanted interneurons in developing mouse neocortex. J. Neurosci. Off. J. Soc. Neurosci. 23, 5113–5122.

Valiullina, F., Akhmetshina, D., Nasretdinov, A., Mukhtarov, M., Valeeva, G., Khazipov, R., Rozov, A., 2016. Developmental Changes in Electrophysiological Properties and a Transition from Electrical to Chemical Coupling between Excitatory Layer 4 Neurons in the Rat Barrel Cortex. Front. Neural Circuits 10, 1. https://doi.org/10.3389/fncir.2016.00001

Valverde, F., López-Mascaraque, L., Santacana, M., De Carlos, J.A., 1995. Persistence of early-generated neurons in the rodent subplate: assessment of cell death in neocortex during the early postnatal period. J. Neurosci. Off. J. Soc. Neurosci. 15, 5014–5024.

Valverde, F.S., Facal-Valverde, M.V., Santacana, M.V., Heredia, M., 1989. Development and differentiation of early generated cells of sublayer VIb in the somatosensory cortex of the rat: a correlated Golgi and autoradiographic study. J. Comp. Neurol. 290, 118–140. https://doi.org/10.1002/cne.902900108

Van der Loos, H., Woolsey, T.A., 1973. Somatosensory cortex: structural alterations following early injury to sense organs. Science 179, 395–398. https://doi.org/10.1126/science.179.4071.395

Varela, C., 2014. Thalamic neuromodulation and its implications for executive networks. Front. Neural Circuits 8. https://doi.org/10.3389/fncir.2014.00069

Varga, Z., Jia, H., Sakmann, B., Konnerth, A., 2011. Dendritic coding of multiple sensory inputs in single cortical neurons in vivo. Proc. Natl. Acad. Sci. 108, 15420–15425. https://doi.org/10.1073/pnas.1112355108

Vetter, P., Roth, A., Häusser, M., 2001. Propagation of action potentials in dendrites depends on dendritic morphology. J. Neurophysiol. 85, 926–937. https://doi.org/10.1152/jn.2001.85.2.926

Viswanathan, S., Sheikh, A., Looger, L.L., Kanold, P.O., 2017. Molecularly Defined Subplate Neurons Project Both to Thalamocortical Recipient Layers and Thalamus. Cereb. Cortex N. Y. N 1991 27, 4759–4768. https://doi.org/10.1093/cercor/bhw271

Vitali, I., Jabaudon, D., 2014. Synaptic biology of barrel cortex circuit assembly. Semin. Cell Dev. Biol. 35, 156–164. https://doi.org/10.1016/j.semcdb.2014.07.009

Waites, C.L., Craig, A.M., Garner, C.C., 2005. Mechanisms of vertebrate synaptogenesis. Annu. Rev. Neurosci. 28, 251–274. https://doi.org/10.1146/annurev.neuro.27.070203.144336

Wang, H.C., Bergles, D.E., 2015. Spontaneous activity in the developing auditory system. Cell Tissue Res. 361, 65–75. https://doi.org/10.1007/s00441-014-2007-5

Ware, M.L., Tavazoie, S.F., Reid, C.B., Walsh, C.A., 1999. Coexistence of widespread clones and large radial clones in early embryonic ferret cortex. Cereb Cortex 9, 636–645.

Washbourne, P., Bennett, J.E., McAllister, A.K., 2002. Rapid recruitment of NMDA receptor transport packets to nascent synapses. Nat. Neurosci. 5, 751–759. https://doi.org/10.1038/nn883

Washbourne, P., Dityatev, A., Scheiffele, P., Biederer, T., Weiner, J.A., Christopherson, K.S., El-Husseini, A., 2004. Cell Adhesion Molecules in Synapse Formation. J. Neurosci. 24, 9244–9249. https://doi.org/10.1523/JNEUROSCI.3339-04.2004

Watakabe, A., Ichinohe, N., Ohsawa, S., Hashikawa, T., Komatsu, Y., Rockland, K.S., Yamamori, T., 2007. Comparative analysis of layer-specific genes in Mammalian neocortex. Cereb. Cortex N. Y. N 1991 17, 1918–1933. https://doi.org/10.1093/cercor/bhl102

Watanabe, M., Inoue, Y., Sakimura, K., Mishina, M., 1992. Developmental changes in distribution of NMDA receptor channel subunit mRNAs. Neuroreport 3, 1138–1140. https://doi.org/10.1097/00001756-199212000-00027

Welker, E., Hoogland, P.V., Van der Loos, H., 1988. Organization of feedback and feedforward projections of the barrel cortex: a PHA-L study in the mouse. Exp. Brain Res. 73, 411–435. https://doi.org/10.1007/bf00248234

Wen, J.A., Barth, A.L., 2011. Input-Specific Critical Periods for Experience-Dependent Plasticity in Layer 2/3 Pyramidal Neurons. J. Neurosci. 31, 4456–4465. https://doi.org/10.1523/JNEUROSCI.6042-10.2011

Wenthold, R.J., Prybylowski, K., Standley, S., Sans, N., Petralia, R.S., 2003. Trafficking of NMDA receptors. Annu. Rev. Pharmacol. Toxicol. 43, 335–358. https://doi.org/10.1146/annurev.pharmtox.43.100901.135803

Wess, J.M., Isaiah, A., Watkins, P.V., Kanold, P.O., 2017. Subplate neurons are the first cortical neurons to respond to sensory stimuli. Proc. Natl. Acad. Sci. U. S. A. 114, 12602–12607. https://doi.org/10.1073/pnas.1710793114

White, E.L., DeAmicis, R.A., 1977. Afferent and efferent projections of the region in mouse SmL cortex which contains the posteromedial barrel subfield. J. Comp. Neurol. 175, 455–482. https://doi.org/10.1002/cne.901750405

Wichterle, H., Garcia-Verdugo, J.M., Herrera, D.G., Alvarez-Buylla, A., 1999. Young neurons from medial ganglionic eminence disperse in adult and embryonic.

Williams, B.P., Price, J., 1995. Evidence for multiple precursor cell types in the embryonic rat cerebral cortex. Neuron 14, 1181–1188. https://doi.org/10.1016/0896-6273(95)90265-1

Williams, S.R., Stuart, G.J., 2002. Dependence of EPSP efficacy on synapse location in neocortical pyramidal neurons. Science 295, 1907–1910. https://doi.org/10.1126/science.1067903

Wimmer, V.C., Bruno, R.M., de Kock, C.P.J., Kuner, T., Sakmann, B., 2010. Dimensions of a projection column and architecture of VPM and POm axons in rat vibrissal cortex. Cereb. Cortex N. Y. N 1991 20, 2265–2276. https://doi.org/10.1093/cercor/bhq068

Winnubst, J., Cheyne, J.E., Niculescu, D., Lohmann, C., 2015. Spontaneous Activity Drives Local Synaptic Plasticity In Vivo. Neuron 87, 399–410. https://doi.org/10.1016/j.neuron.2015.06.029

Wise, S.P., Jones, E.G., 1976. The organization and postnatal development of the commissural projection of the rat somatic sensory cortex. J. Comp. Neurol. 168, 313–343. https://doi.org/10.1002/cne.901680302

Wong, R.K., Prince, D.A., Basbaum, A.I., 1979. Intradendritic recordings from hippocampal neurons. Proc. Natl. Acad. Sci. U. S. A. 76, 986–990. https://doi.org/10.1073/pnas.76.2.986

Wong, R.O., Meister, M., Shatz, C.J., 1993. Transient period of correlated bursting activity during development of the mammalian retina. Neuron 11, 923–938. https://doi.org/10.1016/0896-6273(93)90122-8

Wong-Riley, M.T., Welt, C., 1980. Histochemical changes in cytochrome oxidase of cortical barrels after vibrissal removal in neonatal and adult mice. Proc. Natl. Acad. Sci. U. S. A. 77, 2333–2337. https://doi.org/10.1073/pnas.77.4.2333

Woo, T.U., Beale, J.M., Finlay, B.L., 1991. Dual Fate of Subplate Neurons in a Rodent. Cereb. Cortex 1, 433–443. https://doi.org/10.1093/cercor/1.5.433

Woolsey, T.A., Van der Loos, H., 1970. The structural organization of layer IV in the somatosensory region (S I) of mouse cerebral cortex: The description of a cortical field composed of discrete cytoarchitectonic units. Brain Res. 17, 205–242. https://doi.org/10.1016/0006-8993(70)90079-X

Woolsey, T.A., Welker, C., Schwartz, R.H., 1975. Comparative anatomical studies of the Sml face cortex with special reference to the occurrence of “barrels” in layer IV. J. Comp. Neurol. 164, 79–94. https://doi.org/10.1002/cne.901640107

Xu, Q., Cobos, I., De La Cruz, E., Rubenstein, J.L., Anderson, S.A., n.d. Origins of cortical interneuron subtypes. J Neurosci 24, 2612–2622.

Yoshii, A., Constantine-Paton, M., 2007. BDNF induces transport of PSD-95 to dendrites through PI3K-AKT signaling after NMDA receptor activation. Nat. Neurosci. 10, 702–711. https://doi.org/10.1038/nn1903

Yozu, M., Tabata, H., Nakajima, K., 2005. The caudal migratory stream: a novel migratory stream of interneurons derived from the caudal ganglionic eminence in the developing mouse forebrain. J. Neurosci. Off. J. Soc. Neurosci. 25, 7268–7277. https://doi.org/10.1523/JNEUROSCI.2072-05.2005

Yu, C., Derdikman, D., Haidarliu, S., Ahissar, E., 2006. Parallel Thalamic Pathways for Whisking and Touch Signals in the Rat. PLOS Biol. 4, e124. https://doi.org/10.1371/journal.pbio.0040124

Yuste, R., Gutnick, M.J., Saar, D., Delaney, K.R., Tank, D.W., 1994. Ca2+ accumulations in dendrites of neocortical pyramidal neurons: an apical band and evidence for two functional compartments. Neuron 13, 23–43. https://doi.org/10.1016/0896-6273(94)90457-x

Zheng, C.-Y., Petralia, R.S., Wang, Y.-X., Kachar, B., Wenthold, R.J., 2010. SAP102 is a highly mobile MAGUK in spines. J. Neurosci. Off. J. Soc. Neurosci. 30, 4757–4766. https://doi.org/10.1523/JNEUROSCI.6108-09.2010

Zhu, F., Cizeron, M., Qiu, Z., Benavides-Piccione, R., Kopanitsa, M.V., Skene, N.G., Koniaris, B., DeFelipe, J., Fransén, E., Komiyama, N.H., Grant, S.G.N., 2018. Architecture of the Mouse Brain Synaptome. Neuron 99, 781-799.e10. https://doi.org/10.1016/j.neuron.2018.07.007

Zhu, Y., Li, H., Zhou, L., Wu, J.Y., Rao, Y., 1999. Cellular and molecular guidance of GABAergic neuronal migration from an extracortical origin to the neocortex. Neuron.

Zielinski, B.S., Hendrickson, A.E., 1992. Development of synapses in macaque monkey striate cortex. Vis. Neurosci. 8, 491–504. https://doi.org/10.1017/s0952523800005599

Zito, K., Svoboda, K., 2002. Activity-dependent synaptogenesis in the adult Mammalian cortex. Neuron 35, 1015–1017. https://doi.org/10.1016/s0896-6273(02)00903-0

Zucker, R.S., Regehr, W.G., 2002. Short-term synaptic plasticity. Annu. Rev. Physiol. 64, 355–405. https://doi.org/10.1146/annurev.physiol.64.092501.114547

Zuo, Y., Lin, A., Chang, P., Gan, W.-B., 2005. Development of Long-Term Dendritic Spine Stability in Diverse Regions of Cerebral Cortex. Neuron 46, 181–189. https://doi.org/10.1016/j.neuron.2005.04.001